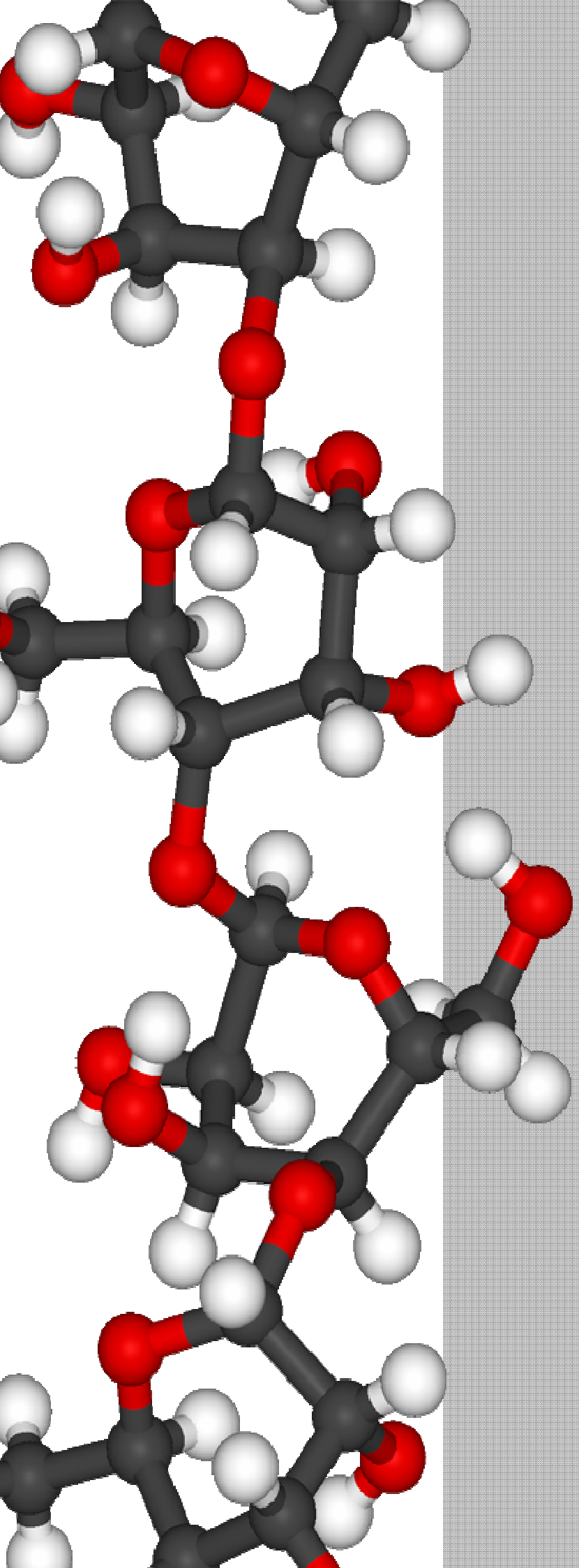

Structure, property and processing relationships of all-cellulose composites

Benoît Duchemin

PhD thesis

2008

Mechanical Engineering
University of Canterbury
Christchurch
New Zealand

Structure, property and processing relationships of all-cellulose composites

Benoît Duchemin

Statement of authenticity

I confirm that the present written work is all my own achievement and does not include any work completed by anyone other than myself.

Acknowledgements

The author would like to thank the Biopolymer Network Limited (New Zealand) for financial assistance and technical support provided to this project. The author is indebted to several staff members at the University of Canterbury in the Mechanical Engineering department: many thanks to Dr Mark Staiger for his valuable supervision through the years; to Dr John Smaill, senior lecturer for the useful discussions; to associate professor Milo Kral, head of the department, for the assistance with TEM, maintenance of the useful group meetings and logistics; to Miss Margot Beck, administrative assistant, for the help in organizing everything; to Miss Elizabeth Sands, Departmental administrator, for her incredible aptitude at managing everything; to Mr Kevin Stobbs, technical officer, for his help organizing and preparing the laboratory work; to Mr Mike Flaws, Senior Technical Officer and Safety Officer, for his help with the SEM and the TEM; to Mrs. Scott Amies, Ken Brown and Paul Wells, respectively senior technical officer, technical officer and senior technician, for their valuable help and advises; to Mr Sato Takanori, PhD fellow and occasional lecturer, for advice and help; to Andy Hamm, PhD fellow, for the useful discussions; to Mademoiselle Karen Denizot, and her infinite help and patience in her task assisting me preparing the foam work. Many thanks too to my friends and colleagues from the other departments: Mme Seema Dean, PhD student from Chemical and process engineering, for the cheerful discussions; to Mr. Manfred Ingerfeld, Biology department, for his help with the TEM; Dr Alexis Pietak, Chemistry department, for her expertise in AFM; Dr Sean Devenish and Miss Annabel Murphy, Chemistry department, for their friendship and the useful advises for my laboratory work; Prof Laurie Greenfield and

Mr Craig Galilee for their help with the grinder; Mr Trevor Berry and Bob Gordon, Chemical and process engineering, for their technical assistance; Mr Stephen Brown for the acquisition of X-ray patterns; Dr Ken Morrison, for his help with the viscometry; thanks to Jack Van Berkel at the Kaikoura field station; no thanks to Dr. Marie Squire, Chemistry technician, for her professionalism; thanks to Dr Jan Wikaira and Prof Ward Robinson, Chemistry department, for the initial X-ray work.

I would also like to thank many of the members of the Biopolymer network: many thanks to Dr Alan Fernyhough, leader of the biomaterials engineering unit at Scion (ex-FRI), for the assistance throughout the Thesis; to Dr Roger Newman, senior scientist at Scion, who brought rigour into my work as well as a deep inside in the macromolecular aspect of cellulose; to Mr Stephen Hill, PhD student and technical officer at Scion, for his help with the solid-state NMR work; to Miss Marie-Joe Le Guen, research assistant as Scion, for her cheerful assistance; to Dr Nick Tucker at Crop and Food for his assistance in the foam work; to Dr Jonathan Caldwell and Dr Joy Woods, research leaders at Agresearch (ex-Canesis, ex-WRONZ), for their help with the TEM work; to Mr Henry Barker and Dr Azam Ali for their help with the mechanical testing. I would especially like to thank Wolfgang Gindl for the useful discussions.

I will never thank enough all of my friends here at University of Canterbury. Thanks to my musician companions as well, long live Sputnik! Merci egalement à mes amis de France et d'Europe pour être restés en contact ou pour m'avoir un jour prêté un bout de canapé : Antoine Laurain, Vincent et Karo, Nicolas et Marie-E, Marie et Luc, Benoit, Stéphane et sa p'tite femme, Jérémie-Eugêne et Billim, Jean, Célia, Virginie, Anne-Gaëlle, Amélie, Pascal et Chloé, Chloé Bonnineau, Heri. Mes excuses à tous ceux que je n'ai pas nommé mais qui comptent néanmoins beaucoup, comme mes potes du bled.

Tout particulièrement à ma famille et à mes parents Sylvie et Jean-Paul, ma soeur Claire, mon cousin Steven, mes cousines Peggy et Hortensia, mes grands parents maternels Odette et

Marius et mes grands-parents paternels, Marthe et Jean. Merci à eux, bien sûr, sans qui rien de tout cela n'aurait été possible : merci infiniment.

Table of contents

Statement of authenticity **2**
Acknowledgements **2**
List of tables **12**
Abstract **15**
1 Introduction **18**
1.1 Overview 18
1.2 Objectives and Thesis outline 19
2 Cellulose: An overview **21**
2.1 Introduction 21
2.2 Chemistry of cellulose 25
2.3 Synthesis 30
2.3.1 Higher plants and algae 30
2.3.2 Bacterial cellulose 36
2.3.3 Synthetic cellulose 36
2.4 Secondary structure 37
2.4.1 Amorphous cellulose 39
2.4.2 Crystalline cellulose 41
2.5 Mechanical properties of cellulose 46
2.6 Extraction of cellulose 49
3 Cellulose Dissolution and Regeneration Routes **51**
3.1 General aspects of cellulose dissolution 53
3.2 Dissolution of cellulose in *N*-methylmorpholine *N*-oxide (NMMO) 54
3.2.1 Introduction 54
3.2.2 NMMO and its hydrates 54
3.2.3 NMMO/water/cellulose system 57
3.2.3.1 Rheological behaviour 58
3.2.3.2 Side-reaction and by-product formation 60
3.2.3.3 Crystallization 60
3.2.4 Stabilizers and additives 61
3.2.5 The lyocell process 63
3.2.5.1 Dope preparation 64
3.2.5.2 Extrusion and dry-jet step 67
3.2.5.3 Coagulation and rinsing 67
3.2.5.4 NMMO recycling 68
3.2.6 Process measurement and analysis 68
3.2.7 Conclusion 70
3.3 Dissolution of cellulose in sodium hydroxide 70
3.3.1 Introduction 70
3.3.2 Dissolution in aqueous NaOH 73
3.3.3 Dissolution in NaOH and additives 74
3.4 Dissolution of cellulose in LiCl/DMAc 79
3.4.1 Introduction 79
3.4.2 The dissolution process 80
3.4.2.1 Cellulose activation 80
3.4.2.2 Solvent preparation 82
3.4.2.3 Cellulose dissolution 82
3.4.2.4 Cellulose precipitation 85
3.4.2.5 Monitoring the preparation 86

3.4.3 Conclusions 87
3.5 Which solvent for an all-cellulose composite? 87
4 All-cellulose composites –a review 90
4.1 Introduction: Overview and benefits over other eco-composites 91
4.2 Anisotropic all-cellulose composites 92
4.2.1 Composites made with continuous fibres 92
4.2.2 Composites made with a strained hydrogel 97
4.3 Quasi-Isotropic all-cellulose composites 97
5 Preliminary investigations into all-cellulose composites 101
5.1 Introduction 101
5.2 Experimental procedures 101
5.2.1 Matrix preparation 101
5.2.2 Matrix regeneration 104
5.2.3 Composite preparation 106
5.3 Conclusions and future work 107
6 Crystallization behaviour of a cellulose hydrogel 109
6.1 Introduction 109
6.2 Experimental procedures 109
6.2.1 Gel preparation 109
6.2.2 X-ray analysis: data extraction and equatorial profile deconvolution 110
6.3 Results and discussion 111
6.3.1 Phase transformations during drying of cellulose gel 111
6.3.2 Peak assignment 111
6.4 Conclusions 116
7 Phase transformations in a model composite made of Micro-Crystalline Cellulose (MCC) 117
7.1 Introduction 117
7.2 Experimental procedures 118
7.2.1 Composite preparation 118
7.2.2 WAXS 119
7.2.3 Solid-state NMR 120
7.2.3.1 Background 120
7.2.3.2 ^{13}C solid-state NMR: an instrument for the scientist interested in cellulose 129
7.2.3.3 Experimental details 136
7.2.4 TEM 137
7.2.5 Optical microscopy 138
7.2.6 Fourier transform infrared spectroscopy (FTIR) 139
7.3 Results and discussion 139
7.3.1 WAXS 139
7.3.2 Solid-state NMR 144
7.3.3 Optical microscopy 152
7.3.4 Transmission electron microscopy (TEM) 153
7.3.5 Fourier transform infrared spectroscopy 158
7.4 Conclusions 166
8 Structure-property relationship of all-cellulose composites 168
8.1 Introduction 168
8.2 Experimental methods 168
8.2.1 Experimental materials 168
8.2.2 Materials characterisation 169

8.3 Results and discussion 170
8.3.1 Microstructural characterisation 170
8.3.2 Mechanical properties and fracture behaviour 172
8.4 Conclusions 178
9 Viscoelastic behaviour of all-cellulose composites in the range of -150°C to 350°C 180
9.1 Introduction 180
9.2 Experimental method 181
9.2.1 Preparation of cellulose and all-cellulose composites 181
9.2.2 Materials characterisation 181
9.3 Results and discussion 182
9.3.1 Viscoelastic behaviour between -150°C and 50°C 182
9.3.1.1 Storage modulus. 182
9.3.1.2 β transition. 183
9.3.1.3 γ peak and other secondary relaxations. 187
9.3.2 Viscoelastic behaviour between 30°C and 350°C 187
9.3.2.1 α_3 transition. 187
9.3.2.2 α_2 transition. 188
9.3.2.3 α_1 transition. 189
9.3.2.4 Refinement of the high temperature thermo-mechanical model. 192
9.4 Conclusions 193
10 Aerocellulose based on all-cellulose composites 195
10.1 Introduction 195
10.2 Experimental methods 196
10.3 Results and discussion 198
11 Conclusions 206
11.1 State-of-the-art 206
11.2 Key questions for the understanding of all-cellulose composites structures 212
11.3 The future of all-cellulose composites and the challenges that lay ahead ... 213
REFERENCES 216
Appendix 1: Brass mould 233
Appendix 2: Sample holder for WAXS of gel specimens 235
Appendix 3: Example of PeakFit® output file 236

List of figures

Figure 1 Life cycle of cellulose in an industrial context 23
Figure 2 Fischer projection, stereo projection and chair projection of alpha (top) and beta (bottom) glucose molecules. 27
Figure 3 Representation of the cellobiose unit..... 28
Figure 4 Representation of the cellulose chain. 28
Figure 5 Cellulose crystal with intra- and intermolecular hydrogen bonds..... 29
Figure 6 Schematic of (a) the plant cell and (b) the cellulose synthase organisation. 32
Figure 7 Schematic representation of the wood cell wall. 33
Figure 8 Fringe fibrillar model (a) and interconnection between the different cellulose allomorphs (b). 38
Figure 9 Specific (a) strength and (b) Young's modulus of natural materials. 48
Figure 10 Formation of N-methylmorpholine-N-oxide..... 55
Figure 11 Conformers of NMMO with calculated energy differences. 56
Figure 12 Complete NMMO-water phase diagram..... 56
Figure 13 Factors influencing dissolution of cellulose in the system NMMO water. 59
Figure 14 Main degradation products of NMMO. 59
Figure 15 Spinnability of cellulose: if the cellulose concentration is too high, the slurry cannot be spun (a). Inversely, if it is too low, the solution will not be sufficiently viscous (c). A balance (b) needs to be achieved..... 62
Figure 16 Lyocell process as described by H. Krässig. 63
Figure 17 Phase diagram cellulose-NMMO-water. 66
Figure 18 The N-Methylmorpholine-N-oxide molecule (1), the exo-centered C-I ion (2) and the ring-centered C-I ion (3). 66
Figure 19 Articles published on the NaOH dissolution route in the last 15 years. 71
Figure 20 Gelation time and G_{gel} as a function of temperature for 4 wt. % cellulose solution 77
Figure 21 Pseudo-phase diagram of cellulose in LiCl/DMAc..... 84
Figure 22 The first all cellulose composites by Nishino: (a) WAXD and SEM micrograph of a cross section and (b) mechanical testing of the material prepared using different manufacturing procedures. 96
Figure 23 Flow diagram representing preliminary trial procedures. 105
Figure 24 Specially designed samples holders with a copper frame used to place the hydrogel in the diffraction chamber. 113
Figure 25 WAXD at four different hydration stages observed during drying of a cellulose hydrogel. 113
Figure 26 Relative intensity of the initial diffraction peak (2θ ~ 13.6º) over the final one (2θ ~ 9.5º) as a function of the water to cellulose weight ratio. 114
Figure 27 Log-log plot of T_1 vs τ_R (both in seconds0 for a ^{13}C spin relaxing by a dipolar interaction with a single proton 1.09 Å away (typical directly bonded C-H distance); in the case of isotropic rotational reorientation and under conditions of complete proton decoupling. Results are shown for 14.1 kG ($\omega_C = 9.48\times10^7$ rad/sec, $\omega_H = 3.77\times10^8$ rad/sec), 23.5 kG ($\omega_C = 1.58\times10^8$ rad/sec, $\omega_H = 6.29\times10^8$ rad/sec), and 51.7 kG ($\omega_C = 3.48\times10^8$ rad/sec, $\omega_H = 1.38\times10^9$ rad/sec) 125
Figure 28 (a) Conventional high-resolution S free induction decay with *I*-spin decoupling. θ_y indicates a $\theta°$ pulse about the y axis of the appropriate rotating frame and H_{1x} continuous irradiation along x. The *S* spins are polarized every ~T_{1S} and then observed following a 90° pulse while continuously irradiating the *I* spins. For purposes of the analysis in the text it is imagined that $T_{1S} >> T_{2S}^*$. $S(t)$ is

the normalized S free induction decay. (b) One particularly simple version of proton-enhanced nuclear induction spectroscopy, using *I-S* cross polarization. Of the *I* spins in ~T_{1I}, the *I* magnetization is spin locked at resonance along H_{1I} in the *I* rotating frame. The *S* spins are brought into contact with the *I* reservoir by applying a resonant H_{1S} such that the Hartman-Hahn condition is satisfied. The spin systems come rapidly to equilibrium causing a small decrease in M_I and a growth of M*s* along their H_1 fields. This is indicated schematically in the figure by the curves in side the H_1 irradiation blocks. The H_{1S} field is then removed and the *S* free induction decay observed while continuing the *I* irradiation for spin decoupling..... 126
Figure 29 Cross-polarization ^{13}C NMR spectra of polycarbonate, with and without magic-angle spinning. The CP spectra are compared to a FT spectrum of the polymer in solution (with solvent lines omitted for clarity of presentation). The FT spectrum is not fully relaxed. 127
Figure 30 Schematics of an NMR probe 128
Figure 31 First published spectra of cellulose II, Whatman CF-1 cellulose, cellulose I and amorphous cellulose..... 130
Figure 32 CP-MAS ^{13}C NMR spectrum of (A) cellulose II, (B) cellulose I_α and (C) cellulose I_β 130
Figure 33 Symmetry and directions of hydrogen bonding in cellulose. (a) Cellulose I_α, in which all chains are crystallographically identical but alternating glucose units in each chain, shaded grey and yellow, differ slightly in conformation. (b) Cellulose I_β, in which chains of two distinct kinds are arranged in alternating sheets. Chains passing through the origin and centre of the unit cell are shaded respectively yellow and grey 134
Figure 34 WAXS diffractograms of MCC before and after activation. Peaks assignments use the monoclinic cellulose I unit cell of Sugiyama *et al.* (1991)..... 141
Figure 35 WAXS diffractograms of all-cellulose composites prepared from activated cellulose by partial dissolution for (a) 1 h and (b) 8 h with values of c shown above each trace..... 142
Figure 36 CrI of the composites..... 143
Figure 37 Solid-state 13C NMR spectra of activated cellulose. Experimental results are labeled S and S'. PSRE subspectra A and B are assigned to crystalline and less-ordered cellulose, respectively..... 146
Figure 38 Solid-state 13C NMR spectra of all-cellulose composites prepared from activated cellulose mixed with solvent at the weight % values shown above each trace and left for 8 h of dissolution. 147
Figure 39 Subspectra A separated from solid-state 13C NMR spectra of all-cellulose composites prepared from activated cellulose mixed with solvent at the weight % values shown above each trace and left for 8 h of dissolution. Labels C-4i and C-4s indicate chemical shifts for the chains of the interior and surface, respectively, of cellulose I..... 147
Figure 40 Subspectra B separated from solid-state 13C NMR spectra of all-cellulose composites prepared from activated cellulose mixed with solvent at the weight % values shown above each trace and left for 8 h of dissolution. Labels C-4a and C-4p indicate chemical shifts for amorphous and paracrystalline cellulose, respectively..... 148
Figure 41 TEM micrographs of the composites obtained by fast precipitation following an 8 h dissolution time with (a) c = 5% and (b) c = 20%. Scale bars are 1 μm..... 154

Figure 42 (a) Aligned and (b) reconstructed TEM micrographs with dimensions 1.47 × 1.47 µm produced with *c* = 20% and t = 8 h. (c) A 3D reconstruction ~60 nm in thickness was obtained, showing the presence of the paracrystalline matrix (black), undissolved MCC (turquoise) and voids (green). 156
Figure 43 (a) First set of aligned TEM micrographs with dimensions 1.23X1.23 µm produced with *c* = 5% and t = 8 h. (b) Second set of aligned TEM micrographs with dimensions 1.47X1.47 µm produced with *c* = 5% and t = 8 h. (c) Three dimensional reconstruction ~60 nm thick obtained from the first set and showing the presence of voids (yellow). (d) Three dimensional reconstruction ~60 nm thick obtained from the second set and showing the presence of voids (green). 157
Figure 44 FTIR spectra of as-received (thick line) and activated (thin line) MCC. 161
Figure 45 FTIR absorbance spectra of all-cellulose composites produced with (a) *c* = 5%, (b) *c* = 10%, (c) *c* = 15% and (d) *c* = 20% in the -CH region. 162
Figure 46 FTIR absorbance spectra of all-cellulose composites produced with (a) *c* = 5%, (b) *c* = 10%, (c) *c* = 15% and (d) *c* = 20% in the -OH region. 164
Figure 47 Position of the maxima in the OH region 3350-3390 cm^{-1} as a function of the initial cellulose concentration (c) and effective dissolution time (t)..... 166
Figure 48 WAXD of all-cellulose composites obtained by slow precipitation for (a) *c* = 5%, (b) *c* = 10%, (c) *c* = 15% and (d) *c* = 20%. 171
Figure 49 *CrI* as a function of *c* and t for activated MCC and all-cellulose composites. The precipitation rate is given in parentheses..... 171
Figure 50 Tensile mechanical properties of all-cellulose composites produced by fast precipitation with t = 1 h (□), t = 4 h (▨) , t = 8 h (▧), t = 48 h (▤) and by slow precipitation (▥). 173
Figure 51 SEM micrographs of the fracture surfaces of all-cellulose composites as a function of *c* and t. (a) *c* = 5% and t = 1 h, (b) *c* = 5% and t = 48 h, (c) *c* = 10% and t = 1h, (d) *c* = 10% and t = 48 h, (e) *c* = 15% and t = 1 h, (f) *c* = 15% and t = 48 h, (g) *c* = 20% and t = 1 h, (h) c = 20% and t = 48 h. (i) and (j) are the fracture surfaces of the composite obtained *via* the slow precipitation route with c=15%. All scale bars are 100 µm, except 5j where it is 10 µm. 176
Figure 52 Schematic of the shear stresses acting during the precipitation of the gel and creating delamination. 177
Figure 53 Tan δ as a function of temperature for various all-cellulose composites at 1 Hz (offset = 0.02). 184
Figure 54 Maximum damping associated with of the β relaxation measured at 1 Hz for t = 1 h (●) and t = 8 h (■), and *CrI* as a function of initial cellulose concentration for t = 1 h (○) and t = 8 h (□). 184
Figure 55 Half-width at half height of the β transition measured at 1 Hz for (a) t = 1 h and (b) t = 8 h. 186
Figure 56 The β transition temperature (°C) as a function of the initial cellulose concentration (*c*) and dissolution time (t) at 1 Hz..... 186
Figure 57 Tan δ plots at 1 Hz between room temperature and 350°C (offset = 0.05). 189
Figure 58 The α_2 transition temperature as a function of *c* and t at 1 Hz. 189
Figure 59 Plots of tan δ (lower curves) and E' for the high precision scan run at 0.2 Hz (□), 0.5 Hz (▲), 1 Hz (■), 2 Hz (○), 5 Hz (●), 10 Hz (+) and 20 Hz (×). 191
Figure 60 WAXS patterns of (a) activated MCC and all-cellulose composites prepared with (b) *c* = 20%, (c) *c* = 15%, (d) *c* = 10% and (e) *c* = 5%. Peaks are assigned according to the monoclinic cellulose I unit cell after Sugiyama *et al.*[72]..... 200

Figure 61 Young's modulus (◊), density (□) and flexural strength (○) of aerocellulose prepared with *c* = 5, 10, 15 and 20%. 203
Figure 62 Graph showing the specific flexural strength (○), specific Young's modulus (◊), flexural strain (×) and CrI (□) of aerocellulose prepared with *c* = 5, 10, 15 and 20%. 203
Figure 63 Scanning electron micrographs of freeze-fractured aerocellulose prepared with (a) and (b) *c*=5%, (c) *c*=10%, (d) *c*=15% and (e) and (f) *c*=20%. 204
Figure 64 Schematic of the physical modifications and process parameters involved in the different steps of all-cellulose composites manufacturing. 208
Figure 65 Various manufacturing paths are possible in order to produce an all-cellulose composite from MCC by partial dissolution in LiCl/DMAc..... 211

List of tables

Table 1 Example of cellulose applications 24
Table 2 Cellulose content of plant material 35
Table 3 Cellulose crystallite dimension.....35
Table 4 Lattice parameters of the most common cellulose allomorphs. 40
Table 5 Effects of different DP and successful additives 62
Table 6 Different dope compositions used by Biganska *et al* 65
Table 7 Examples of dissolution using the NaOH route. 72
Table 8 Examples of all-cellulose composites described in the literature.....94
Table 9 Experimental table summarising the various processing routes used to produce the matrix and composite materials. 102
Table 10 WAXS peaks for cellulose using a molybdenum-source.....114
Table 11 ^{13}C chemical shifts of crystalline celluloses. 134
Table 12 Crystallinity index *CrI* of different all-cellulose composites obtained with an initial cellulose concentration *c* and a dissolution time t. 143
Table 13 Data for starting materials and all-cellulose composites prepared by partial dissolution for 8 h at cellulose concentrations *c* expressed as % of the total weight of cellulose, LiCl and DMAc. 148

List of abbreviations

AFM: Atomic force microscopy

BC: Bacterial cellulose

c: Cellulose concentration on a weight basis

CP/MAS ^{13}C NMR: Cross-polarized Magic angle spinning Nuclear magnetic resonance

CrI: Crystallinity index

DMA: Dynamic mechanical analysis

DMAc: *N,N*-Dimethylacetamide

DP: Degree of polymerization

F: Fraction of crystalline cellulose as estimated by CP/MAS ^{13}C NMR

FTIR: Fourier-Transform Infrared spectroscopy

GFRPs: Glass fibre-reinforced plastics

HWH: Half width at half-height

L: Apparent average crystallite size as estimated by CP/MAS ^{13}C NMR

MCC: Microcrystalline cellulose

MHS: Mark-Houwink-Sakurada

MW: Molecular weight

NMMO: N-methylmorpholine N-oxide

OM: Optical microscopy

rf: Radio frequency

SEC: Size exclusion chromatography

SEM: Scanning electron microscopy

t or D: Crystallite thickness

TC: Terminal complex

TEM: Transmission electron microscopy

WAXD: Wide angle X-ray diffraction

WAXS: Wide angle X-ray scattering

X: Fraction of cellulose chains contained in crystallite interior as estimated by CP/MAS ^{13}C NMR

Abstract

Cellulose is the main load-bearing component in plant fibre due to its covalent β-1→4-link that bonds glucose molecules into a flat ribbon and tight network of intra- and intermolecular hydrogen bonds. It is possible to manipulate the intra- and intermolecular hydrogen bonds in order to embed highly crystalline cellulose in a matrix of non-crystalline cellulose, thereby creating self-reinforced cellulose composites. Cellulose is an excellent choice of raw material for the production of sustainable and high-strength composites by self-consolidation of cellulose since it is readily biodegradable and widely available. Nowadays, the cellulose industry makes extensive use of solvents. A multitude of solvents for cellulose is available but only a few have been explored up to the semi-industrial scale and can qualify as "sustainable" processes. An effective solvent for cellulose is a mixture of the LiCl salt and organic solvent *N,N*-Dimethylacetamide (DMAc). Once cellulose has been dissolved, the cellulose/LiCl/DMAc mixture can be precipitated in water. Preliminary results showed that a solution of 1 wt.% kraft cellulose in 8 wt.% LiCl/DMAc that was precipitated in water formed an hydrogel where cellulose chains were held in their amorphous state and in which no crystalline phase was detected by wide angle X-ray diffraction (WAXD). The initially amorphous cellulose started crystallizing by cross-linking of hydrogen bonds between the hydroxyl groups of the cellulose chains when the cellulose gel was dried and the water to cellulose ratio reached 7 g/g. The final form was poorly crystalline but distinct from amorphous cellulose. In order to study all-cellulose composites at a fundamental level, model all-cellulose composite films were prepared by partly dissolving microcrystalline cellulose (MCC) powder in an 8% LiCl/DMAc solution. Cellulose solutions were precipitated and the resulting gels were dried by vacuum-bagging to produce films approximately 0.2-0.3 mm thick. Wide-angle X-ray scattering (WAXS) and solid-state ^{13}C NMR spectra were used to characterize molecular packing. The MCC was transformed to relatively slender crystallites of cellulose I in a matrix of paracrystalline and amorphous cellulose. Paracrystalline cellulose was distinguished from amorphous cellulose by a displaced and relatively narrow WAXS peak, by a 4 ppm

displacement of the C-4 ^{13}C NMR peak, and by values of $T_2(H)$ closer to those for crystalline cellulose than disordered cellulose. Cellulose II was not formed in any of the composites studied. The ratio of cellulose to solvent was varied, with greatest transformation observed for $c < 15\%$, where c is the weight of cellulose expressed as percentage of the total weight of cellulose, LiCl and DMAc. The dissolution time was varied between 1 and 48 h, with only slight changes occuring beyond 4 h. Transmission electron microscopy (TEM) was employed to assess the morphology of the composites. During dissolution, MCC in the form of fibrous fragments were split into thinner cellulose fibrils. The composites were tested in tension and fracture surfaces were inspected by scanning electron microscopy (SEM). It was found that the mechanical properties and final morphology of all-cellulose composites is primarily controlled by the rate of precipitation, initial cellulose concentration and dissolution time. All-cellulose composites were produced with a tensile strength of up to 106 MPa, modulus up to 7.6 GPa and strain-to-failure around 6%. The precipitation conditions were found to play a large role in the optimisation of the mechanical properties by limiting the amount of defects induced by differential shrinkage.

Dynamic mechanical analysis was used to study the viscoelasticity of all-cellulose composites over temperatures ranging from -150°C to 370°C. A β relaxation was found between -72 and -45°C and was characterized by an activation energy of ~77.5±9.9 kJ/mol, which is consistent with the relaxation of the main chain through co-operative inter- and intramolecular motion. The damping at the β peak generally decreases with an increase in the crystallinity due to enhanced restriction of the molecular motion. For $c \leq 15\%$, the crystallinity index and damping generally decreased with an increasing dissolution time, whereas the size distribution of the mobile entities increases. A simple model of crystallinity-controlled relaxation does not explain this phenomenon. It is proposed that the enhanced swelling of the cellulose in solution after higher dissolution times provides a more uniform distribution of the crystallites within the matrix resulting in enhanced molecular constriction of the matrix material. For $c = 20\%$, however, the trend was the opposite when the dissolution time was

increased. In this case, a slight increase in crystallinity and an increasing damping were observed along with a decrease in the size distribution of the mobile entities. This phenomenon corresponds to a re-crystallisation accompanied with a poor consolidation of the composite. A relaxation α_2 at ~200°C is attributed to the micro-Brownian motion of cellulose chains and is believed to be the most important glass transition for cellulose. The temperature of α_2 decreased with an increase in crystallinity supposedly due to enhanced restriction of the mobile molecular phase. A high temperature relaxation which exhibited two distinct peaks, $\alpha_{1,2}$ at ~300°C and $\alpha_{1,1}$ at ~320°C, were observed. $\alpha_{1,2}$ is prevalent in the cellulose with a low crystallinity. A DMA scan performed at a slow heating rate enabled the determination of the activation energy for this peak as being negative. Consequently, $\alpha_{1,2}$ was attributed to the thermal degradation onset of the surface exposed cellulose chains. $\alpha_{1,1}$ was prevalent in higher crystallinity cellulose and accordingly corresponds to the relaxation of the crystalline chains once the amorphous portion starts degrading, probably due to slippage between crystallites. The relative $\alpha_{1,1}/\alpha_{1,2}$ peak intensity ratio was highly correlated to the amount of exposed chains on the surface of the cellulose crystallites.

Novel aerogels (or aerocellulose) based on all-cellulose composites were also prepared by partially dissolving microcrystalline cellulose (MCC) in an 8 wt.% LiCl/DMAc solution. Cellulose gels were precipitated and then processed by freeze-drying to maintain the openness of the structure. The density of aerocellulose increased with the initial cellulose concentration and ranged from 116 to 350 $kg.m^{-3}$. Aerocellulose with relatively high mechanical properties were successfully produced. The flexural strength and modulus of the aerocellulose was measured up to 8.1 MPa and 280 MPa, respectively.

1 Introduction

1.1 Overview

Cellulosic fibre-reinforced composites (also referred to as biocomposites) based on thermoplastic matrices have recently generated interest as they promise less environmental impact when compared with more traditional composites based on synthetic fibres. Furthermore, the theoretical mechanical properties of biocomposites are impressive when based on the strength and stiffness of crystalline cellulose.[1, 2] The Young's modulus of the native cellulose crystal has been measured to be as high as 138 GPa along the chain axis.[3] Consequently, its longitudinal tensile strength could reach 2.76 GPa, taking into account defects and other physical factors that reduce its strength.[4] However, the theoretical mechanical properties of biocomposites are difficult to achieve due to the inherently poor interfacial bonding between the cellulose and most thermoplastics.

The chemical incompatibility between an hydrophobic matrix and cellulose fibres that comprise a large number of hydroxyl groups results in poor interfacial bonding.[5, 6] The resulting lack of interfacial bonding leads to inefficient stress transfer, resulting in low mechanical strength and stiffness.[5-7] In fact, the strength and stiffness of biocomposites rarely exceeds 300 MPa and 30 GPa, respectively.[8] In order to tackle the issue of interfacial bonding, several different approaches have been attempted. The most common approach involves modifying the chemistry of the fibre or matrix in order to improve chemical compatibility and enhance interfacial bonding. Treatments such as silane and alkali treatments, acetylation, chemical grafting and corona discharge have been implemented with varying degrees of success.[5-7, 9-12] It has also been possible to promote mechanical bonding by using highly defibrillated nano-sized forms of cellulose with a higher surface area to volume

ratio. Cellulose nanostructures (or whiskers) have been prepared from cotton [13], potato pulp [14], sugar beet [15], tunicin [16], wheat straw [17] or *via* hydrolysis of bacterial cellulose.[18] Whiskers provide biocomposites with mechanical properties comparable to synthetic composites.[19, 20] While these treatments can improve the mechanical properties of biocomposites they also add cost and complexity to their formulation.

Recently, monocomponent (or all-cellulose) composite materials[1] have been developed in which the matrix is formed from dissolved and then precipitated cellulose while the reinforcement is in the form of undissolved or partially dissolved cellulosic fibres.[22-30] Partial dissolution of crystalline cellulose has been trialled to overcome issues of a highly viscous matrix, where the starting material is either pulp. Nishino *et al.* reported strength and storage modulus values of up to 480 MPa and 45 GPa, respectively, for ramie fibre-reinforced cellulose.[23] Most studies related to all-cellulose composites are based on the LiCl/*N,N*-Dimethylacetamide (DMAc) solvent system for the dissolution of the cellulose.[22-29], filter paper [24, 29], long fibres [25] or microcrystalline cellulose (MCC) [26, 27] All-cellulose composites are an evolution in biocomposites where greater chemical compatibility between the matrix and reinforcement results in exceptional mechanical properties.

1.2 Objectives and Thesis outline

This work aims to unravel some of the more fundamental aspects of all-cellulose composites. Cellulose is introduced in Chapter 2 by covering some of the chemico-physical data of the cellulose molecule itself, and also general information about its secretion from the cell, plant cell wall and several methods used to extract cellulose from plants. Since the concept

[1] Anecdotally, the concept of cellulose reinforced with cellulose appeared first in a mysterious and somewhat visionary article entitled "Cellular Fabric" published in Nature in 1993. The author the journalist David Jones, well known for confronting accepted notions of technical feasibility, suggested the use of *in-situ* cellulose polymerization to reinforce wood as well as other porous materials. Jones suggested cellulose-metal hybrid composites for damping out noise and holding oil for lubrication.[21]

of all-cellulose composites inevitably involves cellulose dissolution, Chapter 3 provides a short review of three different cellulose dissolution and regeneration methods. The NMMO method is reviewed as it is the most important "green" dissolution process applied at the industrial scale. The low-temperature NaOH dissolution method is then covered as it appears to hold some promise as a safe, simple method that is exempt of polluting by-products. Finally, the LiCl/DMAc dissolution route is covered in Chapter 3. A bibliography on all-cellulose composites is presented in Chapter 4. Chapter 5 reports on the difficulties encountered during the preliminary stages of this investigation of all-cellulose composites. Chapter 6 is an X-ray diffraction study of the intermolecular hydrogen bonding between cellulose chains during drying of the cellulose hydrogel. The partial dissolution of microcrystalline cellulose (MCC) was studied in depth with chemical spectroscopy and TEM in Chapter 7 by changing some manufacturing parameters. Chemical spectroscopy was performed with wide-angle X-ray diffraction (WAXD), cross-polarized magic angle spinning ^{13}C solid-state NMR (CP/MAS ^{13}C NMR) and Fourier-transform infrared spectroscopy (FTIR). Optical microscopy (OM) and transmission electron microscopy (TEM) were helpful to gain insights into the composite morphology and fracture mechanics. Tensile testing and fracture analysis in Chapter 8 revealed which parameters were the most influential on the stiffness and tensile strength. In Chapter 9, dynamic mechanical analysis (DMA) demonstrated the influence of the phase composition (amount and distribution) on the viscoelasticity of all-cellulose composites. Finally, Chapter 10 examines the possibility of manufacturing aerogels (or *aerocellulose*) based on all-cellulose composites.

2 Cellulose: An overview

2.1 Introduction

Plastics are said to account for 7-8% of the global use of crude oil.[31, 32] However, as oil resources are depleted, it is logical to seek for other sources of sustainable and renewable polymers. Cellulose is by far the most abundant polymer on earth, constituting around 70% of the total biomass. Its photoinitiated biosynthesis amounts to approximately 1.3×10^9 ton a year, whereas the plastic production amounts to about 10^8 ton a year.[32, 33] It is an inexhaustible resource if managed carefully as Nature regenerates it in a relatively short period of time. Furthermore, cellulose readily biodegrades and is said to integrate a closed carbon cycle (Figure 1). The concept of closed carbon cycle is that the same amount of CO_2 is produced during the material combustion or degradation as absorbed by the plant during its growth.

Cellulose is mainly found in wood and other plants but can also be extracted from algae and bacteria. As a way to rationalize agricultural production, it has become evident that crops such as corn, hemp or straw can further be taken advantage of by extracting their fibres for non-food uses.[34] Through the use of otherwise waste crop resources, petroleum could be further conserved. Industrial pollution linked to cellulose results from the industrial processes used and not from cellulose itself.[33] Of course, many applications such as paper and textile make an extensive use of cellulose and these are on-going topics of research. However, new prospects for this wonderful resource are also being developed, and not only because cellulose is renewable. Many research centres (CERMAV in France, The Cellulose Society of Japan, BOKU and Lenzing in Austria, Biopolymer Network in New Zealand) are involved with cellulose-based products as varied as smart textiles or eco-composites. Many projects are also aiming at bringing together the various competences inherent to the development of cellulosic

materials in an industrial framework.[35, 36] For example, the recently created European Polysaccharide Network Of Excellence (EPNOE) aims at bringing the expertise of 16 European laboratories from 9 countries together to develop products based on natural resources.

Cellulose is attracting many new research projects aimed at exploiting its versatility in different industrial applications as varied as reinforced plastics, biofuel or biomedical implants (Table 1). Cellulose is biocompatible, derivatizable and offers a broad range of possible applications as it can interact with many other polymers.[35-37] The chirality and biocompatibility of cellulose leads to applications where proteins and antibodies might be immobilized and enantiomeric molecules separated.[38] The piezoelectric properties of cellulose have been used in small electromechanical devices.[38]

Cellulose crystallite solutions can spontaneously form chiral nematic phases. By casting films from those chiral nematic phases, it is possible to form cellulose papers with specific optical properties.[39] Thus, different ink pigments that cannot be reproduced by photocopying or printing could have potential applications in security papers.[39] Cellulose crystals can also be oriented in a magnetic or electric field, paving the way to new applications.[40, 41]

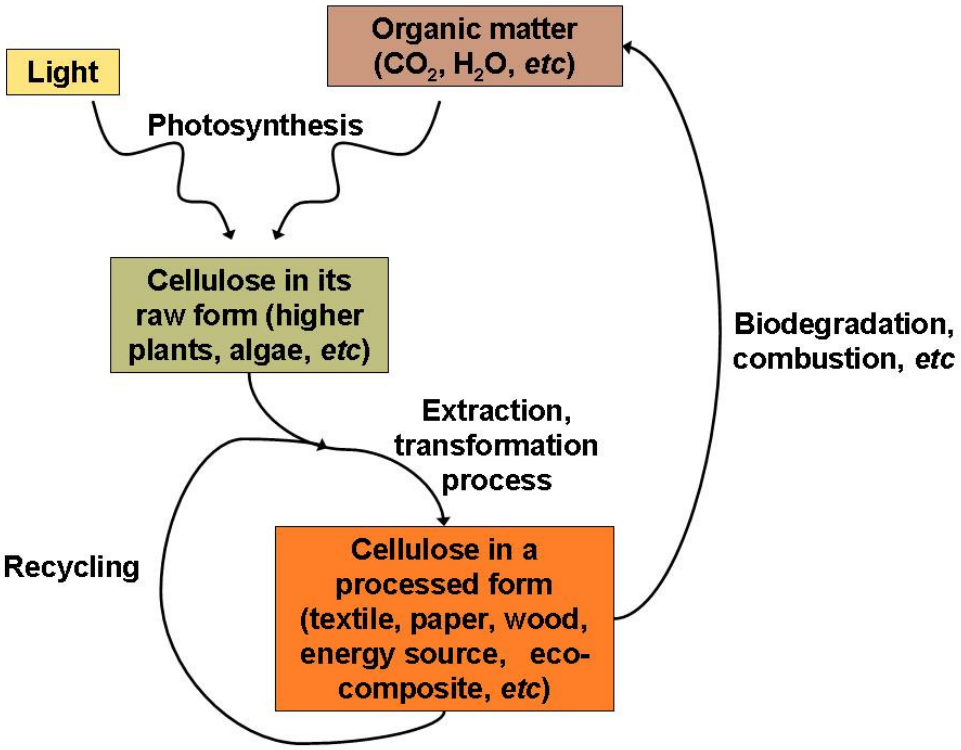

Figure 1 Life cycle of cellulose in an industrial context

Table 1 Example of cellulose applications

Field of application	**Application**	**Product**
Biochemistry	Ultrafiltration membranes	Membrane
Biochemistry	Fractionation membranes	Membrane
Biochemistry	Dialysis membranes	Membrane
Biomedical	Bacterial cellulose wound dressing	Hydrogel
Biomedical	Artificial blood vessels	Hydrogel
Biomedical	Cartilage scaffolds	Hydrogel
Biomedical	Wound dressing	Cotton wool
Chemistry	Filtration	Filter paper (acid-hydrolysed cotton linters)
Chemistry	Purification of chemical systems	Clouding polymers
Civil engineering	Concrete reinforcement	Fibres
Civil engineering	Water balance control in building industry materials (concrete)	Cellulose ethers
Civil engineering	Tunneling and slurry supported excavations	Carboxy methyl cellulose
Commodity	Generic paper, kraft, cartoon	Paper pulp from hemp, linen, wood, *etc*
Commodity	Cosmetic use	Cotton wool
Commodity	Filtration	Filter paper (acid-hydrolysed cotton linters)
Commodity	Cleaning, liquid absorption	Sponges
Commodity	Hi-fi	Bacterial cellulose audio membranes, loudspeaker or MP3 player composite cases
Commodity	Packaging	Cellophane
Electrical	Transformer insulation	Paper impregnated with insulation oil
Electrical	Conductive mats	Cellulose doped with carbon nanotubes
Energy production	Biofuel	Ethanol
Energy production	Electricity	Microbial fuel cells to generate electricity by digesting cellulose
Energy production	Heat by direct combustion	Wood
Food	Texturizer, stabilizer and fat replacer	Microcrystalline cellulose
Mechanical	Polymer composites reinforcement	Fibres, whiskers, microcrystals…
Mechanical	Composite matrix	Cellulose derivatives, regenerated cellulose
Mechanical	Smart paper	Electroactive paper
Medical	Excipient/drug carriers	Compressed microcrystalline cellulose
Optical	Contact lens	Hydrogel
Optical	Iridescent pigments for security paper	Dried cholesteric phase
Optical	Chiral nematic suspensions of cellulose	Liquid
Paint	Stabilizer	Resin, gels, additives
Textile	Man-made fibres (viscose, Lyocel, Tencel, *etc)*	Regenerated wet-spun cellulose fibres
Textile	Smart textiles	Modified regenerated cellulose fibres
Textile	Natural fibres (cotton, hemp, flax…)	Natural fibres
Textile	Disposable towels, tissues, underwears...	Non-woven soft fabrics

2.2 Chemistry of cellulose

Anselme Payen (1795-1871), a French chemist, first discovered and isolated cellulose from green plants.[42] Payen reported its elemental composition in 1842.[33] Cellulose is a linear polymer made of glucose units assembled by groups of two in cellobiose units.

Glucose

Glucose is an hexose, which is a six atom ring. In the conventional representation (Fisher representation), the carbon atoms are numbered from 1 to 6 (Figure 2). Carbon 1 is the potentially aldehydic carbon, and carbon 6 is the carbon atom standing out of the chain. In this form, the sugar is called a pyranose sugar, giving glucose its formal name: glucopyranose. Both α and β forms of glucose exist. The α form first one has its –OH group attached to the carbon 1 above the ring, on the same side as the carbon 4, whereas β has the same –OH group below the ring (Figure 2).[1] The six-membered pyranose ring is not perfectly flat and hexagonal as the stereo projection would suggest; it could have either a *boat* or *chair* form. However, it is found in the *chair* form which is more stable. Also, a C1 conformation where the hydroxyl groups lie nearly in the ring plane (*equatorial hydroxyls*) is preferred. The opposite conformation, 1C, has its hydroxyl groups normal to the ring plane (*axial* groups) which tends to promote instability.[1]

Cellobiose

When the two–OH groups that are attached to the carbons of two glucose rings come sufficiently close in the presence of the appropriate enzyme, a C-O-C group can be created by forming and expelling a water molecule also referred to as *condensation*. The link is called α or β depending on whether the hexoses are in the α or β form. Usually the β form is stronger, leading to less labile molecules compared to the α form.[1] The condensation reaction between

two glucopyranoses in their β form leads to the creation of a C_1-O-C_4 link and the disaccharide cellobiose. This link is annotated as the β-1→4-link. The creation of cellobiose requires the tilting of one of the glucose units for stereochemical reasons. As a result, a hydrogen bond is formed between the ring oxygen and the hydroxyl group attached to the C_3 of the adjacent molecule. (Figure 3)

Cellulose

Cellulose is a linear polymer of β-D-glucose residues linked together by 1,4-links to form a flattened ribbon structure that is a long assembly of cellobiose units. (Figure 4) In wood, the ribbon is ~3.5-5 μm long when determined by extrapolation of the degree of polymerization (DP).[42]

The basic chemical formula of cellulose is $C_{6.DP}H_{10.DP+2}O_{5.DP+1}$.[33] The DP varies tremendously from about 20 in the case of laboratory synthetized cellulose to about 3000 for wood and up to 8000 for ramie.[33] Other estimates have been given with several measurement methods but might seem unreasonably high. Summaries of typical DPs are available in the literature (e.g. Krässig (2002)[33] or Preston (1974) [1]). Usually there is a large number of glucose units in most cellulose sources except synthetic cellulose. Consequently, we can write the approximation:

$$C_{6.DP}H_{10.DP+2}O_{5.DP+1} \sim (C_6H_{10}O_5)_{DP} \text{ or } (C_6H_{10}O_5)_n \quad (1)$$

Where n is the number of units per chain. While other plant polysaccharides (such as lignin) are normally branched structures, cellulose is a linear polymer that occurs naturally in the crystalline state.[43] Cellulose chains are highly hydrophilic due to the presence of large numbers of hydroxyl groups. Cellulose is also very stable due to the β-1→4-link that is

reinforced by an intrachain hydrogen bond. This intrachain bond links the ring oxygen with the C_3 hydroxyl group of the adjacent molecule(Figure 5).[1, 44] Another intrachain hydrogen bond is also found between the hydroxymethyl group oxygen and C_2 hydroxyl group. The existence of this bond for the crystalline states has been proven by both FTIR spectroscopy and X-ray diffraction.[44-47]

In the natural state, approximately 40 to 70 of these chains are held together via O_6-O_3 hydrogen bonding to form a crystalline fibrous structure approximately 3 nm in diameter, also referred to as a microfibril.(Figure 5) Cellulose is chemically stable, normally insoluble and does not thermally degrade below ~200°C in air.[33]

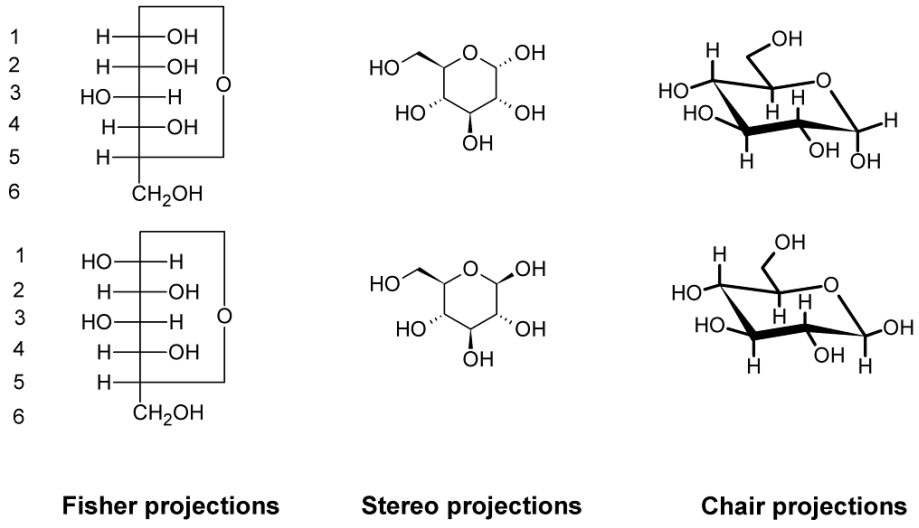

Figure 2 Fischer projection, stereo projection and chair projection of alpha (top) and beta (bottom) glucose molecules.

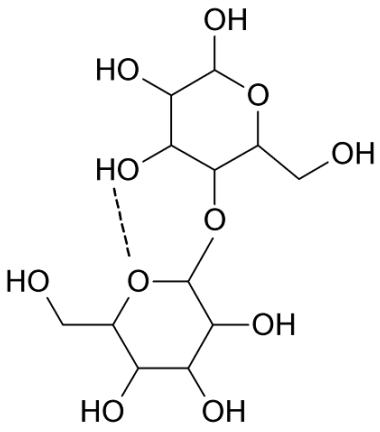

Figure 3 Representation of the cellobiose unit.

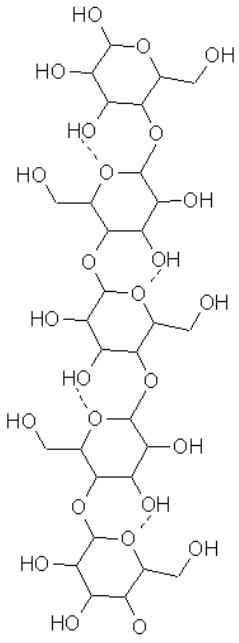

Figure 4 Representation of the cellulose chain.

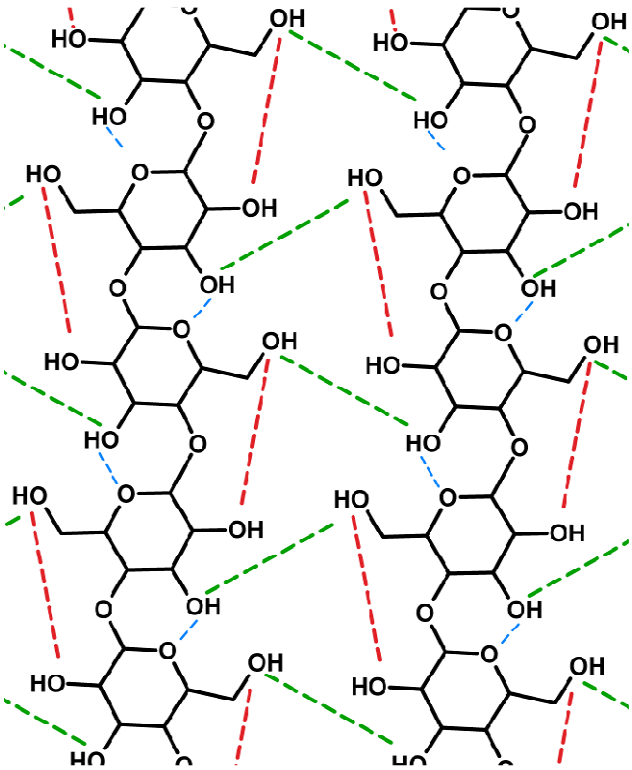

Figure 5 Cellulose crystal with intra- and intermolecular hydrogen bonds.

2.3 Synthesis

Cellulose can be synthesised in eukaryotic[2] and prokaryotic[3] cells, extending from plants, algae, fungi, protists[4] and animals. Laboratory-synthesised cellulose is also possible but has a limited DP.[48, 49]

The most plausible theory to date as to the synthesis of native cellulose microfibrils infers the extracellular association of pre-synthesized (1-4)-β-D-glucans by hydrogen bonding. As reported later by Preston (1974), Colvin first suggested that the glucan chains extruded at the surface of the cell will hydrogen bond to form thin sheets.[1] These thin sheets are forced to coalesce side-by-side by shifts in electron cloud distribution (London forces) to form the microfibril. Native cellulose chains are held together by the hydrogen bonds between the oxygen attached to the C-3 and C-6 molecules. This crystallographic form of cellulose is referred to as cellulose I in order to refer to its crystallographic family, as will be detailed in Chapter 2.4.2.

2.3.1 Higher plants and algae

Cellulose biosynthesis is the result of an original process in higher plants and some algae. As initially proposed by Roelofsen in 1958, a terminal enzyme complex (TC) located at the tip of the cellulose microfibril controls the assembly of the microfibril.[50-52] TCs have

[2] any cell or organism that possesses a clearly defined nucleus; this description excludes bacteria and blue-green algae. The eukaryotic cell has a nuclear membrane, well-defined chromosomes (bodies containing the hereditary material), mitochondria (cellular energy exchangers), a Golgi apparatus (secretory device), an endoplasmic reticulum (a canal-like communication system within the cell), and lysosomes (digestive apparatus within many cell types). (Encyclopædia Britannica. 2007. Encyclopædia Britannica Online. 22 Mar. 2007)

[3] any self-contained cell or organism that lacks internal unit membranes. Bacteria are among the best-known prokaryotic organisms. Prokaryotes lack a nuclear membrane and most of the components of eukaryotic cells. The cell membrane consists of a phospholipid unit membrane and constitutes the cell's primary osmotic barrier. The cytoplasm includes ribosomes that carry out translation and protein synthesis. The nuclear region usually consists of circular, double-stranded deoxyribonucleic acid (DNA). Many prokaryotes also contain accessory, self-replicating genetic structures, called plasmids, with additional dispensable cell functions, such as encoding proteins to inactivate antibiotics. The flagella are distinct from those of eukaryotes in design and movement. The organelles that are present, such as storage vesicles, are surrounded by a nonunit membrane consisting principally of proteins. (Encyclopædia Britannica. 2007. Encyclopædia Britannica Online. 22 Mar. 2007)

[4] any member of the kingdom Protista, a group of eukaryotic, predominantly unicellular microscopic organisms. They may share certain morphological and physiological characteristics with animals or plants, or both. The protists comprise what have traditionally been called protozoa, algae, and lower fungi. (Encyclopædia Britannica. 2007. Encyclopædia Britannica Online. 22 Mar. 2007)

several possible morphologies: linear, rosette or octamer. Their morphology seems to be restricted to rosettes in vascular plants; octamer TCs are found in algae only.[51, 52]

- In all vascular plants, cellulose is synthesized by a complex known by its morphology with a six-fold symmetry. This synthase complex is called a rosette TC and it emerges through the cell membrane. It seems to have some degree of freedom in its lateral motion within the cell membrane.[51]
- Brown proposed a model based on thin sectioning where the rosettes are formed by six subunits where the cellulose chains are catalysed. TCs are composed of both hydrophilic and hydrophobic regions and it is believed that the most central part of the rosettes is facing the cytoplasm. (Figure 6).[51]

The exact process accompanying the polymerization of glucan residues into a cellulose chain, the crystallization of those chains, their extrusion out of the plasma membrane and the role of some lipids as intermediates in the biosynthesis is still not fully understood and thus remains an on-going topic of research.[51]

The organization of the cell wall structure is the well accepted model described by Preston and Frey-Wyssling (Figure 7).[1, 53] The plasma membrane is surrounded by a cell wall where cellulose is deposited. The whole cell is 10–100 μm in diameter. Cell walls are a superimposition of layers where cellulose microfibrils lie nearly parallel to each other. They are 0.1 to 100 μm thick and act as sleeves that will accommodate the physiological need of the growing cell. In the early stages of the cell growth, a primary wall will surround the plasma membrane and simply adapt its size to the growing cell. When the cell reaches its maximum size, appositions of layers against the

(a)

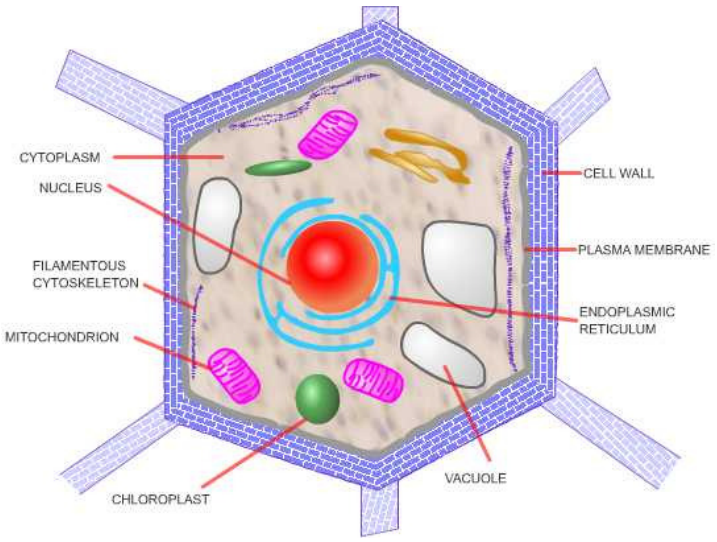

(b)

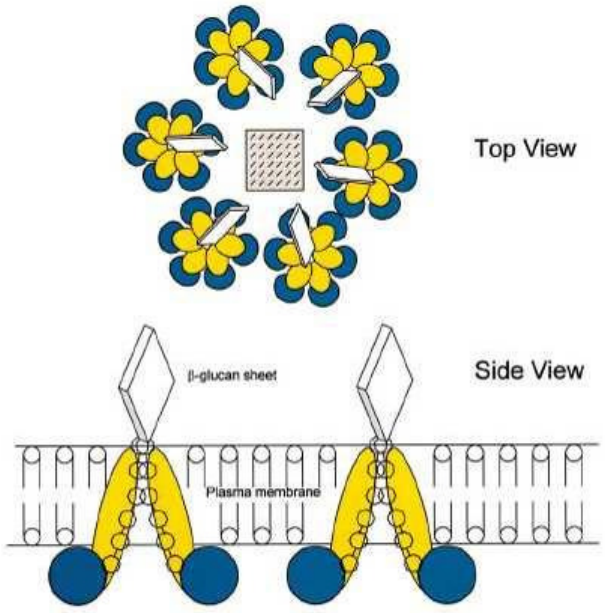

Figure 6 Schematic of (a) the plant cell and (b) the cellulose synthase organisation [51].

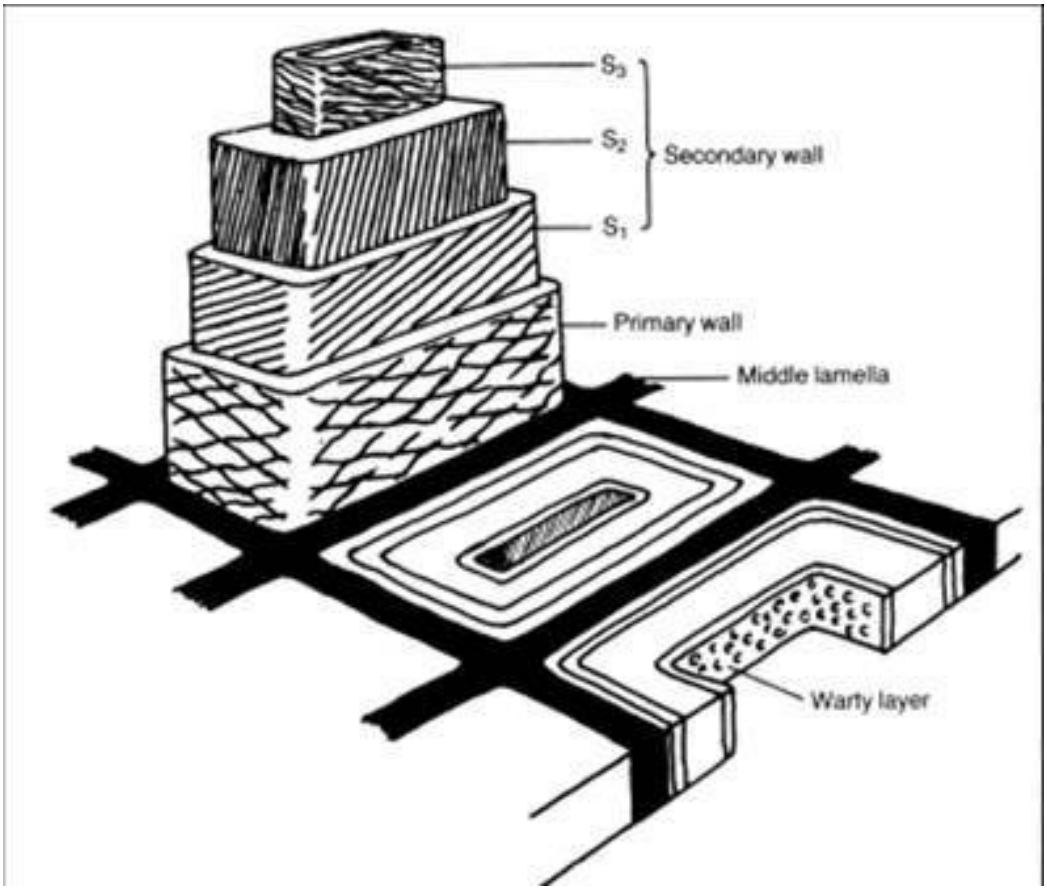

Figure 7 Schematic representation of the wood cell wall (aft. [1]).

primary wall will eventually lead to the creation of the secondary wall. The secondary wall is a lot thicker than the secondary wall. The distinction between primary and secondary wall does however not hold true for some algae, because the two walls are indistinguishable in them.[43] Cellulose microfibrils are embedded in a matrix of other polysaccharides and in non-sugar compounds such as lignin in tissues like wood or phloem sclerenchyma (bark tissue). Extensin is a glycoprotein well known to be one of the major components of the primary cell wall.[43] From a static mechanical viewpoint, this matrix material contributes the cohesion of the cellulose assembly by cross-linking and stiffening.[2, 43] From a more complex physiological perspective, matrix materials such as xyloglucans, extensin, pectin or lignin are integrally part

of the dynamic cell expansion process. This one requires the microfibrils to pack in an ordered manner and the cell wall to have different hydrophilic properties across its diameter.[2, 43]

It is generally found that cellulose microfibrils reorient during cell wall thickening, and particularly during the secretion of the secondary cell wall. The primary cell wall generally holds the cellulose microfibrils with a "roughly transverse" orientation, as described by Preston (1974).[1] As a result of this privileged orientation, the primary cell wall can hold radial hydrostatic pressure just like a pressure pipe. The cell exerts pressure against the cell wall (so-called Turgor pressure) from the inside outwards (Figure 6a). This pressure is the osmotic pressure resulting from the hydrostatic pressure produced by the solution in the whole cell assembly divided by the semipermeable plasma membrane. It is due to a differential in the cell solute concentration: the cytoplasm is richer in water than the flaccid cell.[1]

Hence, the new layers deposited by the plasma membrane in the cell wall undergo an increasing strain gradient by moving outwards across the cell wall, progressively reorienting the microfibrils in the cell length direction. This strain gradient is correlated to the Turgor pressure distribution across the cell wall. This mechanism is well expressed in the two independent statements constituting the Multinet Growth Hypothesis of Roelofson:

- Strain increases for a given wall zone as it passes through the wall; the latter one has a strain gradient
- Constant net transverse orientation of the microfibrils laid down on the inner wall face gives the orientation gradient.[43]

Bailey and Vestal identified three concentric layers in the secondary cell wall: S1, S2 and S3 (though S3 is missing in some species such as spruce).[43] S1 is the outer layer and S3 the inner one; cellulose microfibrils generally exhibit a transverse orientation in those layers. S2 is thicker than both S1 and S3, and it is sandwiched between those two. This structure is

easily visible with TEM when pulp fibres undergo delamination when recycled.[54] The cellulose microfibrils in S2 generally exhibit a longitudinal orientation. Henceforth, the orientation of this layer largely dominates the microfibril angle of the cell wall, often referred to as the MFA. The MFA is routinely calculated by X-ray diffraction.[55] Thus, S2 largely dominates the overall strength and stiffness of natural fibres.[2, 43]

The Young's moduli of cellulose fibres is comparable to that of nylon fishing line while the hemicellulose-lignin matrix in which they are embedded is comparable to that of an epoxy resin. Lignin has a Young's modulus of approximately 2 GPa.[56] The proportions of cellulose vary depending on the material from which it is sourced (Table2).

Table 2 Cellulose content of plant material.[43]

Plant material	**Cellulose (%)**
Cotton	95-99
Ramie	80-90
Wood	40-50
Bark	20-30
Mosses	25-30
Bacteria	20-30
Brown and red algae	1-10

Table 3 Cellulose crystallite dimension.

Origin	**Length**	**Width**	**Reference**
Valonia	100-2000 nm	20 nm	Fleming, 2001
Bleached softwood kraft pulp	180 ±75 nm	3-5 nm	Fleming, 2002
Cotton	100-300 nm	7 nm	Fleming, 2003
Tunicate	several microns	15 nm	Podsiadlo, 2005
Wood pulp	/	3-5 nm	Saito, 2006
Cotton	/	3-5 nm	Saito, 2006
Tunicin	/	Fibrils: 50-100 nm; crystals: 3-5 nm	Saito, 2006
Bacterial cellulose	/	Fibrils: 10-20 nm; crystals: 3-5 nm	Saito, 2006
Cotton	/	10-50 nm with average ~25 nm	Earl, 1981
Acetobacter xylinum	/	7 nm	Earl, 1982

2.3.2 Bacterial cellulose

Bacterial cellulose (BC) is a promising source of cellulose and has found applications in biomedical research. Cellulose is produced in a pure form from bacterial strains such as Acetobacter, Achromobacter, Aerobacter, Agrobacterium, Pseudomonas, Rhizobium, Sarcina, Alcaligenes and Zoogloea.[57, 58] The aerobic strain *Acetobacter xylinum* is commonly used to synthesize the BC referred to in the literature; it has the ability to secrete cellulose extracellularly and lacks photosynthetic ability. The cellulose molecules are assembled in the plasma membrane and secreted *via* linear TCs at the surface of the bacterium.[58] The cellulose chains then aggregate into an assembly called a ribbon. In the hydrated state, ribbons about 500 Å wide are formed of several paracrystalline microfibrils with a cross-section of ~10 × 160 Å.[59] After synthesis in the medium bath or reactor, the BC requires to be boiled in a diluted NaOH solution (0.1 N) to facilitate the elimination of non-cellulosic organic matter such the amino compounds of the cells.[58] Strikingly, dried BC sheets exhibit high mechanical properties. In particular, Nishi who studied dried BC sheets found a dynamic Young's modulus approaching 30 GPa.[60] For comparison, standard phenolic resins have a modulus ranking *ca.* 2 GPa.

2.3.3 Synthetic cellulose

Synthesizing cellulose *in vitro* has been a challenge for scientists since 1941. Fifty years have been necessary before the first successful synthesis was reported by Kobayashi in 1991.[48] To date only enzyme-catalyzed routes have been proved successful because of their ability to control polysaccharides regio- and stereo-selectivities. The first successful non-biosynthetic route used a cellulase-catalyzed polymerization of β-cellobiosyl fluoride monomer. As to the DP, it appears to be limited to about 22 because the product precipitation in the tube test hinders far-reaching monomer aggregation to the existing chain.[48, 49]

Synthetic cellulose exists and could open incredible perspectives for new cellulose applications. However, the lack of control of the synthetic process brings physical limitations that impair synthetic cellulose from finding any use in current industrial applications.

2.4 Secondary structure

Cellulose fibrils consist of complex structure wherein cellulose chains are laterally packed together *via* intermolecular hydrogen bonding in a microfibril or linear crystal. The microfibril can contain 1000 chains and be up to 20 nm across in some algae and in tunicates and sea squirts.[33, 61, 62] In most plants, cellulose usually aggregates in linear crystals about 3 nm thick (Table 3).[62] However, the crystal is imperfect and thus it would be more accurate to describe cellulose as a polymer assembly containing crystallites. The understanding of the fine structure of cellulose has challenged researchers since its discovery. From the end of the 1920s onwards, researchers have been trying to correlate data obtained from X-ray diffraction, electron microscopy, polarized light microscopy, infra-red spectroscopy and atomic force microscopy with the chemical and physical data that is available. Cellulose contains both crystalline and disordered material, as measured by Hermans in the late fifties.[63] Thus, cellulose has a variable *degree of order*. In 1963, Hearle tried to imagine the microstructural cellulose aspect in a much-referenced publication.[64] Part of his vision of the cellulose assembly, named the fringed-fibril structure, was sufficiently accurate and broad to embody most of the progress in this field so far. In his own words: “the crystalline regions are regarded as continuous “fringed fibrils” (Figure 8a), composed of molecules diverging

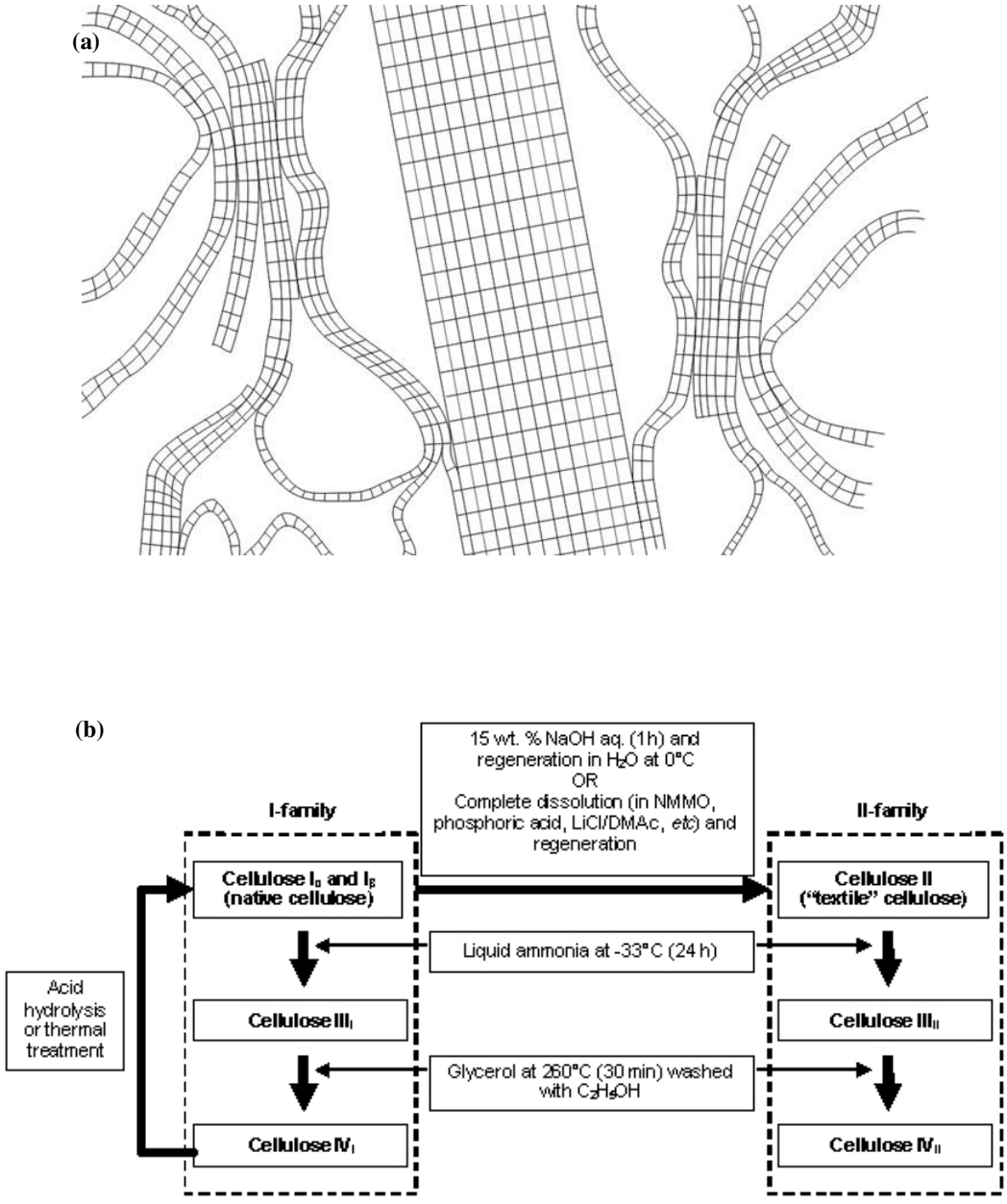

Figure 8 Fringe fibrillar model [64] (a) and interconnection between the different cellulose allomorphs (b) [65].

from the fibrils at different positions of their lengths.[…] It has been assumed that some distortion of the crystal lattice may occur, so that a slight curvature of the fibrils may occur". This accounts for the need to use more modern techniques such as solid-state NMR or electron diffraction to study these structures.

A distinction between amorphous and crystalline cellulose is often made. Crystalline cellulose exists as different allomorphs. By allomorphs, we mean any of at least two distinct crystalline forms of the same substance. Those allomorphs feature distinct lattice dimensions, chain orientation and group conformation (Table 4 and Figure 8b).

2.4.1 Amorphous cellulose

There is vigorous debate in the cellulose field as to how a distinction between amorphous and crystalline phases is made. Different techniques such as WAXD, FTIR, NMR, acid hydrolysis or moisture absorption provide different definitions and values, even if the values strongly correlate.[66-69] The distinction between crystalline and amorphous can be made using acid hydrolysis or water sorption in combination with gravimetric methods; it can also be made using spectroscopy tools such as Segal's crystallinity index, Herman's background analysis, relative absorption bands in infrared spectra or differences in solid-state NMR proton-spin relaxation.[66-68, 70-72] However, these techniques only provide a relative gage of the crystallinity. In fact, cellulose exists in a continuum of states varying in order, blurring the true boundary between crystalline and amorphous states. The macromolecular structure features changing intermolecular in-plane and intra-sheet hydrogen bonds, hydroxymethyl group conformations, interplanar distances, parallel or antiparallel chain conformation, lattice distances (if any), lattice distortions and amount of chain coil.

Table 4 Lattice parameters of the most common cellulose allomorphs.

Allomorph	Crystal system	Chain arrangement	*a* (Å)	*b* (Å)	*c* (Å) (chain axis)	*α* (°)	*β* (°)	*γ* (°)
Cellulose I_α [73]	One chain triclinic	Parallel	6.74	5.93	10.36	117	113	81
Cellulose I_β [73]	Two chain monoclinic	Parallel	8.01	8.17	10.36	90	90	97.3
Cellulose II [74]	Two chain monoclinic	Antiparallel	8.10	9.03	10.31	90	90	117.1
Cellulose III_I [75]	One chain monoclinic	Parallel	4.48	7.85	10.31	90	90	105.1
Cellulose III_{II} [76]	Two chain monoclinic	Antiparallel	10.25	7.78	10.34	90	90	122.4
Cellulose IV_I [76]	Two chain orthorhombic	Parallel	8.03	8.13	10.34	90	90	90
Cellulose IV_{II} [76]	Two chain orthorhombic	Antiparallel	7.99	8.1	10.34	90	90	90

Cellulose in its non-crystalline states easily exhibits order to some extent; [77-79] the real content of true amorphous cellulose may be a lot lower than the value provided by either one of the above-mentioned techniques. For example, Kulshreshtha (1973) confronted chemical assays and classic crystallinity measured by X-ray diffraction and claimed that true amorphous cellulose could represent no more than 5% of cotton, even though X-ray spectroscopy indicated 70% content of crystalline material.[77] Caution must be taken when discussing the degree of order of cellulose to address the intermediary states of order, the so-called paracrystalline states.[77-79]

Relatively few studies have focused solely on the preparation and analysis of amorphous cellulose.[45, 69, 80-82] In general, true amorphous cellulose is prepared by ball-milling, grinding or by regenerating it from SO_2 DEA DMSO (diethylamine-

dimethylsulfoxide) solution.[68, 80, 83-85] Interestingly, a recent study reported the possibility to transform crystalline cellulose into amorphous cellulose in hot and compressed water (320°C and 25 MPa).[86]

Amorphous cellulose differs from crystalline cellulose in its hydrogen bonding pattern. Kondo showed that the chains in amorphous cellulose were held together by isotropic intermolecular hydrogen bonds linked to the hydroxyl groups at the C-2 and C-3 positions, resulting in randomly distributed domains.[45] X-ray diffraction and solid-state NMR reveal that the amorphous chains are not straight nor do they have a preferred orientation as in crystalline cellulose. Instead, the chains of amorphous cellulose consist of bent and twisted backbones and the molecules are in a random coil conformation.[70, 80, 87]

2.4.2 Crystalline cellulose

Crystalline cellulose, in contrast to amorphous cellulose, has different interchain links involving hydrogen bonding at the C-6 position.[79] Accordingly, crystalline chains are aligned to some extent and able to present differing degrees of order.

The cellulose I family

In general, native cellulose is the most crystalline allomorph of cellulose. The parallel packing of native cellulose makes it a metastable form when compared to its counterpart cellulose II, which packs in an antiparallel manner. The nascent nature of the cellulose I microcrystal (simultaneous polymerization and crystallization) provides an explanation for this peculiar, otherwise odd, chain arrangement.[88]

The structure of native cellulose has been elucidated only relatively recently. It was in 1984 that Vanderhart and Atalla [89] suggested that cellulose I was composed of two phases. These two phases were further elucidated by Sugiyama who first proposed the unit cell dimensions

for these two phases.[73] Cellulose I_α has a one-chain triclinic ($P1$) structure. Its unit cell parameters are a = 0.674 nm, b = 0.593 nm and along the chain axis, c = 1.036 nm, while α = 117°, β = 113° and γ = 81°. Cellulose I_β has a two chain monoclinic ($P2_1$) structure with lattice parameters a= 0.801 nm, b = 0.817 nm and c = 1.036 nm, while a monoclinic angle γ equals 97.3°. Bacterial or algal cellulose are essentially cellulose I_α whereas cellulose from tunicates or animal cellulose is mostly of the cellulose I_β form.[90-92] Higher plants contain both forms.[93, 94] Kataoka and Kondo used a microscopic FTIR technique to prove that the primary cell wall of coniferous cells was richer in cellulose I_α whereas the secondary cell wall held I_β.[95] In the same study, the cellulose I_α also appeared more crystalline than the cellulose I_β. The authors attributed the difference to changes in the growth environment such as the stresses involved.

Cellulose I_α and I_β can be present simultaneously in the same fibre, but *also* in the same crystallite.[96, 97] In fact, I_α and I_β co-exist as an assembly of brick-like nano-domains aggregated together in the crystal.[98] The lack of crystalline irregularity seems to indicate that the crystalline lattices I_α and I_β self-assemble.[62]

Molecular modelling by the rigid ring method gave a predicted crystal packing energy of -19.5 kcal/mol for cellulose I_α and of -19.9 kcal/mol for cellulose I_β, which is in accordance with the higher stability of cellulose I_β over I_α.[99] Free rotation around C_5-C_6 and C_6-O_6 in this model also predicted the C_6 *trans-gauche* conformation for the two allomorphs, which also correlates with solid-state NMR, synchrotron X-ray and neutron diffraction results.[70, 90, 91, 99, 100] Transformation of I_α to the more stable I_β can be initiated by high temperature annealing or bending, which causes a longitudinal displacement of the sheets of chains with respect to one another.[62, 92, 93, 101, 102]

Atomic Force Microscopy (AFM) is sensitive to atomic level interactions and is used to observe crystallites at the atomic level. Kuuti *et al.* observed a repeating pattern for *Valonia macrophysia* cellulose that was attributed to the crystal surface (110).[103] Li *et al.* observed I_α and I_β with AFM leading to the following conclusions:

- The two lattices are intimately associated
- I_α and I_β phases have the triclinic (010) and monoclinic (110) plane lying parallel to the cell wall surface, respectively, which differs to cellulose from *Valonia.*[97, 104]

X-ray fibre diffraction patterns with a resolution of up to 0.1 nm were obtained at the European Synchrotron Radiation Facility (ESRF) (Grenoble, France). ESRF provides more precisely than any other technique the position of the heavier atoms, carbon and oxygen, in the cellulose chain. The position of the hydrogen atoms involved in the intermolecular and intramolecular hydrogen bonding could be determined by analysis of neutron fibre diffraction data.[105] Nishiyama used synchrotron X-ray and neutron fibre diffraction in a series of papers to ascertain the position of the carbon and oxygen.[90, 91]

It is important to note that cellulose I_β is a more disorganized form of cellulose than cellulose I_α. The intermolecular hydrogen bond O_2-O_6 of I_β covers a wide physical volume, which provides the polymer chains with the flexibility required to maintain the polysaccharide sheets despite relatively high lattice distortions.[90]

Cellulose III_I can be prepared from cellulose I by treatment in liquid ammonia, supercritical ammonia or by treatment in ethylenediamine.[75, 76, 106-108] It has a one chain unit cell and a $P2_1$ space group with lattice parameters of a = 0.448 nm, b = 0.785 nm, c = 1.031 nm and γ = 105.1°.[75]

Cellulose IV_I can be prepared from cellulose III_I with a high temperature treatment (260°C) in glycerol.[107, 109, 110] Several authors' findings pointed towards cellulose IV_I being a disordered form of cellulose I_β because of the size of its unit cell and the reversibility of the transformation I → IV by thermal treatment or acid hydrolysis.[76, 109, 110] Lattice parameters can be found in Table 4.

The cellulose II family

The cellulose II polymorph is obtained by mercerization or regeneration of cellulose from solution. It packs in a space group $P2_1$ with the unit cell parameters a = 8.10 Å, b = 9.03 Å and c = 10.31 Å with the monoclinic angle γ = 117.10°.[74]

Aalboo (1995) using molecular modelling found the packing energy of cellulose II to be -21.4 kcal/mol for cellulose II as determined by the ring method.[99] This method also predicted the *gauche-trans* conformation of the hydroxymethyl group, in accordance with ^{13}C solid-state NMR results and electron diffraction techniques.[70, 99, 100, 111] Applying the latter technique, Langan and co-workers refined the model and suggested that a small portion of *trans-gauche* conformation could possibly be found in the centre chain.[111]

When regeneration is carried out at elevated temperatures, the allomorph cellulose IV can be formed.[63] Thermal treatment such as high pressure steam also provides a pathway to the formation of cellulose IV from regenerated cellulose.[112-115]

Mercerization process and soda-cellulose

Transformation from cellulose I to cellulose II occurs when cellulose is exposed to an alkaline solution of NaOH.[76, 116] The process was named mercerization after it was invented by John Mercer some 150 years ago.[117] It is still used nowadays in the textile industry in order to produce fibres with superior mechanical properties and improved dyability.

Sodium hydroxide is known to change the cellulose crystal lattice, orientation factor, crystallinity and degree of hydrolysis.[117-120] It is also possible to dissolve cellulose with NaOH under certain conditions, as will be detailed in Chapter 3.3. Das and Chakraborty have shown that in the case of bamboo left for one hour in an alkali solution, the overall crystallinity was preserved up to a caustic soda concentration of about 20%.[116] However, the crystallinity content of the material was seriously diminished when the caustic soda concentration was raised to 50%.

At concentrations greater than ~20%, however, the lattice is changed and goes from a parallel packing to an antiparallel packing (Table 4). The lattice transformation depends on experimental conditions and is known to induce several intermediary crystal forms called Na-cellulose or soda cellulose that have antiparallel chain packing.[117, 118] During the immersion of cellulose in the caustic soda solution, the hydrogen in the –OH group is replaced with a Na^+ cation, leading to the solid-state transformation of cellulose to soda cellulose. The most probable composition of soda-cellulose is $C_6H_{10}05.NaOH.2H_20$ and it is believed to have a four chain unit cell with $\alpha = \beta = \gamma = 90°$, a = 8.83 Å, b = 25.28 Å and c = 10.29 Å along the fibre axis.[118] A detailed Na-cellulose phase diagram deduced from solid state ^{13}C NMR was published by Porro *et al.*.[117] Destruction of the soda-cellulose complex by rinsing with distilled water and neutralization with mineral acid results in the formation of cellulose II.[76]

Effect of ball milling or mechanical grinding

The cellulose crystalline structure is changed when relatively harsh mechanical action is applied. In general, the crystallinity is decreased during ball-milling or severe grinding and the process is accompanied by a change in the intermolecular chemical bonding.[84, 121, 122] Kimura *et al.* concluded from WAXD that all forms of cellulose (I, II, III_I and III_{II}) transform to an amorphous state *via* the IV form.[121] They elucidated the crystal structure remaining in

ball-milled samples by acid hydrolysis and treatment with NaOH solutions. Samples that were not fully amorphous after ball-milling recrystallized in a structure where the lattice conformation was identical to that of the starting material. Amorphous cellulose recrystallized into cellulose II -an irreversible change driven by the more stable antiparallel chain conformation.

2.5 Mechanical properties of cellulose

Strength

The ideal strength of cellulose is widely estimated in the literature to be about 13-17 GPa for cellulose I and 9 GPa for cellulose II. Those estimates are based on the rule of the thumb claiming that $\sigma \sim 0.1 \times E$.[4] However, there is no direct measure of this value yet available, and values between $0.01 \times E$ and $0.02 \times E$ seem more realistic in practice.[4] By extrapolation from Chen *et al.*, the maximum theoretical strength of amorphous cellulose is about 800 ± 100 MPa.[123] Wegst *et al.* indexed cellulose's strength to about 1 GPa.[124] As a comparison, silk fibres and Kevlar fibres reach strengths up to 2 and 4 GPa, respectively. Cellulose has the highest efficiency in tension of all natural polymers, outstripping steel by a factor of 2.6 (Figure 9a). These measures take into account the relatively low density of cellulose by comparing the specific strengths of all materials σ/ρ. The native cellulose crystal has a density of about 1.58-1.59 g/cm³ whereas that of pure natural fibre reaches 1.55 g/ cm³.[42, 125]

Deformation of cellulose occurs by a complex stretching and re-organisation of the hydrogen bonds, particularly in the amorphous region.[123, 126-130] Yielding of amorphous cellulose occurs by breaking of hydrogen bonds where more than 90% of these are determined to be intermolecular.[123] Inter-molecular hydrogen bonds can be broken below the yield

point, which explains the hysteresis phenomenon of cellulose at small strains.[123] Yielding of amorphous cellulose occurs at 7-8% strain.[123]

Young's Modulus

An average Young's modulus of 10.3 GPa was calculated for amorphous cellulose using a force-field model.[123] Using X-ray diffraction, Nishino measured the elastic modulus in the direction parallel to the chain axis of several cellulose polymorphs.[3] Cellulose I was found to have a modulus of 138 GPa whereas cellulose IV_I exhibited a lower value of 75 GPa.[3] Ishikawa *et al.* published similar values and ranking for polymorphs sourced from ramie fibre.[107] Such values are higher than that of other engineering materials such as aluminum (70 GPa) or glass fiber (76 GPa).[22] Wegst *et al.* also ranked the specific stiffness of cellulose among the highest of all natural materials (Figure 9b).[124]

(a)

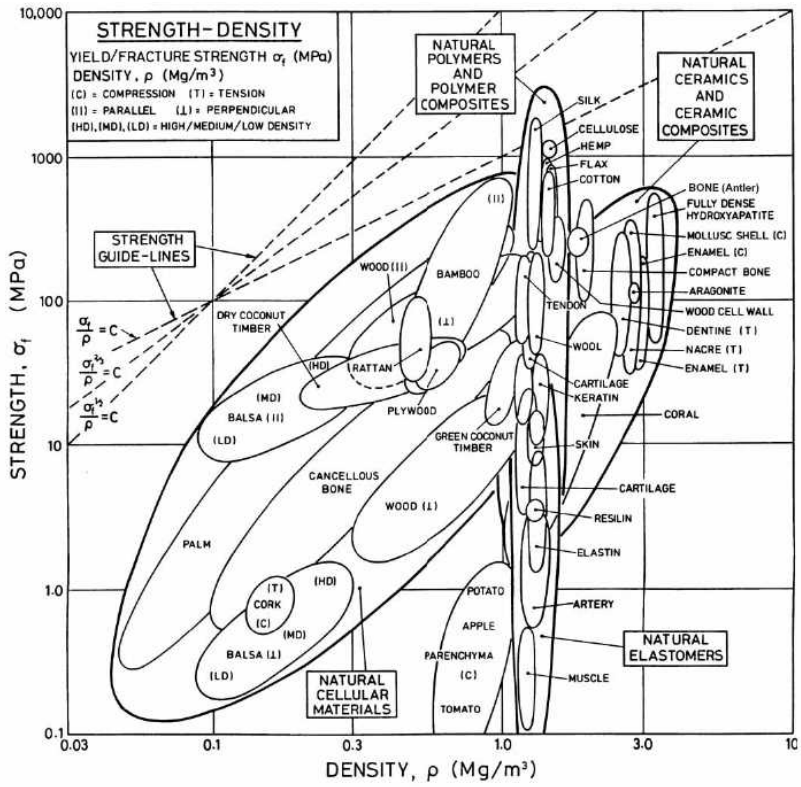

(b)

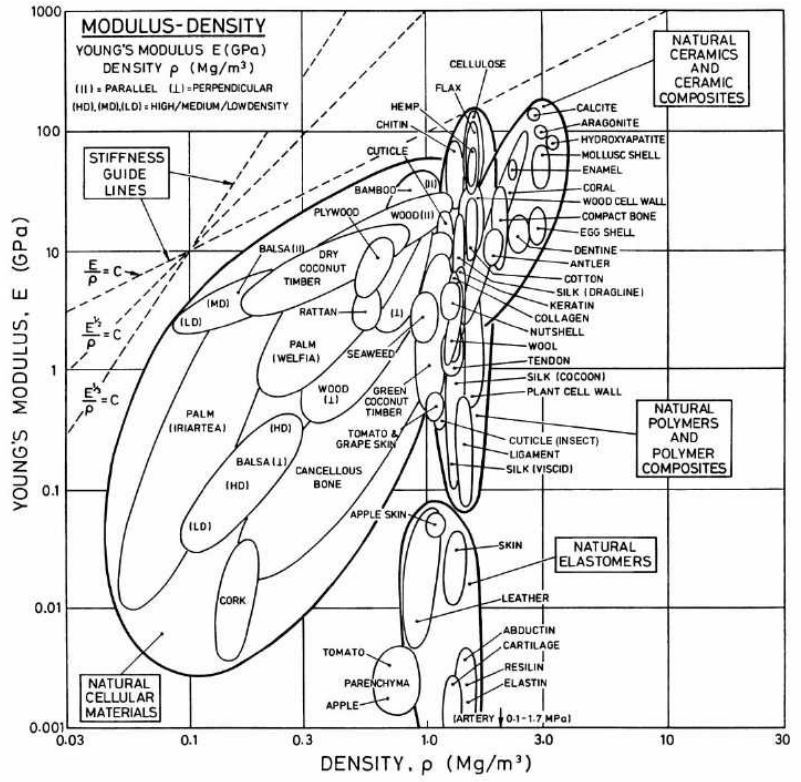

Figure 9 Specific (a) strength and (b) Young's modulus of natural materials.[124]

2.6 Extraction of cellulose

General considerations

A drawback of cellulose obtained from higher plants is its chemical impurity. As detailed previously, natural fibres consist of an assembly of cellulose microfibrils concentrically arranged in a matrix of other organic compounds. Pure cellulose can be extracted from the cell wall by using various mechanical, chemical and enzymatic processes. Field retting is a traditional method that consists of leaving the cut fibre stems in the field in order for micro-organisms and UV to aid the release of single fibres from the stems. Carding, also called mechanical decortication, is another common preliminary step aiming at breaking down large fibre aggregates into smaller ones before further treatment is carried out. It has consequences for the fibre integrity such as strain-hardening for example.[131] Progressive reorientation of the microfibrils under stretching is thought to be the mechanism behind this phenomenon.[131] Thermomechanical pulping, steam explosion, enzymatic retting and mercerization are all four possible treatments that may follow mechanical decortication. They are all aimed at separating the fibre bundles in elementary fibres by extracting amorphous components from the cell wall. Thermomechanical pulping is a common method used to mechanically separate fibres in a liquid media kept at temperatures above 100 ˚C. Mechanical pulps account for 20% of the world pulp production.[132] Steam explosion consists in placing the wet fibres in a high-pressure environment and suddenly releasing the pressure and temperature down to atmospheric conditions. As a result, fibre bundles break down into single fibres and up to 20% of the fibre mass is removed as hemicellulose and pectin.[115, 133, 134] Enzymatic methods are aimed at depolymerising the hemicellulose and breaking the covalent link between lignin and other carbohydrates.[34] Hemicelluloses can also be removed by treatment in hot alkaline solutions followed by neutralization in a mineral acid.[2] When this process is accompanied by fibre stretching, it is commonly referred to as mercerization.

Mercerization is very common in the textile industry. Bleaching is also routinely used in the pulp and paper and textile industries after separation of the fibre bundle into single fibres. This treatment further rids the cellulose of low molecular weight compounds while providing cell wall delignication, giving a pronounced whiteness to the fibre.[34] Bleaching is carried out with hypochlorite, peroxides or chlorine dioxide.[33] Environmentally friendly chlorine-free alternatives do exist such as mixtures of acetic acid/nitric acid.[135]

Microcrystalline cellulose

Microcrystalline cellulose (MCC) consists of short fibre aggregates of nearly pure native cellulose, 3 to 6 μm in size; its DP is usually around 200-400 and its crystallinity index CrI is greater than 75%. MCC can be prepared out of virtually any cellulose source such as wood, cotton, water hyacinth, coconut shells, sugar cane bagasse, ramie, wheat, flax and rice straws, soybean husk, flax fibres and soybean husk.[136] MCC prepapration usually involves bleaching prior to acid hydrolysis. Acid hydrolysis is usually carried out with HCl or H_2SO_4 and is known to decrease the DP by breaking down the glycosidic bonds; elimination of the three dimensional regions of disorder follows.[89, 136, 137] Other more exotic methods to produce microfibrils include high shear refining and cryocrushing.[137] Eichhorn and Young evaluated the value of MCC Young's modulus by Raman spectroscopy and found it to be ~ 25 ± 4 GPa.[138] Applications of MCC range from laboratory grade cellulose (≤ 99% purity) to food additive.

3 Cellulose Dissolution and Regeneration Routes

With the exception of the application of wood products, textile fibres account for most of the demand for cellulose. Natural cellulosic-based fibres have been used in textiles since the beginning of civilization. Flax seeds found in Ramad (Syria) dating back to 7000 B.C. suggest the cultivation of flax. Egyptian mummies wrapped in linen shrouds have also been dated back to 5000 B.C..[139]

Natural fibre quality is subject to geographical conditions including weather, soil types, fungi and fauna pressure. Dissolution of natural cellulosic materials, followed by cellulose regeneration, has provided more consistent material than can be achieved using natural fibres direct from the field. Features like drapability, coloration potential, texture and tenacity are tailored for the intended application. Furthermore, the use of cheap wood pulp (with low DP) as a starting material is a cost-effective alternative to high quality natural fibres. Amongst the known processing routes for cellulose dissolution, only a few are used at an industrial scale. The Viscose process was the first of these processes to be discovered and was developed at around the turn of the 20^{th} century. Social pressures to seek more eco-friendly alternatives due to the environmental impacts of the Viscose process have been raised in the last decade. Indeed, the Viscose process is a long, complicated, inefficient process, also producing sulphur by-products.[33, 140] A dissolution process based on the use of the tertiary aliphatic amine N-oxide hydrates was the subject of extensive research in the seventies. N-methylmorpholine-N-oxide (NMMO), is now successfully used as an organic solvent in an industrial process that produces spun cellulosic fibres under the generic name of Lyocell. Other dissolution methods have been used with success to produce textile fibres. Cellulose can for example be dissolved with LiCl/DMAc to produce high tenacity fibres.[141-143] More recently, attention has been focused on a sustainable process taking advantage of the Q-region in the NaOH cellulose phase

diagram. In the Q region, cellulose can be completed dissolved under certain conditions.[144-148]

The uses of cellulose dissolution goes beyond fibre spinning and is found in a broad range of applications ranging from sponges to synthesis of cellulose derivatives. Ionic liquids (ILs) have recently gained much attention due to their high efficiency and non-volatility which makes them relatively safe to work with. Furthermore, ILs are easily recyclable.[149-155] Other solvents for cellulose include dimethyl sulfoxide/ammonium fluorides [156, 157], dimethyl sulfoxide/formaldehyde [158], inorganic complexes like cuprammonium cuene or cadoxene [159], molten salt hydrates such as $LiClO_4*3H_2O$, $ZnCl_2*4H_2O$ or $LiSCN*2H_2O$ [149, 160], metal complexes [161], LiOH/urea [162, 163], ethylene diamine/potassium thiocyanate [164], NH_4SCN/NH_3 [165], N_2O_4-dimethylformaldehyde and concentrated protonic acids.[159]

Three of these solvents (NMMO, NaOH and LiCl/DMAc) will be reviewed after a brief introduction on cellulose dissolution as these especially hold promise for all-cellulose composites. NMMO is already used at an industrial scale and is generally agreed to be the eco-friendliest solvent system used in an industrial process. Sodium hydroxide is not used industrially yet, but it has the advantage of yielding no hazardous by-product while being cost effective and part of a low temperature process. LiCl/DMAc will also be reviewed since all of the all-cellulose composites produced so far in the literature are based on this solvent system. LiCl/DMAc is a very potent solvent of cellulose, easy to use and can dissolve cellulose at room temperature.

3.1 General aspects of cellulose dissolution

Cellulose dissolution is normally preceded by swelling. Polymer dissolution is accompanied by a decrease in the free energy ΔF of the polymer-solvent systems. ΔF is defined as: $\Delta F = \Delta H - T \Delta S$, where ΔH and ΔS are the changes in the enthalpy and entropy contributions, respectively. One of the common criteria to predict polymer solubility is Hildebrandt's solubility parameter (δ), which is closely related to the cohesive forces between the polymer chains. When the interaction energy of the solvent is close to the cohesive forces of the polymer, the dissolution theoretically only depends on the entropy contribution. However, it is not sufficient for a chemical to simply have δ in the right range to dissolve cellulose.[159]

δ was found to be 28.6 $(J/cm^3)^{1/2}$ for cellulose based on swelling experiments; however, it is closer to 53.4 $(J/cm^3)^{1/2}$ when calculated from the crystalline region cohesion forces.[103] The average solubility parameter of amorphous cellulose, as calculated by Chen and co-workers, amounted to about 38.9 $(J/cm^3)^{1/2}$.[123] Easier side-group accessibility and weaker interchain hydrogen bonding are indeed expected from the amorphous material over its crystalline counterpart.

A contribution to δ from dispersion (δ_d), from dipole-dipole (δ_p) and H- bonds (δ_h) has to be taken into account in order to reflect the complex mechanism at the inter- and intra-molecular levels. By extrapolating δ, δ_h, δ_d and δ_p from the values of cellulose acetates with varying degrees of substitution, Bochek *et al.* established that the energy of one cellulose hydrogen bond was E_h = 25.2 kJ/mol.[166] The authors concluded that amine oxides theoretically had the power to dissolve cellulose if their $E_h \geq 25.0$ kJ/mol, because intermolecular bonds are hydrogen bonds.

3.2 Dissolution of cellulose in *N*-methylmorpholine *N*-oxide (NMMO)

3.2.1 Introduction

The dissolution of cellulose in NMMO is used in an industrial method generally named the Lyocell process. This route was developed in order to replace the polluting Viscose process. Different companies put their own brand names on the fibres produced from this process such as Tencel (Courtaulds), Lyocell (Lenzing), Alceru (TITK Rudolstadt) and Newcell (Akzo Nobel).[33, 167] The dissolution of cellulose in the NMMO/water system also permits the recovery of virtually all the NMMO used in the process. Additionally, NMMO is biodegradable and non-toxic.[167-170]

The fibres produced by the Lyocell process primarily consist of monoclinic cellulose type-II crystallites.[76, 171, 172] Crystalline regions have a length, width and thickness of 12-14 nm, 8-10 nm and 3-4 nm, respectively.[172] They are assembled into strand-shaped bundles with lengths of 150-550 nm, partly assembled into aggregates 30-60 nm in diameter.

The strength and stiffness of regenerated fibres spun from NMMO in the presence of additives can be really good and up to 1.3 GPa and 55 GPa, respectively.[140]

3.2.2 NMMO and its hydrates

NMMO has been approved by the International Union of Pure and Applied Chemistry and is considered to be the official terminology for N-methylmorpholine-N-oxide, although other names such as NMMNO, MMNO and NMO can be found in the literature. NMMO belongs to the family of *cyclic, aliphatic, tertiary amine oxides*, where the nitrogen carries the cyclic and aliphatic groups, as well as the oxygen (Figure 10).[167] The highly polar group N-O (4.38 mD) is responsible for the high hydrophilicity of NMMO and its complete miscibility in water, as it readily forms hydrogen bonds. The N-O bond has a high energy (222kJ/mol) and

thus is easily broken. Hence, NMMO is thermally labile (it can easily be decomposed when subjected to heat), a strong oxidant and sensitive to any catalyst which can break the N-O bond.

NMMO possesses an unrestrained flexible six-membered ring (Figure 10) with five conformations including two chair conformations (1 and 2), two boat conformations (3 and 4) and one twist conformation (5). The two chair conformations are much more stable than the other conformations (Figure 11) and thus it is assumed that only the two chair conformations are found in solution.[168]

The NMMO-water mixtures are denoted $n$$H_2O$-NMMO or NMMO*$n$$H_2O$, where n is the number of water molecules per solvent molecule. For n = 0, the mixture is anhydrous. When the components are mixed in the same proportions (*i.e.* n = 1), the mixture is referred to as monohydrate, having a 13.3 wt.% water content. The monohydrate is the evaporation product of NMMO-water solutions when n > 1.[167] Another important hydrate is the disesquihydrate obtained when n = 2.5 (28 wt.%). Both the monohydrate and disesquihydrate are known to be stable hydrates.[167] Recently, Biganska *et al.* conducted a systematic analysis which found that the stable hydrate observed in the n = 2-2.5 region may well be the dihydrate (23.5 wt.%) - this is still the subject of controversy. An 8H_2O-NMMO hydrate (55.2 wt.%) was also discovered to be a new crystalline stable hydrate.

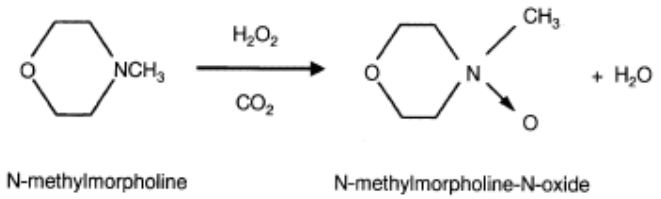

Figure 10 Formation of N-methylmorpholine-N-oxide.[171]

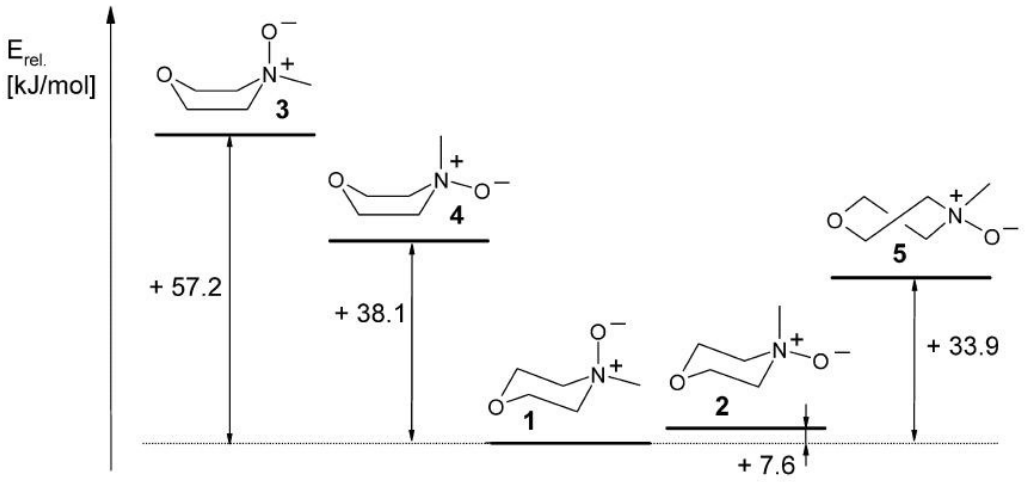

Figure 11 Conformers of NMMO with calculated energy differences.[171]

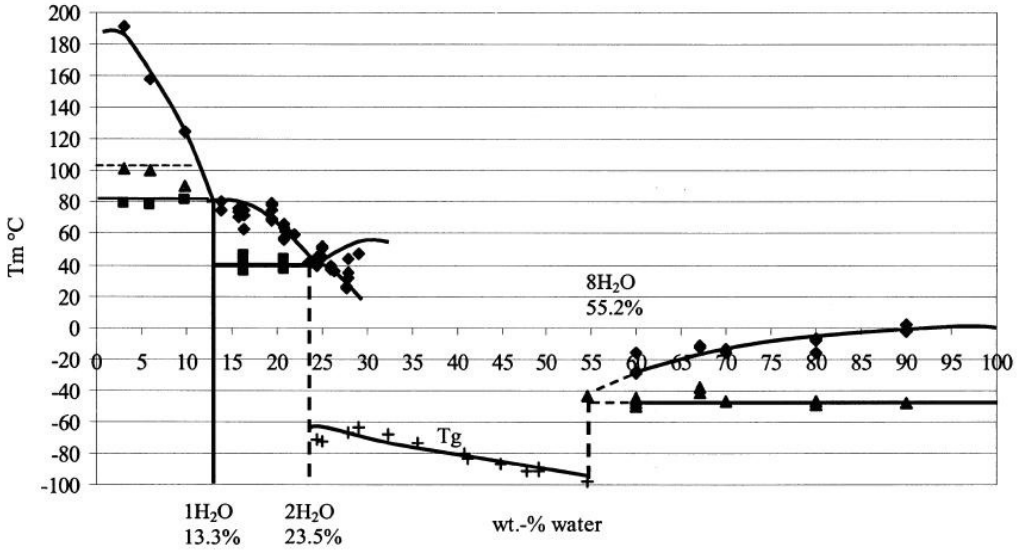

Figure 12 Complete NMMO-water phase diagram.[173]

The complete NMMO/water phase diagram was constructed by Biganska and Navard using Differential Scanning Calorimetry (Figure 12). The melting point of pure NMMO was found to be 170 ºC [171], although more recently it was measured at 184 ºC by DCS.[173] For $n < 1$, a peak found at 110 ºC can be assigned to a solid-solid transition of anhydrous NMMO. For $1 < n < 2$, the phase diagram indicates the existence of a eutectic. Above $n = 2$, the phase diagram exhibits a two-phase region consisting of a liquidus and a solidus. For $2.5 < n < 8$, regardless of thermal path, a glass transition exists at low temperatures (-60 to -100ºC). Above $n = 8$, the phase diagram shows two phase boundaries. The upper boundary is found between 0ºC at 100% water content and -30ºC where the boundary position is not well defined. The lower phase boundary is almost a horizontal line from -45ºC at $n = 8$ down to – 48ºC at 100% water content.

3.2.3 NMMO/water/cellulose system

NMMO is an effective cellulose solvent due to the high polarity and weakness of the N-O bond. Approximately 25% of NMMO is present as conformer 2 in pure water. However, the addition of cellobiose (cellulose monomer obtained by partial cellulose hydrolysis) to the solution favours conformer 1 (*i.e.* NMMO chair conformer with axial oxygen). Conformer 1 has the lowest overall conformation energy and is the least polar of the various conformations. Conformer 1 strongly interacted with the cellobiose and was the only conformer found in solution. In other words, carbohydrates reduce the interaction between water and NMMO.[168] NMMO is able to dissolve cellulose with water contents up to ~17 wt.% ($n = 1.2$). However, maximum cellulose solution percentage depends on its degree of polymerisation. The disesquihydrate does not dissolve cellulose since its two hydrogen bonding positions are already blocked by water. The lower cellulose content is 4 wt.%; below this value, the dissolution temperature gets dangerously close to the decomposition temperature of the

solvent.[167] Consequently, a slurry with a cellulose weight composition frame comprised between ~4 and ~17% seems reasonable. The phase diagram of the ternary NMMO/water/cellulose is given in Figure 12.

Initially, an isotropic solution is obtained when cellulose is dissolved in NMMO*H_2O. An increase in cellulose concentration leads to a mixture of isotropic and anisotropic phases in equilibrium; the latter phase dominates with further increases. The isotropic-anisotropic transition depends on cellulose concentration and molecular weight. High solution temperature, low water content of the mixture, low cellulose concentration or molecular weight and input of mechanical energy (shear stresses) will promote cellulose dissolution (Figure 13). Careful control over these parameters will allow a uniform solution to be readily obtained. Mechanical agitation is commonly used to reduce the temperature of the process and to keep it as far as possible from the degradation temperature of NMMO. The use of aqueous NMMO favours intimate mixing. Stabilizers are added at this point to hinder auto-catalyzed solvent degradation. Excess water is then evaporated by applying a vacuum to the mixture.

3.2.3.1 Rheological behaviour

The cellulose-NMMO-water system can be characterized by rheological measurements of the loss and storage modulus since the system exhibits viscoelastic properties similar to molten polymers.[171, 174]

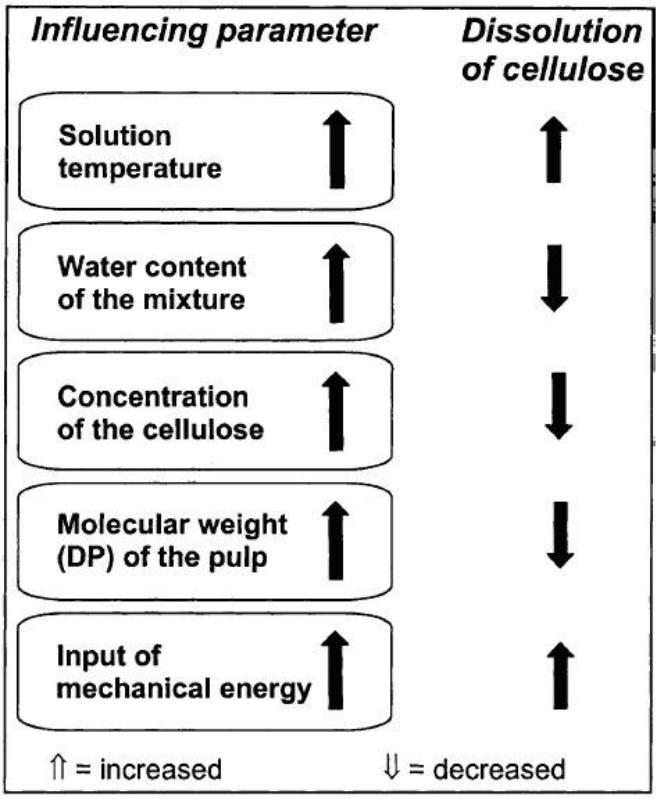

Figure 13 Factors influencing dissolution of cellulose in the system NMMO water.[167]

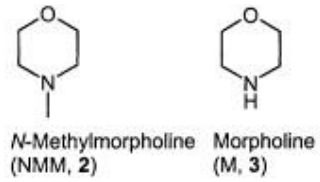

N-Methylmorpholine (NMM, **2**) Morpholine (M, **3**)

Figure 14 Main degradation products of NMMO.[167]

3.2.3.2 Side-reaction and by-product formation

Although cellulose dissolution has been long considered an entirely physical process, it appears that the limitations of the process have chemical origins. Indeed, both cellulose and NMMO undergo degradation reactions during the process.[167, 175] Cellulose is degraded by direct oxidation at its reducing end (peeling). N-methylmorpholine (NMM,**2**) and morpholine (M,**3**) (Figure 14) have been recognized as the two main degradation products.[167, 175] In the eighties, the first wave of studies conducted on the degradation process considered that it was initiated by metal ions and catalyzed by decomposition products of NMMO. Antioxidants and stabilizers were then thought to be sufficient. However, unpredictable explosions of laboratory scale or pilot plant trials demonstrated that NMMO was more labile and oxidising than these estimations would have suggested. As a result, the research for optimized stabilizers was accelerated. Eventually, a safe Lyocell production emerged. This research also underlined the importance of studying the chemical reactions involved in the Lyocell process. A systematic approach was adopted to minimize side-reactions and to avoid their detrimental effects by using proper stabilizers.

3.2.3.3 Crystallization

Solutions of cellulose in monohydrate and anhydrous NMMO crystallise upon cooling, forming spherulites from monohydrate NMMO and cell textures from anhydrous NMMO.[176] NMMO crystallisation is followed by the transcrystallisation of cellulose during which cellulose chains keep the morphology imprinted by NMMO crystallites. Thus, the crystallisation process is governed by the solvent rather than the cellulose. Cellulose crystallisation does not depend on the degree of polymerisation (DP < 1000) and it decreases strongly with increasing cellulose concentration in contrast to classical polymer solutions. Cellulose crystallisation reaches a maximum in the temperature range 21-25 ºC for

monohydrate NMMO solutions. It also appears that the higher the solvent concentration (or the smaller the amount of cellulose), the more rapidly crystallisation occurs.[174] Near room temperature, needles are usually the precursor to spherulite formation.[176] Lyocell has the highest crystallinity index (71.62%) of all man-made fibres.[172]

3.2.4 Stabilizers and additives

The search for stabilizers has originated from the necessity to reduce the radical degradation of NMMO and cellulose chain scission at the working temperatures. Without these additives, the cellulose DP will drop dramatically, leading to poor mechanical properties.

Gallic acid propylester (GPE) [171, 176] and propylgallate (PG) [140, 174] have been used to prevent cellulose degradation. However, the addition of GPE will accelerate the thermal instability of the NMMO-cellulose solution in the presence of metals.[177] Franz *et al.* patented a method for stabilization of the slurry by adding up to 10% mole of organic or inorganic bases.[178]

H. Chanzy *et al.* tried different salts as additives in order to improve the mechanical properties of the fibre (Table 5). It was found that NH_4Cl and $CaCl_2$ increased the fibre properties; LiCl, $MgSO_4$, $(CH_3)_4NCl$, $C_6H_5B(OH)_2$ and P_2O_5 had no effect; and $LaCl_3$, $ZnSO_4$ and $Na_2B_4O_710\ H_2O$ decreased fibre properties. The agents that enhance the mechanical properties are subject to a patent.[179] With respect to this work [140], the results from using NH_4Cl and $CaCl_2$ can be found in the following table. A solution must have the appropriate viscosity in order to be spun. If the viscosity of the solution is too low it cannot be spun. Conversely, excessive cellulose concentrations will hinder cellulose dissolution (Figure 15). The addition of certain alkaline compounds like *N*-methylmorpholine can increase the dilution rate of cellulose in the solution.[180]

Table 5 Effects of different DP and successful additives.[140]

Cellulose type	Additive	Additive proportions	Young's modulus (GPa)	Tenacity (GPa)	Elongation at break (%)
DP 5000 (a)	No additive		40	0.85	4
	NH_4Cl	1 %	39	0.6	3
		2 %	37	0.7	4.5
		3.5 %	55	1.3	4.5
		5 %	53	1.2	5
	$CaCl_2$	1 %	45	0.85	3.5
		2 %	55	0.95	2.6
		5 %	45	1	4
		7 %	48	0.9	4.5
DP 600	NH_4Cl	No additive, 14 % cellulose	21	0.5	16
		2 % (14 % cellulose)	36	0.9	8
		4 % (10 % cellulose)	36	0.8	7
		10 % (4 % cellulose)	31	0.7	6

(a): in these series of experiments, the cellulose content was kept at 2 % w/w solution.

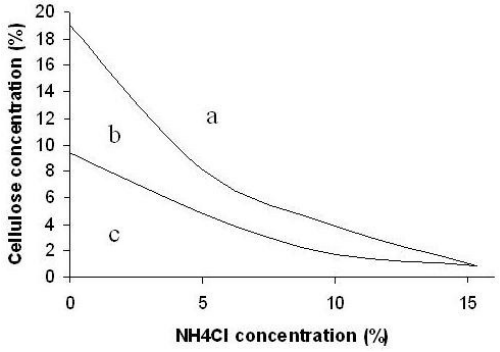

Figure 15 Spinnability of cellulose: if the cellulose concentration is too high, the slurry cannot be spun (a). Inversely, if it is too low, the solution will not be sufficiently viscous (c). A balance (b) needs to be achieved.[140]

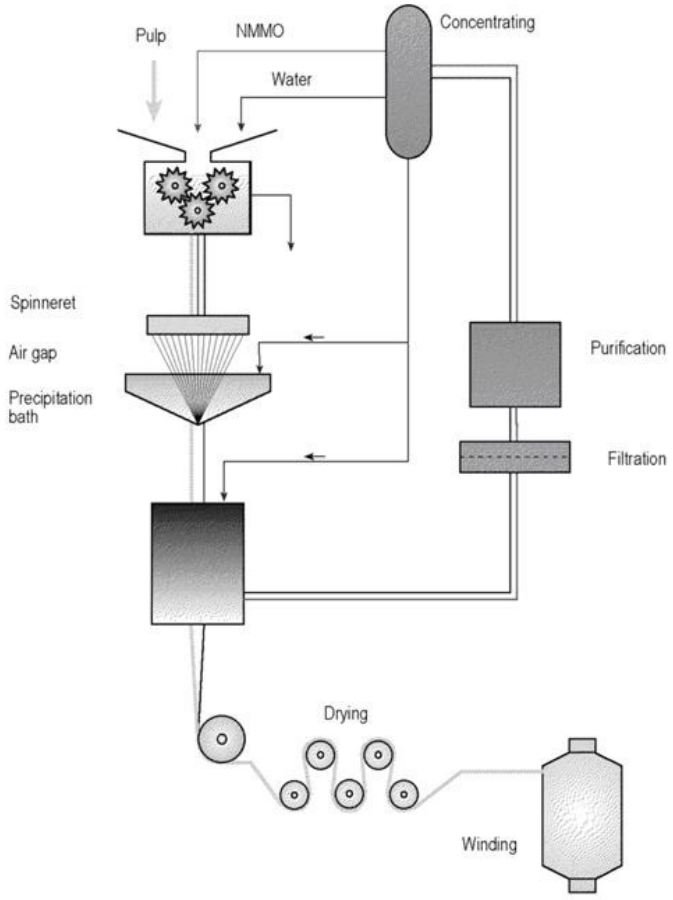

Figure 16 Lyocell process as described by H. Krässig.[33]

3.2.5 The lyocell process

The main steps in the production of Lyocell fibres are listed below and shown in Figure 16. The Lyocell process is also described in a U.S. Patent (No. 4,246,221).[181]

- Preparation of the slurry by dissolution of cellulose (usually pulp or cotton) in a mixture of water, NMMO, stabilizers and additives;
- Extrusion of the viscous dope at high temperatures (generally 90-120 ºC) through an air gap and into a precipitation bath;
- Coagulation of the fibre into a precipitation bath;
- Washing and drying of the fibre; and
- Recovery of the NMMO from the precipitation and washing baths.

The various steps can influence the structural form of the cellulose. Control of the initial viscous dope, dope orientation (shear stresses, shear rates, viscosity, tension applied to the fibre and dimensions of the nozzle), coagulation (fibre dimension and characteristics of the bath such as water purity, temperature and immersion time) and crystallization processes are all paramount. The latter variable is influenced by the slurry characteristics, precipitation conditions, drying and post-treatment conditions. Control of these processing parameters will dictate the final fibre structure and properties.

3.2.5.1 Dope preparation

Firstly, the NMMO-water mixture is produced. The composition of this slurry can be chosen at any point between pure water and the final dope composition (excess water can be removed by water evaporation under low pressures until the monohydrate composition is reached [167]). The slurry dilution degree is chosen to facilitate cellulose dissolution. Extensive dilution will furthermore avoid working at temperatures where the solvent is degraded. Cellulose is then added in the proportions fitting the manufacturing process. The ternary phase diagram is given in Figure 17.

Method 1 [176]

Gallic acid propylester (GPE) was added to NMMO/water solution (~50 wt% of NMMO) and stirred during 10 min. Cellulose pulp was then impregnated at room temperature for 1 h in the same solution with a shovel kneader equipment. Excess water was distilled off by heating and evaporation until Table 6 values are reached. 15 min with 400 mbar pressure and 108–112 ºC temperature were the conditions to be achieved before the dope was spun.

The authors conducted all of the experiments under a dry nitrogen atmosphere as cellulose/NMMO/water systems have a high tendency to exchange water with the ambient air.

Method 2 [140]

14 g of aqueous NMMO and 80 mg of n-propyl gallate were mixed with 170 mg to 1.7 g of V60 cellulose (a dissolving pulp DP=600 cellulose supplied by Buckeye Cellulose Co) or 80 mg up to 210 mg of cotton (DP = 5000). Additive was added (refer to Table 5). A Büchi rotavapor operated at 100 ºC and providing a 15 mm Hg vacuum produced within 7 to 15 min of rapid rotation a yellowish transparent cellulose solution. The solution was returned to atmospheric pressure and a 5 min immersion into a 130 ºC oil bath allowed the slurry to be further spun between 50 and 110 ºC.

Method 3 [170]

Probably the simplest process of the three mentioned, this one provided a homogeneous slurry within an hour of stirring. A mixture of two grams of cellulose, 30ml

Table 6 Different dope compositions used by Biganska *et al.*[176]

Cellulose		Water		NMMO	
wt%	Molar fraction	wt%	Molar fraction	wt%	Molar fraction
3	0.0123	14	0.516	83	0.471
3	0.0119	15	0.526	82	0.451
3	0.0115	16	0.555	81	0.432
3	0.0112	17	0.573	80	0.415
3	0.0109	18	0.590	79	0.398
6	0.0239	15	0.539	79	0.436
8	0.0335	13.5	0.510	78.5	0.456
10	0.0435	12.5	0.489	77.5	0.466

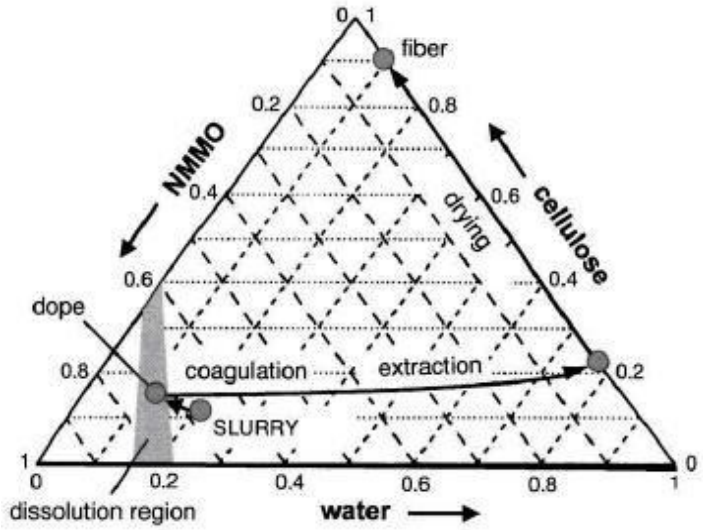

Figure 17 Phase diagram cellulose-NMMO-water.[33, 171]

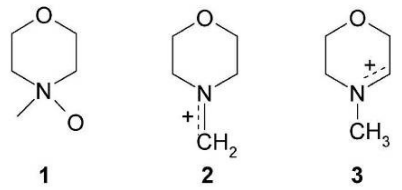

Figure 18 The N-Methylmorpholine-N-oxide molecule (1), the exo-centered C-I ion (2) and the ring-centered C-I ion (3).

NMMO solution, and then 0.1 wt.% of propyl gallate constituted the basis of the preparation. Stirring under vacuum with a temperature up to 105ºC finished removing the excess of water.

3.2.5.2 Extrusion and dry-jet step

The viscosity of the solution will lead to a particular crystallite orientation in the spinneret and air gap that will be preserved until coagulation and crystallization. Consequently, careful control of the extrusion rate and nozzle length/diameter ratio is required.

Fibres of low fibrillation and high mechanical properties can be spun using long air gaps and draw ratios of up to 10. Spin-stretch ratios of at least 3 are advised.[181] A solution with a relatively low cellulose concentration (10% *vs.* 15wt.%) will have decreased chain orientation before entering the coagulation bath due to more rapid relaxation and thus lower (axial) mechanical properties.

3.2.5.3 Coagulation and rinsing

The orientation of the crystallites mostly takes place during the extrusion stage. The coagulation of the cellulose is a diffusion-driven phenomenon. The liquids that can be used in the bath are polar liquids such as water or alcohols in the aliphatic homologous series (from methanol to hexanol). However, water coagulation results in higher strength and lower strain.[171] This is related to the higher degree of crystallinity of the water coagulated fibres. Furthermore, the degree of crystallinity is increased at higher bath temperatures.

In the coagulation bath, the desolvation of cellulose is due to non-solvent induced phase separation. This process is rapid for Lyocell fibre. Complete coagulation of a 50 μm diameter fibre has been estimated to be only 1-2 s.[182]

A post-treatment with an aqueous NaOH solution has also been found to increase the crystallinity.

The use of a surfactant (*e.g.* alkyl amine-oxides, alkyl glycoside, alkyl ethoxylate or water soluble fluorine-containing surfactants) in the coagulation bath has been suggested as a means of reducing the fibrillation of spun fibres, presumably by increasing the amount of fibre cross-linking.[183]

Patents provide further regeneration processes (*e.g.* DD-A 254 199, EP-A-0 427 701, WO93/11287 or U.S. Pat. No. 4,324,593). It is also beneficial both in terms of cellulose degradation and DP loss minimization to adjust the pH of the regenerated (purified and concentrated) solution. Indeed, the introduction into the precipitation bath of an adsorbing resin modified with alkaline groups, an alkaline anion exchanger and an acidic anion exchanger is profitable for the solution stability.[177, 184] A general thorough rinsing in cold tap water follows the previous undertaken steps.

3.2.5.4 NMMO recycling

The recycling of NMMO is achieved by evaporation of the coagulation bath with the resulting product being monohydrate NMMO. This direct process enables the recovery of ~99% of the solvent.[167]

3.2.6 Process measurement and analysis

Viscosity measurement

Rheological measurements are used to determine the storage (G′) and loss (G″) moduli of the slurry any given frequency. The relaxation time of the solution can be estimated from the intersection point of G′ (f) and G″ (f), where f is the frequency of the test. Relaxation time (or viscosity) increases with cellulose concentration or DP.[185] The relaxation time ranges from ~ 50 ms for cellulose with DP = 400 up to ~230 ms for cellulose with DP = 600.[171]

X-ray scattering

Wide angle X-ray scattering (WAXS) is used for the determination of the crystallinity index (CrI) and crystal orientation of regenerated fibres. 2-D scattering diagrams can be obtained by means of a two-circle goniometer.[172] The measurements can be performed over an azymuthal angle ranging from 0 to 180º. The separation of the crystalline and non-crystalline regions permits the calculation of the degree of crystallinity. Biganska *et al.* also performed X-ray scattering experiments with a plane chamber using the Debye-Scherrer method.[176] They found that crystallised solvent orientation was decreasing with cellulose content.

Refractometry

The water concentration of NMMO-water mixtures can be calculated by refractometry.[173] A calibration curve giving the index of refraction of aqueous NMMO using the Karl-Fischer technique can be established.[140]

NMMO concentration

The NMMO concentration can be determined by titration with H_2SO_4. H_2SO_4 of known concentration is added to the NMMO solution until it reaches a defined pH.[173]

Limitations: Degradation reactions and precautions of use

The NMMO degradation reaction involves mainly three molecules: NMMO (**1**) and two species formed by cleavage of the N-O bond, the *exo*-centered C-I ion (**2**) and the ring-centered C-I ion (**3**) (Figure 18). The C-I ions will catalyze the parent amine N-oxide degradation, leading to the above-mentioned exothermic reaction. However, the ion **2** is largely predominant as **3** will react with water in an endothermic and bimolar reaction to form **2**.[186] The

exothermic reaction rate can be controlled by using certain metals and avoiding others for the pipes and devices in contact with the solution, according to US patent No. 5,766,530.[177, 184] This material should contain no metal of the group consisting of copper, molybdenum, tungsten or cobalt. However, it has been observed as being beneficial to use at a minimum of 90% up to a depth of at least 0.5 μm, preferably more than 1 μm, at least one element of the group consisting of titanium, zirconium, chromium and nickel in elementary form and/or in the form of compounds provided that the remaining material does not contain any of the above-mentioned catalysis favourable metals.

3.2.7 Conclusion

NMMO is an organic solvent that has the capacity to dissolve cellulose. The use of NMMO in industry stems from the good properties of the regenerated cellulose that are derived from using NMMO and the eco-friendliness of NMMO. However, elevated working temperatures, dangerous degradation reactions, high cost (NZD $300/100 g), special equipment requirements (beakers and pipes made of titanium, zirconium, *etc.*) and the need for constant monitoring limit the use of NMMO for applications in advanced composite materials manufacturing. Furthermore, important side-reactions and by-product formation would interfere with a simple and safe eco-composite manufacturing process.

3.3 Dissolution of cellulose in sodium hydroxide

3.3.1 Introduction

In the search for environmentally friendlier non-derivatizing dissolution paths for cellulose, there has been a great deal of trials. Some of the most successful solvents reported in the literature are organic solvents or sometimes, organic solvents in combination with a salt. A

new exciting method that involves a low-energy, extremely simple and relatively safe process has recently been developed and seems to be grandly expanding, judging by the number of publications on the topic: sodium hydroxide aqueous solutions at low temperatures (Figure 19). The first traces of this method found in the literature involve the placement of a modified –but non derivatized- form of cellulose in an aqueous solution of sodium hydroxide at low temperatures.[83, 144, 187, 188] In the last three years, however, some authors have made a significant progress in making this method a lot more efficient by adding urea and/or thiourea in the mixture of NaOH and water. (see for example refs [146, 162, 189]) A recent publication proved the feasibility of a textile fibre made with the NaOH/urea dissolution route at a semi-industrial scale.[145]

Some of the dissolution methods are detailed in Table 7. Usually, the alkaline solvent is cooled down to subzero temperatures, with or without cellulose. Once the subzero temperature is attained, the mixture is often stirred under thawing, resulting in the dissolution of the polymer. Some authors centrifuge the solution to separate the undissolved portion from

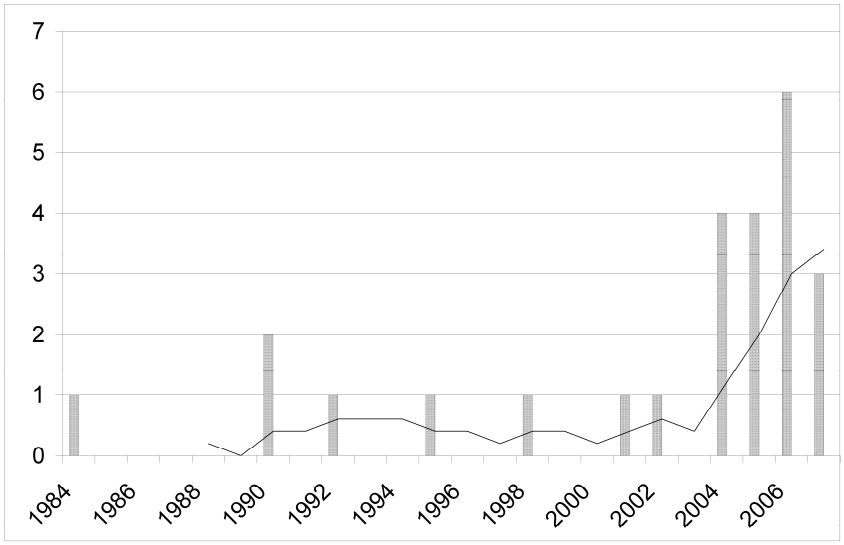

Figure 19 Articles published on the NaOH dissolution route in the last 15 years.

Table 7 Examples of dissolution using the NaOH route.

Cellulose source	Cellulose concentration	NaOH concentration	Additives	Preparation	Coagulant	Reference
Steam exploded soft wood pulp (DP = 331)	5 wt. %	9.1 wt. %	None	Cellulose added to the aqueous NaOH at 4°C, followed by stirring for 8 h and centrifugation to exclude the undissolved part	At 15 °C: H_2SO_4, HCl, CH_3COOH, H_3PO_4. At 5 °C: H_2SO_4 and HCl.	(Yamashiki T. 1992)
Low DP cellulose, Avicel, linter regenerated from 0.5 M Cupriethylenediame hydroxide, amorphous celluloses, non-lignified samples.	~4-5 wt. %	~8-9 wt. %	None	Cellulose was swollen in NaOH and water at room temperature, frozen to - 20 °C, then thawed. An amount of water equal to the initial one was added, and shaked the mixture was shaked.	Acidic aqueous medium, water or heating to 40°C.	(Isogai and Atalla 1995; Isogai and Atalla 1998)
Alkali soluble cellulose (DP = 408)	10 grams	9 wt. %	None	Stirring at 500 rpm for 8 h at -5°C followed by centrifugation at 9000G to exclude the indissoluble cellulose fraction. The cellulose solution had a concentration of 4.8 wt. % cellulose.	H_2SO_4 at 10 wt. % for 10 min at 10 °C (after optimisation)	(Cao and Tan 2006)
Avicel (DP = 250)	In general lower than 5 wt. % to ensure a solubility superior to 90 %.	1.6 to 2.6 M	None	The freeze-thaw process described by Isogai was followed by water evaporation in order to increase the cellulose concentration in the membrane.(Isogai and Atalla 1995; Isogai and Atalla 1998) Then, glycerin was used to cover the membrane and form a protective layer on which HCl is slowly added to precipitate the membrane. The membrane was then rinsed with distilled water and isopropyl alcohol.	HCl 0 to 8.4 M	(Kuo and Hong 2005)
Soft wood pulp with DP = 1060 and hard wood pulp with DP = 994	5 wt. %	9.1 wt. %	None	The wood pulp was steam exploded first, mixed with the aqueous NaOH for 8 h at 4 °C and then centrifuged at 7500 rpm for 60 min in order to extract the undissolved portion.	1.3 wt. % aqueous HCl	(Yamashiki, Matsui et al. 1990; Yamashiki, Matsui et al. 1990)
Cotton linter with DP ~540	5 wt. %	1.5 M	Thiourea at 0.65 M	The mixture was cooled to -5°C for 4 h, then thawed with intermittent stirring at 0-4 °C. Centrifugation at 7000 rpm for 30 min helped to get rid of the insoluble portion.	H_2SO_4 between 2 and 30 wt. %	(Zhang, Ruan et al. 2002)
Cotton linters with DP = 330 and 620	7.5 wt. % for the lowest DP and 5 wt. % for the highest one	9.5 wt. %	Thiourea at 4.5 wt. %	The solvent was pre-cooled between -8 °C and -10°C, the cellulose was added and stirred for 5 minutes at room temperature.	10 wt. % H_2SO_4, HCl and CH_3COOH, NH_4Cl	(Ruan, Zhang et al. 2004)
Cotton linter pulp sheets (DP = 600 and 700)	Up 7.6 g for 100 g of solvent (Table #)	8 wt. %	Thiourea : 6.5 wt. %. Urea: 8 wt. %	Cellulose was dissolved in solvents pre-cooled to temperatures between -8 and -12°C (after optimisation)	Gelation occurs at any temperature but is the slowest at 0 °C.	(Jin, Zha et al. 2007)
Cotton, Borregaard or Buckeye fibres	N.C.	7.6 wt. %	Urea at 12 wt. %	The mixture was cooled to -5°C	Not studied	(Cuissinat and Navard 2006)
Various dissolving pulps	1 mole of cellulose for 1050 g of solvent solution was necessary for complete dissolution	7 wt. % (after trials)	Urea at 30 wt. % (after trials)	-25 °C for about 12 h	Water	(Kunze and Fink 2005)
Cotton linters with DP between 242 and 1210 as well as aborbent cotton with DP = 2000	4 wt. %	6 to 10 wt. % (7 wt. % was found to work best)	Urea from 2 up to 20 wt. % (12 wt. % was found to produce a dissolution maximum)	The solvent was pre-cooled between -5 °C and -20°C (an optimal value of -10°C was found), the cellulose was added and stirred for 5 minutes at room temperature.	Gelation occurs at any temperature but is the slowest at 0 °C. In a preliminary paper, the authors used a bath with 15 wt. % H_2SO_4/10 wt. % Na_2SO_4. Later on, they also reported the use of a double coagulation bath: the first one containing 8 wt. % H_2SO_4/12 wt. % Na_2SO_4, and the second one 4 wt. % $H2_SO_4$ at 10 to 20 °C. Other coagulants like HOAc, $(NH_4)_2SO_4$, H_2O, C_2H_5OH and $(CH_3)_2CO$ were reported.	(Cai, Zhang et al. 2004; Cai and Zhang 2005; Cai and Zhang 2006; Mao, Zhou et al. 2006; Cai, Zhang et al. 2007)

the truly dissolved cellulose. After this step, the cellulose can either be transformed into a gel by a thermal path or it can be precipitated in an acidic medium.

3.3.2 Dissolution in aqueous NaOH

It is well known that NaOH strongly interacts with cellulose. NaOH can swell it and the maximum swelling is obtained at a soda concentration of 8-10%.[159] This region is also the region where, under certain conditions such as reasonable DP and low temperature, cellulose dissolves the best and forms the so-called cellulose Q supposedly because of the cellulose hydrate structure.[190] The Q region is located between 8 and 9 wt.% and below 4 °C.[117] Dissolution has however been reported for a larger range of concentrations, between 7 and 12 wt.%.[83, 191] In fact, it is well known for at least fifty years that cellulose presents a portion readily soluble in NaOH.[192]

Historically, the first report of cellulose dissolution was done by Kamide in 1984 who managed to dissolve a cellulose regenerated from a cuprammonium solution in 8-10 wt.% aqueous NaOH at 4 °C; in 1990, Yamashiki *et al.* in a series of papers reported the dissolution of steam exploded softwood and hardwood pulp in similar conditions.[193, 194] The way the dissolution occurs has been studied and several authors came up with models. NaOH can form an hydrate with water, and this hydrate has the capacity to bond with one or two hydroxyl groups of the glucopyranose unit.[190] The amorphous regions (in the X-ray diffraction acceptation of the term) will first be dissolved and the dissolution will create new amorphous regions that will undergo the same transformation.[190]

The parameters that can obstruct or favour complete polymer dissolution are the temperature to which the water/NaOH/cellulose mixture is cooled down, the cellulose concentration in the aqueous media and the supramolecular characteristics (lattice type, DP, *etc*) of the raw material itself.[83] For example, Kuo and Hong have shown that an insufficient cellulose concentration in the aqueous solution would lead to the formation of granulates when

a cellulose solution is directly precipitated in an HCl bath.[195] This was attributed to the formation of gas bubbles acting as structural defects in the membrane under too "vigorous" precipitation. Higher DPs prevent the dissolution process from occurring. Some authors have explained this result by a more difficult disruption of the long range orders inherent to the higher DPs.[83, 187, 193, 194] In general, low DP (< 500) celluloses dissolve well, regardless of their lattice type.[83, 187] However, linter celluloses behave differently. Indeed, they dissolve best when they are regenerated from a solution. In general then, they belong to the cellulose II lattice type or they are amorphous. It was particularly striking to see that mercerized cellulose linters with a type II lattice could be dissolved only to 32%, suggesting a dissolution mechanism driven by the extent of long range orders in crystallites rather than by the lattice type.[83, 187]

The literature reports the successful manufacturing of films and fibres using carefully chosen cellulose sources, dissolution and precipitation conditions.[144, 195, 196] Unanimously, the regenerated material belongs to the cellulose II lattice type.[144, 196]

3.3.3 Dissolution in NaOH and additives

It is of particular interest to note that the addition of thiourea and/or urea to the mixture has the ability to completely dissolve cellulose at subzero temperatures (Table 7). Total dissolution will get the cellulose chains in a random coil conformation, which consequently displaces the C4 peak found in NMR to values between 79 and 81 ppm.[70, 87, 146, 162, 197, 198] This was observed for some of the methods described in this section.

Urea

Certainly, NaOH on its own does not seem to be the best solvent and it certainly does not replace powerful organic solvents.[117] It can only partially dissolve celluloses of low DP. Thus, scientists have tried to use this first approach and have refined it by bringing into play

some additives. Urea was found to be a successful candidate from a practical, environmental and simplicity standpoint. Cuissinat and Navard performed in a recent work a comparative study of different solvents on natural fibres.[189, 199] In particular, they compared the dissolving role of NaOH and NaOH/urea at low temperatures on a range of natural fibres. In the absence of stirring, none of those solvents could spontaneously dissolve the natural fibres indeed, but swelling and ballooning were observed.[199] The quality of the solvent can be quantified by the size of the balloons and the kinetics of their formation; both were superior when urea was added to NaOH.[199] Cai *et al.* have trialled a range of parameters for the dissolution of cellulose using NaOH in combination with urea.[162] They found out that a stable and powerful solvent was obtained by mixing 7 wt.% NaOH and 12 wt.% urea in an aqueous solution pre-cooled to – 10 °C; the cellulose which was dissolved had a DP ~ 700. After stirring for 5 min at 3000 rpm, the cellulose appeared dissolved; centrifugation at 4000 rpm and 5 °C for 10 min was found useful for degassing.[200] On the same year, both Cai *et al.* and Kunze and Fink showed that soda and urea hydrates work in synergy to separate the cellulose chains from each other.[162, 201] They also prevent cellulose from regenerating its intermolecular hydrogen bonding by forming a stable "hydrate coat" on their surface.

The temperature is of major interest in this process: temperatures which are not located in the -10 to -25 °C range do not seem to allow the dissolution, whatever the solvent composition.[201]

Eventually, the complexity of the aqueous system cellulose-soda-urea is only revealed through its gelation behaviour. The cellulose molecules in a dispersion of free water, soda hydrates and urea hydrates should be visualized as a metastable system in a process of gelation. The polymer chains assemble *via* hydrogen bonding, and the process is irreversible under temperature variations. The kinetics of this process is affected by any of the system parameters. Cai and Zhang conducted a fairly systematic rheological study where the effect of temperature, time, cellulose molecular weight and concentration were assessed.[200] The first parameter,

temperature, is known to affect the energy of the hydrogen bond. As the hydrogen bond is crucial in the formation of the gel, so is temperature. In general, Cai and Zhang explained the aggregation of cellulose molecules at higher temperatures by the inter-and intramolecular bonding occurring between hydroxyl groups of cellulose; those are prevalent at higher temperatures over those between the solvent and the polymer.[200] A similar behaviour was also observed by Isogai when cellulose was simply dissolved in NaOH.[83, 187] The nature of the gel is very different too depending on the polymer concentration: at low cellulose concentrations (less than 2-2.5 wt.%), the cellulose solutions behave much like a liquid, whereas at higher ones (between 4 and 5 wt.%), they behave more like an elastic solid. This was explained by the higher density of junction points between the polymer chains. The same behaviour owes for molecular weight and the cellulose concentration. There is a restriction though, as to the gelation of the system: it appeared that diluted cellulose solutions did not have the capacity to form that gel if their concentration was too low (typically, inferior to 3 wt.% for a cellulose with a DP ~ 700). This singularity could potentially originate from the lack of chain entanglement. As would be expected then, the gelation temperature decreases with an increasing average molecular weight. Eventually, the gelation time peaks at about 0°C but becomes shorter at either low temperatures (below -8 °C) or higher ones (above 15 °C). This phenomenon is, once again, probably best explained by the relative solvent-cellulose to cellulose-cellulose energy ratio being maximised around 0 °C. A graph that was obtained for the same cellulose of DP ~700 and for a cellulose concentration of about 4 wt.% is shown in this work (Figure 20).

Other than the natural gelation of the system, the dissolved cellulose can also be coagulated. Different coagulants can be used to produce membranes with different pore geometries due to the exchange by diffusion between solvent and coagulant.[202] As a consequence from the use of different coagulants, dry or wet membranes prepared from the same cellulose solution exhibit different mechanical properties.[202] In a similar manner, the

coagulant concentration and the time for which the membrane is left in the coagulant bath can also affect the membrane morphology and mechanical properties.[203] Tensile strengths up to about 90-100 MPa and elongations at break culminating at 17% were obtained after air-drying the wet membranes at ambient conditions.[202, 203]

Recently, the same group of authors reported the successful spinning of a textile fibre using this process in a pilot plant. The mechanical properties achieved are close to those of commercial rayon fibre, with a tensile strength reaching about 220 MPa and an extension at break as high as 18% in some cases.[145] The regenerated material exhibited typical cellulose II WAXD and CP/MAS ^{13}C NMR spectra.[145, 148, 162]

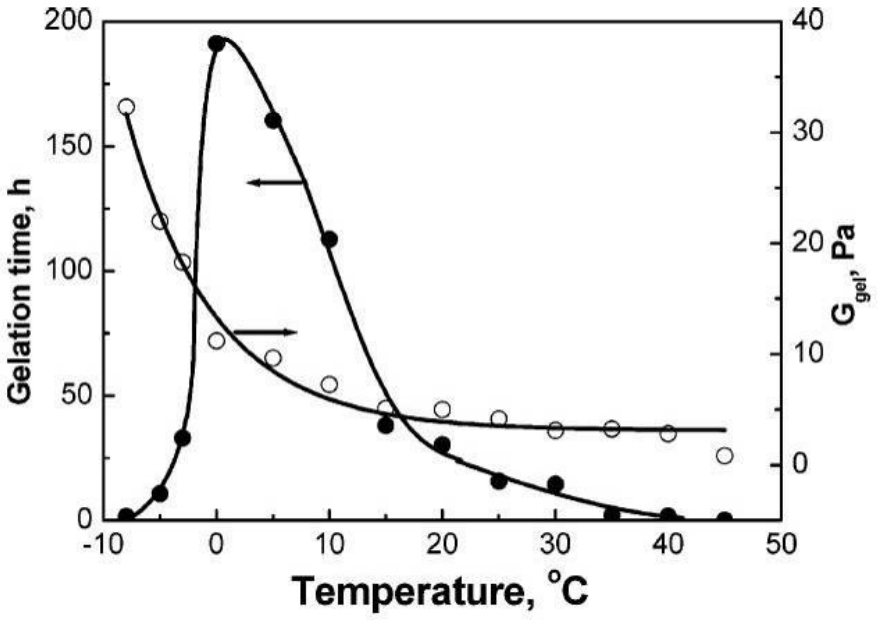

Figure 20 Gelation time and G_{gel} as a function of temperature for 4 wt. % cellulose solution.[200]

Thiourea

A few methods that deal with the addition of thiourea to NaOH are available in the literature.[146, 147, 203-206] All of those papers are coming from a group working in the department of Chemistry of the Wuhan University in China. Studies show that thiourea is a better additive to NaOH than urea.[206] However, in the conditions described by Zhang *et al.*, the solvent does not necessarily completely dissolve cellulose. A 1.5M NaOH/ 0.65 M thiourea

composition could dissolve ~22% of a cotton linter with DP ~1070 and ~ 77% of a cellulose with DP ~ 540; it could however totally dissolve a cellulose II sample that had a DP~670. The dissolved portion, however, has a ^{13}C NMR spectra similar to cellulose dissolved in LiCl/DMAc, indicating a true dissolution with the cellulose chains in a random-coiled conformation.[142, 205] In a similar way to the other methods, the NaOH/thiourea solvent needs to be cooled to subzero temperatures. Dissolution of cellulose involves mixing it with the solvent and stirring under thawing. The dissolved cellulose undergoes thermal gelation, as described in the previous section. The parameters of gelation once again depend on the starting material, but in general it is sufficient to heat up the dissolved material to 60 °C, regardless of the cellulose concentration or molecular weight.[205] Interestingly enough, the cellulose chains retain their random coil conformation in the thermally formed gel. This suggests the formation of a physical cross-linked network held by the hydrogen bonding interaction between the cellulose chains.[146, 205] The mixture can also be coagulated in the right solvents. Ammonium sulphate [$(NH_4)_2SO_4$] is one of them and has been studied for the coagulation of microporous membranes.[203] The concentration of the coagulating solution in ammonium sulphate and the time for which the membrane was immersed could dramatically affect the mechanical properties of the final dry product.[203] Good tensile strength (up to 100 MPa) and elongation at break (10%) of the air-dried membranes were obtained with the adequate coagulation parameters.[203] Fibres were spun in a pilot plant and had mechanical properties comparable to commercial rayon fibre: a tensile strength of 2.2 $cN.dtex^{-1}$ (250 MPa) and an elongation at break of 2.1% could be reached.[147]

For cellulose dissolved by the present route, there are two ways to precipitate the material. The first one is thermal gelation, and the other one is the straight-forward solution casting method where the dissolved cellulose is simply placed into a bath of coagulant (such as a 5 wt.% $(NH_4)_2SO_4$). Fascinatingly, the two methods produce very different gel morphologies at the microscopic scale.[204] As a result of the solvent-coagulant inter-diffusion, the solution

casting method produces an interconnected porous network where the cellulose comes in a flaky shape. The thermal gelation method produces a structure with round-shaped particles aggregates. Those obtained by low temperature gelation are more spherical than those obtained by a higher temperature gelation method. This dissolution technique is also of great interest to produce hydrated membranes with potential applications such as filtration or tissue engineering. Eventually, it should be pointed out that the regenerated material belongs to the cellulose II family.[146, 203, 206]

Urea and thiourea in combination

In a recent publication, Jin *et al.* reported the use of urea and thiourea in combination. The authors claimed that the combination produces a solvent with the capacity to fully dissolve more cellulose than any of the NaOH/urea or NaOH/thiourea formulations on their own.[198] What's more, the dissolved cellulose appeared more stable and did not precipitate in solution.

3.4 Dissolution of cellulose in LiCl/DMAc

3.4.1 Introduction

Another solvent used with the aim of dissolving cellulose is *N,N*-dimethylacetamide (DMAc or DMA). DMAc does dissolve cellulose derivatives such as cellulose acetate or (hydroxypropyl)cellulose on its own.[207-209] It is only when conjugated with lithium chloride (LiCl) that DMAc has the power to dissolve cellulose. In 1980, McCormick qualified LiCl/DMAc as being the only functioning lithium salt-organic solvent combination for cellulose dissolution.[141] The system LiCl/DMAc is used as a non-degrading (or as the least degrading) solvent to determine cellulose molecular weight (MW) distribution.[210, 211] NMR has proved that the solvent does not form chemical bonds with cellulose.[212] These results have also been confirmed by MW measurement.[213] Consequently, this solvent is probably

the most appropriate one for molecular mass distribution investigation of cellulose using size exclusion chromatography SEC.[211, 214, 215]

As a non-degrading solvent, it has in recent times also been proved useful in the acetylation of cellulose under homogeneous solution conditions or for the preparation of low DS cellulose derivatives by ring-opening esterification.[216, 217] Among the exotic applications of this solvent, the preparation of fibres elaborated from a blend of cellulose and silk fibroin positively holds an interesting position.[218]

Also, LiCl/DMAc/cellulose viscous solutions can be spun and regenerated into high strength (up to 350 MPa) and high modulus (up to 22 GPa) fibres.[219]

The solvent can be recycled with a high recovery rate, which accounts for its eco-friendliness.[220]

Using this solvent, a matrix could be formed in which fibres could be embedded in order to form an all-cellulose eco-composite[22, 221].[23, 26, 28] Masson and co-workers utilized the LiCl/DMAc system to form blend films from cellulose with poly(vinyl alcohol), polyacrylonitrile, poly(ε-caprolactone) and nylon 6.[222] Williamson *et al.* (1998) utilized it for the manufacturing of semi-interpenetrating networks of Poly(*N,N*-dimethylacrylamide) and cellulose. A six-fold increase in modulus was obtained when compared to the sole matrix.[222, 223] The method was also used to dissolve and regenerate bacterial cellulose from *Acetobacter xylinum* with the final goal to produce a wound dressing containing a humectant.[224] Eventually, Saga *et al.* patented in 1999 a way to obtain a highly transparent, high strength, cellulose gel that could be used for ophthalmic devices such as soft contact lens.[225]

3.4.2 The dissolution process

3.4.2.1 Cellulose activation

Cellulose needs to undergo the so-called “activation procedure” during which the fibre is penetrated with a polar medium.[226] Without this procedure, it takes years for the

dissolution to proceed.[227] Crystallinity and dissolvability are decoupled: amorphous celluloses obtained by ball-milling dissolve just as poorly as highly crystalline ones in the absence of the activation procedure.[227] Furthermore, the activation step does not affect cellulose crystallinity. Rather, it is the pore structure that seems to dominate the ease of dissolution. The activation procedure increases the size of the pores with radii smaller than 1 nm.[228] An increase in pore size homogeneity via mercerization was also shown to be an important factor to facilitate the dissolution of cotton linters; those would not dissolve otherwise.[220] In this precise case, the change in pore structures was attributed to the effect of mercerization on hemicelluloses.[216]

Before being effectively dissolved in the solvent LiCl/DMAc, the secondary hydrogen bonds of cellulose can be broken; further swelling brought by LiCl in solution will then lead to a facile dilution. The activation procedure can either be carried out at high temperatures by refluxing dry cellulose in DMAc at 150 °C or by a step procedure involving solvent exchange. The latter one was found to yield more reproducible results, and so we will describe it more in depth.[229] This activation procedure method is decomposed into three main steps according to the often-mentioned patent from Turback.[226] First, the fibres are soaked in water in order to achieve intermicellar swelling. Soaking them twice at 40 °C for no more than one hour was found satisfactory in all cases.[229] Soaking into methanol, ethanol, isopropanol, acetonitrile, tetrahydrophuran or acetone and thorough filtering follows.[226, 230] Two repetitions with DMAc for no less than 45 min were found to complete the procedure successfully.[229] The cellulose material should then be dried and protected from water as further contact with water was shown to cancel the solvent exchange effect and hinder dissolution, probably by pore size decrease.[228] Those different steps aim at a correct solvent exchange.

3.4.2.2 Solvent preparation

It is usually recommended that the LiCl/DMAc mixture be stirred at elevated temperatures in order to obtain homogeneous slurry.[213] DMAc degrades at 165 °C; this temperature is the upper limit in the process. Dupont (2003) showed that warm DMAc (40 °C) had a better ability to dissolve LiCl than either room temperature or hot (100 °C) DMAc.[229]

There is an interesting controversy existing over the solubility of LiCl in DMAc. People reported concentrations of 8 to 13 wt.% LiCl throughout the literature; however, a maximum of 8.46 wt.% at 25 °C was experimentally determined.[231] Both LiCl and DMAc are strongly hygroscopic, and so is their mixture. It is thus easy for this solution to absorb water that, in turn, will artificially increase the LiCl solubility value. After careful LiCl drying in a vacuum oven (5 days at 0.2 atm and 80 °C) and DMAc dehydration (over molecular sieve 4 Å; process repeated twice), we could for example not achieve in our laboratory an homogeneous 9 wt.% LiCl/DMAc mixture even after slight heating and over several days with constant stirring. The mixture has to be kept under dry atmosphere or nitrogen as it is hydrophilic.

3.4.2.3 Cellulose dissolution

The cellulose used can originate from practically any source such as cotton, bast fibres, wood pulp, or regenerated cellulose.[141, 142, 221, 226] Stirring is critical during the dissolution process to overcome the difficulty levied by the fibre/solvent heterogeneous mixture.

It has been reported that the solubility of cellulose increases with LiCl content.[213] A 9 wt.% LiCl/DMAc mixture was reported at 80°C by McCormick and Dawsey (1990).[230] Timpa (1991) found that 8 wt.% LiCl was necessary to dilute cotton cellulose and McCormick found that a 6 wt.% LiCl solution was necessary for complete cellulose dissolution.[142, 210] However, Röder in a light scattering study also showed that, at concentrations of 6 wt% LiCl and 1wt% cellulose, large anisotropic particles were found; they were described as highly

swollen fringed micelles that could be part of the former crystalline regions of cellulose.[232] In the same paper, the author showed that further dilution with pure DMAc from 9 to 0.9 wt.% LiCl had the potential to drive those aggregates away. Dupont claimed that an 8 wt.% LiCl could totally dissolve cellulose amounting to 1wt.%.[229]

There are two different ways of preparing the mixture: either the LiCl/DMAc is prepared first (as described above) and then the cellulose is added, or both cellulose and DMAc are mixed together followed by LiCl addition.[233]

The dissolution mechanism is believed to imply a macrocation $[DMAc_n + Li]^+$ creating weak interactions with the cellulose oxygens from the hydroxyl groups or ring, a Li^+ cation interacting with the carbonyl group oxygens of the DMAc molecules and a Cl^- anion disrupting the cellulose hydrogen bonds.[212] The existence of the $[DMAc]_xLi^+$ and $[cellulose]Cl^-$ complexes is corroborated by the species migration observed in electrolysis cells.[234]

The mixture cellulose/LiCl/DMAc exists in four different phases. By varying the cellulose concentration, it can be made purely isotropic, isotropic with small solid fibres, isotropic with a cholesteric mesophase, and the latter one plus small solid fibres (Figure 21). A cholesteric mesophase, also called chiral nematic, can be defined as a stack of very thin oriented layers of polymer which will selectively reflect one component of circular polarized light. The pitch of the cholesteric mesophase, defined as the double of the length of a periodic stack, reduces with LiCl addition.[233] In the case of an 8 wt.% LiCl/DMAc solution and for a cellulose with a DP ~288, Conio *et al.* showed that the cellulose/LiCl/DMAc system is isotropic for cellulose concentrations below ~11 wt.% cellulose.[235] Between

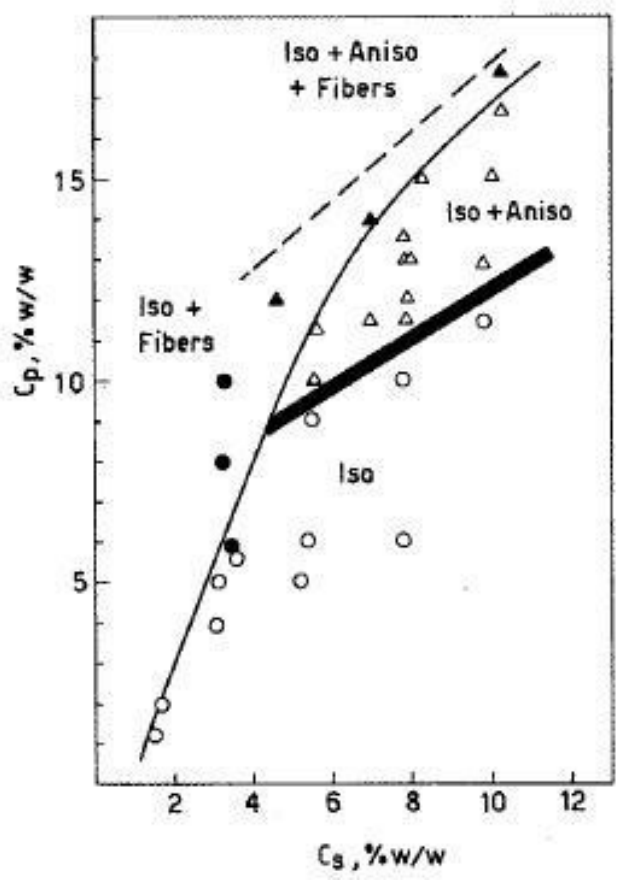

Figure 21 Pseudo-phase diagram of cellulose in LiCl/DMAc.[235]

Above ~15 wt.% cellulose, a solid insoluble phase is also found. Thus, the cellulose regenerated from an 8 wt.% LiCl/DMAc solution with more than ~15 wt.% cellulose will also contain some undissolved cellulose.

Heating the slurry also facilitates cellulose dissolution. However, it is necessary to dissolve the cellulose at temperatures as low as possible to avoid cellulose degradation.[210] A. Potthast *et al.* reported that above 85 °C *N,N*-dimethylketeniminium ions are highly reactive intermediate cleaving glycosidic bonds. Jerosch *et al.* (2001) reported decreases in molecular weights for solutions stirred at temperatures as low as 40-50 °C.[236] The result of it is a significant loss of cellulose degree of polymerization.[237] For high concentrations of dissolved cellulose and LiCl (superior to about 6 wt.%), low dissolution temperatures of 4-5 °C

were found to accelerate dissolution over room temperatures *ca.* 20 °C.[229, 231] But lower temperatures mean that more LiCl (*ca.* 1 wt.%) is necessary to dissolve the same amount of cellulose.[231]

It was shown that cellulose molecules in LiCl/DMAc overlap when the cellulose concentration is above *ca.* 0.3 wt.%.[238] Solutions of cellulose can become quite thick even at cellulose concentrations as low as 3 wt.%.[231] In compliance with the MHS equation, the viscosity of the solution increases with the molecular weight of the cellulose.[185]

Refluxing of cellulose in LiCl/DMAc solutions can show coloration due the formation of chromophoric condensation products.[239] Furthermore, secondary chromophores can be formed by reaction with the cellulose structure.

In the end, cellulose/LiCl/DMAc can be kept for several years at room temperature.[210] According to McCormick, solutions with relatively high cellulose concentration (8 to 10 wt.%) might be unstable. However, the same author used high temperatures. Those have been demonstrated, since then, to induce quick cellulose degradation.[210, 236, 237]

3.4.2.4 Cellulose precipitation

Water or methanol are successful coagulants.[23, 141, 142, 219, 221, 226] Minute amounts of water (lower than 0.01 M) have been shown to lead to the formation of aggregates in solutions with low salt concentrations, such as those used for SEC; those aggregates correspond to fringe micelles.[240] Tolerable amounts of residual water decrease with increasing cellulose concentrations.[231] Henceforth, one has to be very careful with any cellulose/LiCl/DMAc mixture as any absorbed water will rapidly lead to cellulose aggregation and corrupt the SEC results. To the knowledge of the author, there has been so far no conclusion as to the exact mechanism leading water to impair the solvating power of LiCl.[231] However, Dupont (2003) showed that higher salt concentrations (8 wt.%) produced very stable solutions that could be kept for several months.[229]

Water precipitated gels will generally exhibit some turbidity due to sub-micron order heterogeneities.[238] Those heterogeneities can be assumed to be cellulose molecular aggregates that occur in parallel to the phase separation between the cellulose gel and the LiCl/DMAc.

3.4.2.5 Monitoring the preparation

Viscosity measurements are classically performed to assess the MW or equivalent DP. It has been found that the viscosity increases with the MW and generally with the concentration.[63, 241] This will be attributed to inner and outer associations of the molecular chains in solution.

According to this theory, the Mark-Houwink-Sakurada (MHS) equation links MW and intrinsic viscosity with the formula:

$$[\eta] = K \cdot M_w{}^a \qquad (2)$$

K and a are two constants determined for a given solvent at a given concentration. The intrinsic viscosity is given in cm^3/g. Of course, LiCl/DMAc can also be used as a solvent. The parameters K and a have been determined by McCormick *et al.[142]* for a 9 wt.% LiCl/DMAc solution as being:

$$K = 1.278.10^{-4}$$

$$a = 1.19$$

Unfortunately, a recent study (Potthast *et al.*, 2002) has shown that the LiCl solubility was restricted to 8.46 wt.%.[242] This high LiCl concentration can plausibly be explained by the absorption of water by the system, as explained in paragraph 3.5.2.2. The parameters of the equation should be recalculated for a solvent system exempt of water. However, some authors skilled in the art use cupriethylenediamine (CED) at 0.5 M to dissolve cellulose and perform measurements of the intrinsic viscosity.[213, 241] This latter one will give the molecular weight according to the relationship:

$$[\eta] = 1.01 \cdot 10^{-4} M_w^{0.9} \quad (3)$$

CED is meant to well preserve cellulose from degradation, as compared to many other solvents. Another method complementing the viscosity is the light scattering measurement. The molecular weight can be calculated once the refractive index increment is known from the formula:

$$\frac{1}{M_w} = \frac{2 \cdot \pi^2 \cdot n_B^2}{\lambda^4 \cdot N \cdot R_B} \cdot \left(\frac{dn}{dc}\right)^2 \cdot I_B \cdot \left(\frac{c}{H_\theta}\right)_{c=0,H=0} = 0.491 \cdot \left(\frac{dn}{dc}\right)^2 \cdot I_B \cdot \left(\frac{c}{H_\theta}\right)_{c=0,H=0} \quad (4)$$

where n_B, R_B and I_B are, respectively, the refractive index, the Rayleigh ratio, and the scattered intensity at 90° of benzene.[241]

Also, H_Θ is defined as:

$$H_\theta = \frac{(I - I_0) \cdot \sin\theta}{1 + \cos^2\theta} \quad (5)$$

Those two theories are used for size exclusion chromatography.

3.4.3 Conclusions

It has been seen that the use of LiCl/DMAc brings a neat advantage over its counterpart NMMO. Indeed, it does not have any thermal runaway; furthermore, no additive or particular equipment needs to be used, and it was claimed to be recyclable with a high recovery rate. The procedure is simple: cellulose needs to undergo solvent exchange (for example, water, acetone and then DMAc) to break secondary hydrogen bonds and enlarge the pore structure. Once it is soaked with DMAc, the salt LiCl will bring intermicellar swelling and effective dissolution. A simple coagulation bath or evaporation procedure suffices to regenerate the cellulose.

3.5 Which solvent for an all-cellulose composite?

NMMO is a very good solvent for cellulose and it is already used at an industrial scale. It has several advantages that seem to be obvious requirements for the conception of an eco-

composite: it is non-toxic, recyclable and the complexity of its by-products, side-reactions and thermal runaways is well understood thanks to extensive research. However, new composite materials involve a different process than fibre spinning or film blowing, and we believe that the intricacy of cellulose dope preparation using NMMO is a serious impairment to a safe and simple preparation of thick cellulose materials. NMMO was costly when purchased in small quantities and the special glassware needed prevented the study of NMMO in the present work.

The dissolution route using NaOH was also studied. One the one hand, this route seemed to be the eco-friendliest, safest and the most uncomplicated method of them all. NaOH solutions do not produce toxic fumes which makes them easy to handle. The base chemicals are cheap and easy to access; no expensive specialty chemical needs to be used. When HCl is used as a coagulating medium, the only by-product in this process is the innocuous sodium chloride. Dissolution of cellulose in NaOH does not necessitate the use of high temperatures; at the rise of the new millenary, low energy processes are preferred because they are both financially and environmentally more economical. On the other hand, NaOH does not efficiently dissolve all cellulose sources like both LiCl/DMAc and NMMO do. As a consequence, new methods with higher efficiency and based on NaOH emerged.[198] They consist in the addition of urea or thiourea or both to the NaOH solution. However, their development occurred only in the very last three years, which prohibited their use in the present work. Succinct work on those solvents was however carried on in our laboratory.

The LiCl/DMAc system is often regarded as the most effective solvent for cellulose as it possesses the ability to completely dissolve high molecular weight (MW > $1.0*10^6$) cellulose.[228] As a result, a broad range of partial dissolution conditions was obtained in order to extrapolate for the use of other solvents, including less potent ones. To date, all the literature concerning all-cellulose composites involve LiCll/DMAc use. This solvent is hence used in the present work for the sake of scientific intercomparability.[22-24, 26-28, 221] The main disadvantages of this dissolution path lie in the need for a pre-treatment (or activation

procedure) which unfortunately can make its use expensive and time-consuming. DMAc in combination with LiCl is also highly toxic, corrosive and volatile. Health and safety issues are thus high.

As a concluding remark, the concept of green chemistry has been pushed forward extensively in the last years, because there is a physical and moral obligation to change the consumption and production comportments of the society.[243, 244] At the exact cross-road of green chemistry and cellulose dissolution exploration, a new class of solvents called ionic liquids has emerged.[155] Those appear to combine all the encouraging aspects of the three solvents reviewed here: extra low volatility, very low cost due to easy and quasi-total recycling, fast and complete dissolution power for a broad range of cellulose sources and absence of pre-treatment requirement. Regrettably, ionic liquids in cellulose dissolution are a new field of expertise. Most of the literature on this topic dates from the last three years. This hindered the use of ionic liquids in this Thesis, but there is a great deal of chances to see them used in all-cellulose composites within the next few years.

4 All-cellulose composites –a review

"Cellophane was invented by Jacques E. Brandenberger, a Swiss textiles engineer in 1908. After witnessing a wine spill on a restaurant tablecloth, Brandenberger initially had the idea to develop a clear coating for cloth to make it waterproof. He experimented, and came up with a way to apply liquid Viscose to cloth, but found the resultant combination of cloth and Viscose film too stiff to be of use.[192] However the clear film easily separated from the backing cloth, and he abandoned his original idea as the possibilities of the new material became apparent. Cellophane's low permeability to air, grease and bacteria makes it useful for food packaging." (Wikipedia, August 2007)

The above story could be thought as a metaphor, reflecting the difficulties encountered in eco-composite manufacturing. Firstly, cellophane is produced by the Viscose process and it contains a large portion of cellulose crystals embedded in regenerated cellulose.[192] It can therefore be considered as an all-cellulose eco-composite. However, Viscose as a process involves harsh chemicals because cellulose dissolution is in point of fact hard to achieve. True cellophane is readily biodegradable but its production process involves polluting sulphur by-products, which is why it has largely been discarded from the industrial landscape.

However, cellophane film is a successful green nano-composite itself if the manufacturing process is ignored. Nonetheless, it is a lot harder to accommodate raises in scale to produce an eco-composite with a thickness sufficient for structural applications like synthetic matrices reinforced with man-made fibres. The incompatibility between an hydrophobic matrix (cellulose acetate, polyester, epoxy, *etc*) and an hydrophilic reinforcement (textile fibre) is a major limitation of eco-composites. Under certain conditions, the interfacial problem also exists when regenerated cellulose is applied to a native cellulose cloth. In effect, this is the same dilemma Brandenberger faced when Viscose could simply be peeled off the

backing cloth. This chapter will explore approaches that circumvent the problem of interfacial incompatibility in such composite materials.

4.1 Introduction: Overview and benefits over other eco-composites

The need to improve the compatibility between the cellulose and matrix in which it is embedded led to the notion that cellulose itself could perhaps be utilised as the matrix. Nishino *et al.* were the first to apply this approach, giving rise to a new class of high strength, biodegradable materials known as all-cellulose composites.[22-24, 221] Nishino synthesised all-cellulose composites by immersing untreated plant fibres (ramie fibre) into a solution of dissolved conifer craft fibre.[23] The dissolved cellulose was subsequently regenerated to form a cellulose matrix that surrounded the ramie fibres. The longitudinal strength of the composite was as high as 480 MPa, indicating that stress transfer in all-cellulose composites is more efficient than for other types of cellulose-polymer biocomposites.[23] An extremely good thermal stability with a 20 GPa storage modulus at 300 °C is one of their remarkable features.[23] The difficulty arising from this approach lies in the cellulose content of the matrix. It would be desirable to have a solution of dissolved cellulose with a high cellulose content in order to minimize the matrix shrinkage during regeneration and hence maintain good bonding between the matrix and the reinforcement. However, cellulose solutions with a high cellulose content have a very high viscosity which makes the impregnation difficult.

Following on from this work, Nishino and Gindl partially dissolved cellulose I with the idea of utilising the dissolved portion of cellulose to form the surrounding matrix.[24, 26-29] In these studies cellulose I was sourced from microcrystalline cellulose (MCC), beech pulp and filter paper. The resulting isotropic composites had strengths and moduli values as high as 243 MPa and 14.9 GPa, respectively, which compares well with randomly oriented short glass fibre reinforced epoxy composites.[24, 29]

Similar composites have also been prepared by using esters such as cellulose acetate butyrate (CAB) as the matrix.[9, 245] While those composites were based primarily on cellulose, esterification altered the polarity of the matrix relative to the fibres and mechanical performance was not as high as for true all-cellulose composites. Gindl and Keckes (2004) reported a tensile strength of 129 MPa for CAB reinforced with bacterial cellulose, compared with 480 MPa for a true all-cellulose composite prepared by regeneration (Table 8).[24, 245] In a similar way, Zhang and coworkers used a benzylation process to prepare a matrix that was then mixed with unreacted sisal fibres.[246] Some other authors prepared composites out of one material; their approach consisted in getting a thermoplastic sleeve formed around an unreacted cellulose core. For example, Matsumura *et al.* proposed a partial esterification process by hexanoylation and Gandini *et al.* a partial oxypropylation of the cellulose fibres [247-249] Matsumara reported a tensile strength 25 MPa and a Young's modulus of 1.3 GPa for partially derivatized wood pulp fibres consolidated in a composite of cellulose ester and cellulose (Table 8).[249]

4.2 Anisotropic all-cellulose composites

4.2.1 Composites made with continuous fibres

Composites with continuous fibres have usually involved the preparation of a matrix material made of cellulose dissolved in DMAc containing LiCl. The matrix material is then used to impregnate long fibres such as ramie fibres.[22, 23, 250] In order to prepare the matrix, cellulose fibre such as coniferous pulp fibres or MCC is dissolved in DMAc containing 4-8 wt.% LiCl. Fibres went through an activation procedure consisting in the sequential impregnation in water, acetone, DMAc and then vacuum drying. The details of this procedure are outlined in Section 3.4.2.1. 0.5-3 wt.% cellulose fibre was then immersed in the LiCl/DMAc solution. 1-1.5 wt.% cellulose solutions were most favourable for the creation of

an all-cellulose composite. After stirring at room temperature for 24-48 h, a clear solution was obtained, at which stage the cellulose was assumed to be dissolved.

The next step involved the use of the above-mentioned cellulose solution to impregnate and consolidate long cellulose fibres. The long fibres may originate from different sources including bamboo, ramie, flax, hemp, papyrus, kenaf, cotton linter or sisal. Cellulose fibres are used as-received or activated by immersion in DMAc in order to encourage the interdiffusion of the dissolved cellulose molecules at the interface. A length of 1-25 cm was trialled although lengths of 5 to 15 cm were found to be optimal for easy impregnation. The fibres were placed in a mould, clamped in place and then impregnated with the cellulose solution. The mould can be made from any material as long as it is resistant to the solvent.

For a successful lay-up, the matrix material was applied directly to the fibre with the aid of a brush or a roller. Usually, 2-4 ml of solution provided enough matrix material to bond ~ 1 g of long fibres. The mould was then held at room temperature for 10-20 h followed by immersion in water or ethanol for 1-2 days to induce regeneration of the cellulose. Thorough rinsing at this stage eliminated all of the DMAc and LiCl from the cellulose replacing it with water. At this stage, the cellulose is regenerated and swollen in water in the form of a gel. The gel was dried at room temperature for 12-24 h and then vacuum dried at 50-70 °C for 24-48 h.

Table 8 Examples of all-cellulose composites described in the literature.

Reference	Nishino, 2004 [23]	Nishino, 2005 [24, 29]	Gindl, 2005 [26]	Gindl, 2006 [28]	Matsumara, 2000 [249]
Type	The reinforcement is embedded into a fully dissolved cellulose matrix	Partial dissolution of the reinforcement	Partial dissolution of the reinforcement	Partial dissolution of the reinforcement	partially derivatized cellulose esters
Raw materials	Cellulose from coniferous craft matrix and reinforcement from non-pretreated ramie fibre	Filter paper (Toyo Roshi Kaisya, Ltd., No. 5C, for quantitative chemical analysis)	Aldrich microcrystalline cellulose	Dissolving-grade beech pulp	wood pulp fibres
Solvent and cellulose concentrations	3 wt. % cellulose in 8 wt. % LiCl/DMAc	Unknown cellulose concentration in 8 wt. % LiCl/DMAc	2 to 4 g of cellulose in 8 g LiCl added to 100 mL DMAc	Unknown cellulose concentration in 8 gLiCL and 100 mL DMAc	reaction with a mixed p-toluene sulfonic/hexanoic anhydride system in a non-swelling (cyclohexane based) reaction medium
Impregnation time	24 and 72 h	6 to 12 h	12 h	10 h	
Drying process/consolidation process	12 h at RT and 24 h at 60°C in a vacuum	100°C for 12 h then 60°C foo 24 h in a vacuum	"dehydration between two sheets of paper"	Pressing at 80°C and 200 MPa	Pressing 4 min at 155-170 °C under 310 kg/cm²
Matrix content	~ 20 % (vol.)	77 to 84 % (vol.)	24% up to 59 % cellulose I crystallites	~ 20 % (vol.)	
Strength of the material	480 ± 50 MPa	up to 211 MPa	215-243 MPa	154 ± 17 MPa	up to 25 MPa
Youngs modulus	45 GPa (dynamic)	up to 8.2 GPa	12.6-14.9 GPa	12.2 ± 0.9 GPa	up to 1.3 GPa

As a result, an all-cellulose composite with orthotropic mechanical properties was created. (Figure 22) The mechanical properties of the long fibres were essentially retained in the composite. The tensile strength was ~ 300-550 MPa and 10-17 MPa in the fibre and transverse directions, respectively. The storage modulus was ~ 45 GPa at 25 °C in the fibre direction. Pre-treating the fibres resulted in improved transverse mechanical properties although slightly decreased in the fibre direction. A stronger fibre-matrix interface develops when the fibres are activated, as evidenced by fibre breakage rather than fibre pull-out.

Recently, Qin *et al.* showed that a similar all-cellulose composite reinforced with ramie fibres impregnated with a matrix obtained by dissolution of ramie fibre could have its mechanical properties enhanced by mercerization of the composite.[30] For example, the tensile strength could be enhanced by 15-95% after mercerization. Qin *et al.* also showed that unsatisfactory impregnation was obtained when the matrix concentration in cellulose was too low (~1% wt./v) due excessive matrix shrinkage. A significant amount of interfacial defects could also be linked to the use of a matrix with a high cellulose content (~7% wt./v). An explanation for the presence of these defects lies in the high viscosity of the matrix at high cellulose concentrations, leading to poor impregnation.[30]

Finally, all-cellulose composites could also be obtained by simply partially dissolving ramie or flax fibres without any need for the addition of a matrix material.[25]

(a)

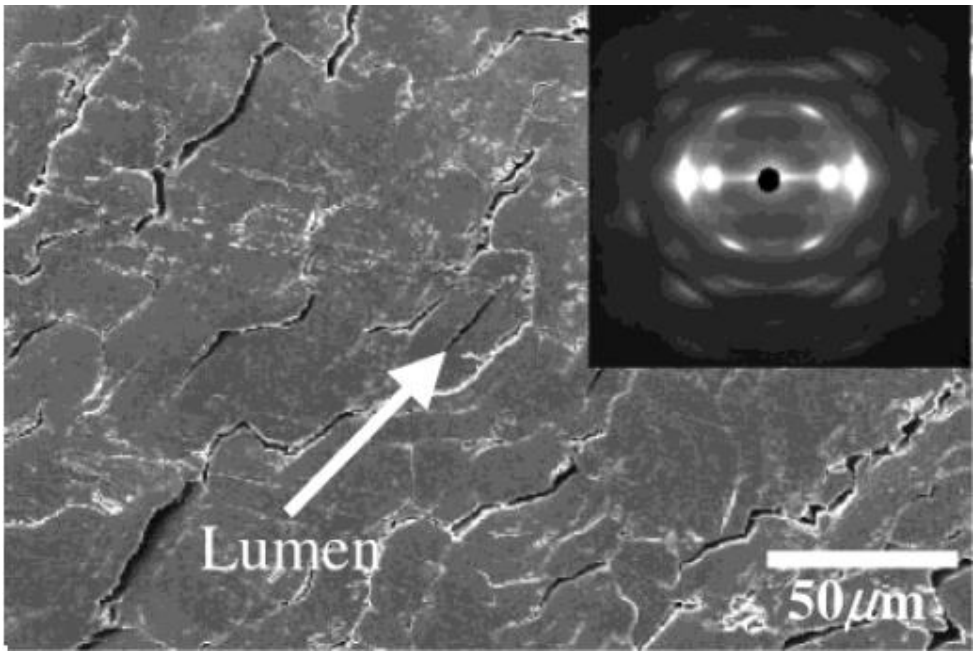

(b)

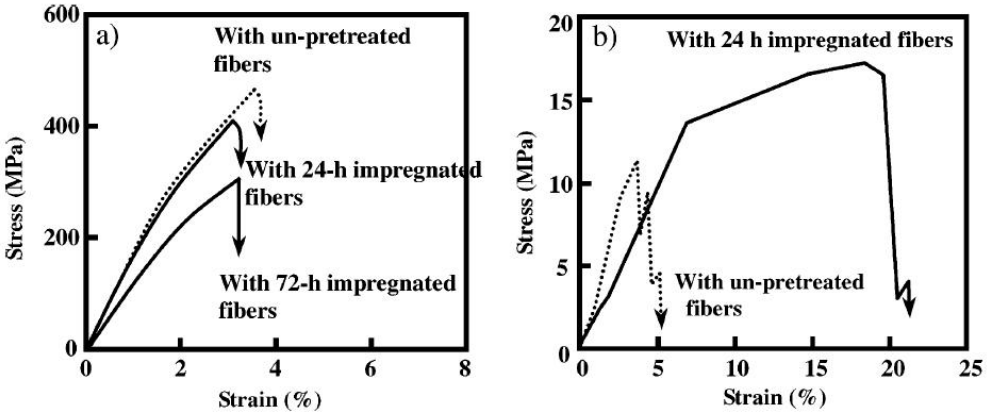

Figure 22 Nishino's first all cellulose composites: (a) WAXD and SEM micrograph of a cross section and (b) mechanical testing of the material prepared using different manufacturing procedures.[23]

4.2.2 Composites made with a strained hydrogel

Cellulose is a composite material consisting of amorphous and crystalline phases. Orientation in both of these phases can be induced by stretching the cellulose to produce greater mechanical properties in the direction of stretching.[251, 252] Orientation is typical for regenerated cellulose fibres and films, the latter mostly found in the form of cellophane. The concept of a strained hydrogel where a cellulose hydrogel produced from completely dissolved cotton linter was stretched was introduced by Kondo *et al.*.[79, 253, 254] As a result, a non-crystalline but orientated form of cellulose, "nematic ordered cellulose", was produced, although the mechanical properties of this novel material were not investigated.[79] Recently, Gindl reported a similar process where Lyocell fibres were completely dissolved in LiCl/DMAc and cast into a gel that was dried in the form of a film.[252] The process involved pre-treatment of the Lyocell fibres by dehydration in each ethanol, acetone and DMAc for 4 h. 2 g of fibres were then mixed with 8 g of LiCl in 100 ml of DMAc. The solution was stirred for 10 min in order to dissolve the cellulose fibre and then cast into a Petri dish where it was left for 12 h at ambient conditions before being dehydrated. Subsequent rehydration in distilled water, monoaxial stretching and drying achieved an orientated state in the final film. A draw ratio of 1.5 resulted in an increase in tensile strength from 201 to 396 MPa and a threefold increase in Young's modulus (8.5 up to 26.4 GPa) while the elongation at break was reduced from 19.6% to 4.3%. The molecular orientation occurred both in the amorphous and crystalline regions.[27, 172, 252-255]

4.3 Quasi-Isotropic all-cellulose composites

Nishino had been developing the concept of all-cellulose composites by simple impregnation of cellulose fibres with a solution of dissolved cellulose.[23] However, the high viscosity of a cellulose solution hinders impregnation of cellulose fibres.[24, 29, 185] It is easier to use a low viscosity LiCl/DMAc solvent to penetrate the reinforcement. The partial

dissolution is able to provide sufficient matrix phase to bond the remaining portion of undissolved cellulose. The idea of partially dissolving cellulose fibres to consolidate them into a composite material was first reported by Nishino and Arimoto.[24]

Only a few published papers by two main groups of authors directly address the required method for making all-cellulose composites.[24, 26, 28, 29] In the first instance, Nishino *et al.* started with a filter paper that was first pre-treated in distilled water, acetone and DMAc followed by drying.[24, 29] The next step involved immersing 3 wt.% of paper in an 8 wt.% LiCl/DMAc solution, then consolidating it with a press at 0.1 MPa for 1 h and immersing it in methanol to prevent the LiCl/DMAc from dissolving the cellulose material further. At this stage, cellulose formed as a gel form and was made stable. The cellulose composite then underwent a two step drying process to complete consolidation: 100°C for 12 h followed by 60°C for 24 h in a vacuum.

In the second instance, Gindl *et al.* used a slightly different approach.[26] The starting material was a MCC in a powder form. As such it could not be easily compressed during dissolution. The cellulose powder was activated with DMAc according to the standard step procedure described above. 2 to 4 g of activated MCC was then mixed for 5 min with a solution containing 8 g LiCl in 100 ml DMAc. The mixture was poured in large Petri dishes and then left at ambient conditions for 12 h. The solvent was then replaced by distilled water and then dried between gently compressed sheets of paper. In a recent study by Gindl *et al.*, disks of beech pulp with a diameter of 12 cm and thickness of 1.5 mm were used. The pre-treatment procedure was essentially the same as usual (dehydration was conducted sequentially with distilled water, methanol, acetone and finally DMAc). The disk was immersed in a solution of 8 g LiCl in 100 ml DMAc for 10 h in order for dissolution to proceed. Finally, the composite was precipitated with water and the solvent was eliminated by keeping the composite immersed in water for 5 days. Excess water was then removed by pressing the gel

between tissue paper. The drying process was performed in a hot-press at 80 °C with the pressure slowly ramped up to 200 MPa.

Thus, the main differences between the methods used by these two groups are the following:

- The starting material can either be laboratory filter paper, cellulose powder or dissolving grade beech pulp.
- In the case where MCC was used, the solvent and cellulose mixture was left at ambient for 12 h, which is generally sufficient to induce gelation and halt further dissolution. This step is useful in that it helps maintain flat samples. The shape of the sample is likely to be lost by placing it directly into a water bath.
- The final drying stage can be performed, with or without increased temperatures and pressures.

Despite these differences, the composites exhibit the same X-ray patterns with a cellulose I peak at ~ 22-22.7° that includes a peak or shoulder at ~ 20-20.4°. The latter peak is attributed to cellulose of low crystallinity and thought of as being the cellulose matrix, formed by partial dissolution and precipitation of part of the starting cellulose. It only appears as a shoulder in the case of partially dissolved beech pulp, supposedly due to the low rate of dissolution that takes place.[28] The low crystallinity peak usually becomes more prominent as the cellulose concentration in the solvent mixture is decreased or as the dissolution time increases. The literature describes composites with a tensile strength of 154 to 210 MPa and Young's modulus of 8.2 to 14.9 GPa.[24, 26, 28, 29] The strain at failure is in the order 3-10% and is generally found to increase with a decrease in the initial cellulose content, supposedly due to the matrix material which is a more ductile material than its highly crystalline counterpart. Similarly, the disordered matrix material shows less re-orientation under strain than cellulose I crystals.[27]

As a concluding remark, all-cellulose composites can exhibit higher mechanical properties than natural fibres mixed with synthetic resins and compare favourably with randomly oriented glass fibre reinforced resin. The high mechanical properties are explained by

the increased chemical compatibility between matrix and reinforcement when both are of the same polarity, unlike hydrophilic/hydrophobic mixtures that are typical of natural fibre reinforced composites.

5 Preliminary investigations into all-cellulose composites

5.1 Introduction

The objective was to find a method for manufacturing a monocomponent composite material wholly based on cellulose. This goal has been achieved through a series of experimental trials, although the process parameters still need to be optimised. The LiCl/DMAc solvent system was used to produce a regenerated cellulose matrix. A wide range of cellulosic materials were trialled for the fabrication of a composite matrix (hemp, *Pinus radiata* pulp, sisal, cotton) and reinforcement (hemp, linen yarn, *Phormium tenax* whisker, *Pinus radiata* pulp). The reinforcements were usually impregnated with the above-mentioned matrix *via* extrusion or hand lay-up and dried in order to produce an all-cellulose interfaceless eco-composite.

5.2 Experimental procedures

5.2.1 Matrix preparation

Cellulose was derived from various sources including hemp, cotton, wood pulp and sisal. Hemp, cotton and *Pinus radiata* pulp were used as received while sisal was submitted to a NaOH treatment. The preparation of the matrix was carried out by initially immersing cellulose in distilled water at room temperature for 48 h. This was followed by immersion at room temperature in acetone for 48 h and DMAc. Residual fibre was removed from the solution by decantation. This process is referred to as the "activation" procedure. The wet cellulose was then vacuum-dried for 40 h at 60^{o}C by placing the samples in a temperature-controlled desiccator. A cellulose solvent consisting of DMAc solution with 8 wt.% LiCl was mixed with the dried cellulose in the weight ratio of 99:1, respectively, agitated with a magnetic stirrer at room temperature until the solid phases (salt and cellulose) had disappeared and then held at room temperature for a period of several days. After this process,

Table 9 Experimental table summarising the various processing routes used to produce the matrix and composite materials.

Number	**1**	**2**	**3**	**4**	**5**
Description	Pure matrix left in a Petri dish	The matrix was poured on the fibres in the mould	Extrusion with high fibre qty/funnel diameter ratio. Fibres were clamped in between two brass plates or placed in the mould	Laminate manufacturing out of the previous sample The stack was clamped to apply pressure onto it	Extrusion with low fibre qty/funnel diameter ratio
Matrix material	Sisal	Pulp	Pulp	Pulp	Pulp
Fibre	/	Hemp	Linen yarn	Linen yarn	Hemp
Product left half a day at room temperature before rinsing	N	Y	N	N	Y
Pressure	N	N	Y (clamps)	Y (clamps)	Y (clamps)
Result	Brittle and inconsistent film. Porosities.	Partial impregnation due to gel viscosity. The gel does not spread over the fibres.	Partial impregnation. Obvious lack of matrix. The matrix there looks successfully distributed over the specimens, though.	Once again, matrix lacks.	The impregnation looks good.
Discussion	Suggest the need for pressure during the manufacturing.	The gel is too viscous to penetrate a bundle of fibre. A more consistent way of mixing as to be found.	A way of controlling the ratio regenerated fibre/ matrix in the final product has to be found. Better wetting will be achieved using more matrix material.	It has been possible to create a laminate out of composite sheets. Small parts can be manufactured and then assembled using some more gel.	Using more matrix material during the impregnation step is the way to go. Extrusion is a possible way of wetting the fibres with the matrix. It has not been possible to quantify accurately the relative amounts of regenerated cellulose and fibres before manufacturing.

Table 9 Experimental table summarising the various processing routes used to produce the matrix and composite materials.

Number	6	7	8	9	10	11
Description	Short fibres and ~20% regenerated matrix in the final product	Gel extrusion through a pipette	Pure matrix in a brass mould	Pure matrix in a brass mould	Partially dissolved fibres were placed into the mould. The product was rinsed unmoulded 48 hrs in water.	Wood pulp and hemp gel. The product was moulded, wetted in water, and then rinsed unmoulded 48 hrs in water.
Matrix material	Pulp	Pulp	Pulp	Hemp	Sisal	Hemp
Fibre	*Phormium Tenax* whisker	/	/	/	Sisal	Wood pulp, pre-soaked in water and then acetone.
Product left half a day at room temperature before rinsing	N	N	N	Y	Y	Y
Pressure	0.14 MPa	N	0.14 MPa	Yes (not quantified yet)	Yes (not quantified yet)	> 11kPa
Result	GOOD fairly consistent sample. D~323 kg/m^3 The volume occupied by the final product is about 22% of the initial one.	Produc-tion of a fibril. Stiff?	The mould was left under running water and samples did oxidize quite badly.	A bath of methanol was used instead of water. 4 samples out of 5 look fine. Stress relaxation is visible after a week time.	Insufficient impregna-tion	Matrix amount ~ 15% (weight measurement in the final product). Impregnation has not been done fully. Obvious porosities in the material.
Discussion	The use of short fibres permits an easy wetting of the fibres. Also, it is easily possible to evaluate the matrix/fibre amounts. However, the sample did not adopt the mould shape. Need for a pressure control.		Perhaps the samples should be placed in the mould after rinsing.	The use of methanol limits brass oxidation. This manufacturing method can probably be used for the preparation of DMA film samples.	Difficulties levied by this method to quantify the amount of matrix/fibre.	Need for more matrix material and a pressure control.

the initially whitish-coloured and turbid solution turned clear as the fibres were dissolved by the solvent. It was assumed that the cellulose was fully dissolved when full transparency was reached. Thus, a 1 wt.% cellulose in LiCl/DMAc solution was obtained. A summary of the results obtained from the dissolution of cellulose from various sources is given in Table 9.

Some authors recommend a treatment with liquid ammonia prior to the activation procedure to remove the hydrophobic lignin that hinders fibre dissolution.[220, 237] The wood pulp and hemp fibre were dissolved as supplied without difficulty and without pre-treatment. Partial sisal dissolution can be explained by incomplete mercerization. Cotton linters were not dissolved. This experiment was conducted in mid 2004. An article published in 2005 showed that cotton dissolves only after complete mercerization, that is after a change from cellulose I to cellulose II.[220]

5.2.2 Matrix regeneration

All trials involved the same basic procedure for matrix regeneration. Figure 23 summarises the various fabrication routes. The gel was shaped and rinsed in water or methanol in order to remove LiCl and replace DMAc with a more volatile solvent before being vacuum dried in a desiccator at 60°C for 48 h.

The first trial in cellulose regeneration (1) involved using a sisal-based gel. A homogeneous solution was poured into a Petri dish, placed in a water bath for 24 h before vacuum drying. A brittle, porous and non-uniformly thick film was produced. In a subsequent trial, a wood pulp-based gel was extruded through a pipette (7). The extrusion was deposited in a beaker of water and vacuum-dried on a brass plate. The high viscosity of the gel created difficulties in manipulating the gel using a thin pipette. However, the use of extrusion to constrain the gel allowed the production of a more consistent product. The use of a brass plate resulted in easier separation of the regenerated film from the substrate when compared with glass.

More regenerated films were produced using a specially designed brass mould (Appendix 1) that also allowed light pressure to be applied during processing. The mould was also designed to produce samples suitable for dynamic mechanical analysis (DMA).

Both wood pulp (8) and hemp (9) gels were trialled using the brass mould. The wood pulp samples were rinsed overnight in the mould under running water. Hemp samples were rinsed by placing the mould for 24 h in methanol. Following rinsing, all samples were vacuum-dried. Unfortunately, brass oxides were absorbed by the regenerated wood pulp samples, making these samples unsuitable for further testing.

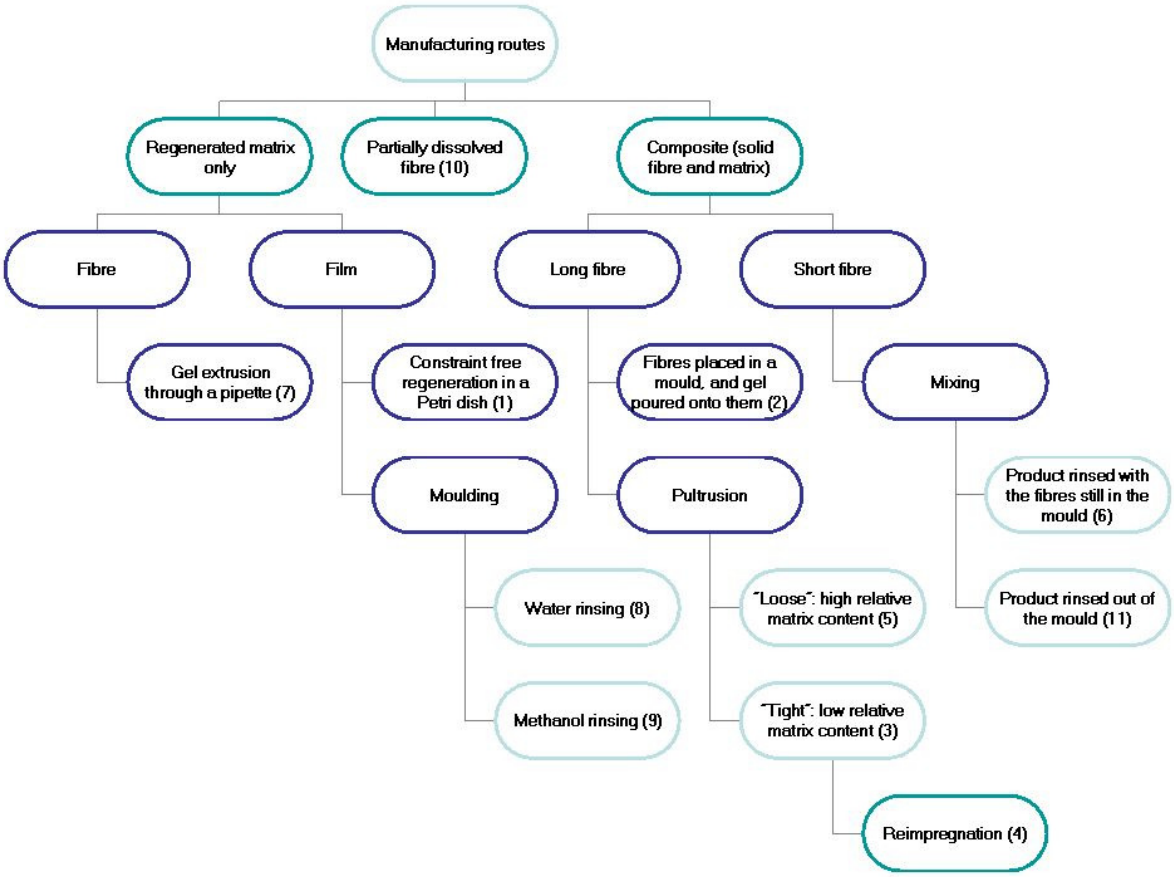

Figure 23 Flow diagram representing preliminary trial procedures.

5.2.3 Composite preparation

The basic steps for preparing the composite materials included impregnating the fibre with a gel, placing the mixture in the brass mould, rinsing to remove LiCl and DMAc and finally vacuum-drying for 48 h at 60°C. Some of the various processing parameters that were investigated included the type of cellulose source, use of long and short fibres, wetting technique, applied pressure during regeneration and type of polar liquid selected for regeneration. The first trials involved combining wood pulp-based gel with hemp fibre bundles placed in a brass mould (2). The composite was rinsed and vacuum dried under mechanical pressure. Only partial impregnation and wetting of the hemp fibre occurred due to the high viscosity of the wood pulp-based gel.

Attempts to improve wetting of the reinforcing fibres was performed by pultruding the fibres through a funnel, which contained the wood pulp-based gel. Fifteen yarns (linear density: 180 g/km; twist: 160 twists/m) were passed through a funnel with a similar diameter (3). The yarns were fully wetted by the gel during pultrusion. The composite was then clamped between two brass plates, rinsed under running water overnight and vacuum-dried. However, consolidation appeared incomplete after drying of the yarns due to extensive shrinkage of the gel. The extrusions obtained by this method were re-impregnated by simple gel deposition, clamped together and placed in methanol overnight (4) although impregnation was still incomplete after this process.

In order to further assess if pultrusion could be a used as an impregnation method, a thin hemp fibre bundle was passed through the funnel containing wood pulp-based gel (5). The extrusion was once again clamped between two brass plates and left in methanol overnight. The dried extrusion appeared consistently consolidated, demonstrating that pultrusion could be a suitable method for fabricating a fully consolidated composite. However, it was difficult to control the relative amounts of fibre and matrix using the pultrusion method. Since an objective

of this work is to compare the properties of these cellulose-based composites with conventional composite materials, it is essential that a fabrication route be developed that offers accurate control over the fibre to matrix ratio.

The fibre to matrix ratio should be easier to control using short fibres by simply mixing the required amount of fibre for a given amount of gel. Defibrillated *Phormium tenax* fibres were combined with a wood pulp-based gel with the goal of achieving ~20% matrix in the final product (6). The two components were mixed up in a beaker, poured into a mould and left overnight in methanol. The composite was then vacuum-dried under a pressure of 0.14 MPa. A fully consolidated sample was produced using this method, although some porosity was present, suggesting that a higher pressure during consolidation or superior wetting is required.

For all of the above processing, it would be preferable to use water for the rinsing step since methanol is toxic. However, water rapidly oxidises the brass mould (brass was selected rather than stainless steel for ease of manufacturing). Thus, "out-of-the-mould" rinsing was trialled, using wood pulp for both the fibre and matrix (11). The wood pulp was in the form of kraft and required softening by solvent exchange using water, followed by acetone. Once the kraft lost its "structure" it was then combined with the wood pulp-based gel and poured into a mould. The composite samples were removed shortly after moulding and then stirred in water for 24 h to remove the DMAc and LiCl. The rinsed composite samples were then returned to the mould and vacuum dried under 0.14 MPa of pressure. The resulting product from this process was consistent and had the advantage of eliminating methanol from the rinsing step.

5.3 Conclusions and future work

A route was developed for manufacturing regenerated films of cellulose. This process will be used for making samples suitable for the X-ray diffraction study. Water rinsing was successfully used for sample preparation. This rinsing method is simple and inexpensive.

Cellulose-based composites can be made using short or long fibre reinforcement, although clearly the process requires further optimisation. Short fibres permit easier control over the relative amounts of matrix and reinforcement.

Despite the obvious ease of manufacturing, many features of all-cellulose composites remain unclear. Hydrogen bonding between fibre and matrix might belong to a crystalline or amorphous phase and could possibly be monitored using solid-state NMR in conjunction with WAXD and FTIR.

The density of the highest quality composite produced in this work was ~330 kg/m^3 (*c.f.* ~1550 kg/m^3 for pure cellulose), suggesting the presence of large numbers of voids, that will be examined with the help of TEM. Extensive shrinkage associated with the regenerated cellulose matrix is the most likely explanation. Improvements are required on surface quality of the samples because ASTM standards for mechanical testing require defect free surfaces. For example, greater control over the applied pressure is required to shape and press the composites. A hot-press or a vacuum bagging technique could be used in the future.

In Chapter 6, the crystallisation of the gel will be monitored as the water evaporates with the aim of understanding the regeneration mechanisms. Plotting the equatorial intensity distribution profile from WAXD enables the determination of the relative amounts of amorphous and crystalline phase present. This data will provide information regarding the rate of crystallisation during cellulose regeneration. During composite formation the spatial molecular behaviour of the cellulosic components will be changing, passing from an amorphous to a semi-crystalline phase. Supposedly, the polymer chains will realign and re-order with a possible backbone straightening as the matrix material transforms from a supposedly completely amorphous to a more ordered state. Wide angle X-ray diffraction (WAXD) is a convenient method to observe these transformations and changes in crystallinity.

6 Crystallization behaviour of a cellulose hydrogel

6.1 Introduction

This Chapter focuses on the crystallization behaviour of *Pinus radiata* hydrogel that was prepared using the LiCl/DMAc solvent system and subsequently rinsed with water. Wide angle X-ray diffraction was used to monitor in-situ matrix dehydration. The water removal is found to drive the crystallisation process. Changes in the X-ray diffractogram during drying suggest that the final crystalline form of regenerated cellulose was only reached in the late stages of drying which has important implications for processing all-cellulose composites.

Much remains unknown about the crystallization process of solid cellulose from its hydrated gel state. There is no change in covalent bonding: the cellulose chains do not break and reform. Hence, after dissolution and solvent exchange with water, the main cellulose chains can only be held together by ionic bonding, hydrogen bonding or entanglements. Above a certain water content value, the hydrogel exhibits what is commonly referred to as the amorphous form. When a cellulose hydrogel is dried, some of the hydrogen bonds between the hydroxyl groups of the cellulose chains and water are replaced by hydrogen bonding between neighbouring cellulose chains. Ionic bonding is also likely to change during drying and the entanglement geometrical features are expected to adjust to the overall shrinkage of the material.[200]

6.2 Experimental procedures

6.2.1 Gel preparation

Effective dissolution of cellulose benefits from a so-called “activation procedure” during which the cellulose is penetrated and swollen with a polar medium.[142, 212, 229] Cellulose sourced from *Pinus radiata* pulp was immersed in distilled water at room temperature (15-30^{o}C) for 48 h. This was followed by immersion in acetone at room

temperature for 48 h. Finally, the cellulose was immersed in DMAc at room temperature for 48 h. The cellulose was then vacuum dried for 48 h at 60°C before being immersed in DMAc solution with 8 wt% LiCl at room temperature. The ratio of cellulose to the LiCl\DMAc solution was approximately 1:99 by weight. The mixing was performed with a magnetic stirrer at room temperature, and agitated until the solid phase disappeared. The solution became clear after several days, indicating that cellulose dissolution had occurred.

The cellulose solution was extruded through a glass funnel (about 1 cm in diameter) in a water beaker. The precipitated gel was rinsed for 48 h under running water to remove the DMAc and LiCl. The gel was in a rod shape, approximately 8 cm in diameter. The samples were then clamped into a specially designed holder for the X-ray diffractometer (Figure 24 and Appendix 2).

6.2.2 X-ray analysis: data extraction and equatorial profile deconvolution

X-ray diffraction was performed using MoKα radiation (λ = 0.71013 Å) and data was collected with a Bruker CCD\SMART area detector. Equatorial profiles were recorded with the angle 2θ varying from – 30^o to 30^o after substracting the air scattering background. Samples were weighed before testing to monitor water content. The water content was expressed as the ratio of specimen weight to dried gel weight (referred to as "water weight ratio" in this work) in order for the following results to be directly comparable with Westman's published work on cellulose hydrogels.[256, 257] Between measurements, the gel specimens were dried for 2 min in a desiccator at 60^oC under slight vacuum pressure (~3 kPa). The specimens were all vacuum dried for another 24 h for the final measurements .

The diffraction angles were taken from the local maxima in the equatorial profiles of the diffractograms. The main peak diffraction angle (θ) was substituted into Bragg's equation to calculate the interplanar spacings, d:

$$d = \lambda / (2 \sin \theta) \qquad (6)$$

where, λ is the wavelength of the radiation.

A quadratic baseline was then substracted from the equatorial profiles using PeakFit®. This baseline was chosen asymptotic to the plot. The curve without baseline was smoothed using an automatic Fast Fourier Transform (FFT) procedure in PeakFit®. The curves were then deconvoluted into Gaussian curves with a correlation coefficient greater than 0.98. The half-width at half-height of the peak was used in the Scherrer equation:

$$D = K \lambda / (B \cos \theta) \qquad (7)$$

where, D is the crystal thickness, λ is the radiation wavelength, θ is the diffraction angle and B the diffraction peak width measured at half maximum height.[258] K is a correction factor usually set at 0.9 for this definition of B.[258]

6.3 Results and discussion

6.3.1 Phase transformations during drying of cellulose gel

An initial broad peak at $2\theta = 13.65 \pm 0.28^{\circ}$ in the early stages of drying disappears. During drying, a doublet or triplet of sharper peaks appear in the region $2\theta = 8.9^{\circ} \leq 2\theta \leq 10.2^{\circ}$ (Figure 25). The first peak corresponds to an interplanar distance of $d = 2.98 \pm 0.06$ Å. The peak width is approximately 5º (see Appendix 3) giving a crystal size of cellulose (D) of 7 Å, implying an average of 2 sheets of cellulose per crystallite (D/d). The final peak yields an interplanar distance between 4.0 Å and 4.6 Å and peak width of approximately 2.8º, giving a crystal size of 13 Å, or 3 sheets of cellulose per crystallite.

6.3.2 Peak assignment

Isogai *et al.* (1989) described the WAXS patterns from most of the recognised crystalline forms of cellulose.[110] They used a copper X-ray source. The corresponding values for a molybdenum source were calculated using Equation (6) and the results are reported in Table 10.

The initial glassy state of the hydrogel saturated in water did not match any of these crystalline forms of cellulose. What's more, other authors have observed similar X-ray patterns for cellulose hydrogels, with a corresponding peak at approximately $2\theta = 30\ ^\circ$ due the use of a copper source.[204, 205] In particular, Weng *et al.* performed both WAXS and solid-state ^{13}C NMR on a hydrogel obtained by thermal gelation of cellulose in a NaOH/thiourea solution.[205] The solid-state ^{13}C NMR results showed that the molecules were in the same conformation in the solvent solution and in the hydrogel, suggesting that the cellulose precipitates without altering the random coiled conformation of the cellulose in solution. Further work is required to explain how cellulose chains might stack with an interplanar distance of only 3.0 Å.

All recognised crystalline forms of cellulose show a WAXS peak in the region 9.5° to 10.4°. For relatively small crystallites, such as those considered here, the lattice can expand so that the peak shows a measurable displacement to low values of 2θ.[259] We are therefore unable to use this peak to identify crystalline forms of cellulose in the final state of the hydrogel. A broad shoulder extending to $2\theta = 5°$ is consistent with the presence of cellulose II, as expected in a regenerated cellulose (Table 10).

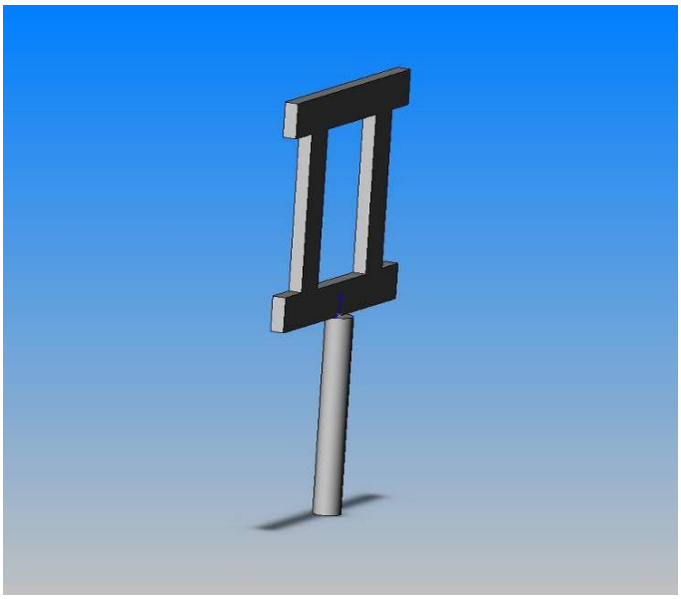

Figure 24 Specially designed samples holders with a copper frame used to place the hydrogel in the diffraction chamber.

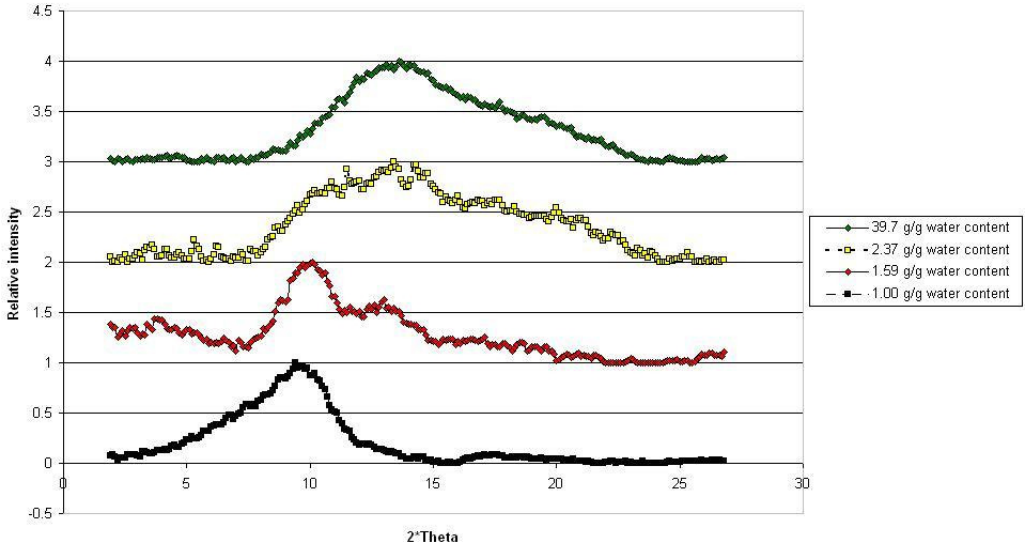

Figure 25 WAXD at four different hydration stages observed during drying of a cellulose hydrogel.

Table 10 WAXS peaks for cellulose using a molybdenum-source.

Form	$2\theta(1\bar{1}0)$	$2\theta(110)$	$2\theta(020)$
Cellulose I	6.8°	7.5°	10.4°
Cellulose II	5.6°	9.1°	10.1°
Cellulose III_I	5.4°	9.5°	9.5°
Cellulose III_{II}	5.6°	9.5°	9.5°
Cellulose IV_I	7.2°	7.2°	10.2°
Cellulose IV_{II}	7.2°	7.2°	10.3°

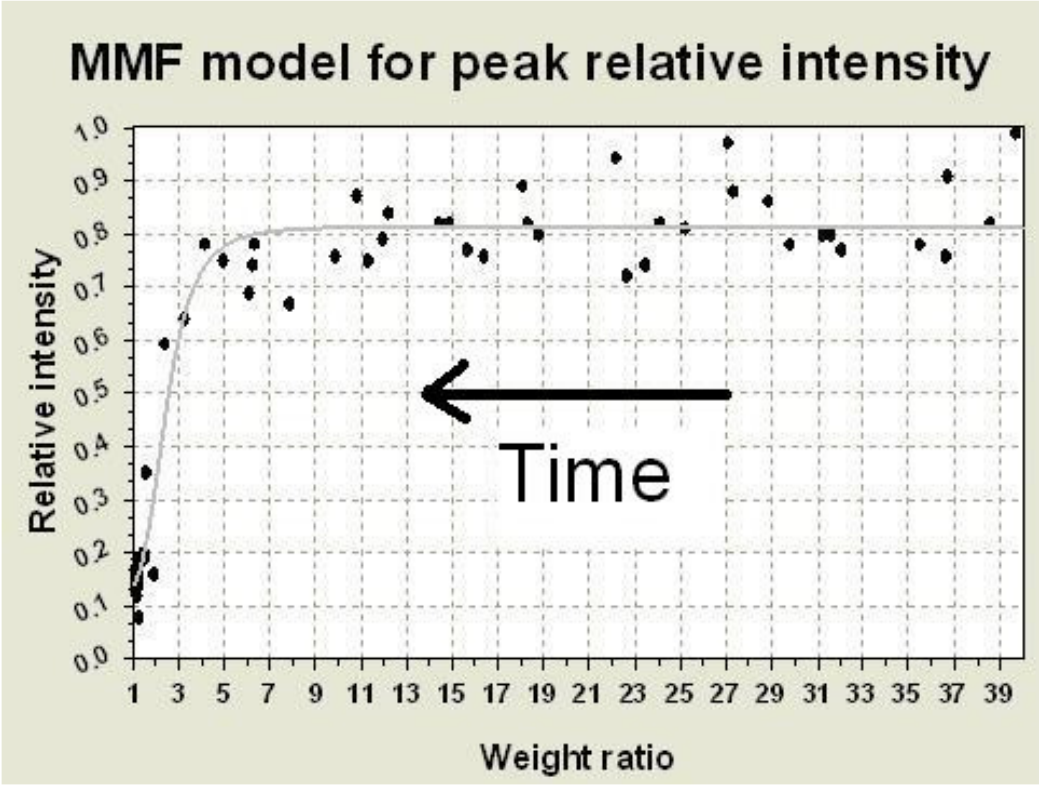

Figure 26 Relative intensity of the initial diffraction peak (2θ ~ 13.6º) over the final one (2θ ~ 9.5º) as a function of the water to cellulose weight ratio.

6.3.3 Comparisons with literature

Cellulose II is the crystalline form most commonly identified in regeneration processes. Cellulose III is known to form *via* a decomposition reaction of native cellulose fibres when placed in liquid ammonia and therefore unlikely to be encountered in the present work (Figure 8b).[33, 76] Cellulose IV is formed along with cellulose II during production of tire cord rayon, but not in production of textile rayon.[112] Cellulose IV can also be produced by recrystallising amorphous cellulose in glycerol at 260°C or by heat-treating high tenacity rayon fibre (Figure 8b).[113, 259] The unit cell of cellulose IV is so similar to the unit cell for cellulose I that some authors doubt the existence of cellulose IV.[109, 110]

The label "Na-cellulose IV" is misleading because this crystalline form of cellulose does not contain sodium. It is derived from Na-cellulose by washing with water, and it represents the final step prior to complete conversion to cellulose II. The most probable crystal structure is a monoclinic unit cell belonging to the group $P2_1$.[76] The unit cell contains two water molecules located between the corner chains. Conversion from Na-cellulose to Na-cellulose IV seems to involve chains aggregating into a sheet structure because of hydrophobic interactions. The unit cell dimensions are similar to those for cellulose II, and we were unable to measure peak positions with sufficient precision to distinguish between cellulose II and Na-cellulose IV in the hydrogel.

The crystal thickness values reported here are smaller than those reported in the literature for regenerated materials, generally between 25 and 40 Å, suggesting that crystallisation within the hydrogel ceases at an earlier stage than in conventional regeneration processes.[33]

6.3.4 Water content versus crystal form

It was found that the WAXS peak for crystalline cellulose appeared only in the late stages of drying. We could plot a curve (Figure 26) reflecting this phenomenon by calculating

the relative intensity of the initial peak at 2θ = 13.6º against the broad deconvoluted peak in the 9.5 º region.

The peak relative intensity equation is used as an indicator for the crystalline change occurring in the late stages of drying. The gel seems, from this point of view, to have relatively steady characteristics until it reaches a weight ratio of about 7 g/g. The first quantities of water escaping from the gel originate from microvoids: the water protons that are not bonded to cellulose are more mobile.[256, 257] In the late stages of drying (5g/g is a typical value), chemical crosslinks in the form of intermolecular H- bonds occurs between cellulose fibrils. This result corresponds to a dramatic dynamic storage modulus increase for degrees of swelling lower than 5 g/g.[260]

6.4 Conclusions

The crystallisation of a cellulose hydrogel obtained by dissolution of *Pinus radiata* was monitored using X-ray diffraction. Results published by Weng *et al.* also suggest that the cellulose molecules retain their random coiled conformation throughout precipitation.[205] The initial gel is characterized by an interplanar distance of 3 Å similar to the interplanar distance of amorphous cellulose. This distance suggests that chains are initially in face-to-face, rather than lateral, contact in the hydrogel. As the cellulose gel is dried, an abrupt change occurs at ~ 7 g/g and the initial amorphous form is replaced by a poorly crystalline material. This material typically contains ~3 sheets of cellulose per crystallite and cannot be identified with any of the known cellulose allomorphs due to the poor resolution of WAXD patterns in the case of small crystallites.

7 Phase transformations in a model composite made of Micro-Crystalline Cellulose (MCC)

7.1 Introduction

Little quantitative data is available on the dissolution or regeneration kinetics using the LiCl/DMAc system. It is known from other studies (*see* Chapter 3) that dissolution kinetics is affected by external factors such as temperature, stirring of the cellulose/solvent solution and the reactants mixed in the solvent. It is also affected by factors intrinsic to the system such as cellulose concentration, LiCl salt concentration, cellulose degree of polymerization, initial cellulose crystalline type, initial crystal size and crystallinity. Varying the cellulose regeneration parameters is also known to provide the material with a whole range of different features. Extrusion spinneret geometry, chemical composition and temperature of the regeneration bath, drying temperature, slurry cellulose concentration and extrusion speed are all known to influence the final void size and orientation, molecular orientation, and skin-core conformations.[171, 196, 251, 261-263] Each of the parameters relating to the dissolution, regeneration and drying of the cellulosic material affects the physical properties of the final product.[140, 142, 168, 171, 181, 182, 212, 235, 237, 251, 264-266]

In this case, it is of particular interest to characterise the dissolution kinetics since all-cellulose composite materials can be readily produced by partial dissolution of the reinforcement. Another bone of contention is the nature of the regenerated material that could not be elucidated by WAXS in the previous chapter.

While the high mechanical properties of all-cellulose composites have been reported, there are very few references to the nature of the allomorphs present in all-cellulose composites.[26] The allomorphs identified in the work by Gindl *et al.* were based solely on WAXD measurements. Generally, all-cellulose composites have poor crystallinity and conclusions based on WAXD results require some precaution. Imperfections in the cellulose crystal means that *paracrystalline* is a more appropriate description of the structure of

cellulose.[259, 267] Moreover, paracrystalline theory demonstrates that increasing disorder in the lattice artificially increases the unit cell parameters and crystallite specific volume.[259] The Scherrer equation also shows that a decrease in lateral crystallite size induces peak broadening.[69, 84] As a result, it is not possible to use WAXD as a means of distinguishing between the low crystalline forms of different cellulose allomorphs.[26, 84] Nishino took a pragmatic position by simply stating that the resulting cellulose allomorph had lower crystallinity than the starting high crystallinity native cellulose.[24] In this chapter, the effect of the cellulose concentration and dissolution time on the regeneration of a partially dissolved cellulose I was studied in order to elucidate the mechanisms of cellulose crystal transformation, their kinetics and the nature of the final material.

7.2 Experimental procedures

7.2.1 Composite preparation

Preparation of composites

Cellulose dissolution using DMAc initially involves an activation step in which the cellulose structure is first swollen via solvent exchange.[212, 229] The increased molecular mobility of cellulose allows the LiCl/DMAc solvent to penetrate the cellulose structure more easily.[142, 227] In the present work, microcrystalline cellulose (MCC) powder (Avicel, Merck, particle size between 20 and 160 μm) was immersed in distilled water at 20°C for 48 h and vacuum-filtered through Whatman No. 1 filter paper, twice immersed in acetone (Biolab, laboratory grade) at 20°C for 24 h and filtered through Whatman No. 1 filter paper to remove the acetone each time, twice immersed in DMAc (Merck, synthesis grade) at 20°C for 24 h and each time filtered through Whatman No. 1 filter paper afterward, vacuum-dried for 48 h at 60°C and then sieved (90 μm). The activated MCC was vacuum-dried for a further 48 h at 60°C and finally sealed in a container for storage. The DP was determined using Bianchi *et al.* (1985) method and found to be 163.[213]

Partial dissolution

A solution of 8.0% (by total weight) LiCl in DMAc was prepared by mixing LiCl (Unilab, 99% purity) and DMAc in a 2 L Schott bottle. The bottle was immediately sealed to prevent moisture absorption. The mixture was mechanically stirred for 24 h until the salt appeared to be completely dissolved.

A portion of 1 g activated MCC was immersed in a Petri dish containing sufficient LiCl/DMAc to achieve cellulose concentrations of c = 5%, 10%, 15% or 20%, where c is expressed as% of the total weight of cellulose, LiCl and DMAc. The solution was placed under vacuum and stirred for 1 h, 4 h, 8 h or 48 h at 20°C. The regeneration of the dissolved cellulose began initially with light spraying of water onto the surface of the gel in order to fix the shape of the final sample. The partially regenerated gel was then carefully transferred to a beaker and immersed in water for 48 h at 20°C. The water was changed at least every 24 h. Residual LiCl or DMAc was removed by further thorough rinsing of the specimen with water. The specimens were then dried 48 h in a vacuum oven at 60°C to ensure complete solidification.

7.2.2 WAXS

WAXS was performed on as-received MCC, activated MCC and on the final composites. X-ray patterns were obtained with a Philips PW1729 diffractometer using Cu K_α radiation (λ = 0.1540 nm), voltage of 50 kV and current of 40 mA with 2θ increased in steps of 0.02°. The X-ray data was smoothened over 30 adjacent points using the adjacent averaging smoothing function in Origin© Pro 7.5 and plots were then area-normalized. Peaks were assigned according to the monoclinic unit cell described by Sugiyama and coworkers.[73] Peak positions and widths were measured from plots by using the method described by Gjønnes and Norman in 1958.[268] We did not use curve fitting software because of the complexity of the diffractograms, with peak positions and widths expected to be related to crystallite dimensions

as well as crystalline forms of cellulose, as discussed below. Instead, we confined precise measurements to samples that had not been in contact with LiCl/DMAc.

The Scherrer equation was used to calculate the crystal thickness by using the half-width at half-height of the peak assigned to (200) planes:

$$D = K\lambda/(B\cos\theta) \quad (7)$$

where D is the crystal thickness, λ the radiation wavelength, θ the diffraction angle and B the full width of the diffraction peak measured at half maximum height prior to smoothing. The correction factor, K, was set to 0.9.[269] A crystallinity index CrI was used as defined by Segal *et al.* (1959) [68]:

$$CrI = 100(I-I')/I \quad (8)$$

where I is the height of the peak assigned to (200) planes, typically located in the range 2θ = 21° to 22°, and I' is the height measured at 2θ = 18°, which is where the maximum appears in a diffractogram of amorphous cellulose.

7.2.3 Solid-state NMR

7.2.3.1 Background

Introduction

Nuclear magnetic resonance in condensed matter has gone a long way its initial discovery in 1946. Strikingly, two research groups discovered it simultaneously: Edward Purcell and co-workers at Harvard and Felix Bloch and co-workers at Stanford University. Their initial discovery was the response of a magnetic nuclei placed in a uniform magnetic field to a continuous radio frequency (rf) magnetic field that was tuned through resonance. Four years later, in 1950, Edwin Hahn made another discovery that would eventually provide one of the main tools for NMR studies: the spin echo. Two pulses with a given delay time between them would yield a signal from the magnetic nuclei at a time equal to that delay time. Magnetic nuclei precess around a magnetic field with a characteristic frequency called the

Larmor frequency. The NMR measure involves disturbing the magnetic equilibrium of the nuclei derived from the main magnetic field. This is performed by submitting the sample to a rf field at the Larmor frequency, and then recording the return of the nuclei to its equilibrium.[270]

The question arising is: how can solid-state NMR be used optimally to analyze cellulose? How can the spectroscopist obtain high resolution spectra where broadening is removed by minimizing the dipolar spin interactions?

Energy dissipation can be described in terms of three different relaxation time constants:

- the spin-lattice relaxation time constant T_1,
- the rotating-frame relaxation time constant $T_{1\rho}$,
- the spin-spin relaxation time constant T_2.

The relaxation properties of ^1H nuclei can be studied directly by ^1H NMR or indirectly by transfer of magnetisation to ^{13}C nuclei.

T_1

The spin-lattice relaxation time T_1 is a time constant due to the return of a nuclei ^1H or ^{13}C from a higher energy level to a lower one. The energy gap between those two energy levels is $E = h\nu$. In an NMR experiment, quanta $h\nu$ of magnetic energy are initially absorbed by the nuclei before being released in the form of thermal energy. During the process, nuclei energy goes up one level and then down to its initial energy level.

If ω_C is the ^{13}C resonance frequency in radians/second and τ_R the rotational correlation time, the value of T_1 is at a minimum when $\omega_C.\tau_R \approx 1$. A given value of T_1 will yield two possible values of τ_R (Figure 27).[271] In the case of biopolymers, often, no solution of τ_R can be excluded on physical grounds. Hence, to determine the correct τ_R, T_1 should be determined at several resonance frequencies by using two spectrometers or otherwise.[271, 272] T_1 in solid

polymers are in the order of tens of seconds, which regrettably makes time-averaging process tedious.[273]

High power decoupling and T_2

A system of rare *S* spins is detected by observing its accumulative effects on an abundant spin system (spins *I*). The *I* and *S* spins cannot be decoupled directly since their mutual interaction is the thermodynamic link used for detection.[274] Instead, the *I* spin thermodynamic energy is used as a source of polarization. Following the *I*-*S* contact, the so-called **cross-polarization (CP)**, the *S* spin decay is directly observed. It is the same *I*-spin irradiation used for the spin locking that initiates the spin decoupling and hence the high resolution. The *S* signals accumulated over the repetition of the cycles until the *I* magnetization is depleted produce a large sensitivity enhancement over a conventional *S* free induction decay (Figure 28).[274]

A matched spin-lock (or Hartman-Hahn) CP experiment is a lot faster than a spin-lattice relaxation one.[273] In the case of polymers, static dipolar interactions lead to a polarization of the carbons by a transfer from nearby protons spin locked in their own rf field.[273] This is what is called a T_2 or spin-spin type process. The advantage of it over a spin-lattice relaxation process is its relatively short duration, around 100 μs. T_2 is depending on the strength of the decoupling field.[275]

$T_{1\rho}$

Spin-lattice relaxation experiments are more sensitive to motions of polymers in the 20 MHz range. Whereas this can provide useful information as to the ^{13}C relaxation parameters, it is not prone to unveil the molecular information required to the understanding of glassy polymers.[273] Ideally, high-sensitivity experiments about the motion of polymers in the 20 kHz area would provide datasets related to slow main chain motions below their glass

transition temperature. The ^{1}H rotating-frame relaxation time constant $T_{1\rho}$ is associated with motions in the 10-100 kHz, which is well adapted. However, as often observed when the proton time relaxation is studied, spin diffusion reduces ^{1}H $T_{1\rho}$ to an average over all the protons in the sample. As an answer to this problem, the low-abundant and well-separated carbons experience largely inferior spin diffusion phenomenon. Therefore, the relatively short ^{13}C $T_{1\rho}$ is a source of useful information. It is dominated by spin-lattice processes.[273]

Magic angle spinning (MAS).

In 1959, Lowe showed that a solid rotating about an axis oriented at an angle θ_H with respect to a uniform magnetic field $H_o\mathbf{z}$ had different spinning echoes decays depending on the angle.[276] The orientation of the spinning axis could be varied with regard to the applied magnetic field H_o and for angles superior to zero, the NMR line shapes could be narrowed while free induction decay was seen to create a series of side-peaks. A maximum effect is maximised when $\theta_H = 54.7^{\circ}$which corresponds to the angle of a cube's diagonal when the primary magnetic field is applied parallel to the cube's ridge.[270] This discovery paved the way to magic angle spinning (MAS) in solid polymers. Its effectiveness was detailed later on in, for instance, Schaefer's *et al.* article published in 1977.[273] The same author showed that MAS could be combined with cross polarization to produce strong signals in highly resolved spectra from all types of carbon. MAS is used to eliminate the angular chemical shift anisotropy, and so those spectra obtained by CP MAS ^{13}C NMR contain *isotropic* chemical shift information in analogy to liquid-state ^{13}C NMR with proton decoupling.[89]

Those highly resolved peaks facilitate the interpretation of the CP ^{13}C NMR spectra of solid polymers (Figure 29).[273]

^{13}C NMR

^{13}C NMR provides detailed spectra of cellulose by supplying excellent signal dispersion.[272] A plethora of information can be extracted from those spectra. For example, the position of the C-1, C-4 and C-6 peaks varies with the non-crystalline content and provides signature for the lattice conformation.[70, 110] Development of ^{13}C NMR provides lines narrow enough to distinguish between the carbons.[273]

NMR apparatus

An NMR facility usually comprises three main components: the spectrometer itself, the probe (Figure 30) and the timing and signal-processing computer.

The spectrometer comprises a powerful solenoid making up for the external magnetic field. The magnetic field is in the order of several Teslas (2 to 9 T). In the case of a double resonance experiment, two synthesizers provide the basic rf for the two frequencies.[274] The intermediate frequency is split into four channels. Three of them are gated through the ^{1}H network and controlled by the pulse programmer in order to produce the ^{1}H pulse sequence signals with relative phases 0°, 90° and 180°. The remaining channel and the other synthesizer makes the ^{13}C signals. Reception is usually made with a tuned preamplifier and dual phase detection produces quadrature free induction decay signals for processing by by complex Fourier transformation. A probe comprising two coils is placed in the main solenoid geometry. A computer is in charge of digitizing and storing the free induction decay

More details are available in the literature.[274] At this stage it should be emphasized the total impossibility to explain in the present work all of the NMR concepts in details. A large amount of literature is available to the reader wanting to explore the NMR subtleties in detail. The next section will instead explain why solid-state NMR historically enabled the comprehension of the cellulose paracrystal.

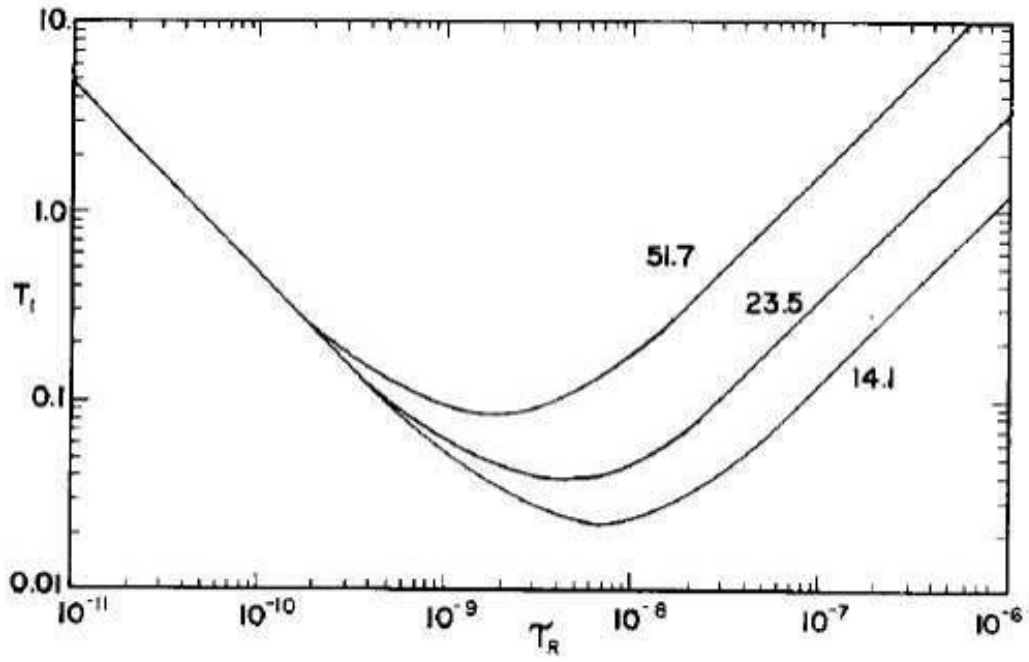

Figure 27 Log-log plot of T_1 vs τ_R (both in seconds0 for a ^{13}C spin relaxing by a dipolar interaction with a single proton 1.09 Å away (typical directly bonded C-H distance); in the case of isotropic rotational reorientation and under conditions of complete proton decoupling. Results are shown for 14.1 kG ($\omega_C = 9.48\times10^7$ rad/sec, $\omega_H = 3.77\times10^8$ rad/sec), 23.5 kG ($\omega_C = 1.58\times10^8$ rad/sec, $\omega_H = 6.29\times10^8$ rad/sec), and 51.7 kG ($\omega_C = 3.48\times10^8$ rad/sec, $\omega_H = 1.38\times10^9$ rad/sec).[271]

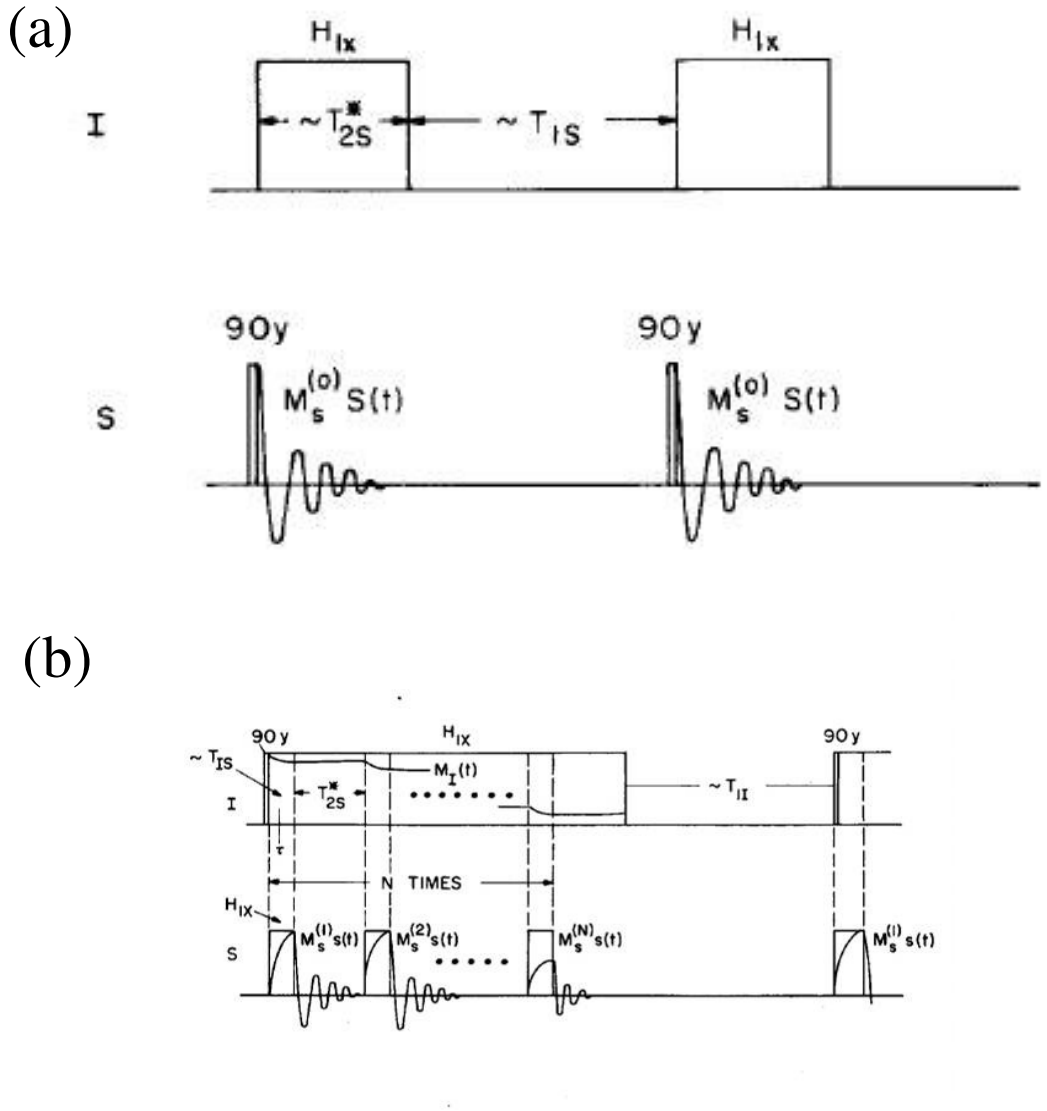

Figure 28 (a) Conventional high-resolution S free induction decay with *I*-spin decoupling. θ_y indicates a $\theta°$ pulse about the y axis of the appropriate rotating frame and H_{1x} continuous irradiation along x. The *S* spins are polarized every ~T_{1S} and then observed following a 90° pulse while continuously irradiating the *I* spins. For purposes of the analysis in the text it is imagined that $T_{1S} >> T_{2S}^{*}$. *S*(*t*) is the normalized S free induction decay. (b) One particularly simple version of proton-enhanced nuclear induction spectroscopy, using *I*-*S* cross polarization. Of the *I* spins in ~T_{1I}, the *I* magnetization is spin locked at resonance along H_{1I} in the *I* rotating frame. The *S* spins are brought into contact with the *I* reservoir by applying a resonant H_{1S} such that the Hartman-Hahn condition is satisfied. The spin systems come rapidly to equilibrium causing a small decrease in M_I and a growth of M*s* along their H_1 fields. This is indicated schematically in the figure by the curves in side the H_1 irradiation blocks. The H_{1S} field is then removed and the *S* free induction decay observed while continuing the *I* irradiation for spin decoupling.[274]

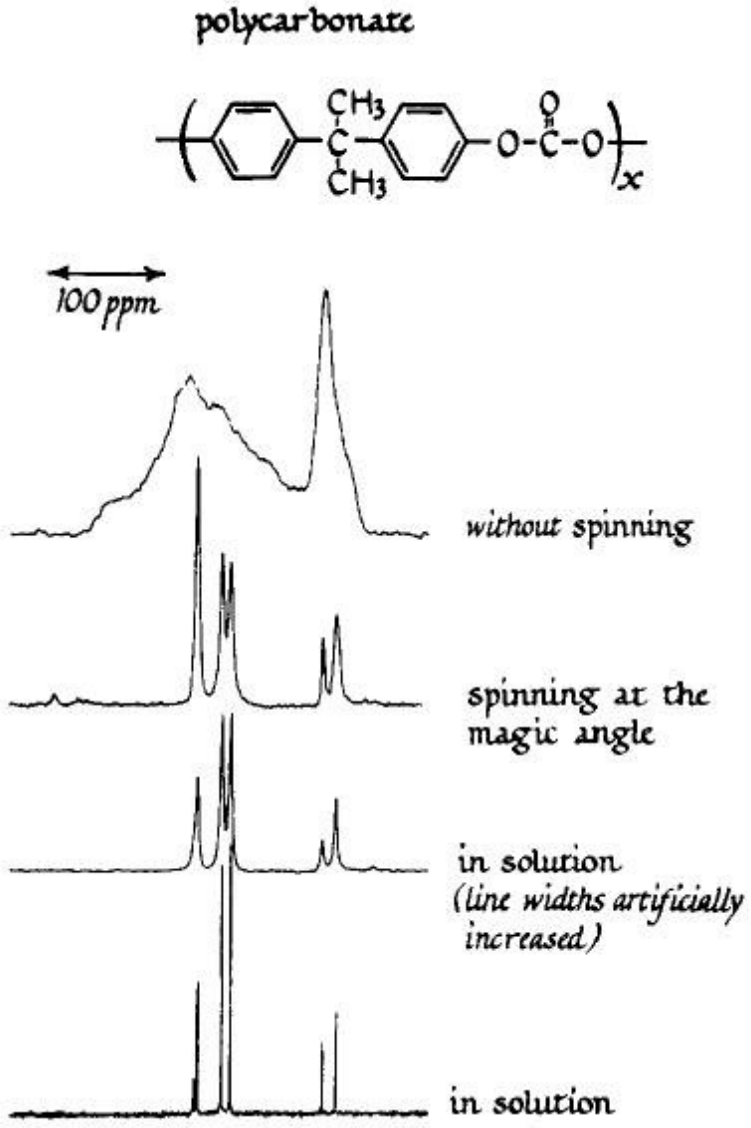

Figure 29 Cross-polarization ^{13}C NMR spectra of polycarbonate, with and without magic-angle spinning. The CP spectra are compared to a FT spectrum of the polymer in solution (with solvent lines omitted for clarity of presentation). The FT spectrum is not fully relaxed.[273]

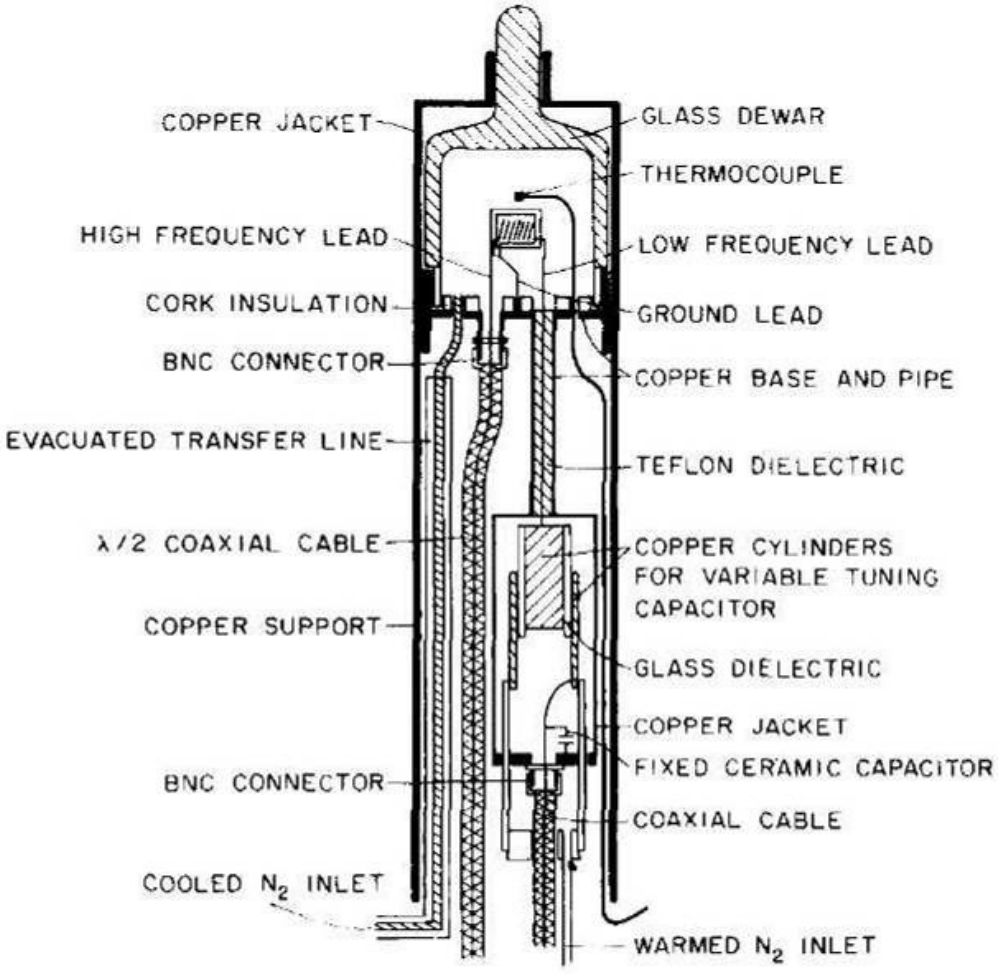

Figure 30 Schematics of an NMR probe.[274]

7.2.3.2 ^{13}C solid-state NMR: an instrument for the scientist interested in cellulose

Whereas cellulose was practically one of the very first materials examined by X-ray spectroscopy (the first X-ray diffraction pattern was taken by Nishikawa and Ono in 1913), 30 years elapsed between Hahn's discovery of the spin-echo in 1950 and the first investigation of cellulose with solid-state NMR.[277] The two first articles addressing this topic, to the knowledge of the author, were simultaneously published in the same April 1980 edition of the Journal of the American Chemical Society.[278, 279] Both used high resolution cross-polarized/magic angle spinning techniques. Atalla and Gast pointed out different peak features between the spectra of cellulose I, cellulose II and amorphous cellulose (Figure 31). They assigned the peaks by analogy to the spectra of low DP cellulose in solution in dimethyl sulfoxide published nearly simultaneously.[278, 280] Earl and VanderHart produced a spectra of cellulose I and assigned the peaks to the different carbons by analogy to the spectra they obtained for glucose and cellobiose in the solid state.[279, 281] Both groups of authors observed shifts of the carbon peaks, a shift of about 1-2 ppm for the resonance lines of C-1 and C-4 and an additional shift of 3-5 ppm for the C-4 and C-6 resonances.[278, 279, 282] A first hypothesis aiming at explaining the shifts observed for the C-4 and C-6 peaks was the possible hydrogen bonding with water. The same authors ran wet and dry samples and could not observe any difference in those peaks. They concluded that the chemical shift dispersion was probably due to some irregularities in the crystal packing. In turn, changes in the hydrogen bonding occur.[279]

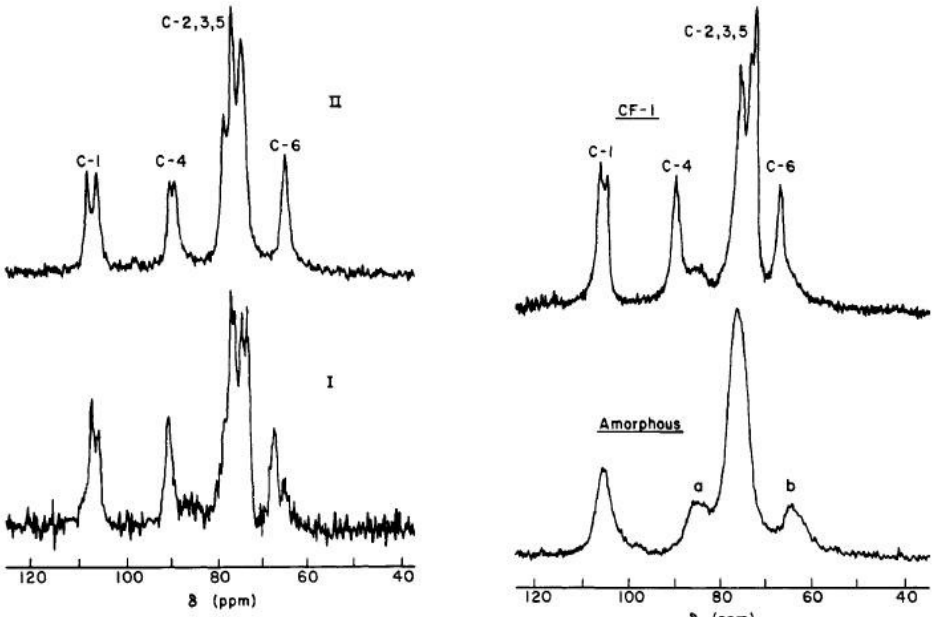

Figure 31 First published spectra of cellulose II, Whatman CF-1 cellulose, cellulose I and amorphous cellulose.[278]

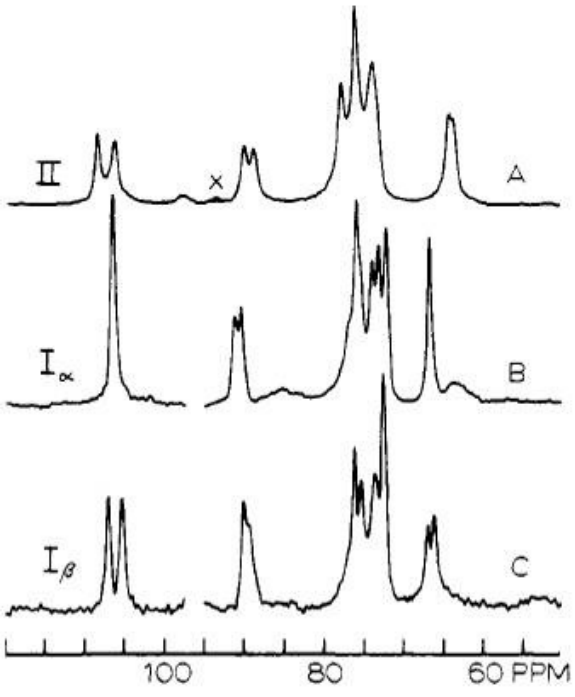

Figure 32 CP-MAS ^{13}C NMR spectrum of (A) cellulose II, (B) cellulose I_α and (C) cellulose I_β [89]

Such irregularities are not observed in the liquid-state NMR spectra as rapid molecular tumbling allows for averaging of carbon resonances; solid-state NMR involves cellulose placed in an environment with inter- and intrachain hydrogen bonds inherent to the crystalline conformation, and that gives birth to extra nuclei peaks.[280, 283] Another pertinent supposition was that the crystalline state of cellulose I implies more packing regularity than chain rigidity. The same author further detailed the idea of a supramolecular morphology affecting the spectra by comparing the NMR signals obtained from various cellulose sources.[282] Certainly, the characterization of cellulose crystallinity is not clear-cut. As pointed out by Earl and VanderHart in 1981: "the definition of crystallinity in cellulose is not entirely straightforward since one must consider the degree of order along the cellulose chain as well as the degree of lateral order or the chain packing".[282] Unquestionably, the notion of paracrystallinity, intrinsic to crystals with lattice distortions, was already lying beneath the concept of lateral order and it was well integrated in the high-resolution ^{13}C NMR spectroscopy studies of cellulose since the beginning.[77, 78, 284] The non-crystalline character of a polymer is expected to give broader lines than the crystalline one.[282] Broad peaks were attributed to less organized surface chains of cellulose whereas sharp ones were attributed to interior cellulose chains with a higher degree of lateral organization. The idea has since largely been accepted and is used in some of the most recent literature.[69, 267] Eventually, the authors pointed "striking" differences such as C-4 and C-6 resonance splitting and shoulder changes between the spectra of cotton, *Acetobacter* and *Valonia.* Peak splitting lead to the conclusion that at least two anhydroglucose moieties existed, maybe due to the existence of two non-equivalent conformations of the cellulose chains in the solid.[282, 285]

Maciel published results in 1982 that clearly showed that carbon peaks were displaced to lower chemical shifts as the crystallinity of the samples was lowered by ball-milling.[286] Though short, the work had the merit to clearly underline the difficulties associated with differentiating between crystallinity, crystal type, long-range order and short-range order

effects. In order to explain the chemical shift splittings in regenerated cellulose, Horii proposed that the "downfield peaks" (peaks with the lower chemical shift) of the C-4 and C-6 resonances were related to non-crystalline portions whereas the upfield ones were related to crystalline ones.[285] The same author proposed an NMR crystallinity index defined by "the integrated fraction f_{NMR} of the downfield resonance with respect to the total resonance of the C-4" after deconvolution of the C-4 resonances in Lorentzian functions. A linear relation between Hermans' crystallinity factor and f_{NMR} was demonstrated and thus corroborated his hypothesis.[71, 285] However, the author stated himself that the multiplicities of the C-1 and C-4 carbon resonances were both related to the crystal structure and to the crystallinity of the samples; the latter one is also true for C-6.

In 1983, Dudley *et al.* suggested that the double C-1 and C-4 peaks of cellulose II could be due to differences in the environment of those carbons arising from the symmetry of the unit cell.[88] They then suggested that a cellulose II unit cell comprising two independent chains was highly probable. On the same year, Horii published a study where the most likely conformations of the hydroxymethyl group were assigned to the different cellulose structures: *trans-gauche* was assigned to native crystalline cellulose, and *gauche-trans* to noncrystalline native, crystalline regenerated and noncrystalline regenerated cellulose.[100]

VanderHart and Atalla published on the next year the formal justification for a distinction between two forms of native cellulose, cellulose I_α and I_β, which could assemble in an *allomorphic composite* (Figure 32).[62, 89] They also discussed in length the inclusion of surface and interior chains in the C-4 and C-6 carbon resonances to come to the conclusion that the sharper resonance (higher chemical shift) reflects crystallite-interior cellulose chains with lateral order whereas the broader one (lower chemical shift) reflects the exterior chains. Of particular interest, they used the water molecule as a probe and detected its response in the cellulose matrix. In 1985, Cael *et al.* published a work corroborating the theory that all spectra of native cellulose could be considered as the linear combination of two spectra with subtle

differences and adjustments as to the results obtained from electron and X-ray diffraction.[283] They suggested that most native celluloses contain crystallite with either two- or eight-chain unit cells. Later on in 1987, Horii reappraised the idea of two native phases, cotton-ramie type I_a and bacterial-Valonia type I_b, respectively corresponding to the previously defined I_β and I_α phases.[287] In 1989, Isogai, Atalla *et al.* published the first comparative study of solid-state CP/MAS ^{13}C NMR spectra of cellulose polymorphs (Table 11).[110] Takahishi presented a similar work emphasising the effects of the starting polymorphs on the final spectra after transition to another polymorph (typically, from cellulose I or II to III or IV) in 1993.[65]

In the early nineties, Newman and Hemmingson presented a couple of papers where a difference in proton spin relaxation time was exploited to separate the crystalline and non-crystalline portions in cellulosic materials.[288, 289] A delayed contact pulse sequence is used to generate two spectra, S and S'. The signal comprises a preparation pulse t_p, a spin-locking pulse t_{sl}, a cross-polarization contact time t_c a data acquisition time t_a followed by a recovery delay t_d.[288] By varying the preparation pulse, it is possible to suppress part of the crystalline signal in one of the ^{13}C spectra. The two spectra can be deconvoluted by linear combination in order to separate the two domains.[69, 70, 288, 289] This technique was used to determine the degree of crystallinity of cellulose in wood [288] and the lignin content of cell walls.[289] Newman's 1993 work is of particular interest as it was showing a degree of molecular order in kraft residual hemicelluloses.[289] Hemicelluloses align to some extent in the cellulose crystallite length and could possibly be partly embedded in it.

Table 11 ^{13}C chemical shifts of crystalline celluloses.[110]

Polymorph	C1	C4	C6
Cellulose I	105.3-106.0	89.1-89.8	65.5-66.2
Cellulose II	105.8-106.3	88.7-88.8	63.5-64.1
Cellulose III_I	105.3-105.6	88.1-88.3	62.5-62.7
Cellulose III_{II}	106.7-106.8	88.0	62.1-62.8
Cellulose IV_I	105.6	83.6-84.4	63.3-63.8
Cellulose IV_{II}	105.5	83.5-84.6	63.7
Amorphous	ca. 105	ca. 84	ca. 63

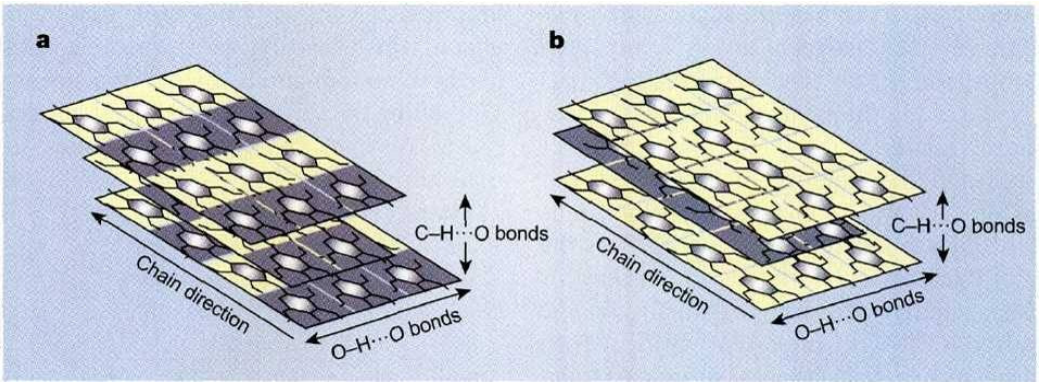

Figure 33 Symmetry and directions of hydrogen bonding in cellulose. (a) Cellulose I_α, in which all chains are crystallographically identical but alternating glucose units in each chain, shaded grey and yellow, differ slightly in conformation. (b) Cellulose I_β, in which chains of two distinct kinds are arranged in alternating sheets. Chains passing through the origin and centre of the unit cell are shaded respectively yellow and grey.[62]

High resolution CP/MAS ^{13}C NMR was useful to study the conversion of cellulose I_α to I_β and prove the coexistence of those two allomorphs in a cellulose composite.[290] In 1993 and 1995, Newman and Hemingson refined the molecular structure study of cellulose microfibrils and showed that the distinction between crystal interior, well-ordered surfaces, poorly ordered surfaces and domains of disorder could be well assessed; they extended this technique to kraft cellulose, cellulose I and II, before and after alkaline treatment and vacuum drying.[70, 265, 289] A great deal of information, such as cellulose allomorph type, crystallinity, crystal size or amorphous components proportions can be extracted directly from biological materials using the same techniques.[69, 94, 101, 291-297] A semi-empirical approach and molecular dynamics were later on used to explain some of the cellulose carbon resonances observed in cellulose I_α, I_β and II.[298] Of particular interest, the work of Kondo *et al.* in 2001 used CP/MAS ^{13}C solid-state NMR along with WAXS, FTIR, AFM and high-resolution transmission electron microscopy (HRTEM) to discern a paracrystalline category that was not belonging to any of the crystalline allomorphs, but yet sufficiently ordered to be distinguished from amorphous cellulose. They used the term "nematic ordered cellulose" in an analogy to nematic phases of liquid crystals that have no long range order but some parallelism in the direction of the molecules.[79]

Further refinement as to the molecular conformations of the hydroxymethyl groups has also been brought lately. For cellulose I_β crystallite surface chains, the most accurate description for the hydroxymethyl group conformation is probably a mixture of *gauche-trans* and *gauche-gauche* conformation, which is reflected by a peak at 60-62.6 ppm and 62.5-64.5 ppm, respectively.[100, 297]

Over the years, CP/MAS ^{13}C solid-state NMR kept on proving being a very valuable tool and provided improved structural data for cellulose I_α, I_β, II, III_I, IV_I.[75, 102, 109, 299-301] The article published in 2003 by M. Jarvis in Nature is a good example of how the solid-state NMR

could contribute the complex model of cellulose I_α and I_β combination in an allomorphic composite (Figure 33).[62]

Generally speaking, solid-state NMR is a remarkable tool as it can provide information about cellulose even if this material is embedded into a matrix of lignocellulosics. In the particular case of cellulose, it is commonly admitted that NMR brings more useful quantitative data about small cellulose crystallites (< 30 Å in width) than does WAXS because it is not limited to the chains interior to the crystals. It shows the cellulose chains that are interior and exterior to the crystals as well as the truly amorphous material.

7.2.3.3 Experimental details

Each composite was crushed to particle dimensions of ~0.5 mm, combined with a similar or larger weight of water, and packed into a zirconium oxide rotor. Excess water was expelled during packing to prepare samples with a typical solids content of 55% by dry weight. The rotor was sealed with a Kel-F® cap.

Solid state CP-MAS ^{13}C NMR spectra were obtained on a Bruker Avance DRX200 FT-NMR spectrometer at a frequency of 50.3 MHz and at a magic-angle spinning frequency of 5 kHz. Each 90° proton preparation pulse of 5 μs was followed by a delay τ, a contact time of 1 ms, acquisition time of 20 ms, and a recycle delay of 1 s. Two spectra were acquired for each sample and labelled **S** (τ = 1 μs) and **S'** (τ = 15 μs). Bold type is used for these symbols since they represent vectors, i.e., lists of the signal heights measured across a range of chemical shifts. Transients from a minimum of 10,000 pulses were averaged in both cases.

Signals from crystalline cellulose were partly suppressed in **S'**, through relatively rapid T_2(H) decay during the delay τ. The discrimination was enhanced by proton spin relaxation editing (PSRE). This method is more commonly used to process spectra modified by rotating-frame relaxation [69] but has been used to process spectra modified by T_2(H).[292] PSRE involves computing linear combinations:

$$\mathbf{A} = k\mathbf{S} + k'\mathbf{S}' \quad (9a)$$

$$\mathbf{B} = (1 - k)\mathbf{S} - k'\mathbf{S}' \quad (9b)$$

The values of k and k' are adjusted until signals assigned to poorly-ordered matter are excluded from **A** and signals well-ordered matter are excluded from **B**. In this case, signals at 80 ppm and 89 ppm were assigned to C-4 in poorly-ordered and crystallite-interior cellulose, respectively.[69] Details concerning the adjustment of k and k' can be found elsewhere.[70] The fraction F of crystalline cellulose in each composite was estimated by dividing the area of **A** by area of **S**.

The subspectra labeled **A** showed two partly-resolved C-4 signals, assigned to crystallite-interior and crystallite-surface glucosyl residues, at 89 ppm and 84 ppm respectively. Signal areas were delimited by the baseline and a vertical line drawn at 86.4 ppm. Relative areas were used to estimate the percentage X of cellulose chains contained in crystallite interiors.[69] Assuming a simplified model of a square cellulose crystallite with cross-sectional dimensions $L \times L$ and only a monolayer of cellulose chains exposed to the surface, an estimate of the apparent average crystallite size can be given by the expression [69]:

$$L = 1.14 / (1 - X^{1/2}) \quad (10)$$

7.2.4 TEM

All-cellulose composite samples were impregnated in spurr resin using a step impregnation procedure. The samples were first soaked in distilled water overnight. They were then dehydrated with acetone by steps of 30 min. Samples were successively soaked in 20%, 40%, 60% and then 80% aqueous acetone and then dehydrated in pure acetone overnight for greater solvent penetration. Acetone was exchanged twice more with 30 min steps. The samples were then soaked in a mixture of 3/4 acetone and 1/4 spurr resin and soaked overnight. This step was repeated twice by replacing the impregnation medium with a mixture of 3/4 spurr

resin and 1/4 acetone, and then finally using pure spurr resin. The samples were then dried at 60°C overnight to cure the resin. A similar procedure was trialled with an acrylic resin (LR white), but the samples were too brittle and inappropriate for microtoming. 100 nm sections were cut on an ultramicrotome (LKB 2128 Ultrotome IV) and placed on copper grids for TEM.

The samples were stained by immersion in uranyl acetate (negative staining). The grids were placed in droplets of uranyl acetate (1% in 50% ethanol) for 10 min, washed in 50% ethanol and two changes of distilled water, and placed in lead citrate for a further 5 minutes, followed by two distilled water rinses. Low resolution TEM was initially performed with a FEI Morgagni TEM with an accelerating voltage of 100 kV.

In order to produce 3-D reconstructions, high resolution TEM with tomography was also performed (Hitachi 300 kV). Gold particles were applied to the TEM grids by placing them for 5 min on each side in a drop of 15 nm gold colloidal suspension. The tomogram was reconstructed out of 87 micrographs obtained by tilting the sample in 1.5° increments from 0° to 64.5° and then from 0° to -64.5°. The micrographs were first stacked and aligned for the 3-D reconstruction. The reconstructed features were then rendered. IMOD (www.bio3d.colorado.edu) was used for the 3-D reconstruction and modelling. Reconstructions were approximately 50-60 nm in thickness.

7.2.5 Optical microscopy

Direct visualization of the dissolution and regeneration steps by optical microscopy (OM) was used to better understand the partial dissolution of cellulose in LiCl/DMAc and its precipitation in water.

The dissolution kinetics of MCC for two different cellulose concentrations were studied. The first solution was prepared by mixing ~0.1 g of activated MCC and ~1 mL of 8 wt.% LiCl\DMAc solution in a small glass beaker, with a resulting mixture comprising less than 10

wt.% cellulose. The second solution was prepared by mixing ~1 g of activated MCC with 4 g of 8 wt.% LiCl\DMAc solution, giving a cellulose concentration of ~20 wt.%.

A single drop from each solution was placed on a glass slide and covered with a glass slide cover. The specimens were then placed in an Olympus BH optical microscope and observed under polarized light. The dissolution process was then recorded in real time for 4 hours with a Spotlight digital camera. For the 20 wt.% specimen, a drop of distilled water was placed along the edge of the glass cover in order to observe water diffusion and hence cellulose regeneration in real-time over a period of 4 h.

7.2.6 Fourier transform infrared spectroscopy (FTIR)

FTIR spectra were acquired in transmission on an FTIR-8201 PC Shimadzu equipped with the software Hyper IR. Transmission FTIR was used to analyze as-received MCC, activated MCC and all-cellulose composites. The composites were first crushed in ~0.5 mm particles. 2 mg of cellulose was mixed with 200 mg of KBr and ball-milled for 5 min. Pellets were made by pressing the mixture for 2 min in a cylindrical mould using a 12 tonne press. Samples were dried at 60°C for 48 h. Spectra were averaged from 16 scans from 4000 to 400 cm^{-1} and obtained with a resolutionof 2 cm^{-1}. The crystallinity index was calculated as the ratio of the absorption peaks at 1372 and 2900 cm^{-1} after Nelson *et al.*.[72]

7.3 Results and discussion

7.3.1 WAXS

Activation of the MCC showed only a minor effect on the WAXS diffractogram (Figure 34). The peak assigned to (200) planes appeared at $2\theta = 22.6°$ and 22.8° in as-received MCC and activated MCC, respectively, as in published WAXS diffractograms for cellulose I.[110, 185, 227] The full widths B at half maximum height were 1.75° and 1.68°, giving crystal thicknesses of 4.5 and 4.9 nm, respectively, according to Equation (7).

Peaks at 2θ = 15.1°, 16.8° and 34.8° in the diffractogram for activated cellulose were also consistent with peaks in published WAXS diffractograms for cellulose I.[110, 227] The crystallinity index *CrI* calculated from Equation (8) decreased from 87% for MCC to 80% after activation (Table 12).

The WAXS diffractograms for all-cellulose composites showed a small shoulder at 2θ = 20.8° that progressively developed into a distinct diffraction peak with decreasing cellulose concentration in the solvent (Figures 35a and 35b). The peak was more distinct in composites prepared with a dissolution time of 8 h (Figure 35b), relative to 1 h (Figure 35a). Plots for other dissolution times indicated that equilibrium was reached after approximately 4 h, with little further change to 48 h. Gindl and Keckes (2005) observed this peak in WAXS diffractograms of all-cellulose composites, and assigned it to regenerated cellulose.[26] They observed a similar peak in a WAXS diffractogram of cellulose produced by dissolving cellulose II in LiCl/DMAc and regenerating it.

The peak at 2θ = 20.8° was 5.0° wide at half maximum height, and this width was too small for the peak to be assigned to amorphous cellulose. Ball-milled cellulose is commonly used as a reference standard for amorphous cellulose. The peak position has been reported as 2θ = 18° [66, 68] or 2θ = 20° [82], but it is generally agreed that the width is approximately 10°. The width of 5.0°, observed in Figure 35, corresponds to a crystallite thickness of D = 1.6 nm according to Equation (7). For (200) planes separated by 0.4 nm that corresponds to crystallites containing just 4 planes.[73]

A commonly-used crystallinity index *CrI*, expressed in Equation (8), exploits the fact that the maximum for amorphous cellulose falls between peaks in the diffractogram for cellulose I. The diffractograms in Figures 35a and 35b showed increasing height at 2θ = 18°, for increasing degrees of transformation, but the value of *CrI* never dropped below 32% (Table 12 and Figure 36).

Gjønnes and Norman (1958) and Ioelovich and Larina (1999) reported lattice expansion in thin crystallites of cellulose I, so that an increase in peak width was associated with a displacement to low values of 2θ.[259, 268] A curve published by Gjønnes and Norman (1958) indicated that an increase in peak width to 7° was sufficient to displace the peak to 2θ = 21°.[268] The peak at 2θ = 20.8° in Figures 35a and 35b is therefore consistent with cellulose I crystallites split to fine dimensions.

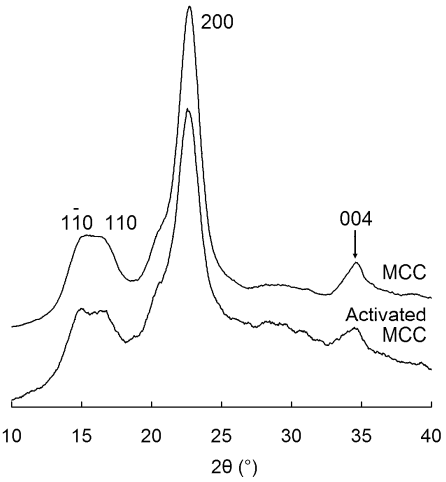

Figure 34 WAXS diffractograms of MCC before and after activation. Peaks assignments use the monoclinic cellulose I unit cell of Sugiyama *et al.* (1991).

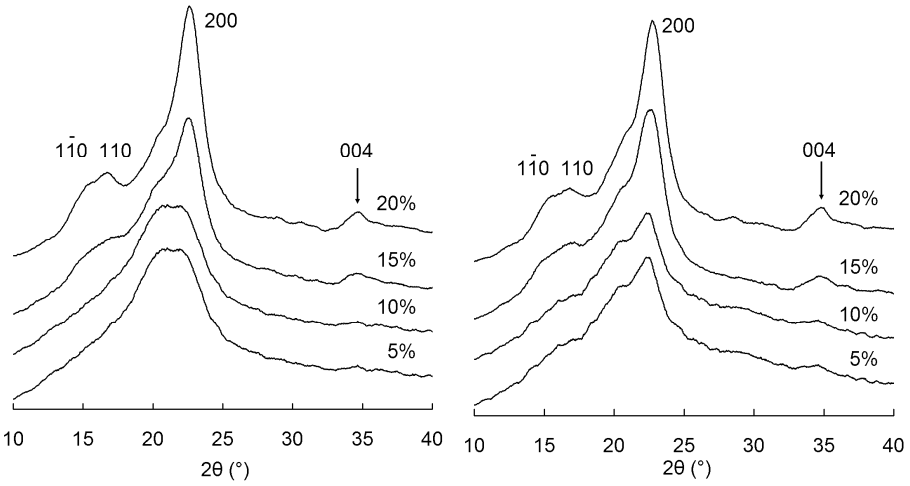

Figure 35 WAXS diffractograms of all-cellulose composites prepared from activated cellulose by partial dissolution for (a) 1 h and (b) 8 h with values of c shown above each trace.

When regenerated cellulose crystallizes to the cellulose II allomorph it shows WAXS peaks at 2θ = 12.1°, 19.8° and 22.0°.[110] Changes in lattice dimensions influence the positions of WAXS peaks for cellulose II, but the pattern of displacements is different from that for cellulose I. Gjønnes and Norman (1960) showed that the peak at 2θ = 19.8° is displaced to higher values, and the peak at 2θ = 22.0° to lower values, as the peaks broaden.[302] Extrapolation from their data suggested that the two peaks might form a single peak, with a width of approximately 7°, at a value of 2θ somewhere between 20° and 21°. Yamashiki *et al.* (1992) confirmed movement towards an intermediate value of 2θ by published WAXS diffractograms for cellulose II as Viscose and cuprammonium rayons, showing a broad peak at 2θ = 20.0° with a shoulder at 2θ = 21.6°.[144] The peak at 2θ = 20.8° in Figure 35b is therefore indistinguishable from the pattern predicted for very narrow crystallites of cellulose II.

Cellulose III, when prepared from cellulose I, shows a strong WAXS peak 2θ = 20.7° and a weaker peak 2θ = 11.7° (Isogai *et al.* 1989).[110] The former peak matched the broad peak in WAXS diffractograms of the most severely treated specimens (Figures 35a and 35b), but the latter was not observed.

Table 12 Crystallinity index *CrI* of different all-cellulose composites obtained with an initial cellulose concentration *c* and a dissolution time t.

CrI	**t = 1 h**	**t = 4 h**	**t = 8 h**	**t = 48 h**
***c* = 5%**	0.43	0.37	0.39	0.36
***c* = 10%**	0.49	0.47	0.39	0.35
***c* = 15%**	0.59	0.54	0.59	0.54
***c* = 20%**	0.68	0.64	0.71	0.67

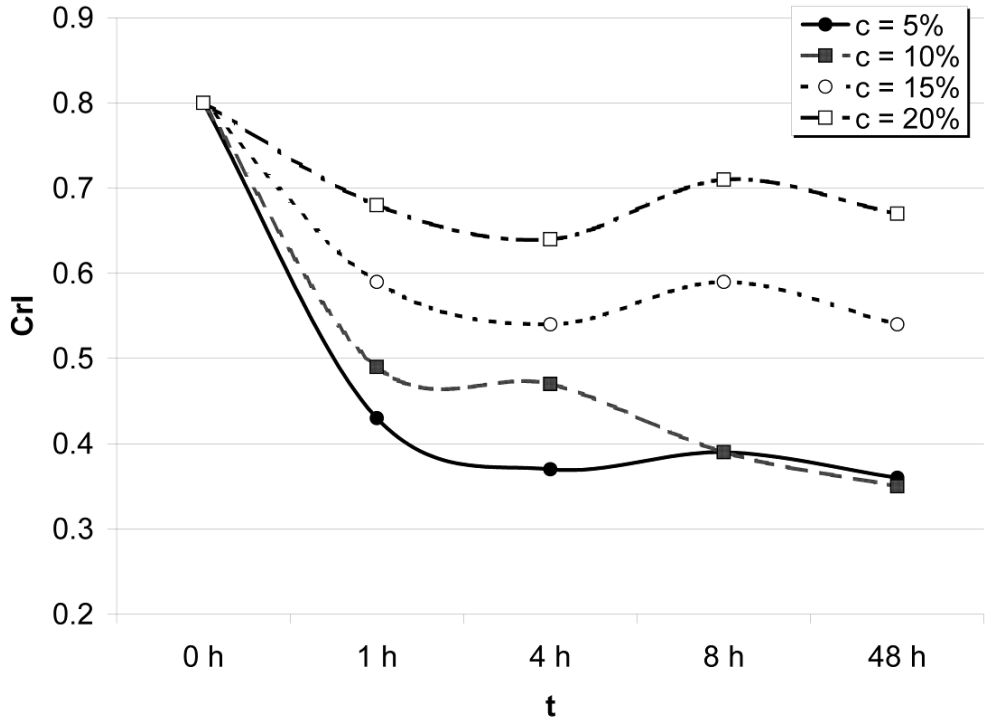

Figure 36 CrI of the composites

The peak assigned to (200) planes of cellulose I remained visible as a shoulder at 2θ = 22.3° in WAXS diffractograms of specimens with the greatest degrees of transformation, i.e., the lower two traces in Figures 35a and 35b. The shoulder was too weak for measurement of the peak width, but the curve published by Gjønnes and Norman (1958) indicated that displacement to 2θ = 22.3° corresponded to a peak width of 3°, for which Equation (7) indicated a crystallite thickness of approximately 3 nm.[268] The diffractogram of MCC (Figure 34) showed a peak assigned to (004) planes. This peak was weak or absent in diffractograms of all-cellulose composites prepared with the greatest degrees of transformation, e.g., the lowest diffractogram in Figure 35b. The disappearance of this peak suggests longitudinal disorder, consistent with a paracrystalline matrix.

7.3.2 Solid-state NMR

The ^{13}C NMR spectrum of activated MCC (Figure 37) resembled a published spectrum of Avicel MCC (Newman and Hemmingson 1995), confirming WAXS indications of little change in molecular packing associated with activation.[70] Minor changes were revealed by PSRE (Figure 37). In the published PSRE results (Newman and Hemmingson 1995) subspectrum **A** accounted for 84% of the area of the total spectrum **S**.[70]This proportion decreased to 73% after activation (Figure 37), indicating transformation of some of the cellulose I to a less ordered form of cellulose. A published ^{13}C NMR study of Avicel MCC indicated a crystallite width of L = 5.9 nm (Newman 1999).[69] Peak areas in subspectrum **A** of Figure 37, interpreted according to the same procedure, indicated a crystallite width of L = 6.3 nm for activated MCC (Table 13).

Figure 38 shows ^{13}C NMR spectra of the composites regenerated after a dissolution time of 8 h. Peaks are assigned to cellulose I, as in Figure 37. Cellulose II would have contributed a peak at 108 ppm, assigned to C-1 in crystallite-interior chains (Hemmingson and

Newman 1995; Newman and Hemmingson 1995).[70, 265] No such peak was detected in Figure 38, so there was no evidence for regeneration to cellulose II in crystallites of sufficient size for chains to be enclosed.

A peak at 89 ppm was assigned to C-4 peak of crystallite-interior chains of cellulose I. This peak was observed in all of the spectra in Figure 38, but decreased with decreasing values of *c*. PSRE was used to split the NMR spectra into subspectra labeled **A** (Figure 39), assigned to crystalline cellulose, and subspectra labeled **B** (Figure 40), assigned to cellulose that was less well ordered.

The fraction *F* of cellulose associated with subspectrum A dropped steadily from 0.84 for MCC to $F = 0.24$ for the composite treated for 8 h at $c = 10\%$, then rose to $F = 0.37$ for $c = 5\%$ (Table 13). The last of these values might have been distorted by the difficulty in separating subspectra A and B.

Relative peak areas within subspectrum A were used to calculate *X*, i.e., the crystallite-interior cellulose expressed as% of crystalline cellulose contributing to subspectrum A. The values (Table 13) confirmed the visual impression (Figures 38, 39) of a steady decline in *X* as the value of *c* was decreased. The values of *X* were used to calculate crystallite widths *L*, according to Equation (10). Values (Table 13) indicated a decrease to $L = 2.3$ nm for the most severe treatment.

The chemical shift for C-4 is particularly sensitive to the conformation of a cellulose chain (Horii *et al.* 1987).[287] Chemical shifts in the range 79 to 81 ppm are characteristic of the random-coil conformation of cellulose dissolved in trifluoroacetic acid (Bock *et al.* 1991) [197] or regenerated as amorphous cellulose (Hirai *et al.* 1990; Newman and Hemmingson 1995).[70, 87] Chemical shifts in the range 84 to 90 ppm are characteristic of the linear conformations of chains in crystalline cellulose (Horii *et al.* 1987).[287] El-Kafrawy (1982) dissolved cellulose in LiCl/DMAc and observed a C-4 peak at 79 ppm, confirming a true solution of random-coil cellulose.[303] All of the traces in Figure 40 showed a dip at 80 ppm,

labeled C-4a, but the fact that the dip did not extend to the baseline suggested a contribution from amorphous cellulose. Most of the C-4 signal area was found in a peak at 84 ppm, i.e., the same chemical shift as reported for C-4 in cellulose chains in linear molecular conformations exposed on the surfaces of cellulose I, with hydroxymethyl groups in the *gauche-gauche* conformation (Newman and Davidson 2004).[304] The C-6 signal area was found in a peak at 62 ppm, also consistent with chains exposed on surfaces of cellulose I (Newman and Davidson 2004).[304]

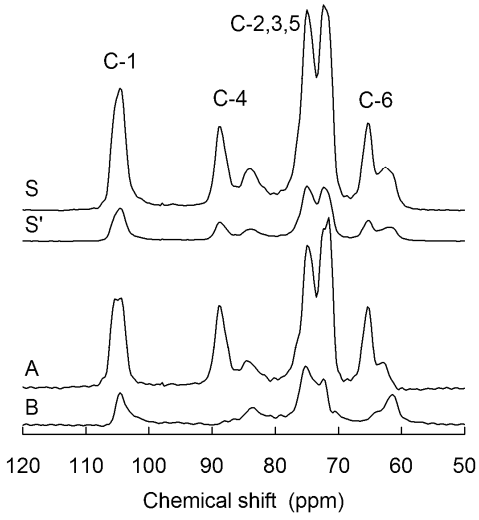

Figure 37 Solid-state 13C NMR spectra of activated cellulose. Experimental results are labeled S and S'. PSRE subspectra A and B are assigned to crystalline and less-ordered cellulose, respectively.

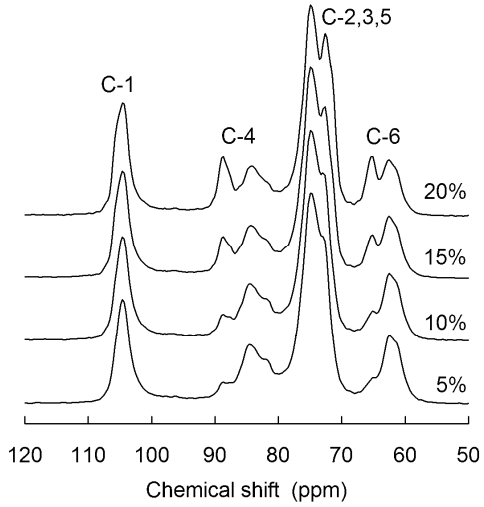

Figure 38 Solid-state 13C NMR spectra of all-cellulose composites prepared from activated cellulose mixed with solvent at the weight % values shown above each trace and left for 8 h of dissolution.

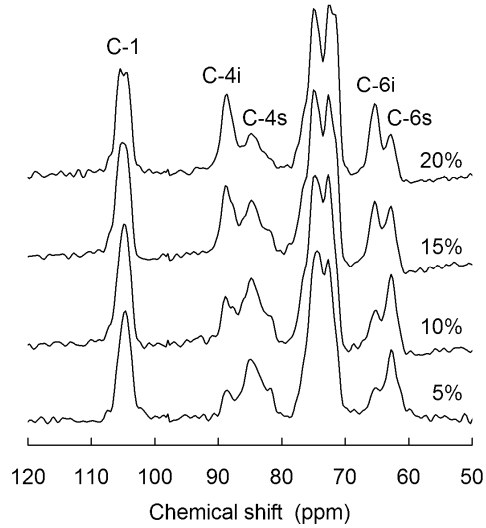

Figure 39 Subspectra A separated from solid-state 13C NMR spectra of all-cellulose composites prepared from activated cellulose mixed with solvent at the weight % values shown above each trace and left for 8 h of dissolution. Labels C-4i and C-4s indicate chemical shifts for the chains of the interior and surface, respectively, of cellulose I.

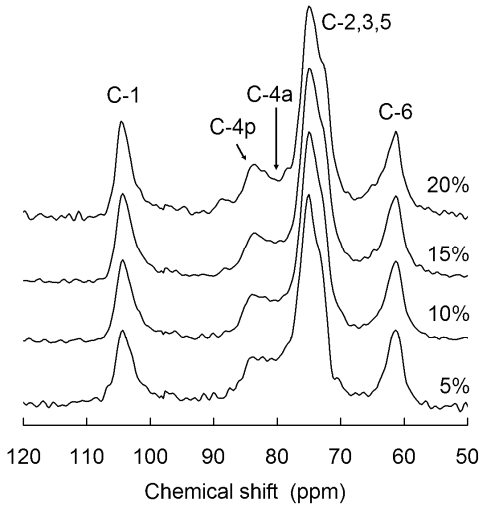

Figure 40 Subspectra B separated from solid-state 13C NMR spectra of all-cellulose composites prepared from activated cellulose mixed with solvent at the weight % values shown above each trace and left for 8 h of dissolution. Labels C-4a and C-4p indicate chemical shifts for amorphous and paracrystalline cellulose, respectively.

Table 13 Data for starting materials and all-cellulose composites prepared by partial dissolution for 8 h at cellulose concentrations *c* expressed as % of the total weight of cellulose, LiCl and DMAc.

Sample	*CrI* (%)	*D* (nm)	*F*	*X* (%)	*L* (nm)
MCC	87	4.5	(0.84)[a]	(65)[a]	(5.9)[a]
Activated	80	4.8	0.73	67	6.3
c = 20%	71	-[b]	0.56	61	5.2
c = 15%	59	-[b]	0.52	49	3.8
c = 10%	39	-[b]	0.24	32	2.6
c = 5%	39	-[b]	0.37	24	2.3

It is possible to construct models for crystallites of cellulose I in which all chains are exposed on surfaces, but the widths must be no more than 2 nm. Such crystallites might be described as 'paracrystalline', so we have used the label C-4p in Figure 40.

The combination of C-4 and C-6 peaks at 84 and 62 ppm, respectively, has also been reported for the NMR spectrum of cellulose IV (Isogai *et al.* 1989).[110] This is consistent with a suggestion that cellulose IV is simply a poorly-crystalline form of cellulose I (Tsuda and Mukoyama 1957; Wada *et al.* 2004).[109, 112] Cellulose IV has been identified as a product of the Viscose process for regenerating cellulose (Tsuda and Mukoyama 1957).[112] It is also an intermediary allomorph formed during the ball-milling of cellulose I or II; extensive ball-milling usually produces amorphous cellulose.[121] Maciel noticed in his 1992 publication that a small peak at 98 ppm corresponding to the C-1 monomer unit of the end group of the cellulose chain appeared after extensive ball-milling.[286] Such a resonance was not observed here, so the analogy between partial cellulose dissolution and ball-milling does not hold true when it comes to the polymer chain cleavage into smaller chains, as it means an superior number of end-groups. This was expected as the LiCl/DMAc solvent is known to cause virtually no cellulose chain disruption.

Chemical shifts for crystallite-surface chains in cellulose II have been reported as 88.0 and 86.5 ppm (C-4s) and 63.2 and 62.9 ppm (C-6s) (Newman and Davidson 2004).[304] Those chemical shifts differ from the values observed in Figure 40. Hong (1998) reported evidence for cellulose III in cellulose fibre regenerated from LiCl/DMAc.[143] The chemical shifts for crystallite-interior cellulose III are similar to those for cellulose II (Isogai *et al.* 1989), but crystallite-surface signals have not been reported.[110]

The relevant proton spin relaxation time constants provide clues to the nature of the matrix. The experiments described in this paper were based on differences in T_2(H) between crystallites and the matrix. Subspectra were separated from spectra of the primary walls of *Arabidopsis thaliana* by Newman *et al.* (1996), and the values of k and k' in Equation (3)

indicated T_2(H) = 8.5 μs and 19 μs for crystalline cellulose and amorphous matrix polysaccharides, respectively.[292] Using the same expressions for *k* and *k*' in the present work indicated T_2(H) = 8.6 μs and 11 μs for crystallites and matrix, respectively. The value of T_2(H) for the cellulosic matrix was not greatly increased over the value for the crystallites, suggesting paracrystallinity rather than amorphicity.

The subspectra stacked in Figure 40 could not be used to determine the relative proportions of paracrystalline and amorphous cellulose, since the C-4 peaks were not resolved. Overlap between the C-4 and C-2,3,5 bands might even account for much of the signal strength in the dip at 80 ppm.

Kondo *et al.* (2001) introduced the concept of 'nematic ordered cellulose' to cover intermediate states of molecular ordering such as those described in this work, i.e., states that display some of the features of each of the crystalline allomorphs of cellulose, yet no perfect match to any one of those allomorphs.[79, 254]

Comparisons between WAXS and NMR

The WAXS index *CrI* showed strong correlations with both of the NMR indices tabulated in Table 13. Linear least-squares fits gave correlation coefficients R^2 = 0.92 and 0.94 for *CrI* against *F* and *X* respectively. The correlation coefficient rose to R^2 = 0.99 for *CrI* against the product *FX*, i.e., crystallite-interior cellulose expressed as % of total cellulose.

The crystallite dimensions *D* and *L* showed similar trends, i.e., decreasing cross-sectional dimensions as a result of partial dissolution. A perfect match was not expected for these parameters, since they represent cross-sectional measurements in orthogonal directions: *D* perpendicular to the (200) planes, *L* across those planes (Newman 1999).[69]

Transformation mechanisms

When considered together, the WAXS and NMR results suggest the following mechanism. Exposure to LiCl/DMAc peels layers of cellulose from crystallites. The residual

core of the crystallite becomes thinner as successive layers are removed. The peeled layers might retain some of the molecular ordering of the cellulose I structure from which they were removed, but are too thin to contain crystallite-interior chains. Those might be precipitated forms of the aggregates present in cellulose solutions that are known to keep reminiscents of the initial cellulose form.[305] When the LiCl and DMAc are washed away, the peeled layers of cellulose are regenerated into a paracrystalline matrix. The paracrystalline structures are sufficiently disordered to show T_2(H) values slightly longer than those characteristic of crystalline cellulose. On the other hand, they are sufficiently distinct from amorphous cellulose to show a WAXS peak just half as broad. They are also sufficiently distinct to show a 4 ppm displacement of the C-4 ^{13}C NMR peak, from 80 ppm for amorphous cellulose to 84 ppm for the matrix of the composites.

The partly-ordered nature of the matrix helps account for the superior mechanical properties observed for all-cellulose composites.

Using relatively high concentrations of cellulose in LiCl/DMAc has several advantages. Above all else, it minimizes the shrinkage undergone by the material during the precipitation and drying stage. This minimizes many manufacturing constraints like large mould opening, shape loss or amount of residual water in the material before drying. There are also financial, environmental and health interests in minimizing the amount of solvent used for a given amount of polymer. Conio *et al.* (1984) suggested that a concentration $c < 15\%$ was necessary for partial dissolution in 8% LiCl/DMAc, and a concentration $c < 11\%$ was necessary for complete dissolution.[235] Our results show that partial dissolution could be observed at $c = 20\%$. More work is required to test whether the degree of transformation was sufficient to provide satisfactory mechanical properties. Transformation was nearly complete for $c = 10\%$, but we detected a trace of residual crystalline cellulose.

7.3.3 Optical microscopy

The preparation of all-cellulose composites with c = 10 and 20% were studied in real time using OM and are on display at the following address: http://picasaweb.google.co.uk/ben.savethequeen/AVI. Video 1 and video 2 respectively show the progressive dissolution of MCC when the cellulose concentration is c = 10 and 20%. Video 3 shows the regeneration following video 2.

Initial swelling was followed by progressive dismantling of the fibril structure (Videos 1 and 2). After 4 h, the MCC particles had lost their initial sharp outline to become more diffuse in appearance. Dissolution was more pronounced in the c = 10% solution, resulting in a homogeneous liquid-like phase with some undissolved and swollen fibrils. In the c = 20% solution, a larger number of swollen MCC particles was still visible after 4 h. Swelling is known to precede cellulose dissolution.[189, 199] The stage at which the fibril has disappeared in the solution is believed to correspond to a complete loss of the initial crystal form or even to dissolution.[86, 156]

The swelling and dissolution process is more rapid in the earlier stages of dissolution. As dissolution proceeds, the solution increases in viscosity which slows the dissolution rate. Simultaneously, an increasing number of solvent macrocations link to the hydrogen bonds of cellulose while the remaining free solvent macrocations must diffuse through an amorphous swollen cellulose network.[212, 234]

The difference in appearance between the 10 and 20% solutions has two possible origins. Firstly, a higher concentration of cellulose leads to higher viscosity.[63, 241] Secondly, the second experiment involves a biphasic system richer in the solid phase, even after extended dissolution times of 4 h. For a given salt concentration of 8 wt.% LiCl in DMAc, there is a cellulose concentration c = 15 wt.% limit above which the solid phase will remain partly undissolved, yielding a biphasic solution.[235] Mixtures with a high cellulose concentration are thus richer in the undissolved solid phase. Since the solvent diffuses more easily in the

amorphous phase, having a higher undissolved content impairs solvent diffusion. Due to its higher viscosity and pronounced biphasic nature, the c = 20% solution is thus expected to be characterized by a less pronounced dissolution.

The same ratio of dissolved to undissolved cellulose could be obtained by varying either the cellulose concentration or dissolution time. However, the amount of dissolved cellulose is not the only parameter of interest. A lower cellulose concentration will lead to a looser cellulose networks characterized by larger pores after regeneration.[261] Thus, it is expected that variations in the cellulose concentration will have direct consequences for the regeneration process. A loose cellulose network enables easier diffusion of the water molecules through it so that systems with a low cellulose concentration suffer from rapid and extensive shrinkage, at least in the early stages of regeneration (Video 3).[306] From a practical point of view, high shrinkage leads to difficulties producing near net shape products. Thus, methods for producing all-cellulose composites with the highest possible initial cellulose concentration are desirable from this standpoint.

7.3.4 Transmission electron microscopy (TEM)

Whereas the as-received MCC exhibited a pronounced orientation of its cellulose fibrils along the fibre, the partly dissolved cellulose was in part replaced by a cellulose phase with little preferential orientation. Further, the non-orientated phase becomes increasingly prevalent as the cellulose concentration is decreased (*e.g.* c = 5% *c.f.* 20%) (Figure 41). The non-orientated phase essentially creates a matrix that surrounds the remaining undissolved cellulose I. As shown in Section 7.3.2, the matrix phase most likely consists of a poorly crystalline form cellulose I and amorphous cellulose. Small undissolved 0.2-5 µm long MCC fibrils are observable for c = 5% after a dissolution time of 8 h (Figure 41a). Conversely, as the cellulose concentration increases (*e.g.* c = 15 and 20%) the original MCC structure dominates the microstructure such that the matrix phase is not clearly distinguishable by TEM (Figure 41b)

due to its low volume fraction. At the higher cellulose concentrations, the regions of matrix phase were less than 0.5 µm wide and sometimes not observable (Figure 41b). This tends to confirm that the surface of the MCC fibres are selectively dissolved and provide chemical bonding between them, giving rise to a self-reinforced composite by selective dissolution as proposed by T. Nishino *et al.*.[24, 29]

TEM was useful for investigating the location and numbers of voids in the all-cellulose composites. Where the cellulose concentration was lower, it was possible to observe circular voids with a diameter of ~100 nm in the matrix (non-oriented phase). These voids were not found to be contiguous with the undissolved MCC (Figure 41a).

Another type of voids, ~50-400 nm wide, were located in the interfacial regions of the matrix and undissolved phases (Figures 41a and b). It is proposed that differential shrinkage between that of the dissolved and undissolved cellulose is responsible for the generation of these interfacial voids in the all-cellulose composites.

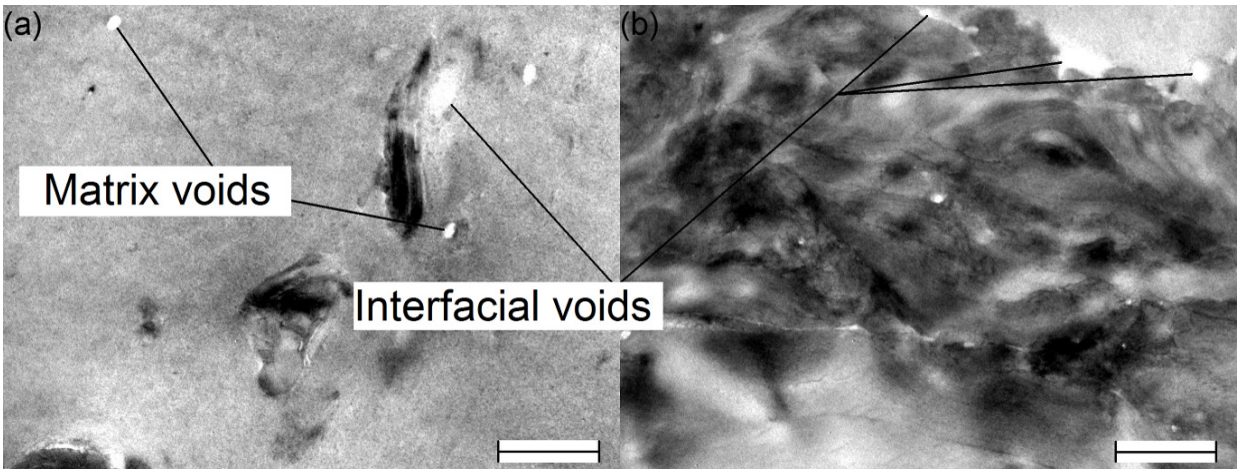

Figure 41 TEM micrographs of the composites obtained by fast precipitation following an 8 h dissolution time with (a) *c* = 5% and (b) *c* = 20%. Scale bars are 1 µm.

The higher crystallinity of the undissolved fibrils consists of a well packed molecular structure that results in less accessible hydroxyl groups compared with the more open structure

of the matrix cellulose. The matrix phase consists of aggregates of 2-3 cellulose chains packed laterally together when precipitated. Consequently, the large number of surface exposed chains with accessible hydroxyl groups in the matrix results in more extensive bonding with water.[304] As a result, different amounts of water are absorbed by the two phases and thus some differential shrinkage at the microstructural level is expected during drying of all-cellulose composites.

HRTEM showed that undissolved MCC fibres (about 200-300 nm in width and 1 μm in length) remain in the composites with c = 20% and are devoid of defects (Figure 42). Undissolved MCC fibres were not observed in the composites with c = 5 % (Figure 43), due to extensive dissolution. The matrix material contained nanovoids with dimensions in the order of 50 nm (Figures 42 and 43). Defects as large as 0.5 μm were also observed and could originate from the nanovoids collapsing together (Figure 43). Again, this suggests that the matrix phase comprises an intrinsic number of defects that arise from the extensive shrinkage undergone by the composite during the precipitation and drying cycles.[261] The observed defects are expected to play an important role in the mechanical behaviour of all-cellulose composites.

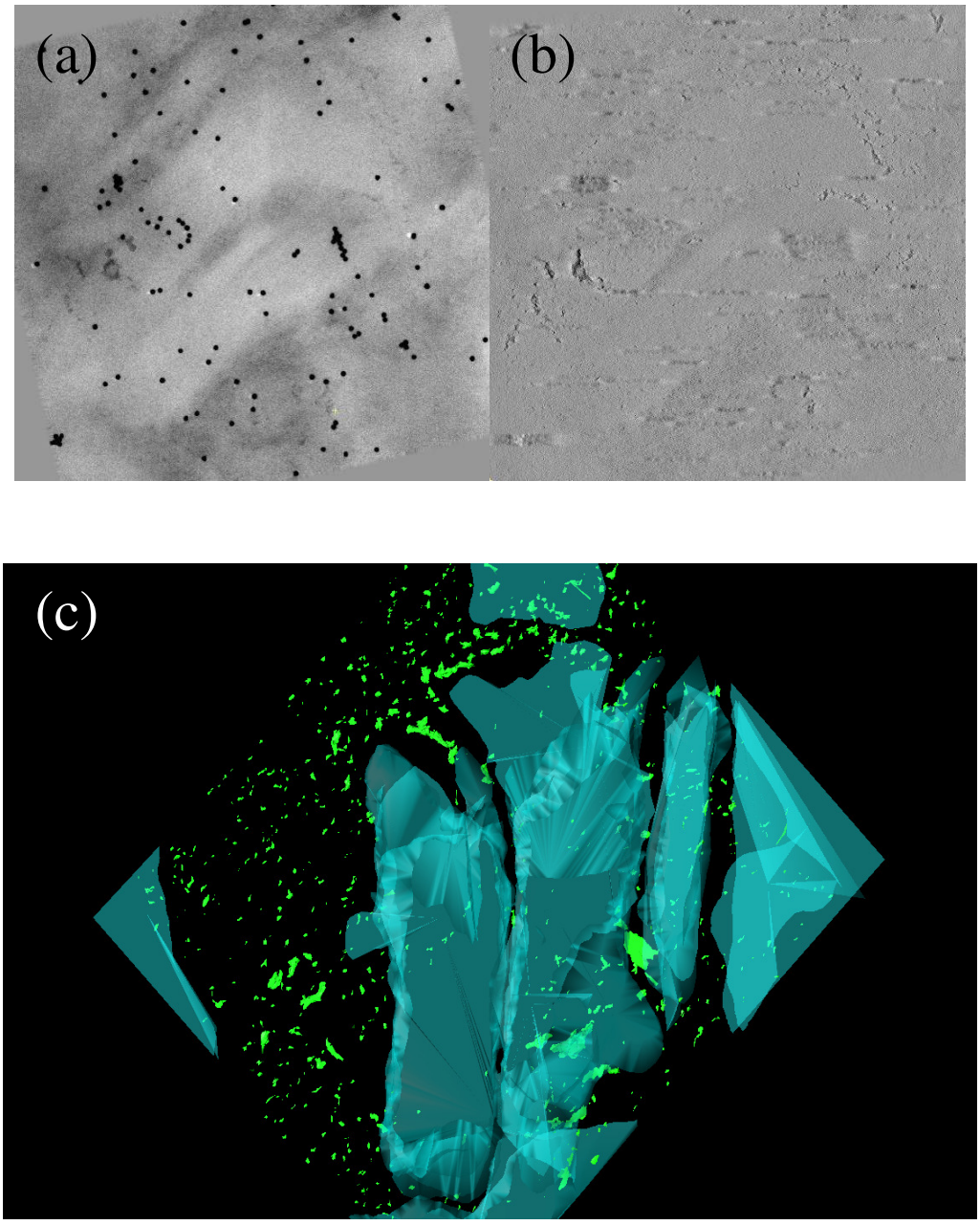

Figure 42 (a) Aligned and (b) reconstructed TEM micrographs with dimensions 1.47 × 1.47 µm produced with c = 20% and t = 8 h. (c) A 3D reconstruction ~60 nm in thickness was obtained, showing the presence of the paracrystalline matrix (black), undissolved MCC (turquoise) and voids (green).

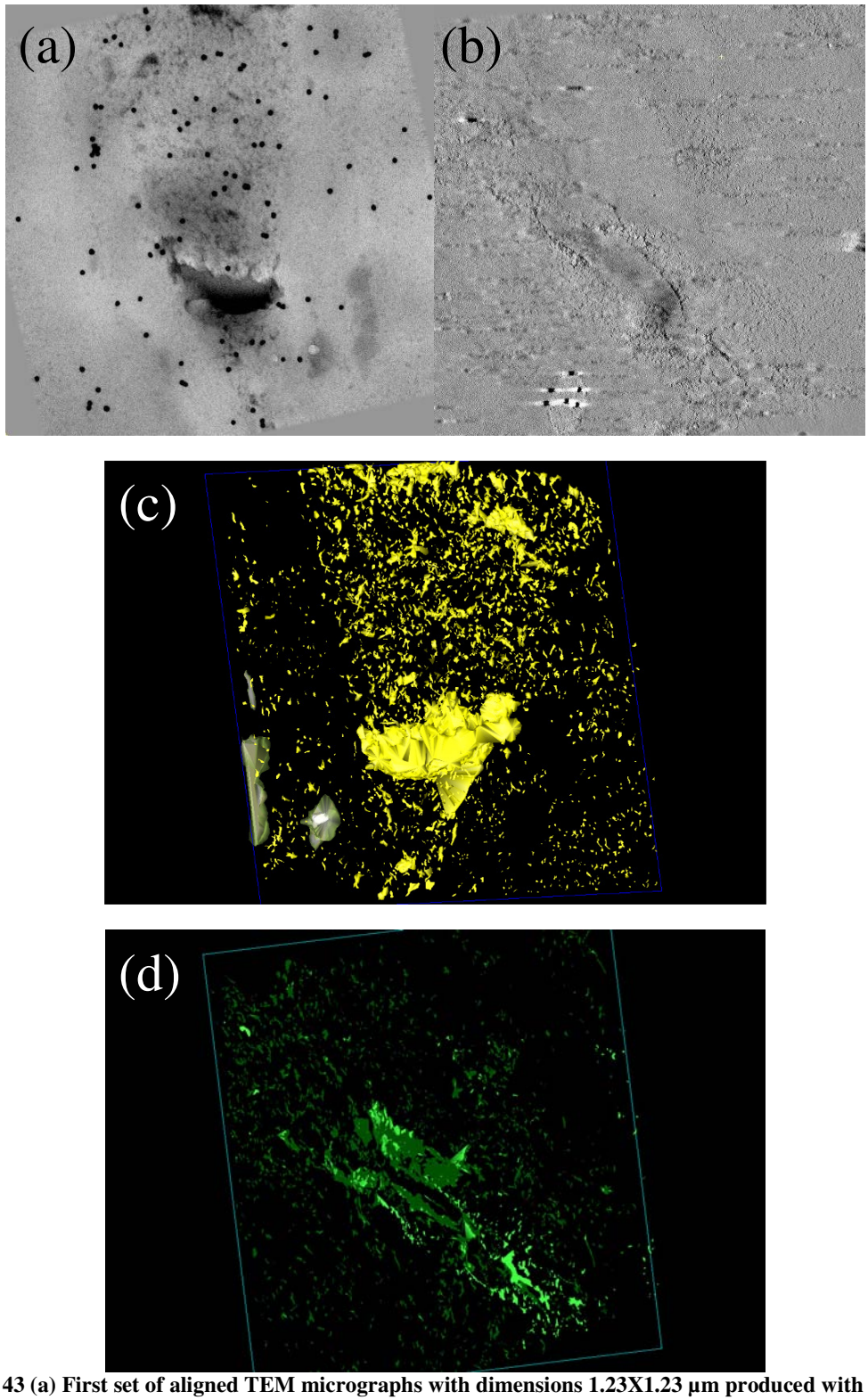

Figure 43 (a) First set of aligned TEM micrographs with dimensions 1.23X1.23 µm produced with *c* = 5% and t = 8 h. (b) Second set of aligned TEM micrographs with dimensions 1.47X1.47 µm produced with *c* = 5% and t = 8 h. (c) Three dimensional reconstruction ~60 nm thick obtained from the first set and showing the presence of voids (yellow). (d) Three dimensional reconstruction ~60 nm thick obtained from the second set and showing the presence of voids (green).

7.3.5 Fourier transform infrared spectroscopy

Crystallinity

The crystallinity index as determined by FTIR spectroscopy was initially 0.36 for the as-received MCC and decreased to 0.32 after activation (Figure 44), which is also in accordance with both the NMR and WAXD results.

-CH region between 1200 and 1450 cm^{-1}

In the -CH region, two adjacent peaks are clearly visible near 1335 cm^{-1} and 1315 cm^{-1} for the activated cellulose. However, they tend to merge for low cellulose concentrations into a diffuse peak near 1318 cm^{-1} (Figure 45) and are distinct for cellulose concentrations *c* of at least 10 wt.%. The peak at ~1335 cm^{-1} is usually attributed to the -OH in-plane bending mode and the peak at 1315 cm^{-1} is attributed to CH_2 wagging motion.[72, 307] There is little, if any, change in the position of those two peaks associated with the passage from cellulose I to regenerated cellulose II. The CH_2 peak was found at 1317 cm^{-1} for cellulose I and at 1315 cm^{-1} for cellulose II.[307] The -OH in plane bending peak was found at 1336 cm^{-1} for cellulose I and at 1335 cm^{-1} for cellulose II.[307] The peak at ~1335 cm^{-1} and the peak at ~1315 cm^{-1} are clearly distinguishable when found in the crystalline forms of cellulose I or II. However, they tend to flatten and merge into one peak with increased ball-milling.[81, 122] As a result, the composites obtained with low cellulose concentrations compare with ball-milled cellulose.

A band at 1420 cm^{-1} (CH_2 scissoring motion) exists in all the composites. An increase in the magnitude of the 1420 cm^{-1} peak with decreasing *c* indicates changes in the environment of the C6 group, which is consistent with a transformation from cellulose I to regenerated or amorphous cellulose.[45, 72, 81, 119, 120, 246, 307]

-CH region between 2850 and 3000 cm^{-1}

The region of CH stretching occurring at low frequencies was also of significance with a peak at ~2900 cm^{-1} and a shoulder at ~2945 cm^{-1} (Figure 46). The 2900 cm^{-1} peak was progressively replaced with a peak at ~2895 cm^{-1} with a shoulder in the vicinity of 2925 cm^{-1} as the initial cellulose concentration was lowered (Figure 46). The intensity of the 2895 cm^{-1} peak was most pronounced for the lowest initial cellulose concentration, and decreased when *c* increased (Figure 46). The displacement of the 2925 cm^{-1} peak to lower values is consistent with a transformation to regenerated or low crystallinity cellulose.[45, 119, 120, 122] However, the broadening of the peak is an indication of the lower crystallinity. In particular, the exact same transformation was observed for prolonged ball-milling.[122] Hence, the transformation undergone by the cellulose powder during the manufacturing of the composite yields a material of low crystallinity analogous to ball-milled cellulose or amorphous cellulose. The resemblance increases with decreasing *c* values.

-OH region between 3200 and 3400 cm^{-1}

Another spectra area gets notably modified: the area assigned to the hydrogen bonds in the lower frequency area (3200-3400 cm^{-1}). In general, the peak maximum was shifted from the initial 3340-3350 cm^{-1} region to 3380-3390 cm^{-1}, and this was seen for all the composites except for the one that had the highest initial cellulose concentration of c = 20 % (Figures 46 and 47).

The changes observed in the 3200-3500 cm^{-1} region usually reflect changes in both the intermolecular and the intramolecular hydrogen bonds.[119, 122, 307, 308] Specifically, a band at 3352 cm^{-1}could clearly be assigned in amorphous cellulose to the intermolecular bonds of the hydroxyl groups located at the C(2) and C(3) positions.[45] It also belongs to the intramolecular hydrogen bonds of native cellulose, as proved by polarized FTIR.[308] In contrast to this, values of 3375-3405 cm^{-1} in native cellulose were assigned to the

intramolecular bonds between C(2) and C(6) by Schwanninger (2004) and to undistinguished intermolecular hydrogen bonds by Liang and Marchessault (1959).[122, 308] Henceforth, the hydrogen bonding scheme of MCC clearly changes during the all-cellulose composite consolidation and the changes are more drastic when c is lower than 15%. The peak shift occurring for $c < 15\%$ is similar to the one reported for cellulose after ball-milling.[122] The absence of change for $c = 20\%$ is due to its similarity with the starting MCC and both WAXD and ^{13}C solid-state NMR also pointed out the lack of extensive transformation in this material.

Cellulose type and comparison between the different regions

Those IR results distinctly show that no cellulose II is formed during the composite consolidation. Instead, a cellulose form analogous to ball-milled cellulose is produced. In this case, as the starting material Avicel is a form of cellulose I, cellulose ball-milling would have produced a form of poorly crystalline cellulose I similar to cellulose IV with a higher proportion of chains exposed to the surface of the crystallites.[70, 121] This statement strongly supports the previous results obtained by WAXD and ^{13}C solid-state NMR in this Chapter.

However, there are differences in changes depending on the region of the spectra involved. The differences in spectra in the region between 1200 and 1450 cm^{-1} were weak for composites with cellulose concentrations higher than, or equal to, $c = 10$ wt.%. In comparison, the differences in spectra that involved hydrogen bonding (typically differences in the 3200-3500 cm^{-1} region) were very pronounced for all the composites up to a concentration of $c = 15$ wt.%. Both regions reflect the changes associated with cellulose conformation, but the region in the 1200 to 1450 cm^{-1} range reflects changes in chain conformation (chain bending and twisting) whereas the –OH region reflects changes in inter- and intramolecular hydrogen bonding. The transformation occurring during all-cellulose composite consolidation would then involve modifications in hydrogen bonding before actually involving any change in the chain conformation. As the solvent penetration within cellulose crystals precedes the actual swelling

of the MCC, inter- and intramolecular changes in hydrogen bonding must precede the changes in the chain conformation linked with the transformation from native cellulose to the paracrystalline matrix identified in Section 7.3.2.

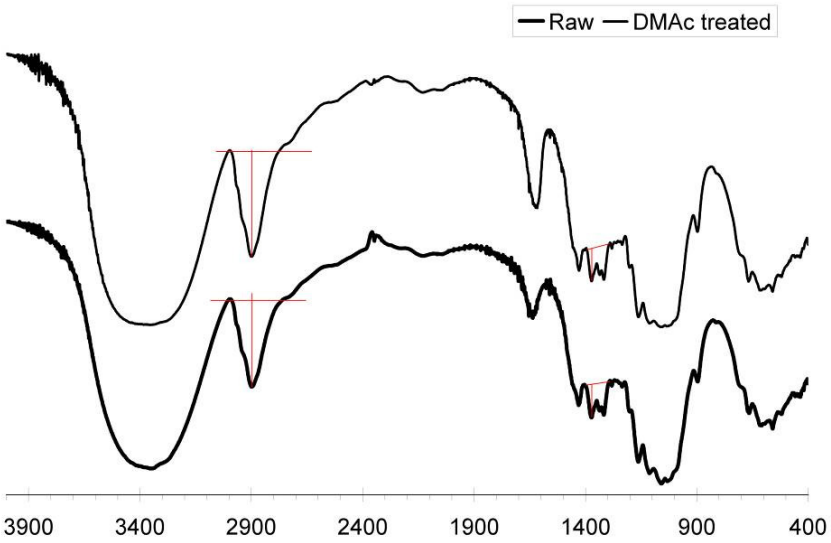

Figure 44 FTIR spectra of as-received (thick line) and activated (thin line) MCC.

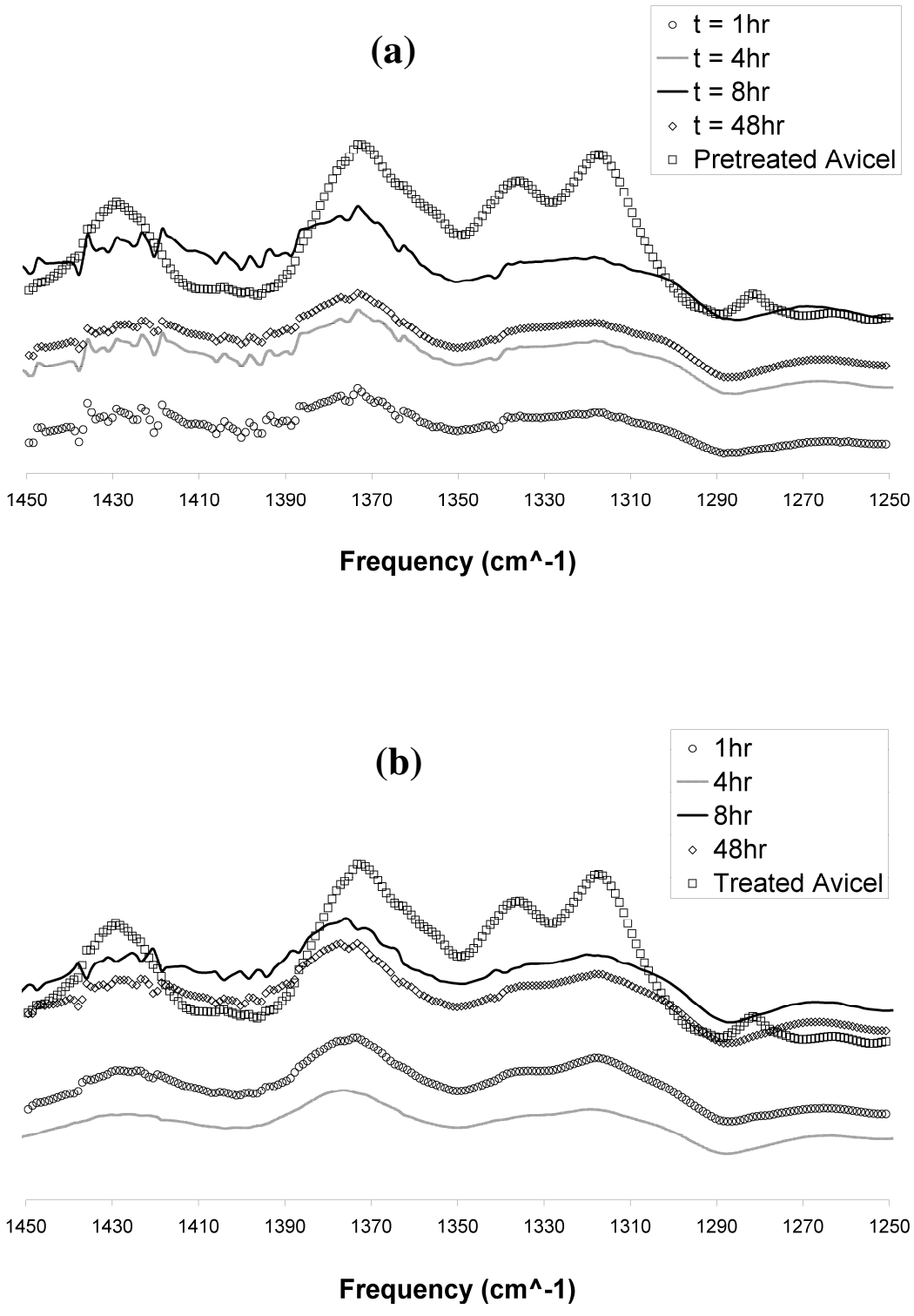

Figure 45 FTIR absorbance spectra of all-cellulose composites produced with (a) c = 5%, (b) c = 10%, (c) c = 15% and (d) c = 20% in the -CH region.

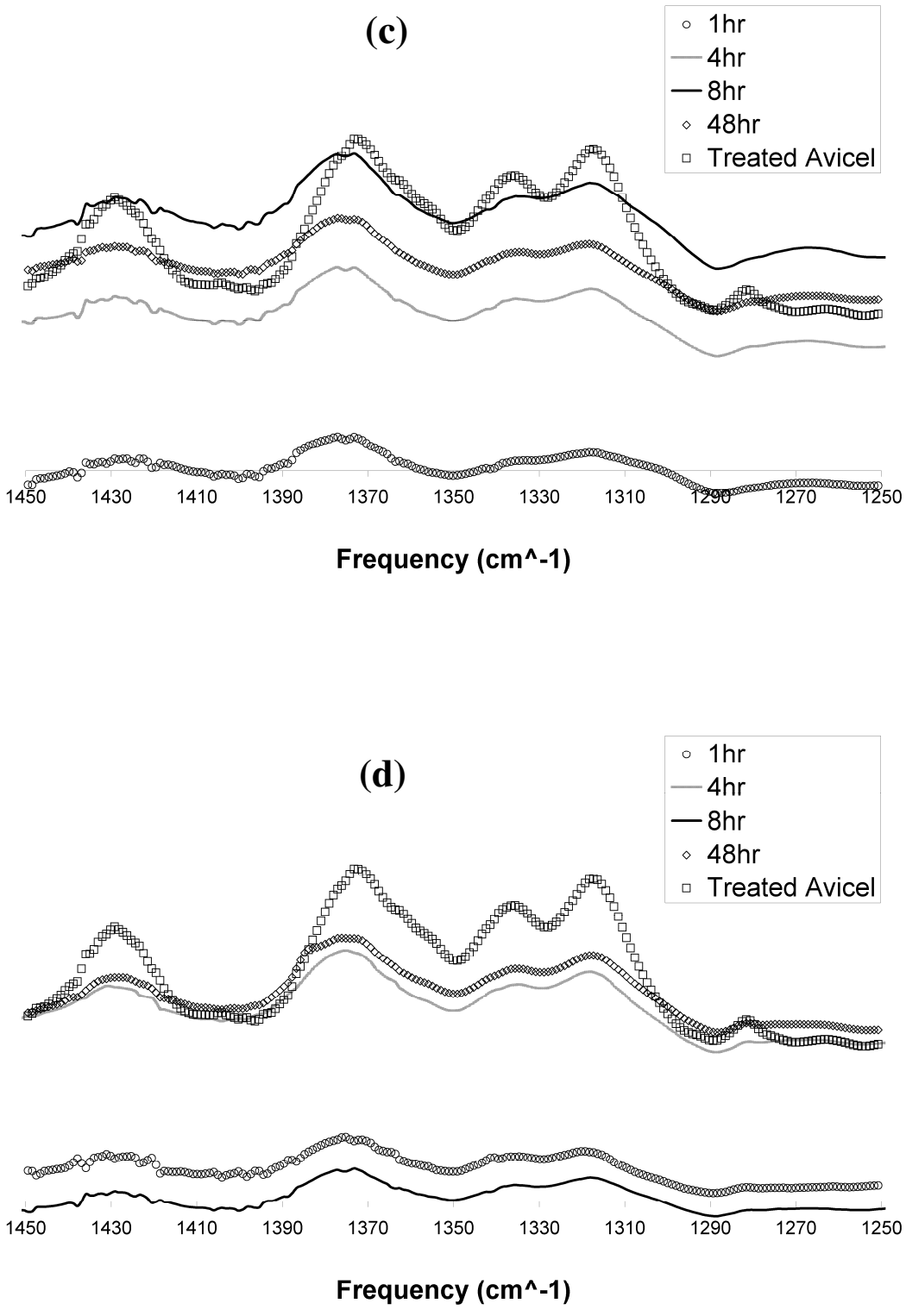

Figure 45 FTIR absorbance spectra of all-cellulose composites produced with (a) c = 5%, (b) c = 10%, (c) c = 15% and (d) c = 20% in the -CH region.

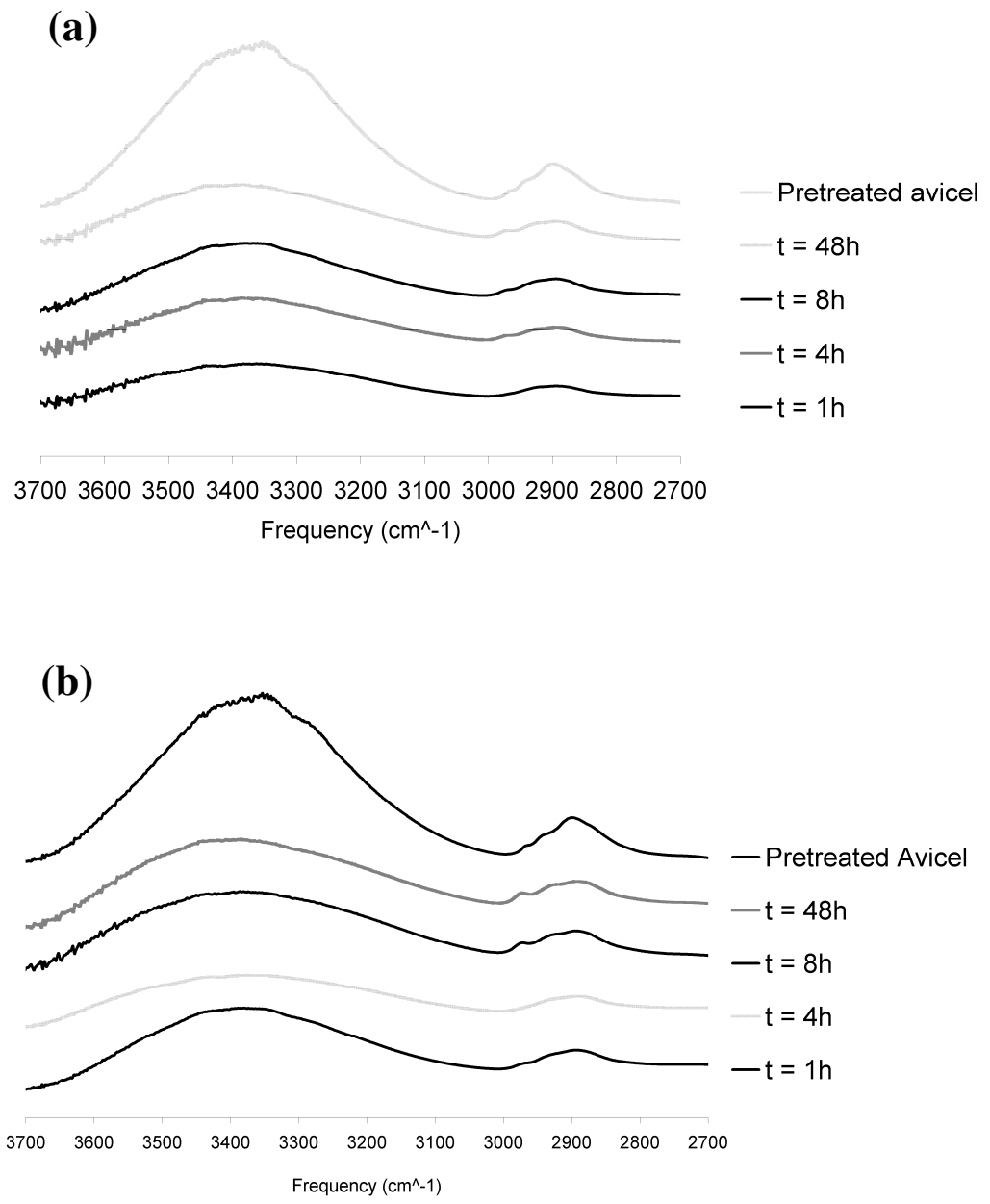

Figure 46 FTIR absorbance spectra of all-cellulose composites produced with (a) *c* = 5%, (b) *c* = 10%, (c) *c* = 15% and (d) *c* = 20% in the -OH region.

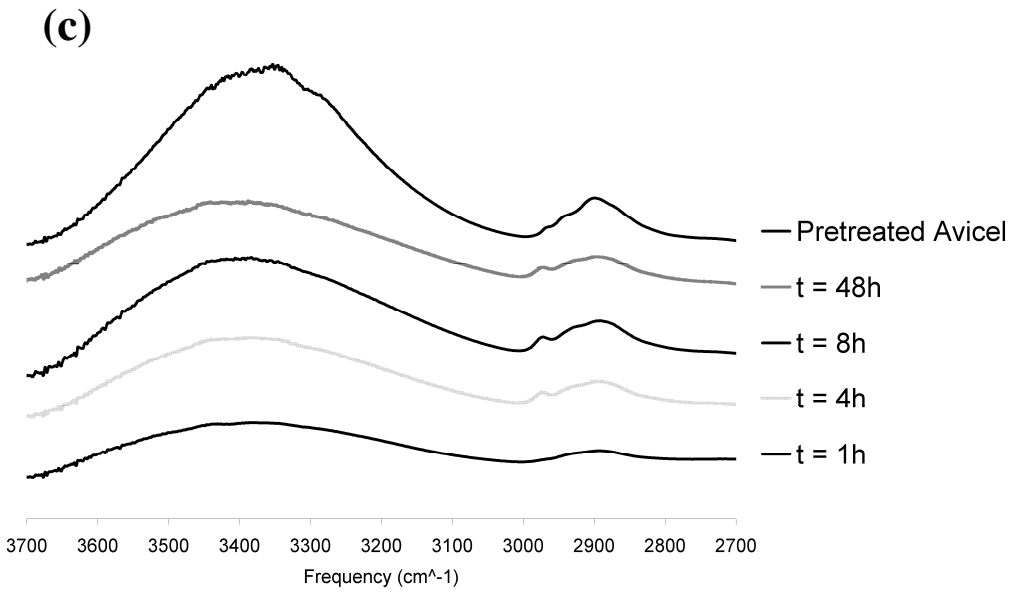

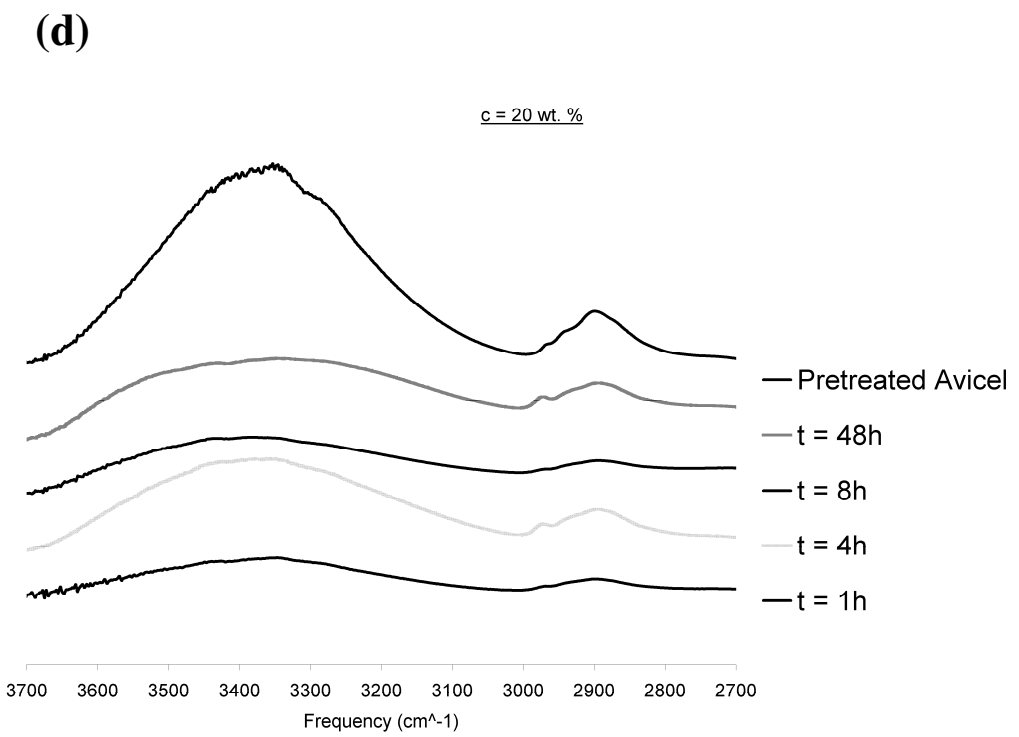

Figure 46 FTIR absorbance spectra of all-cellulose composites produced with (a) *c* = 5%, (b) *c* = 10%, (c) *c* = 15% and (d) *c* = 20% in the -OH region.

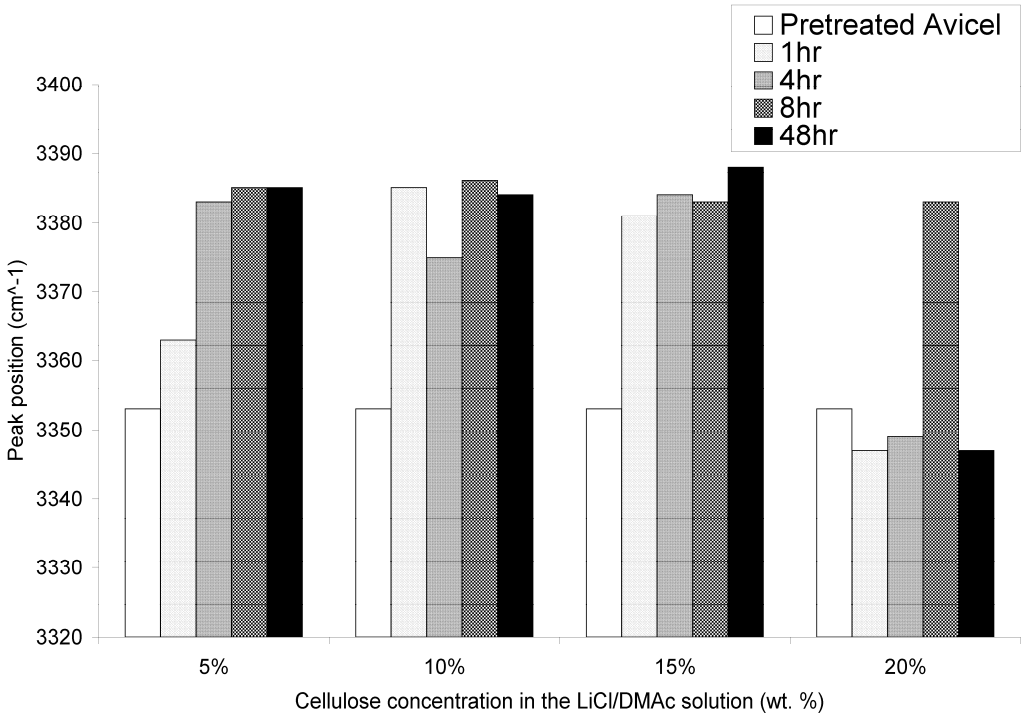

Figure 47 Position of the maxima in the OH region 3350-3390 cm^{-1} as a function of the initial cellulose concentration (c) and effective dissolution time (t).

7.4 Conclusions

Partial dissolution and regeneration of cellulose yielded all-cellulose composites with a matrix comprising a mixture of paracrystalline and amorphous cellulose. The extent of the transformation seems to be more dependent on the initial cellulose concentration than on the dissolution time. The WAXS and NMR results point to distinct differences from a fully amorphous matrix. NMR and FTIR show the absence of cellulose II from the composites. The dissolution proceeds first by a change in the intermolecular and intramolecular hydrogen bonds. This change precedes the swelling of the MCC in the solution which is accompanied by transformations in the chain conformation. The changes in chain conformation result in the formation of the non-crystalline matrix material from the initially highly crystalline MCC. The dissolution of the MCC is a heterogeneous process, with some fibres remaining undissolved.

TEM and HRTEM show the presence of voids in the matrix and at the interface. The quantity, morphology and location of voids is linked to the extent of the cellulose dissolution.

Voids are expected to play an important in the final mechanical properties. In previous works, void network structures observed in regenerated cellulose were detrimental to tensile strength and stiffness.[171] Hence, it would be of particular interest to quantify the voids and their morphology in future work.

In the next Chapter, the consequences of paracrystallinity and molecular changes due to swelling and effective dissolution on the mechanical properties of all-cellulose composites will be tested.

8 Structure-property relationship of all-cellulose composites

8.1 Introduction

The present Chapter takes the next step in examining the relationship between the cellulose structure and mechanical properties of all-cellulose composites produced *via* partial dissolution of MCC powder in an 8.0 wt.% LiCl/DMAc solution. It is reported that the mechanical properties of all-cellulose composites can be maximised by slowing the precipitation rate during processing. The underlying reason for this improvement is found to be the elimination or reduction of internal cracking due to the differential shrinkage during processing. A judicious choice of cellulose concentration and dissolution time can help to optimize the final tensile strength, stiffness and tensile strain to failure.

8.2 Experimental methods

8.2.1 Experimental materials

Initial preparation of cellulose

Microcrystalline cellulose (MCC) powder (Avicel, Merck, particle size range 20-160 μm) was "activated" as described in the previous Chapter. Briefly, activation is used to help swell the cellulose in preparation for dissolution which is accomplished by successive solvent exchange steps using water, acetone and DMAc. The degree of polymerisation (DP) of the MCC was determined to be 163 after the method by Bianchi *et al.*.[213] A solvent solution of 8.0% (by total weight) LiCl in DMAc was prepared by mixing LiCl (Unilab, 99% purity, dried in a vacuum oven at 180°C overnight) and DMAc (Merck, synthesis grade, dried over molecular sieve prior to use) in a 200 ml Schott bottle that was immediately sealed to minimize moisture uptake. The mixture was then mechanically stirred for 24 h until the LiCl was completely dissolved.

Preparation by fast precipitation

2 g of activated MCC was added to a beaker of LiCl/DMAc to give cellulose concentrations of c = 5%, 10%, 15% and 20%, where c is expressed as % of the total weight of cellulose, LiCl and DMAc. The solution was then homogenised with a magnetic stirrer at 20°C for 2 min. A viscous solution resulted which was then poured into Petri dishes and stored under dry atmosphere for effective dissolution times (t) of 1, 4, 8 and 48 h. The precipitation of the dissolved cellulose was initiated with light spraying of water onto the surface of the gel in order to fix the shape of the final sample. This *partially* precipitated gel was then carefully immersed in 3 l glass crystallizer of tap water for 48 h at 20°C and the water was changed at least every 24 h. Residual LiCl or DMAc was then further removed by thorough rinsing of the specimens with water. The specimens were lightly pressed beneath laboratory paper towelling in order to remove excess water and then dried by vacuum bagging for 48 h under a pressure of 0.16-0.24 atm and temperature of 60°C to ensure complete solidification.

Preparation by slow precipitation

All-cellulose films (c = 5, 10, 15 and 20%) were also produced using a slow precipitation route. After casting into Petri dishes and storing for 48 h under dry atmosphere, the samples were then stored under ambient conditions (16 ± 1°C, 52 ± 5 % R.H.) for 50 h in order to undergo slow precipitation. Rinsing and drying were then carried out as previously described.

8.2.2 Materials characterisation

X-ray diffraction (WAXD)

WAXD was performed as described in Chapter 7.2.2. Instead of Origin, the software Excel was used to smoothen the curves whereas both 2.θ at (200) and HWH were manually determined.

Mechanical properties and fracture behaviour

Samples were cut in strips about 0.2 mm thick and 7-8 mm wide and then stored at 55±3% R.H. and 23±2°C for 7 days. Tensile testing was performed on an MTS 858 table-top system with a 2.5 kN load cell at a crosshead speed of 1 mm/min. The specimens were cut into thin strips approximately 8 mm in width with a 35 mm gage length. Fractured tensile samples were mounted on carbon tabs with an angle of 0 or 90° for observation with SEM (JEOL 7000F FE-SEM, accelerating voltage of 5-10 kV). Samples were gold coated with an Emitech K975X using a 25 mA current under 0.2 bar of pressure under Ar.

8.3 Results and discussion

8.3.1 Microstructural characterisation

Partial dissolution was accompanied by a displacement of the (200) diffraction peak to lower values and an overall loss of crystallinity (Chapter 7).[26, 29] In general, the transformation was extensive for c = 5 and 10%. Partial dissolution was observed for all of the composites produced in this work, regardless of the dissolution time or concentration. In general, *CrI* decreased with increasing dissolution, which was primarily controlled by c and t (Figures 48 and 49).

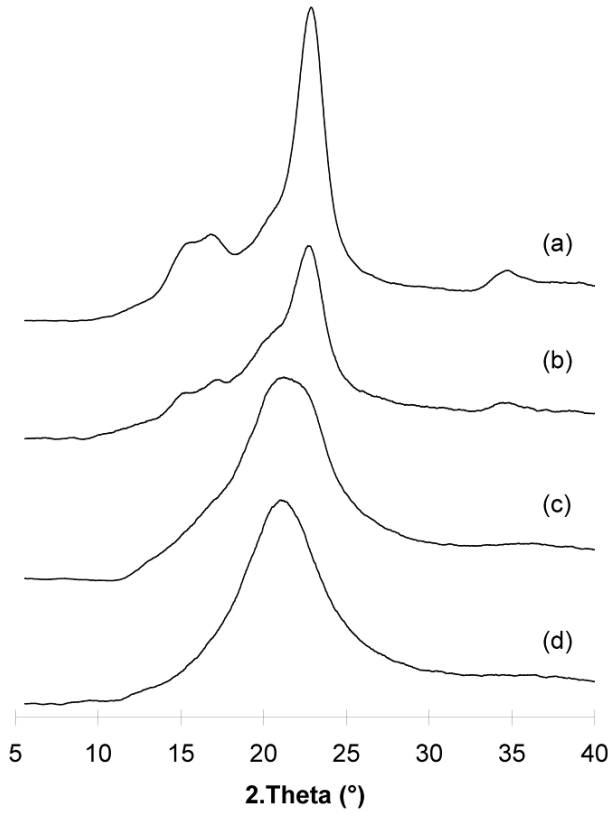

Figure 48 WAXD of all-cellulose composites obtained by slow precipitation for (a) *c* = 5%, (b) *c* = 10%, (c) *c* = 15% and (d) *c* = 20%.

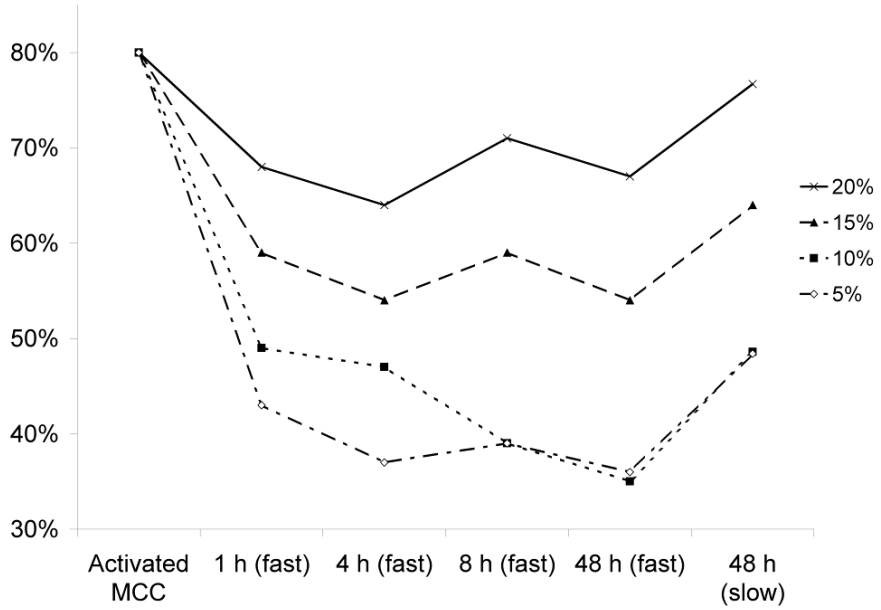

Figure 49 *CrI* as a function of *c* and t for activated MCC and all-cellulose composites. The precipitation rate is given in parentheses.

All of the samples obtained by the slower precipitation had a 10-14% higher CrI than their counterpart obtained with the same dissolution time and using the faster precipitation route (Figure 49). Cellulose aggregates self-associate by solid-liquid phase separation during precipitation; those aggregates can form crystals rather than amorphous cellulose when the phase separation is slow. This was observed previously for the cellulose/LiCl/DMAc system.[227, 240] Hence, it is suggested that the slower precipitation route allows greater time for the cellulose chains to reassemble into an ordered crystalline configuration. The precipitation rate has drastic consequences on the gel in terms of aggregation structure at the submicron scale.[204, 227] In turn, the regenerated cellulose is affected in terms of void content, lateral crystal dimension, orientation, content, and stress, elongation at break and stiffness [171, 219, 309] . Thus, the increase in crystallinity due to the slow precipitation of all-cellulose composites should have a direct impact on their mechanical properties.

8.3.2 Mechanical properties and fracture behaviour

The fast precipitation route yielded lower mechanical properties than the slow precipitation route. The tensile strength is generally highest for cellulose concentrations around 10-15%. The tensile strength was 28-36 MPa for the composite with c = 5%; 20-63 MPa for c = 10%; 24-59 MPa for c = 15%; and 10-23 MPa for c = 20% (Figure 50). The tensile strain to failure was normally in the range 2-5% with a minimum of 0.50±0.23% for c = 20% and t = 4 h and a maximum of 6.86±0.98 % for c = 10% and t = 4 h. The Young's modulus (E) was in the range of 1.5-3 GPa, with a minimum of 1.38±0.54 GPa for an initial cellulose concentration of c = 20% and t = 4 h and a maximum of 3.57±0.95 GPa for c = 20% and t = 48 h (Figure 50).

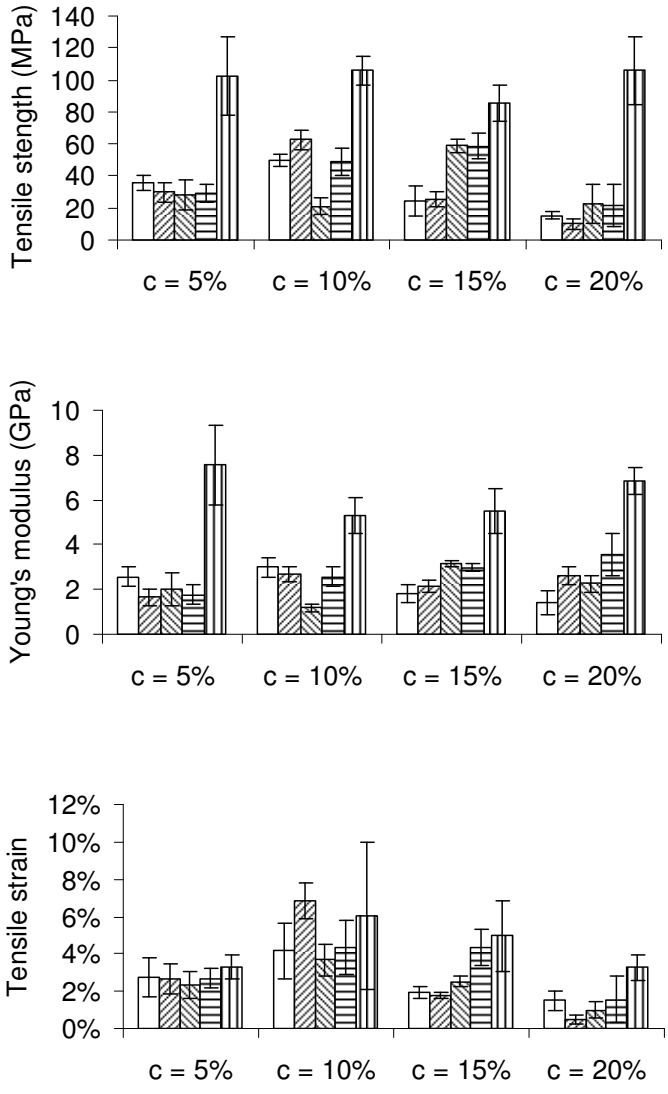

Figure 50 Tensile mechanical properties of all-cellulose composites produced by fast precipitation with t = 1 h ( ), t = 4 h ( ), t = 8 h ( ), t = 48 h ( ) and by slow precipitation ( ).

The composite manufactured with an initial cellulose concentration of c = 5% showed little difference in strength, stiffness or strain regardless of the dissolution time. Dissolution occurs rapidly when the cellulose concentration is low as shown by WAXD (Figure 49) and ^{13}C solid-state NMR. Conversely, the mechanical properties of the two composites with the highest initial cellulose concentrations (c = 15 and 20%) benefited from an extended dissolution time (Figure 50).

In general, the composites obtained by slow precipitation exhibited improved mechanical properties with up to a five fold increase compared with their counterparts obtained *via* the fast precipitation route (Figure 50). Surprisingly, only minor differences in tensile strengths were observed between the different composites, especially when the standard deviation was taken into account. Generally, the tensile strength was in the vicinity of 100 MPa, which compares favourably with many thermoplastics. The Young's modulus was superior for the lowest and highest cellulose concentrations, with a maximum of 7.5 GPa. As might be expected, the strain to failure exhibited the opposite trend with maximums (~6%) found for c = 10-15%. The mechanical properties reported here for all-cellulose composites obtained by partial cellulose dissolution are somewhat lower than that reported in the literature. The precise reason for this is unclear but could be related to the following variables:

(i) the use of compression prior to solvent extraction which was not utilised in the present study [29];

(ii) variations in the precipitation route such as precipitating the cellulose under different atmospheres, precipitation temperature and relative humidity [26, 29]; and/or

(iii) differences in the DP of the cellulose source utilised.[26, 29]

The composites prepared with c = 5% and 10% exhibited smooth fracture surfaces (Figures 51a to 51d) when compared with the composites having c = 15% and 20% (Figures

51e to 51j). Cellulose fibrils of ~100-300 nm in diameter and several microns in length were observed by SEM for c = 20% and t = 1 h (Figure 51g). Hence, MCC is broken into cellulose fibrils during the dissolution although a significant fraction of the cellulose fibrils are not dissolved for the higher concentrations. The amount of undissolved cellulose increases with increasing concentration or decreasing dissolution time as also demonstrated by the WAXD results. The smoother fracture surface exhibited for the lower cellulose concentrations (Figures 51a and 511b) originates from a more thorough dissolution of MCC. In agreement with the present observations is the phase diagram presented by Conio *et al.* that shows for cellulose concentrations less than 11% dissolution is complete, while for c > 15% complete dissolution is hindered.[235] The dissolution reaction is also more rapid with decreasing cellulose concentration and is nearly complete at t = 8 h. Thus, for c = 5% the transformation from cellulose I to a paracrystalline matrix should be largely complete, leaving few fibrils available for pull-out during fracture and resulting in a relatively smooth fracture surface.

A distinct microscopic feature of the all-cellulose composites processed *via* the fast precipitation route was the evolution of a layered morphology. The layers were approximately 0.1-1 μm in thickness and lay parallel to the top surface of the film (e.g. Figures 51a and 51b). In contrast, the composites manufactured *via* the slow precipitation route

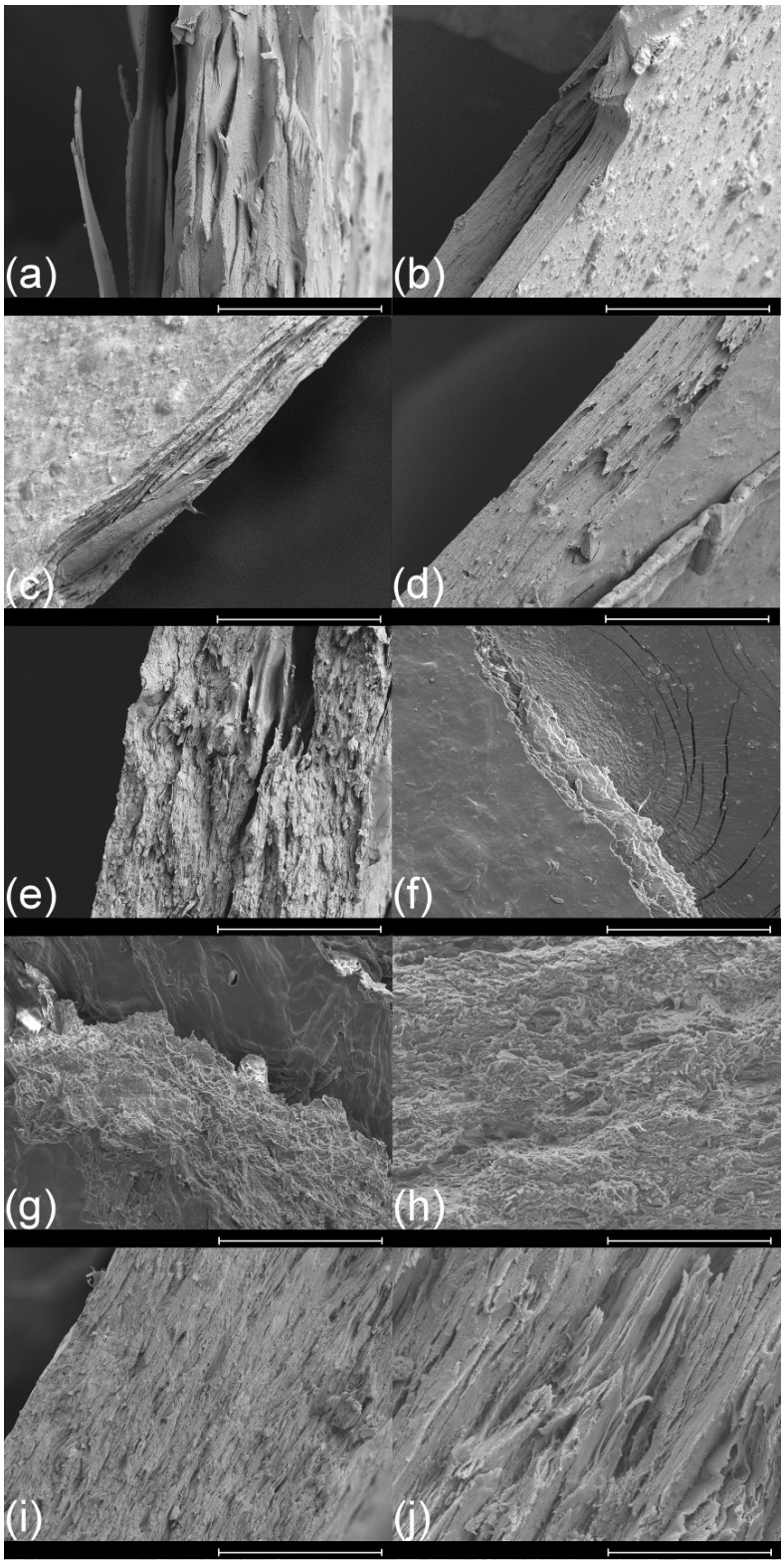

Figure 51 SEM micrographs of the fracture surfaces of all-cellulose composites as a function of *c* and t. (a) *c* = 5% and t = 1 h, (b) *c* = 5% and t = 48 h, (c) *c* = 10% and t = 1h, (d) *c* = 10% and t = 48 h, (e) *c* = 15% and t = 1 h, (f) *c* = 15% and t = 48 h, (g) *c* = 20% and t = 1 h, (h) c = 20% and t = 48 h. (i) and (j) are the fracture surfaces of the composite obtained *via* the slow precipitation route with c=15%. All scale bars are 100 µm, except 5j where it is 10 µm.

do not exhibit such layering. It is proposed that these layers originate from shear stresses created by differential shrinkage of the material during precipitation. Lines of *equi-concentration* of solvent run parallel to the surface of the film since water diffusion would proceed largely in a direction perpendicular to the surface rather than laterally (Figure 52). During removal of the solvent, it could be envisaged that the cellulose at the top surface of the film is precipitated first while the cellulose on the underside of the sample is last to precipitate due to a solvent diffusion gradient through the thickness of the film. The resulting differential shrinkage through the film thickness creates shear stresses of equal intensity in planes parallel to the film surface, resulting in the observed delamination. This phenomenon is probably exacerbated by the high viscosity of the gel. While the upper surface is first to precipitate and shrink, the bottom surface preserves its lateral radial dimension due to adhesion of the gel to the Petri dish. Shrinkage tends to occur to a greater extent in gels with a lower initial cellulose concentration, leading to more prominent delamination.[306]

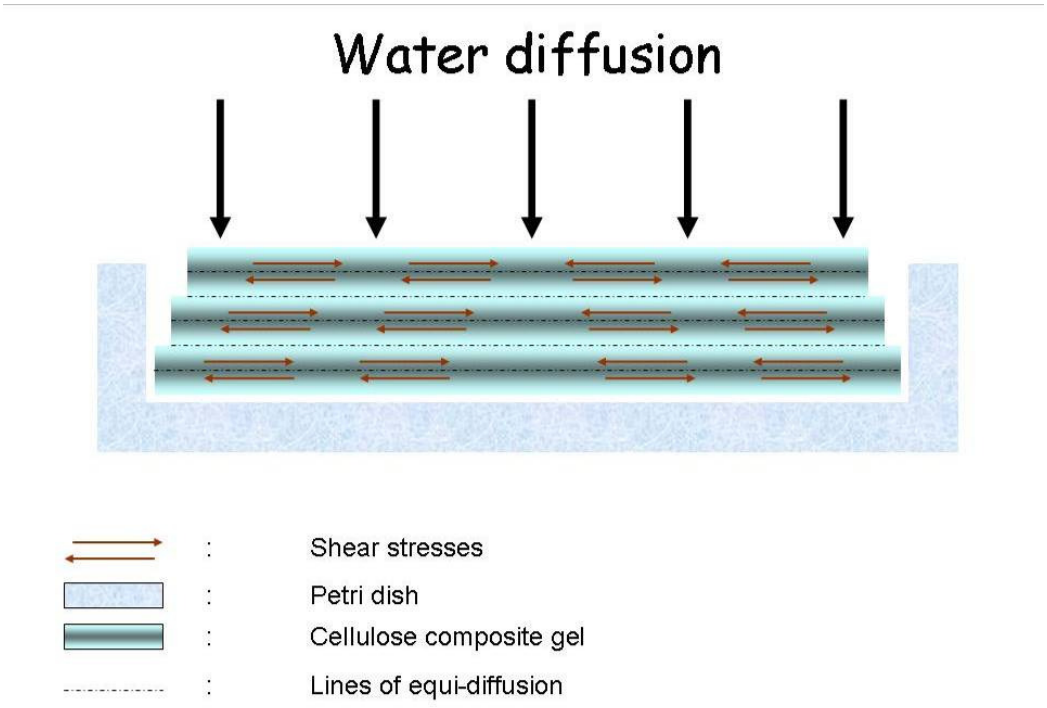

Figure 52 Schematic of the shear stresses acting during the precipitation of the gel and creating delamination.

8.4 Conclusions

The structure-property relationships of all-cellulose composites are made complex by changes to three parameters: dissolution time, initial cellulose concentrations and precipitation rate. These parameters greatly influence the mechanical properties of all-cellulose composites through their effect on the proportion of undissolved cellulose, matrix viscosity, void formation, crystallinity and mechanical properties.

- A composite material where the matrix is a mixture of amorphous and paracrystalline cellulose was created. The paracrystalline material is analogous to a poorly crystalline form of cellulose I. The extent of the transformation usually increases with an increasing dissolution time and a decreasing initial cellulose concentration (Figures 48 and 49).
- The partial dissolution process is graded: the fibril content becomes *progressively* less as the cellulose concentration is decreased, to the benefit of a more homogeneous and non-oriented matrix phase. The size of the fibrils is also a consequence of the dissolution time. Initially large MCC fibrils about 10 µm in diameter are split into finer fibrils about 200-300 nm in width (Figure 51). Exceptionally, a marginal proportion of Avicel fibrils could not undergo extensive dissolution and remained visible in all the materials, even at low concentration (Figure 51c and Figure 41). The distribution of the reinforcement is increasing with the dissolution and precipitation time, probably because of the polymer swelling in the solvent.
- In the end, the biggest improvement came from a slow precipitation method. A hasty precipitation can create a large amount of internal cracks running parallel to the film surface (Figure 51 and 52).
- In general, increasing the dissolution time will create a material with superior mechanical properties (Figure 50), supposedly due to enhanced wetting, MCC

defibrillation and distribution. Assuming that the matrix material is best represented by the lowest cellulose concentrations, then its mechanical properties are equivalent to the composite material with the highest amount of undissolved cellulose.

However, maximising the cellulose concentration has several advantages such as limiting the shrinkage of the material. In an industrial context, it would be interesting to shorten the precipitation step, even though doing so can hinder the integrity of the all-cellulose composite. In the next Chapter it will be shown that a high content in crystalline cellulose will have consequences on the thermomechanical characteristics of the material and on the moisture absorption. A thickness in the order of 0.2-0.3 mm represents a tenfold increase in thickness as compared to cellophane and opens up new possibilities for a material that is produced solely out of renewable resources and that is readily biodegradable.[29, 192] The mechanical properties reported in this work are lower than some of those reported in the literature and this shows the importance of the cellulose selection as well as the importance of a carefully monitored precipitation step.[26, 29]

9 Viscoelastic behaviour of all-cellulose composites in the range of -150°C to 350°C

9.1 Introduction

Hydrogen bonding governs the viscoelastic behaviour of cellulose.[44, 130] Hydrogen bonding in amorphous cellulose in which the C2 and C3 hydroxyl groups mainly participate is isotropic in nature.[45, 72, 90, 91, 111, 130, 308, 310] Conversely, hydrogen bonding in the highly ordered crystalline states occurs via the C6 hydroxymethyl group.[45, 311] As a result of the differences in hydrogen bonding, lower intermolecular cohesive forces are experienced by the amorphous phase. Thus, at lower temperatures mechanical relaxations are largely dominated by the amorphous phase, and denoted as the secondary (β and γ) relaxations. The γ transition originates from the rotation of the hydroxymethyl groups and normally occurs somewhere in the range of -120°C to -90°C depending on the test frequency, moisture content and crystallinity.[128, 312, 313] At higher temperatures, the β transition is observed between -80 and -40°C.[126, 128, 312-314] Activation energies in the range of 69-85 kJ/mol indicate that the β transition is associated with localised main chain mobility of the amorphous phase.[126, 128, 312] At higher temperatures, cellulose exhibits three separate glass transition temperatures, denoted as α_1, α_2 and α_3.[126, 129, 315] The primary α transitions of cellulose originate from long-range cooperative inter- and intra-molecular chain mobility with activation energies greater than 200 kJ/mol.[127, 128, 314, 316] α_3 occurs between 30 and 60°C, α_2 between 140 and 290°C and α_1 between 285-305°C.[127, 130, 309, 313] Manabe *et al.* reported that the α_3, α_2 and α_1 transitions originate from the amorphous regions that have (i) been partially plasticised by absorbed water, (ii) *moderate* intra- and intermolecular hydrogen bonding and (iii) *strong* inter- and intra-molecular hydrogen bonding, respectively.[127] It has been argued that the α_3 peak originates from drying of the film during testing and therefore constitutes an artefact rather than genuine mechanical relaxation.[312]

In the present Chapter, the molecular mechanisms that dictate the thermomechanical behaviour of cellulose are used as a basis for elucidating how mechanical properties of multiphase all-cellulose composites vary with the chosen processing route via microstructural changes. The ratio of undissolved phase (cellulose I) to dissolved phase (matrix of amorphous and paracrystalline phases) in all-cellulose composites was controlled by varying the (i) initial cellulose concentration (c) and (ii) dissolution time (t). It is shown that the dynamic mechanical properties of all-cellulose composites are highly sensitive to the size and distribution of crystallites whilst, interestingly, the total crystallinity plays a less important role.

9.2 Experimental method

9.2.1 Preparation of cellulose and all-cellulose composites

Refer to Section 8.2.1 for the cellulose and solvent preparation. The composites films were prepared as described in the "fast precipitation" subchapter and the samples tested were the specimens obtained for t = 1 h and t = 8 h.

9.2.2 Materials characterisation

Dynamic mechanical analysis (DMA) was performed in tension mode with a Perkin Elmer Diamond DMA under a constant flow (400 ml/min) of dry nitrogen to avoid thermal oxidation. DMA specimens were prepared as thin strips 7-8 mm in width, 0.1-0.4 mm in thickness and 20 mm in gauge length. Specimens were dried under vacuum (24 kPa) at 60°C for 12 h and 100°C for a further 4 h and then stored under vacuum. Specimens were tested as such from -150°C to 50°C but were conditioned at 23°C and 55% R.H. for 1 week before testing from 30°C to 370°C. A heating rate of 2°C/min was used in the temperature (T) range of -150°C to 370°C and a strain of 0.05% was imposed for multiple frequencies in the range of 0.2 to 20 Hz. A composite with c = 20% and t = 1 h was selected for high resolution DMA (*i.e.*

1°C/min between 200 and 270°C, 0.5°C/min between 270 and 300°C and 0.2°C/min between 300 and 330°C) to more clearly distinguish the $\alpha_{1,2}$ and $\alpha_{1,1}$ transitions that partially overlap at ~300°C. The temperature at which the β and $\alpha_{1,2}$ transitions occurred was determined from the local maximum in damping (tan δ). However, it was more convenient to determine the position of $\alpha_{1,1}$ using the local minimum in the storage modulus (E').

The activation energies (ΔH_a) for the $\alpha_{1,1}$ and β transitions were determined with the following equation:

$$\Delta H_a = -R \frac{d \ln f}{d(1/T_{\max})} \qquad (10)$$

where, R is the gas constant (8.31451 kJ/mol), f is the frequency and $T_{\max}$ is the temperature for the local maximum in tan δ.[127, 128] The peak in tan δ associated with the β transition was characterised by measuring the half-width at half height (HWH). To obtain HWH, a horizontal baseline was plotted from the minimum near 0°C (*i.e.* the high temperature side of the β transition). The half width was then taken as the distance to the right of a vertical line that drops down from the maximum in tan δ. This modified method for obtaining HWH avoids the possible over-estimation of HWH due to the presence of the overlapping γ transition that occurs near -100°C. WAXS results are those that were obtained in the previous Chapter.

9.3 Results and discussion

9.3.1 Viscoelastic behaviour between -150°C and 50°C

9.3.1.1 Storage modulus.

A two-fold decrease in the storage modulus (E') was observed as the temperature increases from -150 to 30°C, with values increasing on average from 7.5 GPa to 14.3 GPa. Similar values of E' were reported by Nishino *et al*. for all-cellulose composites obtained by partial dissolution.[29] The relatively large increase in E' at low temperature when compared to

room temperature can be attributed to restricted molecular mobility at lower temperatures due to a decrease in v^f and freezing of absorbed water.[314, 317]

9.3.1.2 β transition.

Between -72 and -45°C the composites exhibited a local peak in tan δ with an activation energy ΔH_a of 77.5±9.9 kJ/mol (Figure 53). This peak can be ascribed to the β transition as shown by Montès *et al.*[128] (85 kJ/mol) for anhydrous samples and Bradley *et al.*[312] (69 kJ/mol) for cellophane. The β transition is largely entropic in nature and will shift temperature according to moisture content. It is ascribed to the mobility of the main chain due to cooperative inter- and/or intramolecular contributions or molecular mobility within the amorphous regions.[128, 317]

Damping associated with the β relaxation usually decreases with increasing concentration but it also tends to be slightly lower for a longer dissolution time at a given concentration ($c \leq 15\%$) despite a decrease in *CrI* (Figure 54). This result shows that the mechanical behaviour of all-cellulose composites is not solely controlled by the crystallinity as described by *CrI*. Overall, the damping decreases with increasing concentration because less amorphous phase is available for mechanical damping. However, this explanation does not satisfy the decrease

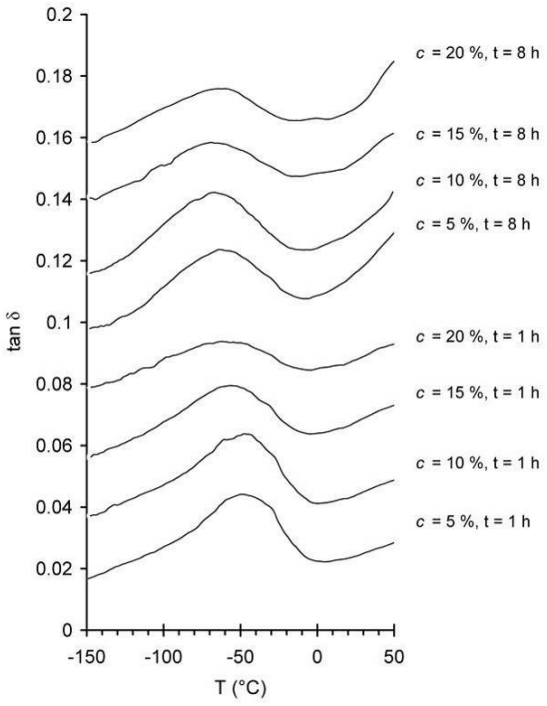

Figure 53 Tan δ as a function of temperature for various all-cellulose composites at 1 Hz (offset = 0.02).

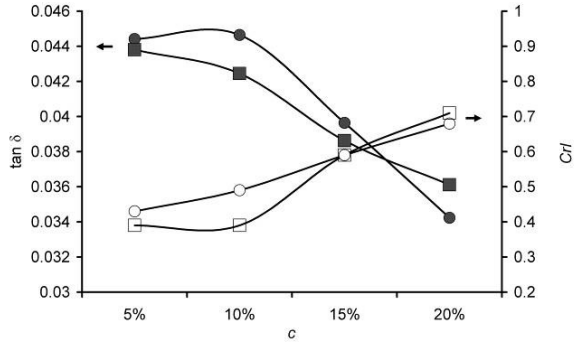

Figure 54 Maximum damping associated with of the β relaxation measured at 1 Hz for t = 1 h (●) and t = 8 h (■), and *CrI* as a function of initial cellulose concentration for t = 1 h (○) and t = 8 h (□).

in damping observed after longer dissolution times since the crystallinity usually decreases ($c \leq$ 15%). A decrease in the amplitude of the β transition has also been attributed to an increase in mechanical coupling between the reinforcement and the matrix, materialised by crystalline and amorphous cellulose in the present work.[318, 319] In the present case, partial dissolution results in some undissolved cellulose crystals being dispersed within the solution. With increasing dissolution time, it is envisaged that diffusion of the surface chains of the dissolving crystals is enhanced, allowing greater entanglement with the surrounding matrix. As a result, a higher volume of interfacial matrix material is generated and restricts the motion of the mobile cellulose chains in the matrix. In parallel, the HWH increases as the dissolution time is increased ($c \leq 15\%$) (Figure 55). HWH usually increases with an increasing distribution of relaxation times or molecular weight distribution of the mobile entities.[319, 320] Since the molecular weight of cellulose is not affected by the action of the LiCl/DMAc solvent, it must be the crystallites that acquire a better dispersion within the matrix that create a broader distribution of relaxation times.

Interestingly for $c = 20\%$, all the above-mentioned trends in CrI, damping capacity and HWH as a function of increasing dissolution time are reversed: CrI increases, tan δ increases and the size distribution of the mobile phase decreases. The increase in CrI and decrease in HWH are likely to be associated with some re-crystallisation process within the MCC where some surface chains would re-align against the interior chains. The increase in tan δ indicates less-than-perfect bonding between the regenerated and undissolved phases. While initial cellulose concentrations less than ~15% can lead to complete dissolution of the cellulose in 8 wt.% LiCl/DMAc, an undissolved portion will always remain for concentrations greater than 15%.[235] As a result, more interfacial defects could potentially be created in partially dissolved cellulose due to an exacerbated heterogeneity in solution and volume restrictions to polymer swelling.

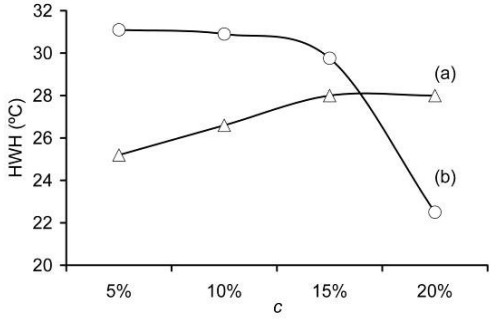

Figure 55 Half-width at half height of the β transition measured at 1 Hz for (a) t = 1 h and (b) t = 8 h.

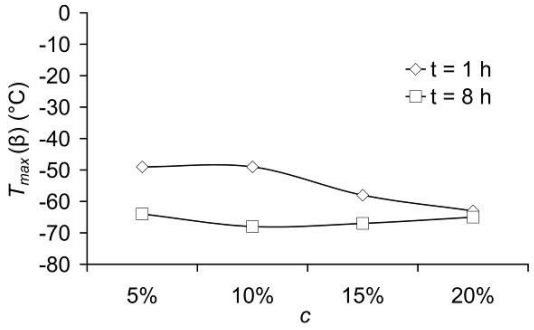

Figure 56 The β transition temperature (°C) as a function of the initial cellulose concentration (*c*) and dissolution time (t) at 1 Hz.

The β transition temperature T_{max}(β) was generally observed to decrease as t was increased from 1 to 8 h, although this appears to be more significant with a lower *c* value (Figure 56). To illustrate this, the β transition temperature of the composites with *c* = 5, 10, 15 and 20% decreased by 15, 19, 9 and 2°C, respectively. This could easily be explained by a decrease in *CrI* induced by an increase of t since a smaller amount of thermal energy would be required to provoke the transition in an all-cellulose composite with less motion restriction, *i.e.* less crystalline cellulose. For t = 8 h, T_{max}(β) is however approximately constant regardless of *c*

and is located in the range -68 to -64°C. As a result, the β relaxation is not controlled solely by the amount of crystallinity. If it was, T_{max}(β) would increase since it is expected that the higher molecular cohesion in the highly crystalline phase would require more thermal energy to relax. Hence, the composites produced in this work must comprise a higher amount of a phase that facilitates their molecular motion and counteracts the thermal effect of the crystalline phase. This phase is not the amorphous cellulose since a higher amount of crystals involves a lower amount of amorphous material available for relaxation. In this case, a facilitated molecular motion could have been artificially created by the presence of voids. Voids were evidenced in the previous Chapter by TEM.

9.3.1.3 γ peak and other secondary relaxations.

A γ transition is reported in the literature around -120 to -90°C, but was observed here only as a broad shoulder (Figure 53).[128, 312, 313] The lack of a distinct γ transition is possibly due to the extensive drying of samples that was carried out.[128, 312]

A secondary relaxation is often detected around -30°C and cannot be explained by a single relaxation process, such as a single hydrogen bond relaxation. The motion of fully bonded glucose rings, on their own or in pair, is preferred.[126] Zhou (2001) demonstrated that this peak could originate from changes in the aggregation state of frozen water or ice crystals.[317] The samples were extensively dried which could explain why this transition was not distinguishable from the main β relaxation.

9.3.2 Viscoelastic behaviour between 30°C and 350°C

9.3.2.1 α_3 transition.

The α_3 transition was observed between 40 and 50°C (Figure 57). α_3 is usually attributed to the motion of chains bound to water molecules by hydrogen bonding and mutual cross-linking that occurs as a result.[127, 129, 130] The activation energy of α_3 was calculated

by Yano *et al.* at 10.9 kJ/mol.[130] An activation energy in this range is consistent with that of hydrogen bonding in the non-crystalline regions.[126] The activation energy of α_3 could not be evaluated in the present work due to the difficulty in determining the α_3 transition temperature.

9.3.2.2 α_2 transition

The α_2 transition temperature was observed around 200°C (Figure 57). It is generally acknowledged that α_2 is a true glass transition since E' abruptly decreases by several orders of magnitude. Manabe et al. attributed α_2 to the micro-Brownian motion of whole polymer segments with "moderate" inter- and intramolecular bonding in the amorphous regions with an activation energy of 200-300 $kJ.mol^{-1}$.[127] As observed previously,[127, 130, 321] the α_2 transition temperature shifts to lower temperatures with an increase in *c* or CrI (Figure 58). Enhanced mechanical coupling between the stiffer, highly crystalline, cellulose and matrix phase could account for this effect. Indeed, mechanical coupling reduces the mobility of the interfacial amorphous regions and a smaller volume ratio of true amorphous phase is available for viscoelastic energy dissipation. As a result, a lower input of thermal energy is necessary for the same mechanical relaxation to happen since a smaller volume ratio of mobile chains is available.

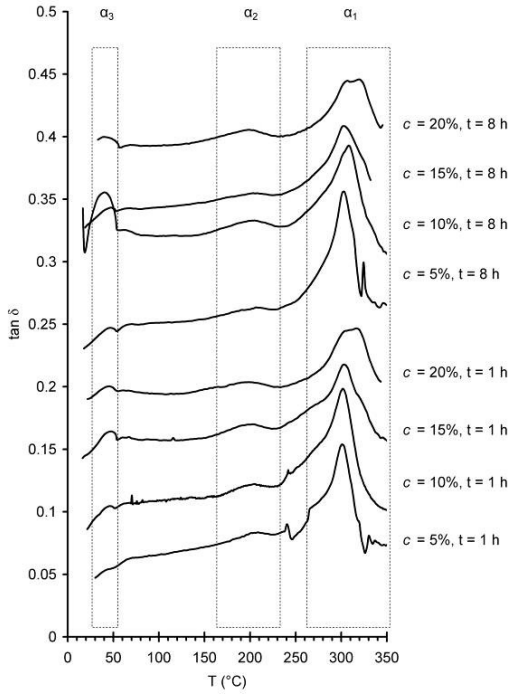

Figure 57 Tan δ plots at 1 Hz between room temperature and 350°C (offset = 0.05).

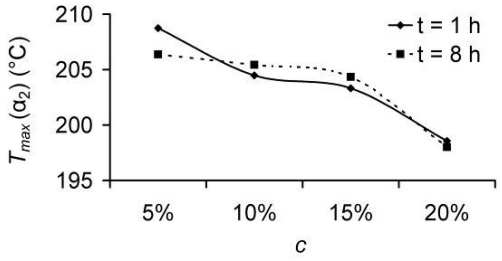

Figure 58 The α_2 transition temperature as a function of *c* and t at 1 Hz.

9.3.2.3 α_1 transition

For the first time, a double peak in tan δ for α_1 was observed in the range of 290-330°C (Figure 58). The lower temperature transition, denoted $\alpha_{1,2}$, was located at ~300°C while a second higher temperature transition, denoted $\alpha_{1,1}$, was observed at ~320°C. α_1 is delicate to monitor because cellulose starts degrading at such high temperatures. Manabe *et al.* reported only one high temperature relaxation peak for α_1 and calculated an overall activation energy of

1210 kJ/mol.[127] The same author inferred that the high temperature motion of amorphous chains with tight inter and intra-molecular bonds were the cause of α_1.[127] The determination of the activation energies of $\alpha_{1,1}$ and $\alpha_{1,2}$ was not possible at normal heating rates (i.e. 2°C/min) due to poor curve resolution. However, by using a very low heating rate, it was possible to calculate the activation energies of $\alpha_{1,1}$ and $\alpha_{1,2}$ for an all-cellulose composite with c = 20% and t = 1 h (Figure 59). T_{max} was shifted to lower values (~290 and 310°C) in the high resolution scan as the lower heating rate also reduced temperature lag. Using Equation (10), the activation energies of $\alpha_{1,2}$ and $\alpha_{1,1}$ were found to be -6170 kJ/mol and 9140 kJ/mol, respectively. $\alpha_{1,1}$ is more important in the composites with a higher *CrI*. Inversely, $\alpha_{1,2}$ is more prevalent in the composites with the lowest *CrI*.

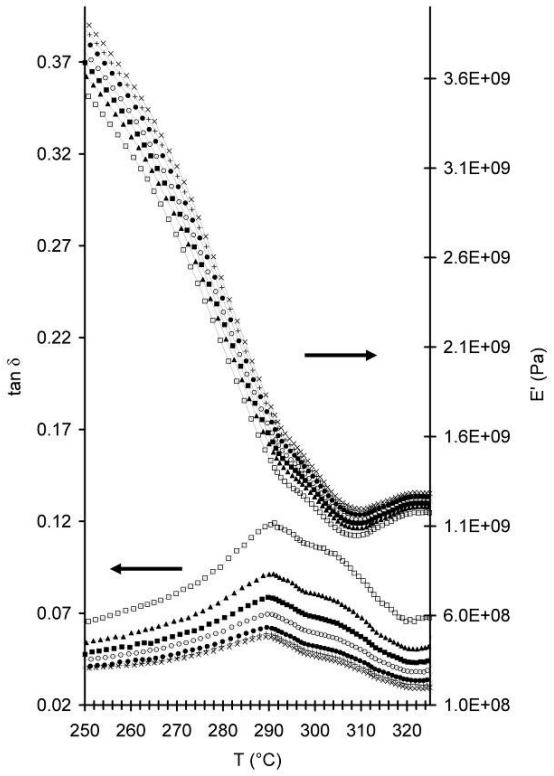

Figure 59 Plots of tan δ (lower curves) and E' for the high precision scan run at 0.2 Hz (□), 0.5 Hz (▲), 1 Hz (■), 2 Hz (○), 5 Hz (●), 10 Hz (+) and 20 Hz (×).

$\alpha_{1,2}$ has a negative activation energy, which is explained by the degradation of the cellulose. $\alpha_{1,2}$ is also predominantly associated with the phase with the highest amount of surface chains.

The observed correlation can be described by considering the processes involved. Firstly, pyrolysis begins around 300°C.[322, 323] CO, CO_2 and CH_4 are released during pyrolysis.[324] The discharge of these carbon compounds signals the destruction of some of the cellulose chains.[325] Hence, $\alpha_{1,2}$ is associated with a relaxation occurring during cellulose degradation. Secondly, the rate of pyrolysis depends on cellulose crystallinity. Amorphous regions are more easily degraded than crystalline regions.[322] Zickler *et al.* conducted X-ray diffraction of wood cellulose during pyrolysis. The results showed that cellulose crystallites were radially degraded by thermal activation, resulting in a decrease in the diameter of the

cellulose microfibril.[326] Thermal degradation is first likely to occur in the surface chains of the cellulose crystallites, since the crystallites are intact until a temperature of ~320°C.[326] As the surface chains are not shown in the X-ray data, it is assumed that below 320°C, only these chains and the amorphous chains are degraded.

9.3.2.4 Refinement of the high temperature thermo-mechanical model.

All-cellulose composites comprise two phases, according to earlier solid-state NMR and WAXD results.[26, 327] Generally, the microstructure consists of large cellulose I crystals embedded in a mixture of amorphous and paracrystalline cellulose. Paracrystalline cellulose comprises very small crystallites ~1.6 nm in width with all of the cellulose chains exposed to the surface.[327] Surface chains possess a different hydrogen bonding pattern to that of interior chains. Interior chains are known to have a strong intermolecular bonding involving the C6 group.[45, 311] This is reflected in the conformation of the C6 group in cellulose I: *trans-gauche*. In contrast, the surface chains are known to have a different NMR signature due to a rotation of the hydroxymethyl group around C5-C6.[328] As a result, C6 is found in a mixture of *gauche-trans* and *gauche-gauche* conformations. Consequently, intermolecular bonding between the surface and the interior chains is different to the one between interior chains.[70, 100, 267] The O6-O2' bond is not present in surface chains making the hydrogen bonding scheme similar to amorphous cellulose.[45, 304] Since hydrogen bonds govern the overall viscoelasticity of cellulose,[44, 130] it is proposed that phases rich in surface chains play a role similar to amorphous cellulose in terms of viscoelasticity at high temperatures, just as they behave similarly in moisture absorption.[70, 304, 328] True amorphous cellulose chains are, however, different to surface chains in that the displacement of the C4 peak in NMR studies shows that they are more coiled.[70, 87, 197]

Thus, Brownian motion of the amorphous and surface chains in the matrix phase is controlled by hydrogen bonding arrangements that are different from those of the interior

chains. Therefore, thermal degradation of the amorphous and surface chains occurs prior to the degradation of the crystalline phase that is more tightly bound.

It is proposed that $\alpha_{1,2}$ is due to the relaxation occurring during the degradation of the cellulose chains with the highest mobility that includes all "accessible" chains in the matrix phase. $\alpha_{1,1}$ is a high energy relaxation that emanates from the high temperature relaxation of the crystalline phase.

9.4 Conclusions

- By varying the processing parameters of all-cellulose composites obtained *via* partial dissolution of MCC, it was possible to produce a range of all-cellulose composites with varying amounts of exposed chains. When the composites were analyzed by mechanical spectroscopy, the contributions of the various phases of cellulose (amorphous, surface chains, crystal interior) to the viscoelastic behaviour and the role of these phases in the composite morphology (matrix, interface, reinforcement) became apparent.
- A more homogeneous crystallite distribution obtained by longer dissolution times largely controls the restriction in the mobility of the cellulose chains in the matrix. The effect of crystallite distribution on viscoelasticity can be greater than the overall crystallinity of the composites, as shown by $T_{max}(\beta)$ placement, HWH variations and tan δ magnitude.
- For solutions with $c \leq 15\%$, the damping at the low temperature β secondary relaxation generally decreases with an increase in crystallite quantity or with a better dispersion of the reinforcement distribution within the matrix. This phenomenon is attributed to enhanced mechanical coupling effect between the undissolved MCC and matrix phase. It shows the importance of the dissolution time on the viscoelasticity of all-cellulose composites, which is not obvious using chemical spectroscopy. For $c = 20\%$, however, contradictory trends in the evolution of the *CrI*, HWH and damping with the dissolution time were observed. A loss of

integrity in the material and a partial recrystallization of the MCC are suggested that could account for these effects.

- The α_2 peak in the 200°C region was displaced to lower temperatures when the crystallinity of the composite was increased, probably also due to a mechanical coupling effect.
- The α_1 relaxation in the 300-320°C region was observed as a doublet in tan δ. The lower temperature transition $\alpha_{1,2}$ is attributed to the thermal degradation of loosely packed chains such as those from the amorphous regions or surface chains of crystallites. The higher temperature transition $\alpha_{1,1}$ is thought to originate from the relaxation prior to thermal degradation of the tightly packed chains within the crystalline regions. The DMA technique applied to this series of model composites provides an indirect measure of the extent of crystalline to amorphous transformation undergone by the MCC during partial dissolution. The high temperature rheology of all-cellulose composites in particular provides a fingerprint for cellulose chains that differ in their hydrogen bonding arrangements.

10 Aerocellulose based on all-cellulose composites

10.1 Introduction

Aerogels were first defined by Kistler as highly porous materials in which the liquid in a gel is replaced with one continuous gas phase.[329, 330] However, capillary action due to the liquid leaving the gel structure would result in collapse of the surrounding gel material. Thus, the highly porous structure of an aerogel is only achieved if the liquid is permitted to leave the gel as a gaseous phase *via* freeze- or supercritical drying. Aerogels are rigid, lightweight materials that are characterised by an extensive interconnected network of voids or pores that possess a very high surface to volume ratio. Hence, aerogels are found in a variety of applications including catalysts, fuel cell electrodes, cosmic dust collectors, insulation materials and energy absorbers.[330-333] Aerogels can be prepared from a broad range of materials ranging from silica to cellulose.[306, 330, 332, 333]

In particular, cellulose is well recognised as being a renewable and biodegradable natural polymer with high mechanical properties in its natural or derivatised forms and thus has potential for use in eco-friendly aerogels. Kistler, the inventor of aerogels, was also one of the first to create aerogels from cellulose.[329] Following on from this, Tan *et al.* reported on the development of aerogels from crosslinked cellulose acetate and cellulose acetate butyrate *via* supercritical CO_2 drying.[334] Following this, Fischer *et al.* recently developed a sol-gel route where cellulose acetate was crosslinked by urethane bonding and dried by supercritical CO_2 drying.[335] Several researchers have also reported successful production of non-derivatised cellulose aerogels (also referred to as aerocellulose).[306, 336, 337]

The preliminary step in creating aerocellulose is to dissolve the cellulose. This is followed by precipitation in a suitable liquid media that acts to penetrate the structure and displace the solvent. For example, cellulose can be dissolved in aqueous calcium thiocyanate, precipitated in methanol and then rinsed with deionised water.[336, 337] Another possible route involves the dissolution of cellulose in hydrated N-methylmorpholine-N-oxide (NMMO),

precipitation in water or alcohol, and finally solvent exchange in an alcohol or acetone.[306] The final step involves using either freeze-drying [336, 337] or supercritical drying[306, 336] with the aim of preventing collapse of the cellulose.

The present Chapter attempts to merge the concepts of aerocellulose and all-cellulose composites with the aim of producing novel types of high strength, biodegradable aerogels. All-cellulose composites have recently been developed as a new class of biocomposite in which the microstructure consists of highly crystalline cellulose embedded in a matrix of regenerated cellulose.[23, 26, 28, 29] All-cellulose composites have some important advantages over other natural fibre biocomposites including greater compatibility between reinforcement and matrix, higher mechanical properties and inherent biodegradability.[23, 26, 28, 29] In this Chapter, all-cellulose composite aerogels have been synthesised *via* freeze-drying of cellulose gels obtained by partial dissolution of microcrystalline cellulose using an 8.0 wt.% LiCl/DMAc solvent system. The resulting aerocellulose was characterised in terms of density, microstructure, phase composition and mechanical properties.

10.2 Experimental methods

Preparation of aerocellulose

Cellulose dissolution using *N,N*-Dimethylacetamide (DMAc) initially involves an activation step in which the cellulose structure is first swollen *via* solvent exchange.[212, 229] The increased molecular mobility of cellulose after activation allows the LiCl/DMAc solvent to penetrate the cellulose structure more easily.[142, 227] In the present work, microcrystalline cellulose (MCC) powder (Avicel, Merck, particle size range 20-160 μm) was activated by immersing in distilled water at 20°C for 48 h and vacuum-filtering through Whatman No. 1 filter paper, twice immersing in acetone (Biolab, laboratory grade) at 20°C for 24 h and filtering through Whatman No. 1 filter paper to remove the acetone each time, twice immersing in DMAc (Merck, synthesis grade) at 20°C for 24 h and each time filtering through Whatman

No. 1 filter paper, vacuum-drying for 48 h at 60°C and finally passing the activated MCC through a sieve (90 μm). The activated MCC was vacuum-dried for a further 48 h at 60°C and finally sealed during storage. The degree of polymerization was 163 as determined using a method after Bianchi *et al.*[213]

A solution of 8.0% (by total weight) LiCl in DMAc was prepared by mixing LiCl (Unilab, 99% purity, dried in a vacuum oven at 180°C overnight) and DMAc (Merck, synthesis grade, dried over 4 Å molecular sieve prior to use) in a 200 ml Schott bottle that was immediately sealed to minimize any moisture uptake. The mixture was mechanically stirred for 24 h to ensure that the LiCl was completely dissolved. 4 g of activated MCC was immersed under constant stirring in a small beaker containing sufficient LiCl/DMAc to achieve cellulose concentrations of c = 5, 10, 15 and 20%, where c is expressed as a total percentage of cellulose on a weight basis. The solutions were stirred for 3 min, poured in Petri dishes and placed under controlled atmosphere (20°C and 33% R.H.) for 24 h. A low humidity atmosphere was employed to initiate gentle precipitation for improved shape retention of the gel. After the initial 24 h step, the gels were placed overnight at 76% R.H. and 20°C. At this stage, precipitation of the cellulose appeared to be complete. The precipitated cellulose was then thoroughly rinsed for 48 h under running tap water. The gels were then frozen overnight at -20°C. The gels were finally freeze-dried at -20°C and ~53 Pa for 48 h to produce samples of aerocellulose approximately 8 mm in thickness and 7-8 cm in diameter.

Materials characterisation

X-ray patterns were obtained with a Philips PW1729 using a Cu target (λ=1.54040 Å), voltage of 50 kV and current of 40mA over the range $5° < 2\theta < 50°$ in 0.02° steps. A crystallinity index (CrI) as defined by Segal *et al.* was used as a measure of the cellulose

crystallinity.[68] The measure was performed manually on graphs plotted from Microsoft Excel.

The bulk density of the aerocellulose was evaluated from the geometric dimensions and mass. Flexural mechanical testing of the aerocellulose was performed in accordance with ASTM-790. 3-point bend tests were conducted on an Instron Model 4444 (500 N load cell) at a crosshead speed of 10 mm/min. Samples were prepared 3-5 mm in height and 9-10 mm in width. A span of 35 mm was used between the sample supports. A minimum of 5 specimens were tested for each type of aerocellulose after conditioning for 40 h at 21±2°C and 55±5% R.H.. The flexural strength (σ_f) and modulus (E_b) were normalised by the density, and the flexural strain to failure (ε_f) was recorded. Samples for field emission scanning electron microscopy (JEOL 7000F FE-SEM) were freeze-fractured, mounted on carbon tabs, gold coated (Emitech K975X High Vacuum Evaporator, 25 mA current, 0.2 bar of Ar pressure) and observed using an accelerating voltage of 3 kV.

10.3 Results and discussion

Wide-angle X-ray scattering (WAXS)

The relationship between initial cellulose concentration and phase composition in aerocellulose tended to follow the same trend as that observed for the all-cellulose composites. The nature of the phase transformations during partial dissolution of MCC in 8 wt.% LiCl/DMAc has been previously analysed by WAXS and ^{13}C solid-state NMR. Partial dissolution of Avicel MCC involves the removal of sheets of cellulose from the surface of the initial cellulose I crystallites of the MCC. Following precipitation and drying, the peeled cellulose sheets assemble into a mixture of amorphous and paracrystalline cellulose, resulting in a biphasic nanostructure. The amorphous and paracrystalline cellulose act as the matrix in which large undissolved cellulose I crystals are embedded. ^{13}C solid-state NMR studies reveal a displacement of the C-4 peak and $T_2(H)$ value that are sufficiently distinct from those

observed for amorphous cellulose or highly crystalline cellulose I thus proving the existence of a paracrystalline phase. Paracrystalline cellulose produced in this work is a form of cellulose I with low crystallinity, analogous to cellulose IV_I and sufficiently small to have all of the chains exposed to the surface. As a result of the phase transformations observed in MCC, the initial (200) peak is displaced from $2\theta = 22.8°$ to $2\theta = 21°$. The transformation of the original cellulose I crystallites into amorphous and paracrystalline phases tends to increase with decreasing cellulose concentration (*c*), while the CrI simultaneously decreases.

Similarly, for aerocellulose a second peak (200) at $2\theta=20.9°$ associated with the paracrystalline matrix material progressively replaces the initial peak of strongly crystalline cellulose at $2\theta = 22.8°$ as *c* is decreased (Figure 60) while CrI decreases. CrI was measured to be 80% for activated MCC but decreased after dissolution to 67% for the composites prepared with *c* = 20%; 55% with *c* = 15%; 38% with *c* = 10%; and 35% with *c* = 5%. In accordance with decreasing CrI, the amount of paracrystalline matrix material created during partial dissolution increases. The crystalline (004) peak at $2\theta = 35°$ gradually disappears as *c* is decreased (Figure 60) which is indicative of longitudinal disorder in the paracrystalline material.

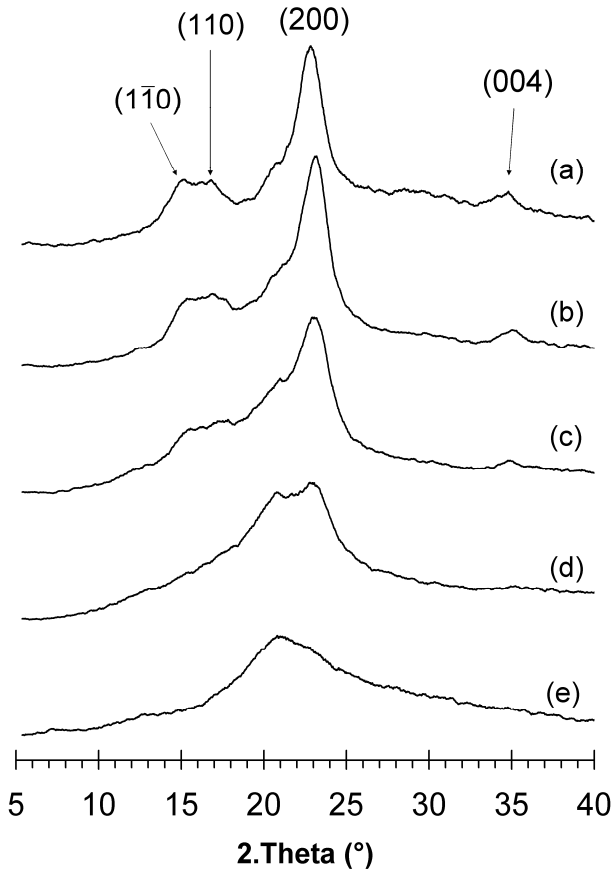

Figure 60 WAXS patterns of (a) activated MCC and all-cellulose composites prepared with (b) *c* = 20%, (c) *c* = 15%, (d) *c* = 10% and (e) *c* = 5%. Peaks are assigned according to the monoclinic cellulose I unit cell after Sugiyama *et al.*[73]

Mechanical properties of aerocellulose

The densities of the aerocellulose were in the range of 120-350 $kg.m^{-3}$. For compositions with a higher *c*, and thus containing higher amounts of undissolved MCC, the density increased and was also higher than the values normally encountered which range between 10 and 200 $kg.m^{-3}$ (Figure 61).[306, 336, 337] Initially, the gels that contain more cellulose per volume unit of LiCl/DMAc may be denser. The difference in density due to *c* persists through the entire precipitation, rinsing and freeze-drying process.[306]

The maxima in flexural strength and stiffness of 8.1 MPa and 280 MPa, respectively, were obtained when *c* = 10-15% (Figure 61). The observed maxima for this cellulose concentration are thought to be attributed to an optimal matrix to reinforcement ratio for a given material density. The specific flexural strength (σ_f) and specific stiffness (E_b) were also determined to take into account the highly variable density of aerocellulose (Figure 62). σ_f and E_b monotonically increase with *c* that shows the undissolved MCC plays an important role as a reinforcement. Whereas Hoepfner reported extremely ductile nanofibrillar aerocellulose,[336] the material studied in this work was rather brittle and normally failed in tension.

The flexural strain to failure is a minimum for the intermediate concentrations (*c* = 10%), although variation in ε_f was low over the concentration range studied. The amount of paracrystalline phase present in aerocellulose was increased with decreasing *c* (*e.g.* $c < 5\%$). Furthermore, low *c* allows more thorough dissolution which should lead to an aerocellulose with a more homogeneous and ductile microstructure. This was reflected in the higher strain to failure values at *c* = 5% (Figure 64). Conversely, aerocellulose with a higher initial cellulose concentration (*e.g.* $c > 15\%$) contains a larger proportion of undissolved highly crystalline cellulose I which reduces the ductility of the aerocellulose. The freeze-fractured surfaces of aerocellulose typically e

xhibit a relatively smooth appearance when the initial cellulose concentration is low with $c < 10\%$ (Figures 63a and b). As discussed, low c tends to produce a more homogeneous material due to the more thorough dissolution of the MCC fibrils which in turn leads to the regeneration of a paracrystalline phase with decreased longitudinal order. In contrast, when the cellulose concentration is increased, the fracture surfaces appear rougher that is indicative of fibril pull-out during fracture. Furthermore, the observed cellulose fibrils were 0.1-1 μm wide which is consistent in scale with the as-received MCC. Concentrations of $c = 15\%$ yield composites with a fracture surface that are intermediate in terms of their roughness. The increase in specific mechanical properties correlates with an increase in the crystallinity index (Figures 60 and 62). A higher crystallinity also translates into a higher proportion of undissolved fibrils as observed directly on the freeze-fractured composite surfaces (Figure 63). This trend in specific mechanical properties is expected since cellulose I is known to be stiffer than both its amorphous and paracrystalline counterparts. The Young's modulus of amorphous cellulose was calculated to be 10.42±1.08 GPa by Chen *et al.*[123] Using X-ray diffraction, Nishino *et al.* measured the elastic modulus in the direction parallel to the chain axis of several cellulose polymorphs. Cellulose I was found to have a modulus of 138 GPa whereas cellulose IV_I, which is similar to the paracrystalline matrix material formed by partial dissolution, exhibited a value of 75 GPa.[3] Ishikawa *et al.* published similar values and ranking of the mechanical properties of cellulose polymorphs based on ramie fibre.[107] Hence, the changes in the specific Young's modulus also reflect the changes in the cellulose molecular structure and correlate with the changes in the *CrI*.

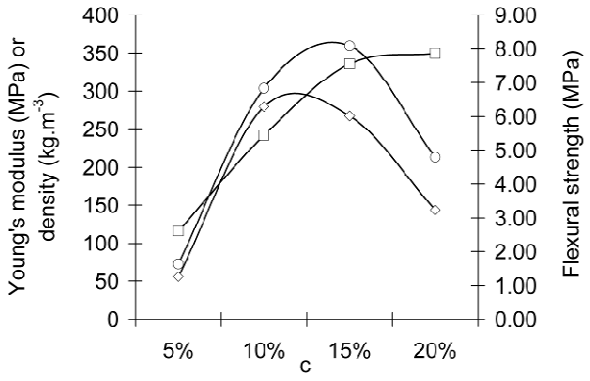

Figure 61 Young's modulus (◊), density (□) and flexural strength (○) of aerocellulose prepared with *c* = 5, 10, 15 and 20%.

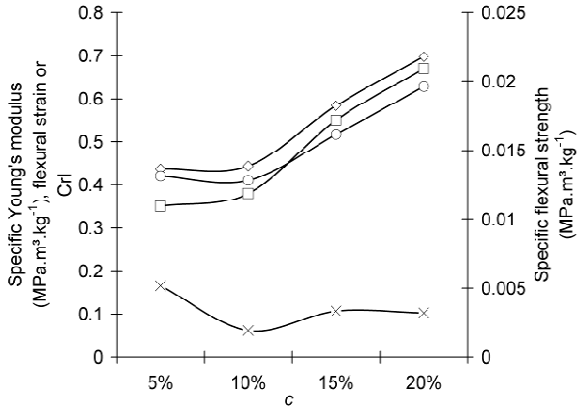

Figure 62 Graph showing the specific flexural strength (○), specific Young's modulus (◊), flexural strain (×) and CrI (□) of aerocellulose prepared with *c* = 5, 10, 15 and 20%.

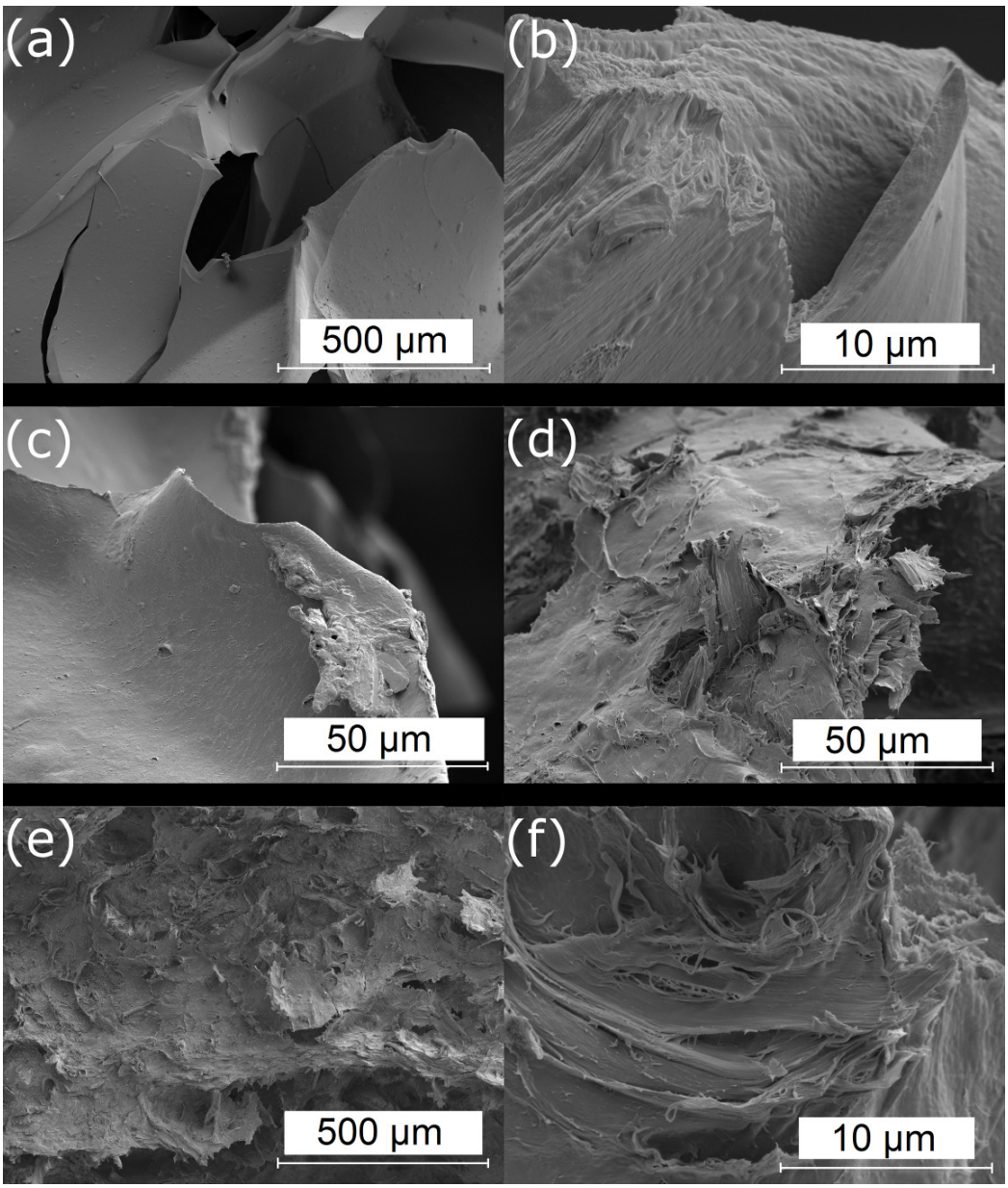

Figure 63 Scanning electron micrographs of freeze-fractured aerocellulose prepared with (a) and (b) *c*=5%, (c) *c*=10%, (d) *c*=15% and (e) and (f) *c*=20%.

10.4 Conclusions

Aerocellulose was successfully produced by dissolving MCC in LiCl/DMAc, precipitating in water and followed by freeze-drying. The resulting aerocellulose exhibits a highly porous structure for which the density increases with the initial cellulose concentration c giving rise to a family of materials with different mechanical characteristics. Overall, the consolidation mechanism is thought to involve the following steps:

- During dissolution in LiCl/DMAc, cellulose layers are peeled away from the crystals and form aggregates in solution. Those aggregates are precipitated by exposure to water. In the final material, they consolidate in a paracrystalline matrix that binds the larger cellulose crystals together. The amount of paracrystalline material is inversely proportional to c;
- The MCC fibrils are broken down into a paracrystalline matrix and split into smaller fibrils. For low cellulose concentrations ($c < 10\%$), the initially large MCC crystallites are almost completely replaced by a paracrystalline phase. Conversely, the materials with a high cellulose concentration ($c > 15\%$) exhibit a relatively different morphology where a large portion of the microstructure consists of fibrils that are consistent in scale with the original non-dissolved MCC or cellulose fibrils.

Generally, the specific flexural strength and stiffness increase with the content of highly crystalline cellulose. Specific mechanical properties similar to polystyrene, dry coconut timber, balsa wood in longitudinal properties and wood in transverse direction [124] make aerocellulose a bio-based, biodegradable and environmentally-friendly alternative to synthetic foams, with applications ranging from structural foams to packaging.

11 Conclusions

11.1 State-of-the-art

All-cellulose composites combine the advantages of being both fully based on an abundant natural resource and being readily biodegradable (Chapter 2). In order to produce all-cellulose composites, it is necessary to select a solvent that is appropriate for cellulose (Chapter 3). Whereas several solvents readily dissolve cellulose, the present study is focused on the LiCl/DMAc system (Chapter 3). All-cellulose composites owe their high mechanical properties to their *interfaceless* nature, which is, in other words, a full chemical compatibility between the crystalline cellulose acting as the reinforcement and the non-crystalline cellulose forming the matrix (Chapter 4). Their mechanical properties compare favourably with glass-fibre reinforced epoxy, which undoubtly constitutes a major benchmark for the industry.

Several manufacturing methods like wet-spinning, film forming, extrusion, vacuum forming, pultrusion or vacuum infusion seem can be used to consolidate all-cellulose composites (Chapter 5). Often, poor consolidation results from matrix shrinkage or poor wetting due to high matrix viscosity (Chapters 4 and 5). All those methods would involve the same basic process comprising three main steps: cellulose dissolution, precipitation and drying (Figure 64).

One condition that should be kept under scrutiny during all-cellulose composites manufacturing, regardless of the method chosen, is the water content at the point where hydrogen bonds start reforming between cellulose chains in the matrix material (Chapter 6). In the case of a 1 wt.% kraft dissolved in 8 wt.% LiCl/DMAc, this water content was evaluated at 7 g/g of cellulose (Chapter 6). When the water content is higher than this value, the cellulose in the hydrogel has a ^{13}C solid-state NMR spectrum analogous to that of cellulose in solution, which is confirmed by a WAXS pattern similar to true amorphous cellulose (Chapter 6).[205] Above a water content of 7 g/g of cellulose, no modification in the cellulose chain

conformation occurs since the water escaping from the hydrogel comes from the more mobile water protons that are trapped in the microvoids of the hydrogel.[256, 257] When the water content is less than this value, water protons that were bound to the cellulose chains are removed and the cellulose chains start re-aligning against each other, forming a low crystallinity matrix material (Chapter 6 and 7). The matrix material could not be strictly identified with the sole use of WAXS due to its lack of crystallinity. Solid-state ^{13}C NMR and FTIR were found to provide a useful supplement of information by showing that the matrix was a mixture of amorphous and paracrystalline cellulose. The paracrystalline phase was similar to a poorly crystalline form of cellulose I, such as cellulose IV_I or ball-milled cellulose I (Chapter 7). In particular, solid-state ^{13}C NMR was useful to show that the cellulose chains in the paracrystalline material were not sufficiently coiled to fall into the amorphous cellulose category. In the case of an all-cellulose composite obtained by partial dissolution of microcrystalline cellulose (MCC), spectroscopy and microscopy techniques provided sufficient evidence for a non-homogeneous material comprising a matrix made of the above-mentioned regenerated cellulose and a reinforcement made of undissolved cellulose. The statement holds true for all the manufacturing paths that were studied (Figure 65). Visibly, the initial cellulose concentration in the solvent system was the main factor controlling the crystallinity *CrI* of the material, followed by the dissolution time (Chapter 7). The precipitation conditions were also found to change the *CrI*, since a slow precipitation by controlled exposure to water vapour, rather than immersion, increased *CrI* by 10% (Chapter 8). Microscopy proved that slow precipitation has the advantage of significantly reducing the defects created by delamination.

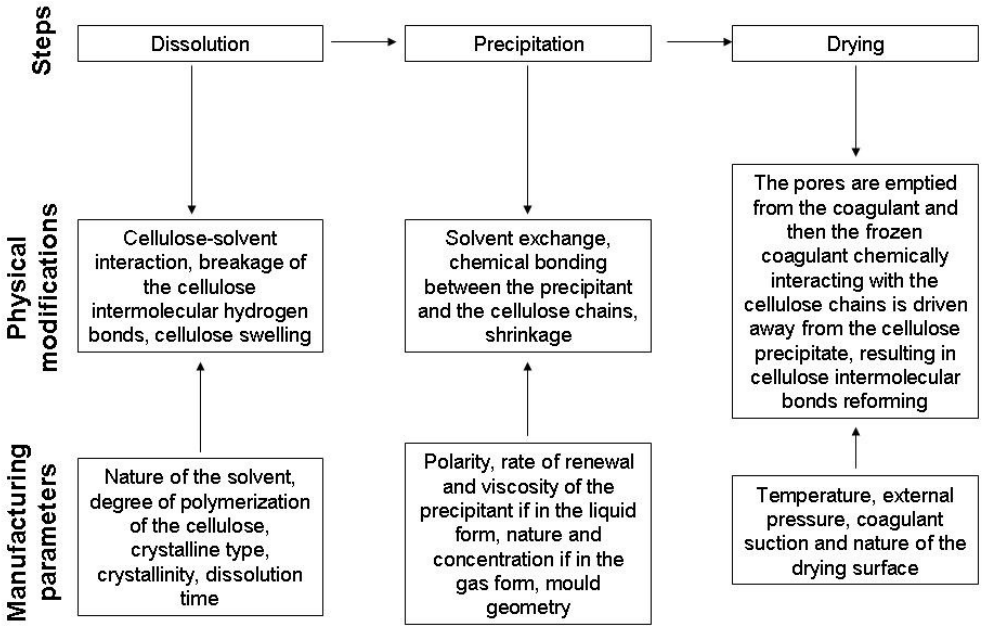

Figure 64 Schematic of the physical modifications and process parameters involved in the different steps of all-cellulose composites manufacturing.

Delamination originates from the differential shrinkage of the partially dissolved cellulose occurring during the precipitation stage. Consequently, the mechanical properties were improved by slow precipitation (Figure 50, Chapter 8). The dissolution time could be used to provide final materials with a more homogeneous microstructure. Indeed, a prolonged dissolution induced enhanced swelling of the MCC which in turn provided a better distribution of the undissolved MCC fibrils within the matrix. All-cellulose composites obtained after thorough dissolution (low initial cellulose concentration and extended dissolution time) exhibited smooth fracture surfaces. On the contrary, all-cellulose composites obtained with a high initial cellulose concentration in the solvent or a short dissolution time displayed large undissolved MCC fibril fragments. Overall, mechanical testing showed that the mechanical

properties of all-cellulose composites obtained *via* a slow precipitation process exhibited little variation when the intial cellulose concentration *c* was varied. In particular, the tensile strength of these materials was consistently ~100 MPa. The stronger intermolecular bonds in the highly crystalline material that was obained by selecting higher initial cellulose concentrations *c* could be compensated for by improved consolidation by thorough dissolution for low *c* values. In this case, improved consolidation might be attributed to the lower viscosity of the cellulose solution.

The two-phase character of the consolidated cellulose, based on undissolved cellulose crystals embedded in a matrix of amorphous and paracrystalline phases, also had an influence on the viscoelastic behaviour of all-cellulose composites (Chapter 9). A series of model all-cellulose composites were used to more closely examine the relationship between the phase composition and microstructure and the viscoelastic behaviour in the temperature range of -150°C to 350°C by studying the secondary (β and γ) and primary ($\alpha_{1,2}/\alpha_{1,1}$, α_2 and α_3) mechanical relaxations with dynamic mechanical spectroscopy.

It was found that damping (β relaxation) decreases with increasing crystallinity, indicating that molecular mobility of the matrix phase in all-cellulose composites is restricted by an increasing proportion of crystalline phase. This observation is readily explained in terms of the accepted paradigm of crystalline-amorphous interfacial interaction effects on the relaxation or damping mechanisms. Inconsistent with this theory was the observed simultaneous decrease in crystallinity and damping with increasing dissolution times for $c \leq 15\%$. Moreover, for $c = 20\%$ the trend was reversed as an increase in dissolution time increased the crystallinity and damping. A systematic relationship between the crystallinity, dissolution time, phase composition and viscoelasticity in all-cellulose composites at first appears to be complex; however, this was elucidated by recognising the changes that take place in the microstructure during processing of this new class of biocomposite. Of particular interest, the amplitude ratio of the high temperature $\alpha_{1,2}$ and $\alpha_{1,1}$ peaks varies according to the extent of transformation

undergone by the MCC during the partial dissolution. The first $\alpha_{1,2}$ peak was attributed to the thermal decomposition of loosely bonded cellulose chains in the amorphous or paracrystalline phase whereas the $\alpha_{1,1}$ peak corresponds to a relaxation of the strongly bonded interior chains in the crystalline phase. Finally, a practical application of all-cellulose composites was explored (Chapter 10). Aerocellulose was obtained from freeze-dried hydrogels of partially dissolved MCC. The freeze-drying process was used in place of the vacuum-bag technique used for the preparation of the specimens studied in Chapters 8 and 9. Freeze-drying has the advantage of preserving the openness of the hydrogel structure during the drying process. The density of aerocellulose increased with the initial cellulose concentration and ranged from 116 to 350 $kg.m^{-3}$. Aerocellulose with relatively high mechanical properties were successfully produced. The flexural strength of the materials reached 8.1 MPa and their stiffness was as high as 280 MPa, which compares with balsa wood.

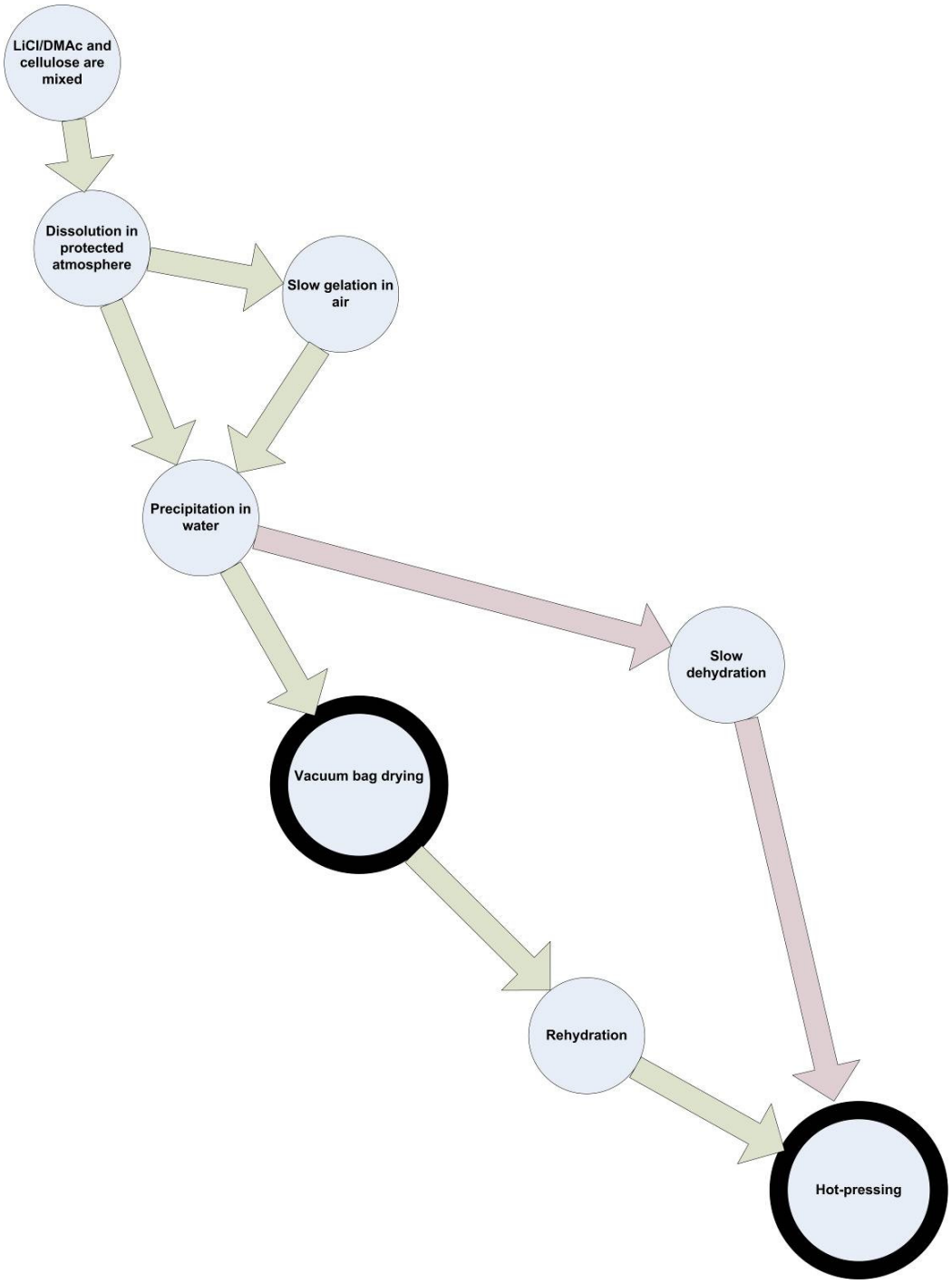

Figure 65 Various manufacturing paths are possible in order to produce an all-cellulose composite from MCC by partial dissolution in LiCl/DMAc.

11.2 Key questions for the understanding of all-cellulose composites structures

At several occasions, the presence of voids in the composite material was demonstrated in this work (Chapters 7 and 9). Unfortunately, the voids were not quantified, even though they undeniably constitute the third "phase" of all-cellulose composites, after the paracrystalline and amorphous matrix and the crystalline reinforcement. From the present work, it appears that voids are controlled by four main factors:

- initial cellulose concentration,
- rate of precipitation,
- drying method, and
- dissolution time.

The distribution of the cellulose chains becomes more homogeneous within the cellulose slurry as the dissolution time is increased. Microscopic heterogeneities are expected to create zones of strain in the drying hydrogel. The strains will be exacerbated by the shrinkage occurring during the precipitation and drying processes, eventually resulting in voids or cracks. As a result of a longer dissolution time, less heterogeneity at the microscopic level in the density distribution of the partially dissolved cellulose is created, and less cracks should occur. In any case, much could be learnt from the quantitative study of the distribution of voids depending on the manufacturing parameters.

Another variable that should be studied in the future is the degree of polymerization. An increase in DP is known to increase the viscosity of the dissolved cellulose solution. Consquently, impregnation of cellulosic fibres (when the composite is prepared by embedding) or diffusion of the cellulose chains within the partially dissolved cellulose should be slower. It is also expected that a higher DP creates regenerated materials with more strength due to the increased proportion of covalent bonds compared to hydrogen bonds.

Finally, this is the first time a regeneration study of a *saturated* solvent solution of cellulose (*i.e.* c = 20%) has been carried out. Unexpected results were obtained such as the re-ordering of the molecules consistent with an increase in crystallinity (Chapters 8 and 9) and a decrease in the size distribution of the mobile entities as indicated by a narrower peak for the β relaxation. Yet, the material appeared to be properly consolidated and it had relatively high mechanical properties. Of all the composites manufactured in this work, all-cellulose composites produced with high initial cellulose concentrations (typically, c = 20%) also had the highest dimensional stability throughout the process due to low shrinkage. It is believed that low shrinkage eases the creation of pre-defined shapes as well as minimizing manufacturing constraints like large mould depths. In the case of cellulose, the composites obtained with a high cellulose concentration also exhibit the lowest moisture absorption.

11.3 The future of all-cellulose composites and the challenges that lay ahead

In the perspective of an industry that will have to find alternatives to petrol, plastic replacements based on cellulose could find their way. Cellulose cannot be digested by humans and so it is a natural resource that would not be used for the production of goods of secondary importance and at the expense of food, as is currently the case with corn. Cellulose can be derived at virtually no cost from items at the end of their life cycle that would otherwise be disposed of. Such items include used textiles, papers, cardboards, and furniture made from wood, bamboo or wicker.

The manufacturing process of all-cellulose composites should be ameliorated by using solvents that do not involve a time-intensive pre-treatment (or activation) step such as LiCl/DMAc. Ideally, solvents that can be recycled and integrated in a low energy (low temperature) process would have a lower environmental impact while being more cost-effective. Succesful candidates include NMMO, sodium hydroxide in combination with urea or thiourea and ionic liquids (Chapter 3). Ionic liquids can be produced that yield concentrated

cellulose solutions with low viscosity, which could facilitate the processing of all-cellulose composites obtained by partial dissolution of cellulose.[338]

Hydrophobicity would be a major advancement for all-cellulose composites as moisture uptake is already a limiting factor for the use of many biocomposites. This hydrophobicity could be obtained *via* suitable surface treatments including traditional oiling, waxing, varnishing or painting. More sophisticated methods are however available to the cellulose scientist, such as grafting of specific hydrophobic groups onto the hydrophilic hydrogen bonds. Recently a treatment based on chemical vapour deposition of polymethylsiloxane has been proposed to transform cellulose into superhydrophobic cellulose, which could have a water contact angle as high as 150º.[339] Another treatment is known that involves the grafting of "fluorinated brushes" also resulting in superhydrophobicity.[340]

Derivatization after consolidation of all-cellulose composites is also a possibility that could, in the future, provide all-cellulose composites that would be water resistant, biodegradable, thermoformable and orthotropic.[9, 103, 157, 166, 245, 249] Such treatments could be carried in the wet form or possibly in supercritical conditions in order to penetrate the composite through its thickness and yield a homogeneous material that could retain some of its initial molecular orientation.

The initial hydrogel form of all-cellulose composites also opens up perspectives for the forming of materials with a pre-determined pore structure.[306, 335, 337, 341] Cellulose can be used as a template and transformed into a different material by functionalization, derivatization or petrifaction.[342, 343] By extrapolation, all-cellulose composites can be used in applications similar to bacterial cellulose (BC). BC was used for gene detection, audio membranes, high resolution dynamic displays or high strength electrically conductive papers.[60, 344-346] Yano *et al.* used the unique nanoporous BC morphology to create optically transparent high strength composite films.[347] BC sheets were also used in cellulose acetate butyrate composites.[245]

In any case, cellulose is the most abundant polymer on Earth and only a positive outcome can be gained by generating more knowledge related to its chemico-physical structure and how to transform it into useful products. Despite their complexity, all-cellulose composites have a tremendous potential and, undeniably, a bright future.

REFERENCES

1. Preston, R.D., *The physical biology of plant cell walls*. 1974, London: Chapman and Hall. 491 illus.
2. Taiz, L. and E. Zeiger, *Plant physiology*. The Benjamin/Cummings series in the life sciences. 1991, Redwood City, Calif: Benjamin/Cummings Pub. Co. xxxii, 559.
3. Nishino, T., K. Takano, and K. Nakamae, *Elastic Modulus of the Crystalline Regions of Cellulose Polymorphs.* Journal of Polymer Science: Part B: Polymer Physics, 1995. **33**(11): p. 1647-1651.
4. Cottrell, A.H., *Strong Solids.* Proceedings of the Royal Society of London. Series A, Mathematical and Physical Sciences (1934-1990), 1964. **282**(1388): p. 2-9.
5. Bledzki, A.K. and J. Gassan, *Composites reinforced with cellulose based fibres.* Progress in Polymer Science, 1999. **24**(2): p. 221-274.
6. Li, Y., Y.-W. Mai, and L. Ye, *Sisal fibre and its composites: a review of recent developments.* Composites Science and Technology, 2000. **60**(11): p. 2037-2055.
7. Zafeiropoulos, N.E., et al., *Engineering and characterisation of the interface in flax fibre/polypropylene composite materials. Part I. Development and investigation of surface treatments.* Composites Part A: Applied Science and Manufacturing, 2002. **33**(8): p. 1083-1093.
8. Madsen, B. and H. Lilholt, *Physical and mechanical properties of unidirectional plant fibre composites- an evaluation of the influence of porosity.* Composites Science and Technology, 2003. **63**(9): p. 1265-1272.
9. Glasser, W.G., et al., *Fiber-reinforced cellulosic thermoplastic composites.* Journal of Applied Polymer Science, 1999. **73**(7): p. 1329-1340.
10. Mwaikambo, L.Y. and M.P. Ansell, *Chemical modification of hemp, sisal, jute, and kapok fibers by alkalization.* Journal of Applied Polymer Science, 2002. **84**(12): p. 2222-2234.
11. Gassan, J. and V.S. Gutowski, *Effects of corona discharge and UV treatment on the properties of jute-fibre epoxy composites.* Composites Science and Technology, 2000. **60**(15): p. 2857-2863.
12. Eichhorn, S.J., et al., *Review of Current International Research into Cellulosic Fibres and Composites.* Journal of materials science, 2001. **36**(9): p. 2107-2131.
13. Wang, Y., X. Cao, and L. Zhang, *Effects of cellulose whiskers on properties of soy protein thermoplastics.* Macromolecular Bioscience, 2006. **6**(7): p. 524-531.
14. Dufresne, A. and M.R. Vignon, *Improvement of Starch Film Performances Using Cellulose Microfibrils.* Macromolecules, 1998. **31**(8): p. 2693-2696.
15. Dufresne, A., J.-Y. Cavaillé, and M.R. Vignon, *Mechanical behavior of sheets prepared from sugar beet cellulose microfibrils.* Journal of Applied Polymer Science, 1997. **64**(6): p. 1185-1194.
16. AziziSamir, M.A.S., F. Alloin, and A. Dufresne, *Review of Recent Research into Cellulosic Whiskers, Their Properties and Their Application in Nanocomposite Field.* Biomacromolecules, 2005. **6**(2): p. 612-626.
17. Helbert, W., J.Y. Cavaillé, and A. Dufresne, *Thermoplastic nanocomposites filled with wheat straw cellulose whiskers. Part I: Processing and mechanical behavior.* Polymer Composites, 1996. **17**(4): p. 604-611.
18. Grunnert, M. and W.T. Winter, *Nanocomposites of cellulose acetate butyrate reinforced with cellulose nanocrystals.* Journal of polymers and the environment, 2002. **10**(1/2): p. 27-30.

19. Henriksson, M. and L.A. Berglund, *Structure and properties of cellulose nanocomposite films containing melamine formaldehyde.* Journal of Applied Polymer Science, 2007. **106**(4): p. 2817-2824.
20. Svagan, A.J., M.A.S. AziziSamir, and L.A. Berglund, *Biomimetic Polysaccharide Nanocomposites of High Cellulose Content and High Toughness.* Biomacromolecules, 2007. **8**(8): p. 2556-2563.
21. Jones, D., *Cellular fabric.* Nature, 1993. **363**(6429): p. 500.
22. Nishino, T., I. Matsuda, and K. Hirao. *Cellulose Self-reinforced Composite*. in *Ecocomp 2003*. 2003. Queen Mary, University of London.
23. Nishino, T., I. Matsuda, and K. Hirao, *All-cellulose composite.* Macromolecules, 2004. **37**(20): p. 7683-7687.
24. Nishino, T. and N. Arimoto. *All-cellulose composite by partial dissolving of fibers*. in *Ecocomp 2005*. 2005. Stockholm.
25. Peijs, T. and F. Vilaseca. *Cellulose-based nanocomposites*. in *Ecocomp 2005*. 2005. KTH, Stockholm.
26. Gindl, W. and J. Keckes, *All-cellulose nanocomposite.* Polymer, 2005. **46**(23): p. 10221-10225.
27. Gindl, W., et al., *Structural changes during tensile testing of an all-cellulose composite by in situ synchrotron X-ray diffraction.* Composites Science and Technology, 2006. **66**(15): p. 2639-2647
28. Gindl, W., T. Schoberl, and J. Keckes, *Structure and properties of a pulp fibre-reinforced composite with regenerated cellulose matrix.* Applied Physics a-Materials Science & Processing, 2006. **83**(1): p. 19-22.
29. Nishino, T. and N. Arimoto, *All-Cellulose Composite Prepared by Selective Dissolving of Fiber Surface.* Biomacromolecules, 2007. **8**(9): p. 2712-2716.
30. Qin, C., et al., *The effect of fibre volume fraction and mercerization on the properties of all-cellulose composites.* Carbohydrate Polymers, 2008. **71**(3): p. 458-467.
31. Czvikovszky, T. and T. Czigány. *Harmonization of plastics and the environment in the 21-st century*. [cited; Available from: www.bmf.hu/conferences/jubilee/czvikovszky.pdf.
32. Usborne, S., *Grow your own plastic*, in *The Independant*. 2007: London.
33. Krässig, H., et al., *Cellulose*, in *Ullmann's Encyclopedia of Industrial Chemistry*, W.-V.V.G. Co., Editor. 2002.
34. Reddy, N. and Y. Yang, *Properties and potential applications of natural cellulose fibers from cornhusks.* Green Chemistry, 2005. **7**(4): p. 190-195.
35. Rosenau, T., *A report from the 2005 Japanese-European Workshop on "cellulose and functional polysaccharides".* Holzforschung, 2005. **60**(5): p. 465.
36. Schurz, J., *'Trends in polymer science' - A bright future for cellulose.* Progress in Polymer Science, 1999. **24**(4): p. 481-483.
37. Vigo, L.V., *Interaction of cellulose with other polymers: retrospective and prospective.* Polymers for advanced technology, 1998. **9**(9): p. 539-548.
38. Kim, J., S. Yun, and Z. Ounaies, *Discovery of Cellulose as a Smart Material.* Macromolecules, 2006. **39**(12): p. 4202-4206.
39. Fleming, K., D. Gray, and S. Matthews, *Cellulose Crystallites.* Chemistry, 2001. **7**(9): p. 1831-1836.
40. Bordel, D., J.-L. Putaux, and L. Heux, *Orientation of Native Cellulose in an Electric Field.* Langmuir, 2006. **22**(11): p. 4899-4901.
41. Sugiyama, J., H. Chanzy, and G. Maret, *Orientation of cellulose microcrystals by strong magnetic fields.* Macromolecules, 1992. **25**(16): p. 4232-4234.
42. O'Sullivan, A.C., *Cellulose: the structure slowly unravels.* Cellulose, 1997. **4**(2): p. 173-208.

43. Young, R.A. and R.M. Rowell, *Cellulose : structure, modification, and hydrolysis*. 1986, New York: Wiley. xix, 379.
44. Hinterstoisser, B. and L. Salmen, *Application of dynamic 2D FTIR to cellulose.* Vibrational Spectroscopy, 2000. **22**(1-2): p. 111-118.
45. Kondo, T. and C. Sawatari, *A fourier transform infra-red spectroscopic analysis of the character of hydrogen bonds in amorphous cellulose.* Polymer, 1996. **37**(3): p. 393-399.
46. Gardner, K.H. and J. Blackwell, *The structure of native cellulose.* Biopolymers, 1974. **13**(10): p. 1975-2001.
47. Kolpak, F.J. and J. Blackwell, *Determination of the Structure of Cellulose II.* Macromolecules, 1976. **9**(2): p. 273-278.
48. Hashimoto, T., et al., *Chemical Reaction at Specific Sites and Reaction-Induced Self-Assembly as Observed by in Situ and Real Time SANS: Enzymatic Polymerization to Synthetic Cellulose.* Biomacromolecules, 2006. **7**(9): p. 2479-2482.
49. Kobayashi, S., J. Sakamoto, and S. Kimura, *In vitro synthesis of cellulose and related polysaccharides.* Progress in Polymer Science, 2001. **26**(9): p. 1525-1560.
50. Saxena, I.M. and R.M. Brown Jr, *Cellulose synthases and related enzymes.* Current Opinion in Plant Biology, 2000. **3**(6): p. 523-531.
51. Brown Jr, R.M. and I.M. Saxena, *Cellulose biosynthesis: A model for understanding the assembly of biopolymers.* Plant Physiology and Biochemistry, 2000. **38**(1-2): p. 57-67.
52. Schuerch, C., A. Sarko, and College of Environmental Science and Forestry. Cellulose Research Institute., *Cellulose and wood--chemistry and technology : biogenesis and structure of cellulose : the cellulose-water system, chemistry of cellulose and wood, surface chemistry of wood and paper, cellulosic membranes : proceedings of the Tenth Cellulose Conference*. 1989, New York: Wiley. xvi, 1638.
53. Frey-Wyssling, A., *The plant cell wall*. 3. completely rev. . ed. 1976, Berlin ; Stuttgart: Borntraeger. xi, 294.
54. Brändström, J., et al., *Ultrastructure of commercial recycled pulp fibers for the production of packaging paper.* Holzforschung, 2005. **59**(6): p. 675-680.
55. Cave, I.D., *Theory of X-ray measurement of microfibril angle in wood.* Wood Science and Technology, 1997. **31**(4): p. 225-234.
56. Bodig, J. and B.A. Jayne, *Mechanics of wood and wood composites*, ed. V.N. Reinhold. 1982, New York: Krieger Publishing Company.
57. Vandamme, E.J., et al., *Improved production of bacterial cellulose and its application potential.* Polymer Degradation and Stability, Biodegradable Polymers and Macromolecules, 1998. **59**(1-3): p. 93-99.
58. Klemm, D., et al., *Bacterial synthesized cellulose -- artificial blood vessels for microsurgery.* Progress in Polymer Science, 2001. **26**(9): p. 1561-1603.
59. Astley, O.M., et al., *Structure of Acetobacter cellulose composites in the hydrated state.* International Journal of Biological Macromolecules, 2001. **29**(3): p. 193-202.
60. Nishi, Y., et al., *The structure and mechanical properties of sheets prepared from bacterial cellulose.* Journal of Materials Science, 1990. **25**(6): p. 2997-3001.
61. Jarvis, M.C. *Celllulose structure and hemicellulose-cellulose association*. in *The hemicelluloses workshop*. 2005. University of Canterbury, Christchurch, New Zealand.
62. Jarvis, M., *Cellulose stacks up.* Nature, 2003. **426**(6967): p. 611.
63. Hermans, P.H., *Physics and chemistry of cellulose fibres : with particular reference to rayon*. Elsevier's polymer series ; 2. 1949, New York: Elsevier Pub. Co. xxii, 534.
64. Hearle, J.W.S., *The development of ideas of fine structure*, in *Fibre structure*, Butterworth, Editor. 1963, The Textile Institute: London-Manchester.
65. Takahashi, M. and M. Ookubo, *CP/MAS 13C NMR and WAXS studies on the effects of starting cellulose materials on transition between cellulose polymorphs.* Kobunshi Ronbunshu, 1993. **51**(2): p. 107-113.

66. Mann, J., *Modern methods of determining crystallinity in cellulose.* Pure and Applied Chemistry, 1962. **5**(6): p. 91-105.
67. Hulleman, S.H.D.v.H., Johanna M.; van Dam, Jan E. G., *Determination of crystallinity in native cellulose from higher plants with diffuse reflectance Fourier-transform infrared spectroscopy.* Carbohydrate Research, 1994. **261**(1): p. 163-172.
68. Segal, L., et al., *An empirical method for estimating the degree of crystallinity of native cellulose using the X-ray diffractometer.* Textile Res. J., 1959. **29**(10): p. 786-794.
69. Newman, R.H., *Estimation of the lateral dimensions of cellulose crystallites using 13C NMR signal strengths.* Solid State Nuclear Magnetic Resonance, 1999. **15**(1): p. 21-29.
70. Newman, R.H. and J.A. Hemmingson, *Carbon-13 NMR distinction between categories of molecular order and disorder in cellulose.* Cellulose, 1995. **2**(2): p. 95-110.
71. Hermans, P.H. and A. Weidinger, *Quantitative X-Ray Investigations on the Crystallinity of Cellulose Fibers. A Background Analysis.* Journal of Applied Physics, 1948. **19**(5): p. 491-506.
72. Nelson, M.L. and R.T. O'Connor, *Relation of certain infrared bands to cellulose crystallinity and crystal lattice types. Part II. A new infrared ratio for estimation of crystallinity in celluloses I and II.* Journal of Applied Polymer Science, 1964. **8**(3): p. 1325-1341.
73. Sugiyama, J., R. Vuong, and H. Chanzy, *Electron diffraction study on the two crystalline phases occurring in native cellulose from an algal cell wall.* Macromolecules, 1991. **24**(14): p. 4168-4175.
74. Langan, P., Y. Nishiyama, and H. Chanzy, *X-ray Structure of Mercerized Cellulose II at 1 Å Resolution.* Biomacromolecules, 2001. **2**(2): p. 410-416.
75. Wada, M., et al., *Improved Structural Data of Cellulose IIII Prepared in Supercritical Ammonia.* Macromolecules, 2001. **34**(5): p. 1237-1243.
76. Zugenmaier, P., *Conformation and packing of various crystalline cellulose fibers.* Progress in Polymer Science, 2001. **26**(9): p. 1341-1417.
77. Kulshreshta, A. and N.E. Dweltz, *Paracrystalline Lattice Disorder in Cellulose .1. Reappraisal of Application of 2-Phase Hypothesis to Analysis of Powder X-Ray Diffractograms of Native and Hydrolyzed Cellulosic Materials.* Journal of Polymer Science Part B-Polymer Physics, 1973. **11**(3): p. 487-497.
78. Hindeleh, A.M. and R. Hosemann, *Paracrystals Representing the Physical State of Matter.* Journal of Physics C-Solid State Physics, 1988. **21**(23): p. 4155-4170.
79. Kondo, T., E. Togawa, and R.M. Brown, *"Nematic ordered cellulose": A concept of glucan chain association.* Biomacromolecules, 2001. **2**(4): p. 1324-1330.
80. Fink, H.-P., et al., *The structure of amorphous cellulose as revealed by wide-angle X-ray scattering.* Polymer, 1987. **28**(8): p. 1265-1270.
81. Nelson, M.L. and R.T. O'Connor, *Relation of certain infrared bands to cellulose crystallinity and crystal lattice types. Part I. Spectra of lattice types I, II, III and of amorphous cellulose.* Journal of Applied Polymer Science, 1964. **8**(3): p. 1311-1324.
82. Schroeder, L.R., V.M. Gentile, and R.H. Atalla, *Nondegradative preparation of amorphous cellulose.* Journal of wood chemistry and technology, 1986. **6**(1): p. 1-14.
83. Isogai, A. and R.H. Atalla, *Alkaline method for dissolving cellulose*, USPTO, Editor. 1995: United States.
84. Maier, G.Z., P.; Stubicar, Mirko; Schurz, J., *The amorphization of different cellulose samples by ball milling.* Cellulose Chemistry & Technology, 2005. **39**(3-4): p. 167-177.
85. Segal, L., M.L. Nelson, and C.M. Conrad, *Experiments on the reduction of the crystallinity of cotton cellulose.* The journal of physical and colloid chemistry, 1951. **55**(3): p. 325-336.

86. Deguchi, S., K. Tsujiib, and K. Horikoshi, *Cooking celluose in hot and compressed water.* Chem. Commun., 2006: p. 3293–3295.
87. Hirai, A., F. Horii, and R. Kitamura, *Carbon-13 spin-lattice relaxation behaviour of the crystalline and noncrystalline components of native and regenerated celluloses.* Cell. Chem. Technol., 1990. **24**(6): p. 703-711.
88. Dudley, R.L., et al., *High-resolution carbon-13 CP/MAS NMR spectra of solid cellulose oligomers and the structure of cellulose II.* J. Am. Chem. Soc., 1983. **105**(8): p. 2469-2472.
89. VanderHart, D.L. and R.H. Atalla, *Studies of microstructure in native celluloses using solid-state carbon-13 NMR.* Macromolecules, 1984. **17**(8): p. 1465-1472.
90. Nishiyama, Y., P. Langan, and H. Chanzy, *Crystal structure and hydrogen-bonding system in cellulose I beta from synchrotron x-ray and neutron fibre diffraction.* J. Am. Chem. Soc., 2002. **124**(31): p. 9074-9082.
91. Nishiyama, Y., et al., *Crystal structure and hydrogen bonding system in cellulose I alpha from synchrotron x-ray and neutron fibre diffraction.* J. Am. Chem. Soc., 2003. **125**(47): p. 14300-14306.
92. Wada, M., T. Kondo, and T. Okano, *Thermally induced crystal transformation from cellulose Ialpha to Ibeta.* Polymer Journal, 2003. **35**(2): p. 155-159.
93. Jarvis, M.C., *Interconversion of the I_α and I_β crystalline forms of cellulose by bending.* Carbohydrate Research, 2000. **325**(2): p. 150-154.
94. Maunu, S.L., *NMR studies of wood and wood product.* Progress in Nuclear Magnetic Resonance Spectroscopy, 2002. **40**(2): p. 151-174.
95. Kataoka, Y. and T. Kondo, *FT-IR Microscopic Analysis of Changing Cellulose Crystalline Structure during Wood Cell Wall Formation.* Macromolecules, 1998. **31**(3): p. 760-764.
96. Imai, T. and J. Sugiyama, *Nanodomains of Iα and Iβ Cellulose in Algal Microfibrils.* Macromolecules, 1998. **31**(18): p. 6275-6279.
97. Li, W., L. Yan, and J. Yang, *AFM study of crystalline cellulose in the cell walls of straw.* Polymer International, 2006. **55**(11): p. 87–92.
98. Hayashi, N., T. Kondo, and M. Ishihara, *Enzymatically produced nano-ordered short elements containing cellulose I[beta] crystalline domains.* Carbohydrate Polymers, 2005. **61**(2): p. 191-197.
99. Aabloo, A., A.D. French, and R.H. Mikelsaar, *Packing energy calculations on the crystalline structure of cellulose I*, in *Cellulose and cellulose derivatives: physico-chemical aspects and industrial applications*, J.F. Kennedy, Editor. 1995, Woodhead publishing Ltd. p. 51-55.
100. Horii, F., A. Hirai, and R. Kitamaru, *Solid-state 13C-NMR study of conformations of oligosaccharides and cellulose.* Polymer Bulletin, 1983. **10**(7): p. 357-361.
101. Sturcova, A., et al., *Structural Details of Crystalline Cellulose from Higher Plants.* Biomacromolecules, 2004. **5**(4): p. 1333-1339.
102. Kono, H., et al., *CP/MAS ^{13}C NMR Study of Cellulose and Cellulose Derivatives. 1. Complete Assignment of the CP/MAS ^{13}C NMR Spectrum of the Native Cellulose.* J. Am. Chem. Soc., 2002. **124**(25): p. 7506-7511.
103. Kennedy, J.F., *Cellulose and cellulose derivatives : physico-chemical aspects and industrial applications*. 1995, Abington: Woodhead. xvi, 589.
104. Sugiyama, J., et al., *Lattice images from ultrathin sections of cellulose microfibrils in the cell wall of Valonia macrophysa Kütz.* Planta, 1985. **166**(2): p. 161-168.
105. Putaux, J.-L., *Morphology and Structure of Crystalline Polysaccharides: Some Recent Studies.* Macromolecular Symposia, 2005. **229**(1): p. 66-71.
106. Ishikawa, A., S. Kuga, and T. Okano, *Determination of parameters in mechanical model for cellulose III fibre.* Polymer, 1998. **39**(10): p. 1875-1878.

107. Ishikawa, A., T. Okano, and J. Sugiyama, *Fine structure and tensile properties of ramie fibres in the crystalline form of cellulose I, II, IIII and IVI.* Polymer, 1997. **38**(2): p. 463-468.
108. Sarko, A., J. Southwick, and J. Hayashi, *Packing Analysis of Carbohydrates and Polysaccharides. 7. Crystal Structure of Cellulose IIII and Its Relationship to Other Cellulose Polymorphs.* Macromolecules, 1976. **9**(5): p. 857-863.
109. Wada, M., L. Heux, and J. Sugiyama, *Polymorphism of Cellulose I Family: Reinvestigation of Cellulose IV$_I$.* Biomacromolecules, 2004. **5**(4): p. 1385-1391.
110. Isogai, A., M. Usuda, T. Kato, T. Uryu, and R. H. Atalla, *Solid-state CP/MAS 13C NMR study of cellulose polymorphs.* Macromolecules, 1989. **22**: p. 3168-3172.
111. Langan, P., Y. Nishiyama, and H. Chanzy, *A Revised Structure and Hydrogen-Bonding System in Cellulose II from a Neutron Fiber Diffraction Analysis.* J. Am. Chem. Soc., 1999. **121**(43): p. 9940-9946.
112. Tsuda, Y. and S. Mukoyama, *The formation of cellulose IV in the viscose spinning.* Bulletin of the Chemical Society of Japan, 1957. **30**(7): p. 718-720.
113. Okajima, S. and K. Inoue, *X-ray diffraction and infrared spectra studies on the fine structure of rayon improved by high temperature steaming.* Journal of Polymer Science: Part A: Polymer Chemistry, 1964. **2**(1): p. 461-480.
114. Kulshreshtha, A.K., *A review of the literature on the formation of cellulose IV, its structure, and its significance in the technology of rayon manufacture.* J. Text. Inst., 1979(1): p. 13-18.
115. Ohshima, N., et al., *Structural analysis for cellulose fibres treated by high pressure steam.* Sen'I Gakkaishi, 2003. **59**(3): p. 83-86.
116. Das, M. and D. Chakraborty, *Influence of alkali treatment on the fine structure and morphology of bamboo fibers.* Journal of Applied Polymer Science, 2006. **102**(5): p. 5050-5056.
117. Porro, F., et al., *Solid-State 13C NMR Study of Na-Cellulose Complexes.* Biomacromolecules, 2007. **8**(8): p. 2586-2593.
118. Nishimura, H., T. Okano, and A. Sarko, *Mercerization of cellulose. 5. Crystal and molecular structure of Na-cellulose I.* Macromolecules, 1991. **24**(3): p. 759-770.
119. Oh, S.Y., et al., *Crystalline structure analysis of cellulose treated with sodium hydroxide and carbon dioxide by means of X-ray diffraction and FTIR spectroscopy.* Carbohydrate Research, 2005. **340**(15): p. 2376-2391.
120. Oh, S.Y., et al., *FTIR analysis of cellulose treated with sodium hydroxide and carbon dioxide.* Carbohydrate Research, 2005. **340**(3): p. 417-428.
121. Kimura, K., Y. Shimizu, and J. Hayashi, *Structural change of cellulose polymorphs by milling*, in *Cellulose and cellulose derivatives*, J.F. Kennedy, Editor. 1995, Woodhead publishing. p. 85-92.
122. Schwanninger, M., et al., *Effects of short-time vibratory ball milling on the shape of FT-IR spectra of wood and cellulose.* Vibrational Spectroscopy, 2004. **36**(1): p. 23-40.
123. Chen, W., G.C. Lickfield, and C.Q. Yang, *Molecular modeling of cellulose in amorphous state. Part I: model building and plastic deformation study.* Polymer, 2004. **45**(3): p. 1063-1071.
124. Wegst, U.G.K. and M.F. Ashby, *The mechanical efficiency of natural materials.* Philosophical Magazine, 2004. **84**(21): p. 2167 - 2186.
125. Lyons, W.J., *Crystal Density of Native Cellulose.* The Journal of Chemical Physics, 1941. **9**(4): p. 377-378.
126. Haughton, P.M. and D.B. Sellen, *Stress relaxation in regenerated cellulose.* Journal of Physics D: Applied Physics, 1973. **6**(17): p. 1998.

127. Manabe, S., M. Iwata, and K. Kamide, *Dynamic mechanical absorptions observed for regenerated cellulose solids in the temperature range from 280 to 600 K.* Polymer Journal, 1986. **18**(1): p. 1-14.
128. Montès, H., K. Mazeau, and J.Y. Cavaillé, *Secondary Mechanical Relaxations in Amorphous Cellulose.* Macromolecules, 1997. **30**(22): p. 6977-6984.
129. Nissan, A.H. and S.S. Sternstein, *Cellulose as a viscoelastic material.* Pure and Applied Chemistry, 1962. **5**(6): p. 131-146.
130. Yano, S., H. Hatakeyama, and T. Hatakeyama, *Effect of hydrogen bond formation on dynamic mechanical properties of amorphous cellulose.* Journal of Applied Polymer Science, 1976. **20**(12): p. 3221-3231.
131. Baley, C., *Analysis of the flax fibres tensile behaviour and analysis of the tensile stiffness increase.* Composites Part A: Applied Science and Manufacturing, 2002. **33**(7): p. 939-948.
132. Kortekaas, S., et al., *Anaerobic treatment of hemp thermomechanical pulping wastewater.* Water Research, 1998. **32**(11): p. 3362-3370.
133. Kohler, R. and K. Nebel, *Cellulose-Nanocomposites: Towards High Performance Composite Materials.* Macromolecular Symposia, 2006. **244**(1): p. 97-106.
134. Dreyer, J., et al., *Comparison of Enzymatically Separated Hemp and Nettle Fibre to Chemically Separated and Steam Exploded Hemp Fibre.* Journal of industrial hemp, 2002. **7**(1): p. 43-59.
135. Xu, F., R.C. Sun, and Q. Lu, *Characteristics of cellulose isolated by a totally chlorine free method from Caragana korshinskii.* Journal of Applied Polymer Science, 2006. **101**(5): p. 3251-3263.
136. El-Sakhawy, M. and M.L. Hassan, *Physical and mechanical properties of mycrocrystalline cellulose prepared from agricultural residues.* Carbohydrate Polymers, 2007. **67**(1): p. 1-10.
137. Chakraborty, A., M. Sain, and M. Kortschot, *Cellulose microfibrils: A novel method of preparation using high shear refining and cryocrushing.* Holzforschung, 2005. **59**(1): p. 102-107.
138. Eichhorn, S.J. and R.J. Young, *The Young's modulus of a microcrystalline cellulose.* Cellulose, 2001. **8**(3): p. 197-207.
139. Sharma, H.S.S. and C.F.V. Sumere, *The Biology and Processing of Flax*. 1992, Belfast: M Publications.
140. Chanzy, H., M. Paillet, and R. Hagege, *Spinning of cellulose from N-methyl morpholine N-oxide in the presence of additives.* Polymer, 1990. **31**(3): p. 400-405.
141. Mccormick, C.L., *Novel cellulose solutions*, in *United States Patents*. 1980, Hopkins Agricultural Chemical co.
142. Mccormick, C.L., P.A. Callais, and B.H. Hutchinson, *Solution Studies of Cellulose in Lithium-Chloride and N,N-Dimethylacetamide.* Macromolecules, 1985. **18**(12): p. 2394-2401.
143. Hong, Y.K., K.H. Chung, and W.S. Lee, *Structure of regenerated cellulose fibers from DMAc/LiCl solution.* Textile Research Journal, 1998. **68**(1): p. 65-69.
144. Yamashiki, T., et al., *New class of cellulose fiber spun from the novel solution of cellulose by wet spinning method.* Journal of applied polymer science, 1992. **44**(4): p. 691-698.
145. Cai, J., et al., *Multifilament Fibers Based on Dissolution of Cellulose in NaOH/Urea Aqueous Solution: Structure and Properties.* Advanced Materials, 2007. **19**(6): p. 821-825.
146. Ruan, D., et al., *Structure and properties of novel fibres spun from cellulose in NaOH/Thiourea aqueous solution.* Macromolecular Bioscience, 2004. **4**(12): p. 1104-1112.

147. Ruan, D., et al., *A Rapid Process for Producing Cellulose Multi-Filament Fibers from a NaOH/Thiourea Solvent System.* Macromolecular Rapid Communications, 2006. **27**(17): p. 1495-1500.
148. Cai, J., et al., *Novel Fibers Prepared from Cellulose in NaOH/Urea Aqueous Solution.* Macromolecular Rapid Communications, 2004. **25**(17): p. 1558-1562.
149. Wu, J., et al., *Homogeneous Acetylation of Cellulose in a New Ionic Liquid.* Biomacromolecules, 2004. **5**(2): p. 266-268.
150. Turner, M.B., et al., *Ionic Liquid-Reconstituted Cellulose Composites as Solid Support Matrices for Biocatalyst Immobilization.* Biomacromolecules, 2005. **6**(5): p. 2497-2502.
151. Turner, M.B., et al., *Production of Bioactive Cellulose Films Reconstituted from Ionic Liquids.* Biomacromolecules, 2004. **5**(4): p. 1379-1384.
152. Zhang, H., et al., *1-Allyl-3-methylimidazolium Chloride Room Temperature Ionic Liquid: A New and Powerful Nonderivatizing Solvent for Cellulose.* Macromolecules, 2005. **38**(20): p. 8272-8277.
153. Swatloski, R.P., et al., *Dissolution of Cellulose with Ionic Liquids.* J. Am. Chem. Soc., 2002. **124**(18): p. 4974-4975.
154. Moulthrop, J.S., et al., *High-resolution 13C NMR studies of cellulose and cellulose oligomers in ionic liquid solutions.* Chem. Commun., 2005. **12**: p. 1557-1559.
155. Zhu, S., et al., *Dissolution of cellulose with ionic liquids and its application: a mini-review.* Green Chemistry, 2006. **4**: p. 325-327.
156. Köhler, S. and T. Heinze, *New Solvents for Cellulose: Dimethyl Sulfoxide/Ammonium Fluorides.* Macromolecular Bioscience, 2007. **7**(3): p. 307-314.
157. Heinze, T., et al., *Effective preparation of cellulose derivatives in a new simple solvent.* Macromolecular Chemistry and Physics, 2000. **201**(6): p. 627-631.
158. Aaltonen, O. and M. Alkio, *Process for producing regenerated cellulosic articles and for recovering the solvent chemicals*, U.S. Patent, Editor. 1982: U.S.A.
159. Turbak, A.F., et al., *A critical review of cellulose solvent systems*, A.S. Series, Editor. 1977: Washington DC.
160. Leipner, H., et al., *Structural changes of cellulose dissolved in molten salt hydrates.* Macromolecular Chemistry and Physics, 2000. **201**(15): p. 2041-2049.
161. Saalwachter, K., et al., *Cellulose Solutions in Water Containing Metal Complexes.* Macromolecules, 2000. **33**(11): p. 4094-4107.
162. Cai, J. and L. Zhang, *Rapid dissolution of cellulose in LiOH/urea and NaOH/urea aqueous solutions.* Macromolecular Bioscience, 2005. **5**: p. 539-548.
163. Cai, J., et al., *Hydrogen-Bond-Induced Inclusion Complex in Aqueous Cellulose/LiOH/Urea Solution at Low Temperature.* ChemPhysChem, 2007. **8**(10): p. 1572-1579.
164. Frey, M.W., et al., *Dissolution of cellulose in ethylene diamine/salt solvent system.* Cellulose, 2006. **13**(2): p. 147-155.
165. Frey, M.W., J.A. Cuculo, and R.D. Spontak, *Morphological characteristcs of the lyotropic and gel phases in the cellulose/NH_3/NH_4SCN system.* Journal of Polymer Science Part B: Polymer Physics, 1996. **34**(12): p. 2049-2058.
166. Bochek, A.M., G.A. Petropavlovski, and A.V. Yakimanski, *Solubility of cellulose and its derivatives*, in *Cellulose and cellulose derivatives: physico-chemical aspects and industrial applications*, J.F. Kennedy, Editor. 1995, Woodhead publishing Ltd: Cambridge.
167. Rosenau, T., et al., *The chemistry of side reactions and byproduct formation in the system NMMO/cellulose (Lyocell process).* Progress in Polymer Science, 2001. **26**(9): p. 1763-1837.
168. Rosenau, T., et al., *On the conformation of the cellulose solvent N-methylmorpholine-N-oxide (NMMO) in solution.* Polymer, 2003. **44**(20): p. 6153-6158.

169. Woodings, C.R., *The development of advanced cellulosic fibres.* International Journal of Biological Macromolecules, 1995. **17**(6): p. 305-309.
170. Liu, X., et al. *Cellulose/Clay Nanocomposites*. in *Ecocomp 2003*. 2003. Queen Mary College, London.
171. Fink, H.-P., et al., *Structure formation of regenerated cellulose materials from NMMO-solutions.* Progress in Polymer Science, 2001. **26**(9): p. 1473-1524.
172. Smole, M.S., et al., *X-ray study of pre-treated regenerated cellulose fibres.* Mat Res Innovation, 2003. **7**(5): p. 275-282.
173. Biganska, O. and P. Navard, *Phase diagram of a cellulose solvent: N-methylmorpholine-N-oxide-water mixtures.* Polymer, 2003. **44**(4): p. 1035-1039.
174. Blachot, J.-F., L. Chazeau, and J.-Y. Cavaille, *Rheological behavior of cellulose/monohydrate of N-methylmorpholine N-oxide solutions. Part 2. Glass transition domain.* Polymer, 2002. **43**(3): p. 881-889.
175. Buitenhuijs, F.A., *The degradation and stabilization of cellulose dissolved in N-Methylmorpholine-N-Oxide (NMMO).* Das Papier, 1986. **40**(12): p. 615–619.
176. Biganska, O., P. Navard, and O. Bedue, *Crystallisation of cellulose/N-methylmorpholine-N-oxide hydrate solutions.* Polymer, 2002. **43**(23): p. 6139-6145.
177. Wolfram, K., *Process for the production of cellulose moulded bodies*, in *United States Patent*. 1997, Lenzing Aktiengesellschaft (AT).
178. Franz, H., et al., *Thermally stable pulp-amine oxide solution for preparation of fibers, films, and molded articles from regenerated cellulose.*, in *Wirtschaftspatent*. 1985: Germany.
179. Chanzy, H.D. and M. Paillet, *Process for the preparation of a shapeable solution of cellulose in the presence of a tertiary amine oxide and an additive*, in *U.S. patent*. 1989, Institut textile de France, Boulogne Billancourt Cedex; Centre de recherche scientifique, Paris, both of France: France.
180. Varga, J.K., *Shapeable tertiary amine N-oxide solution of cellulose, shaped cellulose product made therefrom and process for preparing the shapeable solution and cellulose products*, in *United states patent*. 1982.
181. McCorsley, C.C., *Process for shaped cellulose article prepared from a solution containing cellulose dissolved in a tertiary amine N-oxide solvent*, in *United States Patent*. 1981, Akzona Incorporated (Asheville, NC).
182. Mortimer, S.A. and A.A. Peguy, *The formation of structure in the spinning and coagulation of Lyocell fibres.* Cell. Chem. Technol., 1996. **30**(1-2): p. 117-132.
183. Eibl, M., *Process for the production of cellulose moulded bodies*, in *United States Patent*. 1997, Lenzing Aktiengesellschaft (AT).
184. Wolfram, K., *Process for the production of cellulose moulded bodies*, in *United States Patent*. 1998, Lenzing Aktiengesellschaft (AT).
185. Wei, Y. and F. Cheng, *Effect of solvent exchange on the structure and rheological properties of cellulose in LiCl/DMAc.* Journal of Applied Polymer Science, 2007. **106**(6): p. 3624-3630.
186. Rosenau, T., A. Potthast, and P. Kosma, *Studies on the carbenium-iminium ions derived from N-methylmorpholine-N-oxide (NMMO).* Tetrahedron, 2004. **60**(2): p. 301-306.
187. Isogai, A. and R.H. Atalla, *Dissolution of cellulose in aqueous NaOH solutions.* Cellulose, 1998. **5**(4): p. 309-319.
188. Kamide, K., et al., *Study on the solubility of cellulose in aqueous alkali solution by deuteration IR and [13]C NMR.* Polymer Journal, 1984. **16**(12): p. 857-866.
189. Cuissinat, C. and P. Navard, *Swelling and Dissolution of Cellulose Part I: Free Floating Cotton and Wood Fibres in N-Methylmorpholine-N-oxide-Water Mixtures.* Macromolecular Symposia, 2006. **244**(1): p. 1-18.

190. Roy, C., et al., *Structure of cellulose-soda solutions at low temperatures.* Biomacromolecules, 2001. **2**(3): p. 687-693.
191. Kuo, Y.-N. and J. Hong, *Investigation of solubility of microcrystalline cellulose in aqueous NaOH.* Polymers for Advanced Technologies, 2005. **16**(5): p. 425-428.
192. Inskeep, G.C. and P.V. Horn, *Cellophane.* Ind. Eng. Chem., 1952. **44**(11): p. 2511-2524.
193. Yamashiki, T., et al., *Characterisation of cellulose treated by the steam explosion method. Part 1: Influence of celluose resources on changes in morphology, degree of polymerisation, solubility and solid structure.* British Polymer Journal, 1990. **22**(1): p. 73-83.
194. Yamashiki, T., et al., *Characterisation of cellulose treated by the steam explosion method. Part 2: Effect of treatment conditions on changes in morphology, degree of polymerisation, solubility in aqueous sodium hydroxide and supermolecular structure of soft wood pulp during steam explosion.* British Polymer Journal, 1990. **22**(2): p. 121-128.
195. Kuo, Y.-N. and J. Hong, *A new method for cellulose membrane fabrication and the determination of its characteristics.* Journal of colloid and interface science, 2005. **285**(1): p. 232-238.
196. Cao, Y. and H. Tan, *Preparation and properties of microporous cellulose membranes from novel cellulose/aqueous sodium hydroxide solutions.* Journal of Applied Polymer Science, 2006. **102**(1): p. 920-926.
197. Bock, B., S. Bock, and D. Fengel, *NMR parameters of cellulose in TFA solution.* Holzforschung, 1991. **45**(5): p. 321-324.
198. Jin, H., C. Zha, and L. Gu, *Direct dissolution of cellulose in NaOH/thiourea/urea aqueous solution.* Carbohydrate Research, 2007. **342**(6): p. 851-858.
199. Cuissinat, C. and P. Navard, *Swelling and Dissolution of Cellulose Part II: Free Floating Cotton and Wood Fibres in NaOH-Water-Additives Systems.* Macromolecular Symposia, 2006. **244**(1): p. 19-30.
200. Cai, J. and L. Zhang, *Unique gelation behavior of cellulose in NaOH/urea aqueous solution.* Biomacromolecules, 2006. **7**(1): p. 183-189.
201. Kunze, J. and H.-P. Fink, *Structural changes and activation of cellulose by caustic soda solution with urea.* Macromolecular Symposia, 2005. **223**: p. 175-187.
202. Mao, Y., et al., *Effects of coagulants on porous structure of membranes prepared from cellulose in NaOH/urea aqueous solution.* Journal of Membrane Science, 2006. **279**(1-2): p. 246-255.
203. Ruan, D., et al., *Microporous membranes prepared from cellulose in NaOH/thiourea aqueous solution.* Journal of Membrane Science, 2004. **241**(2): p. 265-274.
204. Liang, S., et al., *Fabrication and Properties of Cellulose Hydrated Membrane with Unique Structure.* Macromolecular Chemistry and Physics, 2007. **208**(6): p. 594-602.
205. Weng, L., et al., *Thermal Gelation of Cellulose in a NaOH/Thiourea Aqueous Solution.* Langmuir, 2004. **20**(6): p. 2086-2093.
206. Zhang, L., D. Ruan, and S. Gao, *Dissolution and regeneration of cellulose in NaOH/thiourea aqueous solution.* Journal of Polymer Science Part B: Polymer Physics, 2002. **40**(14): p. 1521-1529.
207. Marsano, E., E. Bianchi, and A. Ciferri, *Mesophase formation and polymer compatibility. 2. Cellulose acetate/(hydroxypropyl)cellulose/diluent system.* Macromolecules, 1984. **17**(12): p. 2886-2889.
208. Conio, G., et al., *Mesophase Formation and Chain Rigidity in Cellulose and Derivatives .1. (Hydroxypropyl)Cellulose in Dimethylacetamide.* Macromolecules, 1983. **16**(8): p. 1264-1270.

209. Bianchi, E., et al., *Mesophase Formation and Chain Rigidity in Cellulose and Derivatives .5. Cellulose-Acetate in N,N-Dimethylacetamide.* Macromolecules, 1986. **19**(3): p. 630-636.
210. Timpa, J.D., *Application of Universal Calibration in Gel-Permeation Chromatography for Molecular-Weight Determinations of Plant-Cell Wall Polymers - Cotton Fiber.* Journal of Agricultural and Food Chemistry, 1991. **39**(2): p. 270-275.
211. Bikova, T. and A. Treimanis, *Problems of the MMD analysis of cellulose by SEC using DMA/LiCl: A review.* Carbohydrate Polymers, 2002. **48**(1): p. 23-28.
212. Striegel, A.M., *Advances in the understanding of the dissolution mechanism of cellulose in DMAc/LiCl.* J. Chil. Chem. Soc., 2002. **48**(1): p. 73-77.
213. Bianchi, E., et al., *Mesophase Formation and Chain Rigidity in Cellulose and Derivatives .4. Cellulose in N,N-Dimethylacetamide Lithium-Chloride.* Macromolecules, 1985. **18**(4): p. 646-650.
214. Dupont, A.-L. and G. Harrison, *Conformation and dn/dc determination of cellulose in N,N-dimethylacetamide containing lithium chloride.* Carbohydrate Polymers, 2004. **58**(3): p. 233-243.
215. Eremeeva, T., *Size-exclusion chromatography of enzymatically treated cellulose and related polysaccharides: a review.* J. Biochem. Biophys. Methods, 2003. **56**(1): p. 253-264.
216. Ass, B.A.P., G.T. Ciacco, and E. Frollini, *Cellulose acetates from linters and sisal: correlation between synthesis conditions in DMAc/LiCl and product properties.* Bioresource Technology, 2006. **97**(14): p. 1696-1702.
217. Mayumi, A., T. Kitaoka, and H. Wariishi, *Partial substitution of cellulose by ring-opening esterification of cyclic esters in a homogeneous system.* Journal of Applied Polymer Science, 2006. **102**(5): p. 4358-4364.
218. Marsano, E., et al., *Fibres based on cellulose-silk fibroin blend.* Journal of Applied Polymer Science, 2007. **104**(4): p. 2187-2196.
219. Bianchi, E., et al., *Fiber Formation from Liquid-Crystalline Precursors .2. Cellulose in N,N-Dimethylacetamide-Lithium Chloride.* Journal of Polymer Science Part B-Polymer Physics, 1989. **27**(7): p. 1477-1484.
220. Ramos, L.A., et al., *Influence of the supramolecular structure and physicochemical properties of cellulose on its dissolution in a lithium chloride/N,N-dimethylacetamide solvent system.* Biomacromolecules, 2005. **6**(5): p. 2638-2647.
221. Nishino, T., *Cellulose-derived high-strength composites for construction materials and their manufacture*, in *Jpn. Kokai Tokkyo Koho*. 2004: Japan.
222. Masson, J.F. and R.S.J. Manley, *Solid-state NMR of some cellulose/synthetic polymer blends.* Macromolecules, 1992. **25**(2): p. 589-592.
223. Williamson, S.L., et al., *Microstructural Examination of Semi-Interpenetrating Networks of Poly(N,N-dimethylacrylamide) with Cellulose or Chitin Synthesized in Lithium Chloride/N,N-Dimethylacetamide.* Macromolecules, 1998. **31**(23): p. 8134-8141.
224. *Cellulose membrane and method for manufacture thereof*, in *United States Patent*. 1998, The University of Western Ontario.
225. Saga, *Transparent cellulose hydrogel and production process thereof*, in *United states patent*. 1999.
226. Turback, *Solvent system for cellulose*, in *US patent*. 1981, International telephone and telegraph Corp.
227. Ishii, D., D. Tatsumi, and T. Matsumoto, *Effect of Solvent Exchange on the Solid Structure and Dissolution Behavior of Cellulose.* Biomacromolecules, 2003. **4**(5): p. 1238-1243.

228. Ishii, D., et al., *Effect of solvent exchange on the pore structure and dissolution behaviour of cellulose.* Journal of Applied Polymer Science, 2006. **103**(6): p. 3976-3984.
229. Dupont, A.-L., *Cellulose in lithium chloride/N,N-dimethylacetamide, optimisation of a dissolution method using paper substrates and stability of the solutions.* Polymer, 2003. **44**(15): p. 4117-4126.
230. Mccormick, C.L. and T.R. Dawsey, *Preparation of Cellulose Derivatives Via Ring-Opening Reactions with Cyclic Reagents in Lithium-Chloride N,N-Dimethylacetamide.* Macromolecules, 1990. **23**(15): p. 3606-3610.
231. Chrapava, S., et al., *The investigation of the influence of water and temperature on the LiCl/DMAc/cellulose system.* Phys. Chem. Chem. Phys., 2003. **5**: p. 1842 - 1847.
232. Röder, T., B. Morgenstern, and O. Glatter, *Polarized and depolarized light scattering on solutions of cellulose in N,N-dimethylacetamide/lithium chloride.* Macromolecular Symposia, 2000. **162**: p. 87-93.
233. Seurin, M.J. and P. Sixou, *Behavior of Hydroxypropylcellulose Solutions in the Presence of an Inorganic Salt.* European Polymer Journal, 1987. **23**(1): p. 77-87.
234. Stryuk, S., J. Eckelt, and B.A. Wolf, *Solutions of cellulose in DMAc + LiCl: migration of the solute in an electrical field.* Cellulose, 2005. **12**(2): p. 145-149.
235. Conio, G., et al., *Phase-Equilibria of Cellulose in N,N-Dimethylacetamide/LiCl Solutions.* Journal of Polymer Science Part C-Polymer Letters, 1984. **22**(5): p. 273-277.
236. Jerosch, H., B. Lavedrine, and J.-C. Cherton, *Study of the stability of cellulose-holocellulose solutions in N,N-dimethylacetamide-lithium chloride by size exclusion chromatography.* Journal of Chromatography A, 2001. **927**(1-2): p. 31-38.
237. Potthast, A., et al., *Degradation of cellulosic materials by heating in DMAc/LiCl.* Tetrahedron Letters, 2002. **43**(43): p. 7757-7759.
238. Ishii, D., et al., *Investigation of the structure of cellulose in LiCl/DMAc solution and its gelation behavior by small-angle x-ray scattering measurements.* Macromolecular Bioscience, 2006. **6**(4): p. 293-300.
239. Rosenau, T., et al., *Hydrolytic Processes and Condensation Reactions in the Cellulose Solvent System N,N-Dimethylacetamide/Lithium Chloride. Part 1.* Holzforschung, 2001. **55**(6): p. 661-666.
240. Röder, T., et al., *The effect of water on cellulose solutions in DMAc/LiCl.* Macromolecular Symposia, 2002. **190**(1): p. 151-160.
241. Terbojevich, M., et al., *Mesophase Formation and Chain Rigidity in Cellulose and Derivatives .3. Aggregation of Cellulose in N,N-Dimethylacetamide Lithium-Chloride.* Macromolecules, 1985. **18**(4): p. 640-646.
242. Potthast, A., et al., *The cellulose solvent system N,N-dimethylacetamide/lithium chloride revisited: the effect of water on physicochemical properties and chemical stability.* Cellulose, 2002. **9**(1): p. 41-53.
243. Glavic, P. and R. Lukman, *Review of sustainability terms and their definitions.* Journal of Cleaner Production, 2007. **15**(18): p. 1875-1885.
244. Garcia-Serna, J., L. Perez-Barrigon, and M.J. Cocero, *New trends for design towards sustainability in chemical engineering: Green engineering.* Chemical Engineering Journal, 2007. **133**(1-3): p. 7-30.
245. Gindl, W. and J. Keckes, *Tensile properties of cellulose acetate butyrate composites reinforced with bacterial cellulose.* Composites Science and Technology
Developments in carbon nanotube and nanofibre reinforced polymers, 2004. **64**(15): p. 2407-2413.
246. Zhang, M.Q., M.Z. Rong, and X. Lu, *Fully biodegradable natural fiber composites from renewable resources: All-plant fiber composites.* Composites Science and Technology, 2005. **65**(15-16): p. 2514-2525.

247. Gandini, A., et al., *Direct transformation of cellulose fibres into self-reinforced composites by partial oxypropylation.* Polymer, 2005. **46**(24): p. 10611-10613.
248. Matsumura, H. and W.G. Glasser, *Cellulosic nanocomposites. II. Studies by atomic force microscopy.* Journal of Applied Polymer Science, 2000. **78**(13): p. 2254-2261.
249. Matsumura, H., J. Sugiyama, and W.G. Glasser, *Cellulosic nanocomposites. I. Thermally deformable cellulose hexanoates from heterogeneous reaction.* Journal of Applied Polymer Science, 2000. **78**(13): p. 2242-2253.
250. Nishino, T., J.p. association, Editor. 2004: Japan.
251. Fink, H.-P., et al., *Structural aspects of new cellulose fibres and films from NMMO-solution.* Recent res in Polymer science, 1998. **2**: p. 387-403.
252. Gindl, W., et al., *Changes in molecular orientation and tensile properties of uniaxially drawn cellulose films.* Biomacromolecules, 2006. **7**(11): p. 3146-3150.
253. Togawa, E. and T. Kondo, *Change of morphological properties in drawing water-swollen cellulose films prepared from organic solutions. A view of molecular orientation in the drawing process.* Journal of Polymer Science Part B-Polymer Physics, 1999. **37**(5): p. 451-459.
254. Togawa, E. and T. Kondo, *Unique structural characteristics of nematic ordered cellulose - Stability in water and its facile transformation.* Journal of Polymer Science Part B: Polymer Physics, 2007. **45**(20): p. 2850-2859.
255. Gindl, W. and J. Keckes, *Strain hardening in regenerated cellulose fibres.* Composites Science and Technology, 2006. **66**(13): p. 2049-2053.
256. Westman, L. and T. Lindström, *Swelling and mechanical properties of cellulose hydrogels. I. Preparation, characterization, and swelling behavior.* Journal of Applied Polymer Science, 1981. **26**(8): p. 2519-2532.
257. Westman, L. and T. Lindström, *Swelling and mechanical behaviour of cellulose hydrogels. III. temperature effects on the swelling and compliance levels studied by dilatometry and 1H-NMR spectroscopy.* Journal of Applied Polymer Science, 1981. **26**(8): p. 2545-2559.
258. Davidson, T.C., R.H. Newman, and M.J. Ryan, *Variations in the fibre repeat between samples of cellulose I from different sources.* Carbohydrate Research, 2004. **339**(18): p. 2889-2893.
259. Ioelovich, M. and E. Larina, *Parameters of crystalline structure and their influence on the reactivity of cellulose I.* Cellulose Chemistry and Technology, 1999. **33**(1-2): p. 3-12.
260. Westman, L. and T. Lindström, *Swelling and mechanical properties of cellulose hydrogels. VI. Dynamic Mechanical Properties.* Holzforschung, 1987. **41**(4): p. 225-230.
261. Zhang, Y., et al., *Formation and characterization of cellulose membranes from N-Methylmorpholine-N-oxide solution.* Macromolecular Bioscience, 2001. **1**(4): p. 141-148.
262. Kim, D.B., et al., *Double crystallization behavior in dry-jet wet spinning of cellulose/N-methylmorpholine-N-oxide hydrate solutions.* European Polymer Journal, 2002. **38**(1): p. 109-119.
263. Moss, C.E., et al., *Microfocus small-angle X-ray scattering investigation of the skin-core microstructure of lyocell cellulose fibres.* Journal of Applied Polymer Science, 2001. **83**(13): p. 2799-2816.
264. Parker, M.E., J.E. Bronlund, and A.J. Mawson, *Moisture sorption isotherms for paper and paperboard in food chain conditions.* Packaging technology and science, 2006. **19**(4): p. 193 - 209.
265. Hemmingson, J.A. and R.H. Newman, *Changes in molecular ordering associated with alkali treatment and vacuum drying of cellulose.* Cellulose, 1995. **2**(1): p. 71-80.

266. Rydholm, S.A., *Pulping processes*. Wiley-interscience. 1965, New York.
267. Larsson, P.T. and P.-O. Westlund, *Line shapes in CP/MAS 13C NMR spectra of cellulose I.* Spectrochimica Acta Part A: Molecular and Biomolecular Spectroscopy, 2005. **62**(1-3): p. 539-546.
268. Gjønnes, J. and N. Norman, *The use of half width and position of the lines in the x-ray diffractograms of native cellulose to characterize the structural properties of the samples.* Acta Chem. Scand., 1958. **12**(10): p. 2028-2033.
269. Murdock, C., *The form of the X-ray diffraction bands for regular crystals of colloidal size*. Physical review, 1930. **35**(1): p. 8-23.
270. Massiot, D., *Progrès récents de la résonance magnétique nucléaire du solide pour la caractérisation structurale des matériaux.* Spectra Analyse, 2002. **21**(224): p. 27-33.
271. Doddrell, D., V. Glushko, and A. Allerhand, *Theory of Nuclear Overhauser Enhancement and ^{13}C-^{1}H Dipolar Relaxation in Proton-Decoupled Carbon-13 NMR Spectra of Macromolecules.* The Journal of Chemical Physics, 1972. **56**(7): p. 3683-3689.
272. Newman, R.H. *Solid-state NMR as a tool for studying dancing molecules*. in *The hemicelluloses workshop 2005*. 2005. University of Canterbury, New Zealand.
273. Schaefer, J., E.O. Stejskal, and R. Buchdahl, *Magic-Angle ¹³C NMR Analysis of Motion in Solid Glassy Polymers.* Macromolecules, 1977. **10**(2): p. 384-405.
274. Pines, A., M.G. Gibby, and J.S. Waugh, *Proton-enhanced NMR of dilute spins in solids.* The Journal of Chemical Physics, 1973. **59**(2): p. 569-590.
275. Rothwell, W.P. and J.S. Waugh, *Transverse relaxation of dipolar coupled spin systems under rf irradiation: Detecting motions in solids.* The Journal of Chemical Physics, 1981. **74**(5): p. 2721-2732.
276. Lowe, I.J., *Free Induction Decays of Rotating Solids.* Physical Review Letters, 1959. **2**(7): p. 285-287.
277. Takahashi, Y. and H. Matsunaga, *Crystal structure of native cellulose.* Macromolecules, 1991. **24**: p. 3968-3969.
278. Atalla, R.H., et al., *Carbon-13 NMR spectra of cellulose polymorphs.* J. Am. Chem. Soc., 1980. **102**(9): p. 3249-3251.
279. Earl, W.L. and D.L. VanderHart, *High resolution, magic angle sampling spinning carbon-13 NMR of solid cellulose I.* J. Am. Chem. Soc., 1980. **102**(9): p. 3251-3252.
280. Gast, J.C., R.H. Atalla, and R.D. McKelvey, *The 13c-n.m.r. spectra of the xylo- and cello-oligosaccharides.* Carbohydrate Research, 1980. **84**(1): p. 137-146.
281. Pfeffer, P.E., K.M. Valentine, and F.W. Parrish, *Deuterium-induced differential isotope shift carbon-13 NMR. 1. Resonance reassignments of mono- and disaccharides.* J. Am. Chem. Soc., 1979. **101**(5): p. 1265-1274.
282. Earl, W.L. and D.L. VanderHart, *Observations by high-resolution carbon-13 nuclear magnetic resonance of cellulose I related to morphology and crystal structure.* Macromolecules, 1981. **14**(3): p. 570-574.
283. Cael, J.J., et al., *The cellulose crystallites: a perspective from solid-state carbon-13 NMR.* Macromolecules, 1985. **18**(4): p. 819-821.
284. Hosemann, R., et al., *The Alpha-Star-Constant, Equilibrium State and Bearing Net Planes in Polymers, Bio-Polymers and Catalysts.* Journal of Physics C-Solid State Physics, 1985. **18**(5): p. 961-971.
285. Horii, F., A. Hirai, and R. Kitamaru, *Solid-state high-resolution 13C-NMR studies of regenerated celluloses samples with different crystallinities.* Polymer bulletin, 1982. **8**(2-4): p. 163-170.
286. Maciel, G.E., et al., *Carbon-13 NMR and order in cellulose.* Macromolecules, 1982. **15**(2): p. 686-687.

287. Horii, F., A. Hirai, and R. Kitamaru, *CP/MAS carbon-13 NMR spectra of the crystalline components of native celluloses.* Macromolecules, 1987. **20**(9): p. 2117-2120.
288. Newman, R.H. and J.A. Hemmingson, *Determination of the degree of cellulose crystallinity in wood by carbon-13 nuclear magnetic resonance spectroscopy.* Holzforschung, 1990. **44**(5): p. 351.
289. Newman, R.H., J.A. Hemmingson, and I.D. Suckling, *Carbon-13 nuclear magnetic resonance studies of kraft pulping.* Holzforschung, 1993. **47**(33): p. 234-238.
290. Yamamoto, H. and F. Horii, *CPMAS carbon-13 NMR analysis of the crystal transformation induced for Valonia cellulose by annealing at high temperatures.* Macromolecules, 1993. **26**(6): p. 1313-1317.
291. Newman, R.H., *Estimation of the relative proportions of cellulose I_α and I_β in wood by carbon-13 NMR spectroscopy.* Holzforschung, 1999. **53**(4): p. 335-340.
292. Newman, R.H., L.M. Davies, and P.J. Harris, *Solid-State 13C Nuclear Magnetic Resonance Characterization of Cellulose in the Cell Walls of Arabidopsis thaliana Leaves.* Plant Physiol., 1996. **111**(2): p. 475-485.
293. Udhardt, U., S. Hesse, and D. Klemm, *Analytical investigation of bacterial cellulose.* Macromolecular Symposia, 2005. **223**(1): p. 201-212.
294. Martins, M.A., et al., *A solid state 13C high resolution NMR study of raw and chemically treated sisal fibers.* Carbohydrate Polymers, 2006. **64**(1): p. 127-133.
295. Ibett, R., D. Domvoglou, and M. Fasching, *Characterization of the supramolecular structure of chemically and physically modified regenerated cellulosic fibres by means of high-resolution carbon-13 solid-state NMR.* Polymer, 2007. **48**(5): p. 1287-1296.
296. Newman, R.H., et al., *Leaf-fibre lignins of Phormium varieties compared by solid-state 13C NMR spectroscopy.* Holzforschung, 2005. **59**(2): p. 147-152.
297. Newman, R.H., *Homogeneity in cellulose crystallinity between samples of Pinus Radiata wood.* Holzforschung, 2004. **58**(11): p. 91-96.
298. Koch, F.T., et al., *Calculation of solid-state 13C NMR spectra of cellulose Iα, Iβ and II using a semi-empirical approach and molecular approach.* Macromolecular Chemistry and Physics, 2000. **201**(15): p. 1930-1939.
299. Kono, H. and Y. Numata, *Two-dimensional spin-exchange solid-state NMR study of the crystal structure of cellulose II.* Polymer, 2004. **45**(13): p. 2004.
300. Wickholm, K., P.T. Larsson, and T. Iversen, *Assignment of non-crystalline forms in cellulose I by CP/MAS 13C NMR spectroscopy.* Carbohydrate Research, 1998. **312**(3): p. 123-129.
301. Jarvis, M.C., *Relationship of chemical shift to glycosidic conformation in the solid-state13C NMR spectra of (1 --> 4)-linked glucose polymers and oligomers: anomeric and related effects.* Carbohydrate Research, 1994. **259**(2): p. 311-318.
302. Gjønnes, J. and N. Norman, *X-ray investigations on cellulose II and mixtures of cellulose I and II. 2. Lateral order in cellulose II.* Acta Chemica Scandinavica, 1960. **14**: p. 689-691.
303. El-Kafrawy, A., *Investigation of the cellulose/LiCl/dimethylacetamide and cellulose/LiCl/*N*-methyl-2-pyrrolidinone solutions by ^{13}C NMR spectroscopy.* Journal of Applied Polymer Science, 1982. **27**(7): p. 2435-2443.
304. Newman, R.H. and T.C. Davidson, *Molecular conformations at the cellulose-water interface.* Cellulose, 2004. **11**(1): p. 23.
305. Schulz, L., B. Seger, and W. Burchard, *Structures of cellulose in solution.* Macromolecular Chemistry and Physics, 2000. **201**(15): p. 2008-2022.
306. Innerlohinger, J., H.K. Weber, and G. Kraft, *Aerocellulose: aerogels and aerogel-like materials made from cellulose.* Macromolecular Symposia, 2006. **244**(1): p. 126-135.
307. Carillo, F., et al., *Structural FTIR analysis and thermal characterisation of lyocell and viscose-type fibres.* European Polymer Journal, 2004. **40**(9): p. 2229-2234.

308. Liang, C.Y. and R.H. Marchessault, *Infrared spectra of crystalline polysaccharides. I. Hydrogen bonds in native celluloses.* Journal of Polymer Science, 1959. **37**(132): p. 385-395.
309. Hongo, T., et al., *Super-molecular structures controlling the swelling behavior of regenerated cellulose membranes.* Polymer Journal, 1996. **28**(9): p. 769-779.
310. Marechal, Y. and H. Chanzy, *The hydrogen bond network in I_β cellulose as observed by infrared spectrometry.* Journal of Molecular Structure, 2000. **523**(1-3): p. 183-196.
311. Sugiyama, J., J. Persson, and H. Chanzy, *Combined infrared and electron diffraction study of the polymorphism of native celluloses.* Macromolecules, 1991. **24**(9): p. 2461-2466.
312. Bradley, S.A. and H. Carr, *Mechanical loss processes in polysaccharides.* Journal of Polymer Science: Polymer Physics Edition, 1976. **14**(1): p. 111-124.
313. Yamane, C., et al., *Structures and mechanical properties of cellulose filaments spun from cellulose/aqueous NaOH solution system.* Polymer Journal, 1996. **28**(12): p. 1039-1047.
314. Menard, K.P., *Dynamic Mechanical Analysis: A Practical Introduction*, ed. C. Press. 1999: CRC Press. 208.
315. Eyring, H., *Viscosity, Plasticity, and Diffusion as Examples of Absolute Reaction Rates.* The Journal of Chemical Physics, 1936. **4**(4): p. 283-291.
316. Starkweather, H.W., *Aspects of simple, non-cooperative relaxations.* Polymer, 1991. **32**(13): p. 2443-2448.
317. Zhou, S.-M., et al., *Influence of Water on Structure and Mechanical Properties of Regenerated Cellulose Studied by an Organized Combination of Infrared Spectra, X-ray Diffraction, and Dynamic Viscoelastic Data Measured as Functions of Temperature and Humidity.* Macromolecules, 2001. **34**(5): p. 1274-1280.
318. Alberola, N. and A. Bergeret, *Physical modeling of the interphase in amorphous thermoplastic/glass bead composites.* Polymer Composites, 1994. **15**(6): p. 442-452.
319. Dufresne, A., *Dynamic mechanical analysis of the interphase in bacterial polyester/cellulose whiskers natural composites.* Composite Interfaces, 2000. **7**(1): p. 53-67.
320. McCrum, N.G., B.E. Read, and G. Williams, *Anelastic and Dielectric Effects in Polymeric Solids*. 1967: Wiley New York. 127.
321. Salmén, N.L. and E.L. Back, *The influence of water on the glass transition temperature of cellulose.* Tappi, 1977. **60**(12): p. 137-140.
322. Essig, M., G.N. Richards, and E. Schenck, *Mechanisms of formation of the major volatile products from the pyrolysis of cellulose*, in *Cellulose and wood- Chemistry and technology*, C. Schuerch, Editor. 1988, John Wiley and Sons: Syracuse. p. 841-862.
323. Tsujiyama, S.-I. and A. Miyamori, *Assignment of DSC thermograms of wood and its components.* Thermochimica Acta, 2000. **351**(1-2): p. 177-181.
324. Yang, P. and S. Kokot, *Thermal Analysis of Different Cellulosic Fabrics.* Journal of Applied Polymer Science, 1996. **60**(8): p. 1137-1146.
325. Yang, H., et al., *Characteristics of hemicellulose, cellulose and lignin pyrolysis.* Fuel, 2007. **86**(12-13): p. 1781-1788.
326. Zickler, G.A., et al., *In situ X-ray diffraction investigation of thermal decomposition of wood cellulose.* Journal of Analytical and Applied Pyrolysis, 2007. **80**(1): p. 134-140.
327. Duchemin, B., R. Newman, and M. Staiger, *Phase transformations in microcrystalline cellulose due to partial dissolution.* Cellulose, 2007. **14**(4): p. 311-320.
328. Viëtor, R.J., et al., *Conformational features of crystal-surface cellulose from higher plants.* The Plant Journal, 2002. **30**(6): p. 721-731.
329. Kistler, S.S., *Coherent Expanded-Aerogels.* J. Phys. Chem., 1932. **36**(1): p. 52-64.
330. Kistler, S.S., *Method of producing aerogels*. 1937: United States.

331. Hrubesh, L.W., *Aerogel applications.* Journal of Non-Crystalline Solids, 1998. **225**(1): p. 335-342.
332. Burchell, M.F., G. Graham, and A. Kearsley, *Cosmic dust collection in aerogel.* Annual Review of Earth and Planetary Science, 2006. **34**: p. 385-418.
333. Guilminot, E., et al., *Use of cellulose-based carbon aerogels as catalyst support for PEM fuel cell electrodes: Electrochemical characterization.* Journal of Power Sources, 2007. **166**(1): p. 104-111.
334. Tan, C., et al., *Organic Aerogels with Very High Impact Strength.* Advanced Materials, 2001. **13**(9): p. 644-646.
335. Fischer, F., et al., *Cellulose-based aerogels.* Polymer, 2006. **47**(22): p. 7636-7645.
336. Hoepfner, S., L. Ratke, and B. Milow, *Synthesis and characterisation of nanofibrillar cellulose aerogels.* Cellulose, 2007. **15**(1): p. 121-129.
337. Jin, H., et al., *Nanofibrillar cellulose aerogels.* Colloids and Surfaces A: Physicochemical and Engineering Aspects, 2004. **240**(1-3): p. 63-67.
338. Fukaya, Y., A. Sugimoto, and H. Ohno, *Superior Solubility of Polysaccharides in Low Viscosity, Polar, and Halogen-Free 1,3-Dialkylimidazolium Formates.* Biomacromolecules, 2006. **7**(12): p. 3295-3297.
339. Li, S., et al., *Facile transformation of hydrophilic cellulose into superhydrophobic cellulose.* Chem. Commun., 2007(46): p. 4857 - 4859.
340. Nystrom, D., et al., *Superhydrophobic bio-fibre surfaces via tailored grafting architecture.* Chemical Communications, 2006(34): p. 3594-3596.
341. Gavillon, R. and T. Budtova, *Aerocellulose: New Highly Porous Cellulose Prepared from Cellulose-NaOH Aqueous Solutions.* Biomacromolecules, 2008. **9**(1): p. 269-277.
342. Shin, Y., et al., *Hierarchically Ordered Ceramics Through Surfactant-Templated Sol-Gel Mineralization of Biological Cellular Structures.* Advanced Materials, 2001. **13**(10): p. 728-732.
343. Vogli, E., et al., *The Conversion Process of Cellulose Fiber into Ceramic Fibers*, in *Ceramics - Processing, Reliability, Tribology and Wear*, G.M. Prof. Dr, Editor. 2006. p. 207-212.
344. Shah, J. and R.M. Brown, *Towards electronic paper displays made from microbial cellulose.* Applied Microbiology and Biotechnology, 2005. **66**(4): p. 352-355.
345. Yoon, S.H., et al., *Electrically Conductive Bacterial Cellulose by Incorporation of Carbon Nanotubes.* Biomacromolecules, 2006. **7**(4): p. 1280-1284.
346. Tabuchi, M., *Nanobiotech versus synthetic biotech?* Nature biotechnology, 2007. **25**(4): p. 389.
347. Yano, H., et al., *Optically Transparent Composites Reinforced with Networks of Bacterial Nanofibers.* Advanced Materials, 2005. **17**(2): p. 153-155.

Appendix 1: Brass mould

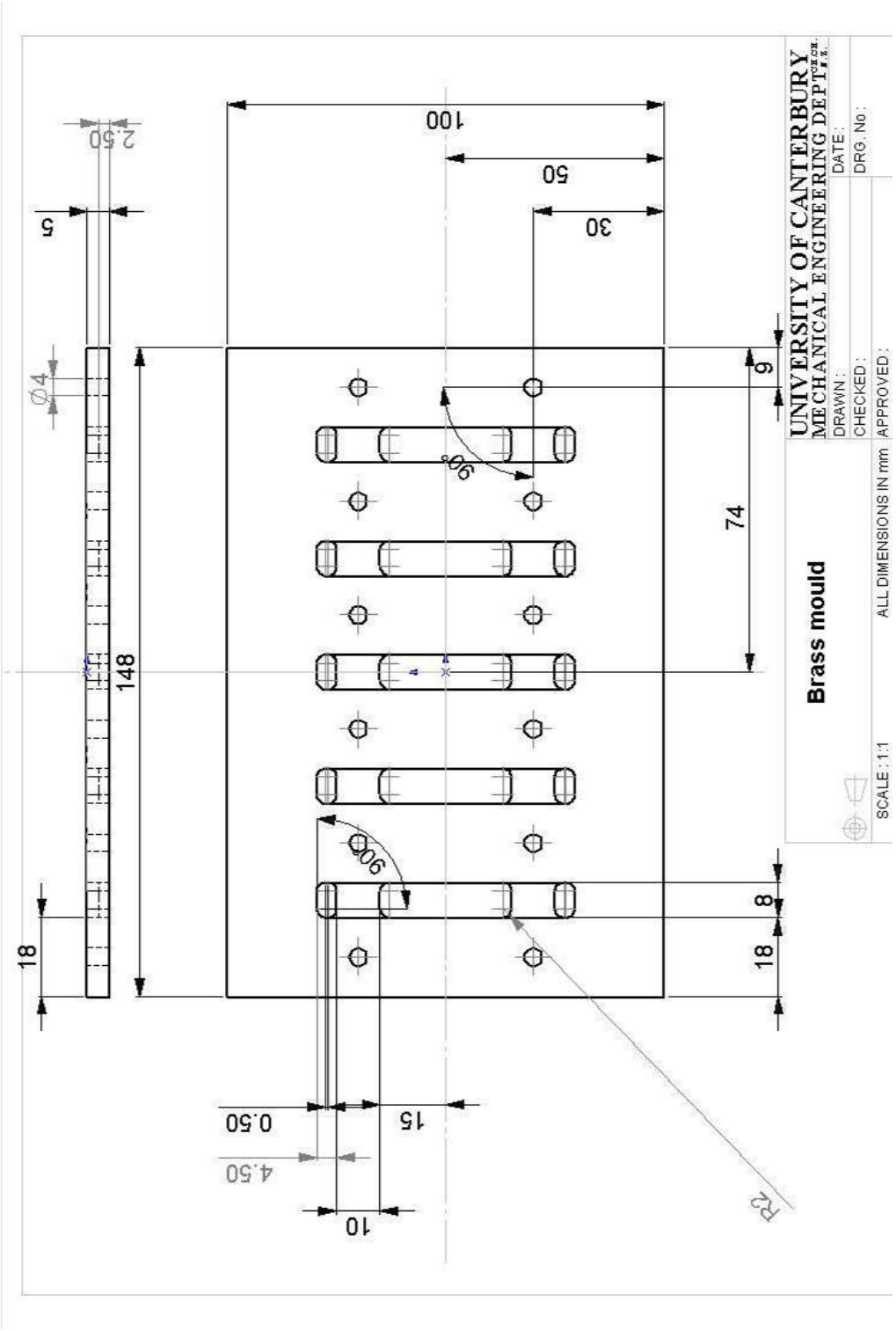

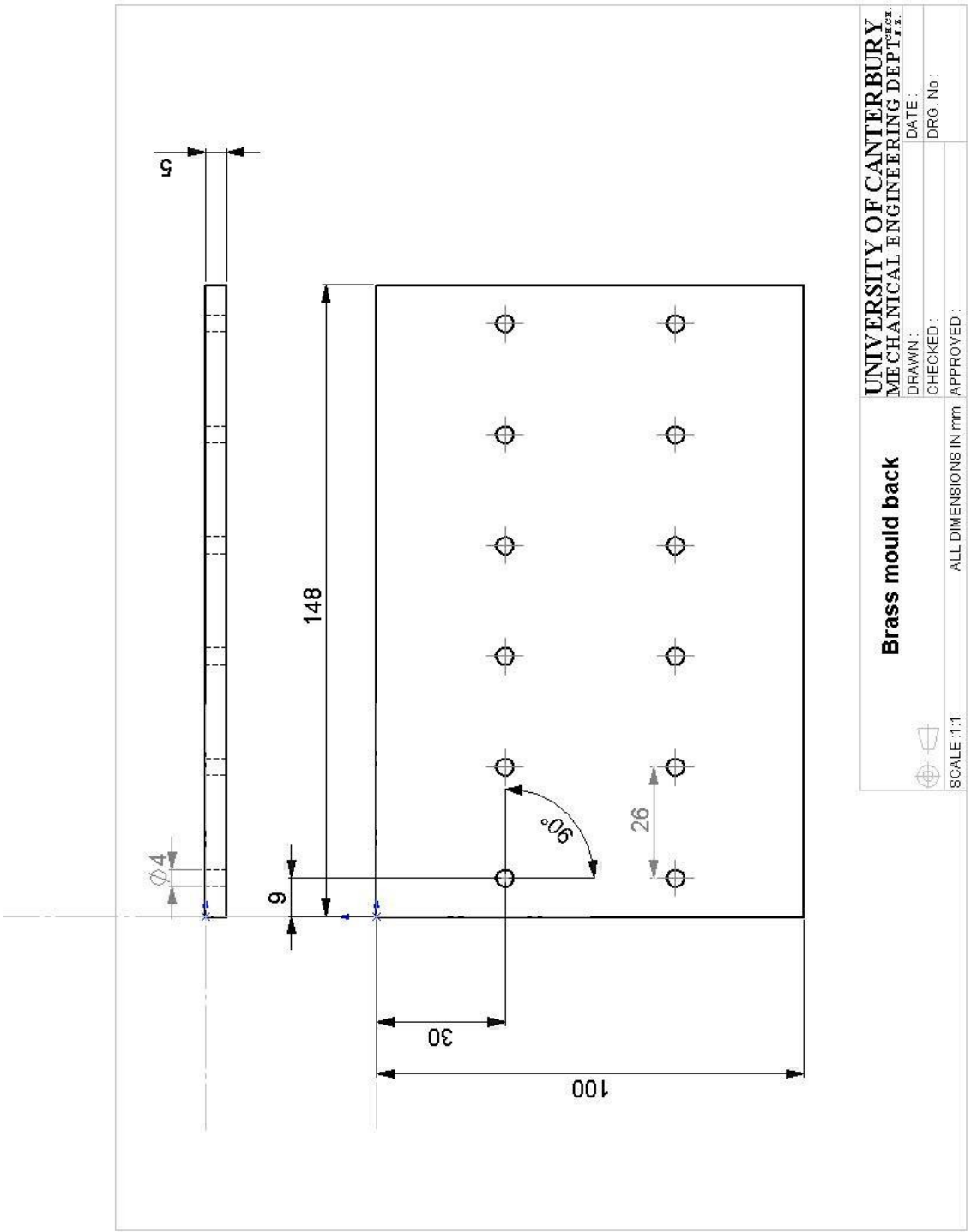
5
148
6
Ø4
90°
26
30
100
Brass mould back
UNIVERSITY OF CANTERBURY
MECHANICAL ENGINEERING DEPT.
DRAWN :
DATE :
CHECKED :
DRG. No :
SCALE 1:1
ALL DIMENSIONS IN mm
APPROVED :

Appendix 2: Sample holder for WAXS of gel specimens

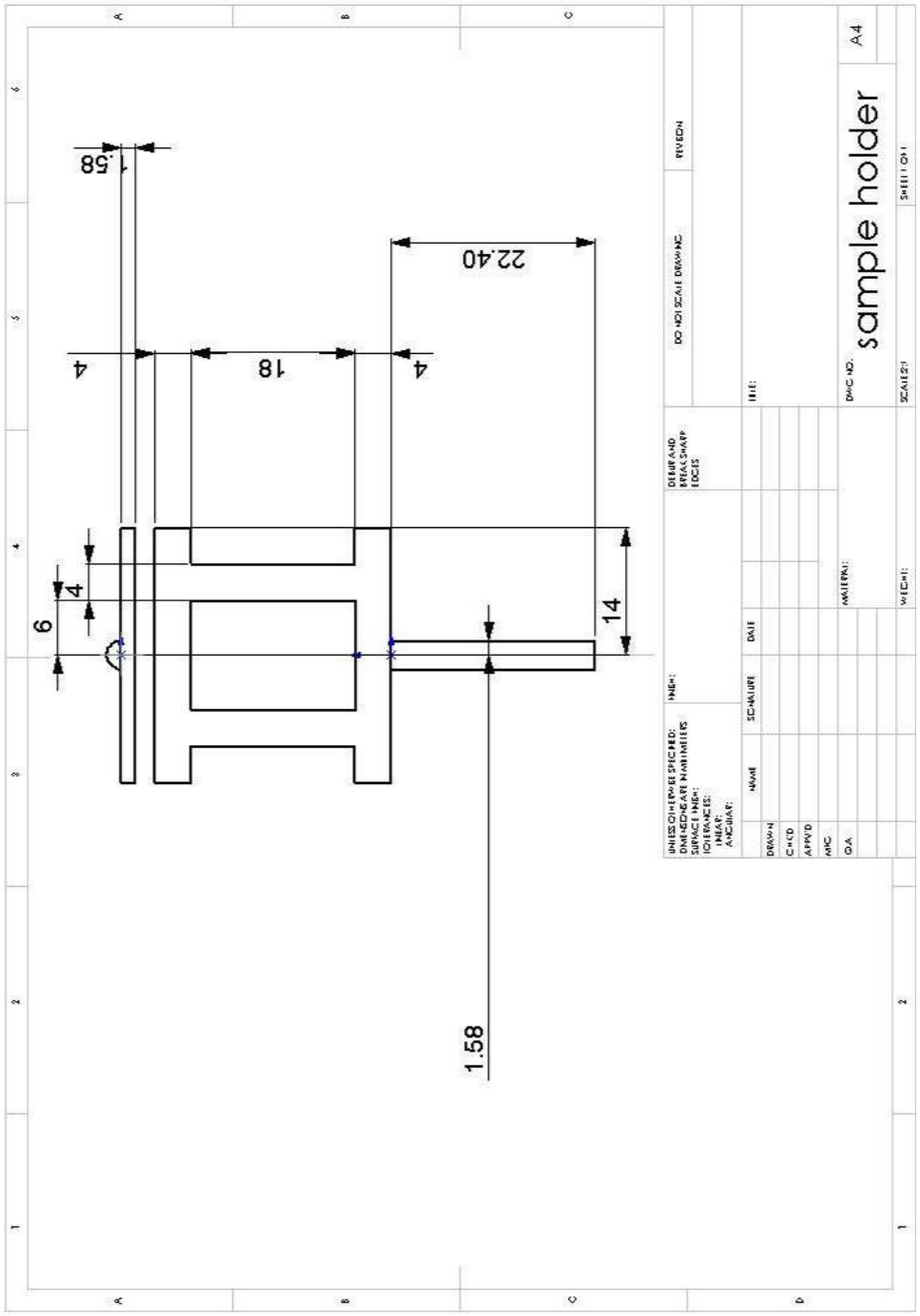

Appendix 3: Example of PeakFit® output file

Description: C:\Documents and Settings\benoit duchemin\Bureau\Equatorial profiles\WOrk file\m
X Variable: 2*theta
Y Variable: Intensity
File Source: c:\documents and settings\benoit duchemin\bureau\equatorial profiles\work file\s1-001.txt

Fitted Parameters

r^2 Coef Det	DF Adj r^2	Fit Std Err	F-value
0.98163534	0.97657568	656.477996	203.530283

Peak	Type	a0	a1	a2
1	Gauss Amp	1372.21643	3.37200000	0.93253888
2	Gauss Amp	1334.05044	4.54800000	1.10200866
3	Gauss Amp	556.385294	6.50800000	1.10200866
4	Gauss Amp	334.020661	8.27200000	1.10200866
5	Gauss Amp	12551.0204	13.6636971	2.09965968
6	Gauss Amp	3061.22449	17.7394209	1.10200866
7	Gauss Amp	4795.91837	19.8440980	1.44706276
8	Gauss Amp	204.081633	21.5812918	1.10200866
B	Quadratic Bg	-1831.8863	350.897510	-10.782974

Measured Values

Peak	Type	Amplitude	Center	FWHM	Asym50	FW Base	Asym10
1	Gauss Amp	1372.21643	3.37200000	2.19596124	1.00000000	4.39567368	1.00000000
2	Gauss Amp	1334.05044	4.54800000	2.59503208	1.00000000	5.19449707	1.00000000
3	Gauss Amp	556.385294	6.50800000	2.59503208	1.00000000	5.19449707	1.00000000
4	Gauss Amp	334.020661	8.27200000	2.59503208	1.00000000	5.19449707	1.00000000
5	Gauss Amp	12551.0204	13.6636971	4.94432071	1.00000000	9.89708745	1.00000000
6	Gauss Amp	3061.22449	17.7394209	2.59503209	1.00000000	5.19449707	1.00000000
7	Gauss Amp	4795.91837	19.8440980	3.40757238	1.00000000	6.82096568	1.00000000
8	Gauss Amp	204.081633	21.5812918	2.59503208	1.00000000	5.19449707	1.00000000

Peak	Type	Anlytc Area	% Area	Int Area	% Area	Centroid	Moment2
1	Gauss Amp	3207.59476	3.15010691	2981.10186	2.93530772	3.50762707	0.66515372
2	Gauss Amp	3685.08232	3.61903674	3646.81295	3.59079250	4.57867326	1.13532677
3	Gauss Amp	1536.91760	1.50937233	1536.88455	1.51327573	6.50810218	1.21396244
4	Gauss Amp	922.673979	0.90613743	922.673973	0.90850033	8.27200004	1.21442283

5	Gauss Amp	66056.8529	64.8729545	66056.8520	65.0421209	13.6636973	4.40856876
6	Gauss Amp	8456.10021	8.30454646	8456.10021	8.32620198	17.7394209	1.21442309
7	Gauss Amp	17395.9873	17.0842092	17395.9505	17.1287229	19.8440833	2.09389276
8	Gauss Amp	563.740014	0.55363643	563.737740	0.55507789	21.5812710	1.21432101
	Total	1.0182e+05	100.000000	1.0156e+05	100.000000		

Parameter Statistics

Peak 1 Gauss Amp

Parm	Value	Std Error	t-value	95
Amp	1372.21643	2.648e+06	0.00051821	-5.253e+06 5.2556e+06
Ctr	3.37200000	332.302602	0.01014738	-655.98846 662.732457
Wid	0.93253888	121.454458	0.00767810	-240.05946 241.924534

Peak 2 Gauss Amp

Parm	Value	Std Error	t-value	95
Amp	1334.05044	2.2617e+06	0.00058984	-4.486e+06 4.4891e+06
Ctr	4.54800000	928.611290	0.00489764	-1838.0183 1847.11426
Wid	1.10200866	1025.03028	0.00107510	-2032.7804 2034.98446

Peak 3 Gauss Amp

Parm	Value	Std Error	t-value	95
Amp	556.385294	1.0034e+06	0.00055452	-1.99e+06 1.9914e+06
Ctr	6.50800000	1212.93409	0.00536550	-2400.2164 2413.23237
Wid	1.10200866	737.307000	0.00149464	-1461.8750 1464.07906

Peak 4 Gauss Amp

Parm	Value	Std Error	t-value	95
Amp	334.020661	2.398e+05	0.00139292	-4.755e+05 4.7615e+05
Ctr	8.27200000	537.262169	0.01539658	-1057.7727 1074.31670
Wid	1.10200866	117.396505	0.00938707	-231.83813 234.042144

Peak 5 Gauss Amp

Parm	Value	Std Error	t-value	95
Amp	12551.0204	5606.71382	2.23856983	1426.08381 23675.9570
Ctr	13.6636971	0.19855227	68.8166252	13.2697263 14.0576679
Wid	2.09965968	0.46903054	4.47659485	1.16900134 3.03031803

Peak 6 Gauss Amp

Parm	Value	Std Error	t-value	95
Amp	3061.22449	52205.4052	0.05863808	-1.005e+05 1.0665e+05
Ctr	17.7394209	4.55960073	3.89056455	8.69218388 26.7866580
Wid	1.10200866	2.01490445	0.54692850	-2.8959989 5.10001622

Peak 7 Gauss Amp

Parm	Value	Std Error	t-value	95
Amp	4795.91837	77377.2578	0.06198098	-1.487e+05 1.5833e+05
Ctr	19.8440980	24.2138627	0.81953459	-28.201459 67.8896549

Wid 1.44706276 25.3676553 0.05704361 -48.887869 51.7819944

Peak 8 Gauss Amp

Parm	Value	Std Error	t-value	95
Amp	204.081633	1.3715e+05	0.00148797	-2.719e+05 2.7235e+05
Ctr	21.5812918	140.641998	0.15344842	-257.48294 300.645528
Wid	1.10200866	86.7831635	0.01269842	-171.09462 173.298633

Baseline Quadratic Bg

Parm	Value	Std Error	t-value	95
a0	-1831.8863	9600.07222	-0.1908201	-20880.512 17216.7397
a1	350.897510	1089.32387	0.32212414	-1810.5574 2512.35240
a2	-10.782974	33.8456710	-0.3185924	-77.940128 56.3741806

Analysis of Variance

r^2 Coef Det	DF Adj r^2	Fit Std Err
0.98163534	0.97657568	656.477996

Source	Sum of Squares	DF	Mean Square	F
Regr	2.2805665e+09	26	87714094	203.53028
Error	42665373	99	430963.36	
Total	2.3232318e+09	125		

Details of Fit

Set Convergence	State	Iterations	Minimization	Extent
1E-6	Not Fitted	0	PVII Lim	1/1

Curvature Matrix	Constraints				Violated
Full	None	- None	- None	- None	- None 0